On Stretched Flows of Carreau Fluid with Heat Transfer: Modeling and Analysis

By

Muhammad Irfan

A Thesis
Submitted in the Partial Fulfillment of the
Requirements for the Degree of

DOCTOR OF PHILOSOPHY
IN
MATHEMATICS

Supervised by

Prof. Dr. Masood Khan

Department of Mathematics
Quaid-I-Azam University
Islamabad, Pakistan
2019

Author's Declaration

I, **Muhammad Irfan,** hereby state that my PhD thesis titled **On Stretched Flows of Carreau Fluid with Heat Transfer: Modeling and Analysis** is my own work and has not been submitted previously by me for taking any degree from the Quaid-I-Azam University Islamabad, Pakistan or anywhere else in the country/world.

At any time if my statement is found to be incorrect even after my graduate the university has the right to withdraw my PhD degree.

Name of Student: **Muhammad Irfan**

Date: **22-Nov-2019**

Plagiarism Undertaking

I solemnly declare that research work presented in the thesis titled **"On Stretched Flows of Carreau Fluid with Heat Transfer: Modeling and Analysis"** is solely my research work with no significant contribution from any other person. Small contribution/help wherever taken has been duly acknowledged and that complete thesis has been written by me.

I understand the zero tolerance policy of the HEC and **Quaid-i-Azam University** towards plagiarism. Therefore, I as an Author of the above titled thesis declare that no portion of my thesis has been plagiarized and any material used as reference is properly referred/cited.

I undertake that if I am found guilty of any formal plagiarism in the above titled thesis even afterward of PhD degree, the University reserves the rights to withdraw/revoke my PhD degree and that HEC and the University has the right to publish my name on the HEC/University Website on which names of students are placed who submitted plagiarized thesis.

Student/Author Signature

Name: **Muhammad Irfan**

On Stretched Flows of Carreau Fluid with Heat Transfer: Modeling and Analysis

By

Muhammad Irfan

CERTIFICATE

A THESIS SUBMITTED IN THE PARTIAL FULFILLMENT OF THE REQUIREMENTS FOR THE DEGREE OF THE

DOCTOR OF PHILOSOPHY IN MATHEMATICS

We accept this thesis as conforming to the required standard

1. _____
Prof. Dr. Sohail Nadeem
(Chairman)

2. _____
Prof. Dr. Masood Khan
(Supervisor)

3. _Saleem Asghar 22/11/2019_
Prof. Dr. Saleem Asghar
(External Examiner)

Department of Mathematics, COMSATS University, Park Road Chak Shahzad, Islamabad.

4. _____
Prof. Dr. Muhammad Sajid (T.I)
(External Examiner)

Department of Mathematics & Statistics International Islamic University, Sector H-10 Islamabad.

Department of Mathematics
Quaid-I-Azam University
Islamabad, Pakistan
2019

Certificate of Approval

This is to certify that the research work presented in this thesis entitled **On Stretched Flows of Carreau Fluid with Heat Transfer: Modeling and Analysis** was conducted by **Mr. Muhammad Irfan** under the kind supervision of **Prof. Dr. Masood Khan**. No part of this thesis has been submitted anywhere else for any other degree. This thesis is submitted to the Department of Mathematics, Quaid-i-Azam University, Islamabad in partial fulfillment of the requirements for the degree of Doctor of Philosophy in field of Mathematics from Department of Mathematics, Quaid-i-Azam University Islamabad, Pakistan.

Student Name: **Muhammad Irfan**   Signature:_____

External committee:

a) **External Examiner 1**:   Signature: _Saleem Asghar_
   Name: **Prof. Dr. Saleem Asghar**   22/11/2019
   Designation: Professor
   Office Address: Department of Mathematics, COMSATS University, Park
   Road Chak Shahzad, Islamabad.

b) **External Examiner 2**:   Signature:_____
   Name: **Dr. Muhammad Sajid (T.I)**
   Designation: Professor
   Office Address: Department of Mathematics & Statistics, Faculty of Basics
   Applied Sciences International Islamic University, Islamabad.

c) **Internal Examiner**   Signature:_____
   Name: **Prof. Dr. Masood Khan**
   Designation: Professor
   Office Address: Department of Mathematics, QAU Islamabad.

Supervisor Name: Signature:_____
Prof. Dr. Masood Khan

Name of Dean/ HOD   Signature:_____

Prof. Dr. Sohail Nadeem

_____ Dedication

To my sweet Mother

whose wisdom and patience will never be forgotten.

To my dear father

for their tender love and support have put me where I am now.

To my brother and sister

for immense support and encouragements.

&

Pakistan armed forces

Acknowledgement

All praise for **Allah**, the creator, the Glorious and the Merciful Lord, who guides me in darkness, helps me in difficulties and enables me to view stumbling blocks as stepping stones to the stars to reach the ultimate stage with courage. I am nothing without my **Allah** but I can achieve everything with His assistance. All of my veneration and devotion goes to our beloved **Prophet Hazrat Muhammad** the source of humanity, kindness and guidance for the whole creatures and who declared it an obligatory duty of every Muslim to seek and acquire knowledge. May **Allah** shower His countless blessings upon **Muhammad, His family** and companions.

I express deepest gratitude to my respected, affectionate and devoted supervisor and **Prof. Dr. Masood Khan** for his intellectual guidance, constant encouragement, suggestions and inexhaustible inspiration throughout my research work. He was the backbone of this research work with constructive criticism and extensive discussions. In short his tireless work, unique way of research and devotion to his profession cannot be expressed in words.

I wish to express my heartiest thanks and gratitude to my parents **Mr. and Mrs. Shabbir Ahmed** the one who can never ever be thanked enough for the overwhelming love, kindness and care they bestow upon me. They support me financially as well as morally and without their

proper guidance it would not been possible for me to complete my higher education. I am also thankful to each and every member of my family. Special thanks to my brother **Muhammad Usman** and **Bhabi,** my brother in law **Mr.** and **Mrs. Raheel Islam** and my cousin **Mrs. Touqeer.** I spend good time with the kids in our family like nephew **Muhmmad Ayan**, **Muhammad Hesham** and niece **Mahnoor Fatima**.

I would like to express my gratitude to respected teachers **Prof. Dr. Muhammad Ayub**, **Prof. Dr. Tasawar Hayat**, **Prof. Dr. Sohail Nadeem**, **Prof. Dr. Tariq Shah**, **Dr. Asif Ali**, **Dr. Khalid Saifullah**, **Dr. Babar Majeed Mirza, Dr. Umar Hayat** and **Dr. Muhammad Aslam**. These are all those people who made me what I am today, they polished me at different stages of my life and taught me whatever I am today.

For this dissertation I would like to thank my oral defense committee, **Prof. Dr. Saleem Asghar** and **Prof. Dr. Muhammad Sajid,** for letting my defense be an enjoyable moment, and for your brilliant comments and suggestions, thanks to you.

I gratefully acknowledge my co-advisor **Dr. Waqar Azeem Khan** my seniors **Dr. Muhammad Waqas, Dr. Hashim, Dr. Shahid Farooq** and Ph.D fellows **Dr. Aamir Hamid**, **Mr. Muhammad Ijaz Khan, Dr. Latif, Miss Humara Sardar, Mr. Kaleem, Mr. Jawad Ahmed, Mr. Yasir and Mr. Usman Ali** for their brilliant ideas and important contribution in refining my research work. Their professional guidance has nourished

*and polished my intellectual skills and I will always remain thankful to them. I am also thankful to some of my ex-friends and class fellows **Mudassar Rehman, Dr. M. Shoaib, Imdad Ullah, Fiaz Ur Rehman** and **Sohail Rehman** for their supporting behavior and beautiful time with everlasting memories.*

*I want to give a special thanks to my friend **Miss Fehmida Riaz** from the core of my heart whose moral support and useful suggestions encouraged me at every step. It is great pleasure for me to mention the name of my friends **Dr. Madiha Rashid** and **Miss Kiran Chohan** for their support and guidance.*

*I enact my heartiest and deepest thanks to all my **lab fellows** who were there in lab during my Ph.D session **(05-2-2016 to 22-11-2019)**.*

*I am also grateful to **Mr. Sheraz, Mr. Zahoor Jan, Mr. Sajid Mehmood, Mr. Muhammad Sajid, Mr. Safdar, Mr. Bilal and Mr. Irfan** for their support at every time.*

In the end thanks to all my research fellows and to those people who directly and indirectly helped me during my research work.

Muhammad Irfan

22-Nov-2019

Abstract

This thesis aims at understanding and improving the existing knowledge in the area of generalized Newtonian fluids. The main focus in this work is given to the mathematical modeling and computation of three dimensional flow of Carreau rheological model that can describe both the shear thinning and shear thickening characteristics of fluids. Consequently, three dimensional boundary layer equations for both steady and unsteady cases are established. Utilizing Boussinesq estimates the governing flow and heat transfer expressions of Carrau fluid model influenced by a bidirectional stretched surface have been framed. The appropriate conversions reformed the modeled partial differential equations (PDEs) into ordinary differential equations (ODEs) and results are established both numerically as well as analytically by employing bvp4c scheme and homotopy analysis method (HAM), respectively. The performance of influential parameters for shear thinning-thickening cases are graphed, tabulated and conferred. Additionally, a comparative study has been reported in both graphical and tabular forms with available literature.

The consideration of non-Newtonian fluids have noteworthy utilizations in the area of energy, deferrals, genetic disciplines, polymer clarification, imitation fibers compound inventions, geophysics and refined materials, etc. Regardless of such attentions, various researchers are still affianced to scrutinize further the streams of non-Newtonian fluids. The contributions in this thesis include mathematical modeling of Carreau fluid in three dimension with elucidations of results of considered problems. The results for the velocity, temperature and concentration fields for both shear thinning-thickening cases are reported. The results showed that the velocity components have conflicting performance for the local Weissenberg numbers for shear thinning and shear thickening cases. It was also noted that the enhancing values of the power law exponent intensify the fluid velocities for both instances. Further, the temperature of Carrau fluid for shear thinning case intensifies for higher estimation of the local Weissenberg numbers; however, for shear thickening fluid a different behavior is observed.

Contents

Chapter 1

Review and Some Fundamental Relations

1.1   Introduction

This chapter reports the background of research and theoretical establishment of the thesis body. The essential facts for the flow and heat transfer of non-Newtonian fluids are provided in literature review. Furthermore, it highlights the significance of reviewing such fluids, especially, the Carreau rheological model. A brief narrative of all chapters of the thesis is incorporated in this chapter. Additionally, some essential worthwhile laws for forming momentum, energy and concentration terminologies are integrated. The basic notions of bvp4c approach and homotopy analysis method (HAM) are also reported.

1.2   Background

Due to the rapid growth of recent engineering expertises, there has been a massive quantity of exertions situate in the fluid flow and heat transport mechanism over the stretched surfaces by the numerous scientists owing to their widespread solicitations in engineering and industry. Boundary layer flow and heat transport are significant in numerous metallurgical processes like depiction of plastic films, fabrication of papers, annealing of copper cords, preservation of an enormous copper plate which might be an electrolyte etc. Initially, the pioneering exertion on

2D viscous fluid flow over a stretched sheet was reported by Crane [1]. Later on the problem related to stretching sheet has broadly discussed under numerous liquid models [2, 3]. Flow by an exponentially shrinking sheet for Eyring–Powell fluid with thermal radiation was analyzed by Ara *et al.* [4]. They renowned that the mass suction parameter intensified the velocity field, while divergent behavior is detected in suction parameter. Assessment of boundary-layer flow through nanoparticles past a stretchable surface was examined by Ishfaq *et al.* [5]. They reported that the consequence of Brownian motion parameter is insignificant on the Nusselt number.

The analysis of non-linear difficulties dealing with flow of non-Newtonian liquids has gained remarkable devotion during the former few decades. The behavior of nonlinear materials in present-day has attained countless thoughtfulness because of their built-up and industrial determination. In numerous applications, non-Newtonian materials have sizeable worth throughout the earliest limited spans. In these materials there is no linear correlation between stress tensor and deformation. The remarkable feature of these liquids are their advanced apparent viscosities and therefore, laminar flow circumstances intensify considerably compared to Newtonian liquids. The applications correlated for these materials are biological progressions, geophysics and genetic disciplines, reservoir manufacturing, petroleum diligence, biochemical, nuclear-powered trades, polymer elucidation, synthetic fibers, cosmetic developments, splatters, antibiotics, bubbles, colloidal and deferral elucidations, adhesives, stone undercoat and soap suds, Ophthalmic fibers, emollients, malleable polymers, granulated materials, compound and diet dispensation are few specimens of non-Newtonian materials. Undoubtedly, all non-Newtonian ingredients on the basis of their behavior in shear are not predicted by one constitutive relationship. Simple shear rate and stress terminologies cannot designate entirely the rheological structures of non-Newtonian fluids. Numerous investigators have exposed their concern to scrutinize nonlinear materials. If a liquid spectacles a nonlinear communication to the strain rate then it is termed as non-Newtonian liquid. It is remarkable that the interruption of non-Newtonian liquids and their energetic features comprise numerous difficulties caused by addition of rheological properties existing in the governing constitutive expressions. Despite of all such densities, numerous investigators are still betrothed to inspect the streams of non-Newtonian liquids under different features. Therefore, numerous nonlinear models concerning non-Newtonian liquids have been

proposed and scrutinized in studies ($[6-9]$) and the references therein.

In 1972, modern rheologist Carreau [10] established an efficacious relation which is used enthusiastically up to date that can well describe the characteristics of nonlinear viscoelastic materials named as Carreau fluid model. The Carreau liquid model was endorsed to visualize the properties of shear thinning/thickening liquids of several non-Newtonian liquids. The Carreau liquid model has caught the thoughtfulness of numerous investigators and engineers through the last few years owing to its wide-ranging uses, such as asphalt splatters, aqueous, polymers deferral and fluxes. In view of its aptitude to access the rheological performance at precise low as well as precise high shear rate, the Carreau viscosity model executes to be a worthy approach for a huge number of shear thinning/thickening liquids. For instance, Chhabra and Uhlherr [11] reported experimentally the Carreau liquid model and studied the creeping motion via shear-thinning elastic fluids over sphere. They investigated that the Carreau viscosity equation is precisely established for the impacts of elasticity and shear thinning on sphere drag. The flow of Carreau liquid of blood through a tapered artery was analyzed by Akbar and Nadeem [12]. Khan and Hashim [13] presented a new formulation for 2D Carreau fluid and examined numerically the boundary layer flow over a nonlinear stretching sheet. They observed that fluid velocity is reduced for shear thinning case with higher Weissenberg number, while the performance is quite opposite for shear thickening case. Khan *et al*. [14] investigated Carreau fluid flow over a sensor surface with time dependent thermal conductivity. They established that for emergent values of squeezing parameter the velocity field arises. Hayat *et al*. [15] explored Carreau nanofluid over a stretched flow in the presence of the convectively heated surface. A virtual study in a limiting sense with prevailing solutions is made in this examination. The results showed that the skin friction coefficient augments for the intensification in material parameter. Moreover, they established that the larger power law exponent rises the velocity component. To exploit the features of improved heat flux on Carreau fluid flow, Hashim and Khan [16] made their study. The homogeneous/heterogeneous reactions are reported in this scrutiny. The heat transfer rate is implicitly enriched to escalation in wall thickness parameter and conflicting impact is noticed for the thermal relaxation parameter. The radiative flow of Carreau fluid with temperature jump and suspension of liquid particle were stated by Kumar *et al*. [17]. The impacts of thermal radiation and convective condition were also deliberated in

7

this examination. They established that the temperature of Carreau liquid and thickness of the thermal boundary layer were enhancing functions of thermal radiation. Few endeavors in this trend can be accessed in references ([18 − 21]).

Fluid heating and cooling are one of the utmost noteworthy and stimulating phases for numerous applications of heat transfer in various industries for example; containing chemical growths, transportation, industrial, fabrication, microelectronics, etc. By rising in the heat transfer amount in industrialized applications there will be decline in time dispensation, intensification in the life of equipment's, and valid in energy. Moreover, conventional liquids viz. paraffin, water, ethylene glycol (EG), inflating oil, etc., are broadly used in numerous productions. However, they do not have adequate proficiency of heat transfer because of their low thermal conductivity and this frequently edges their usage in high heat flux devices, e.g., substantial processing, microelectronics maintenance and stellar thermal antennas. On the other hand by diffusing dense nano-sized particles to conventional liquids rises the thermal conductivity which spectacles advanced thermal assets. Nanofluids, the engineered fluids with insulated efficacious nanoparticles, have disclosed an unexpected thermo-physical properties and new functionalities, and thus have maintained a widespread nature of important applications. The deferral of non-metallic and metallic nanoparticles in base liquids like aquatic and paraffin are known as nanofluids. These fluids are the diffusion of dense particles of magnitude lesser than 100 nm in size. Exclusively, nanoliquids have exposed intentionally better-quality ability of heat transport as linked to traditional working fluids. Moreover, utilizing nanofluid as a forthcoming heat transport liquid with higher thermos-physical aspects is an effective approach to enhance the thermal enactment of energy systems. Furthermore, nanofluids have developed as superior candidates for numerous applications in heat transport; for instance, in hybrid-powered purposes, drag bargain, in crunching, solar water reheating, nuclear vessel cooling numerous others. In the research features, the sort of nanofluid has been extended to a higher magnitude. The current sort of nanoparticles for interrupting in liquids can be categorized according to the thermal aspects which are as follows: Firstly, premier thermal conductivity for example $CNTs$, graphene and diamond etc. Secondly, metallic simples with abundant thermal conductivity such as, Au, Cu, Ag, Al, Fe, etc. Lastly, some metallic or non-metallic mixtures like CuO, Al_2O_3, ZnO, TiO_2, SiC, etc. As a consequence of the assortment of the exploration features and

element varieties in nanofluids, it is flattering gradually challenging to extant a broad analysis on all classes of nanofluids. Choi [22] in 1995 introduced the term nanofluid who established an experimental analysis and exposed to the world about the development of thermal conductivity of nanofluids. Later on, Buongiorno [23] established a precise model to scrutinize the thermal assets of base liquids. He reported that the Brownian motion and thermophoresis enhance the thermal properties of base liquids. Analytically the entropy generation characteristics in MHD $Cu - H_2O$ nanoliquid were scrutinized by Ellahi et al. [24]. The impact of power law index in the existence of thermal radiation is occupied. Khan and Khan [25] scrutinized the impact of generalized Burgers fluid by exhausting the nanoparticle over a stretched surface. It was noted that the rate of heat transfer of nanoliquid at the wall and the nanoparticle volume fraction amount reduced by enhancing the values of thermophoresis parameter; however, quite opposed effect was noted for Brownian motion parameter in this scrutiny. Numerical solutions for 3D magneto viscous nanofluid was established by Mahanthesh et al. [26]. Khan and Khan [27] investigated MHD power law nanofluid by utilizing zero mass flux condition. Numerical scheme, namely shooting technique was implemented to resolve the governing nonlinear ODEs. They noted that both the Brownian and thermophoresis parameters were augmenting functions of temperature distribution. The characteristics of the nanoparticles condition on 3D radiative flow of Burgers nanofluid were explored by Khan et al. [28]. This investigation showed that the concentration field collapsed rapidly correlate to the Deborah number when compared with the Brownian motion parameter. Hayat et al. [29] analyzed numerically the stagnation point flow of carbon–water nanofluid. The properties of melting heat and thermal energy were also deliberated in this exploration. They establish that the amassed values of melting parameter resembled to greater velocity and fewer temperature. Khan et al. [30] considered the generalized Burgers nanoliquid with the influence of chemical response. The impact of nonlinear thermal radiation in the existence of the zero mass flux condition was also explored. Waqas et al. [31] inspected numerically the flow of Carreau nanoliquid in the presence of MHD and thermal radiation. They established that for the velocity component the influence of local Weissenberg number is quite conflicting. Dogonchi et al. [32] inspected the heat transfer flow of magneto nanoliquid between two parallel plates with the effects of thermal radiation. Impact of chemical species with variable thickness of nanoliquid owing to rotating disk was examined

9

by Hayat *et al.* [33]. This scrutiny exhibited that the radial, axial and azimuthal velocities were enriched for intensification in disk thickness parameter. The heat transport phenomenon on unsteady Carreau magneto nanofluid towards the cone packed subject to alloy nanomaterials was discussed numerically by Raju *et al.* [34]. They reported that the heat transfer amount heightened for the viscous variation parameter. Recently, Hayat *et al.* [35] investigated fluid flow of magneto nanoliquid subject to nonlinear stretched surface. They analyzed that the pressure and velocity field declined for power law index. The convective phenomenon in Fe_3O_4-water nanofluid subject to magnetic source was explored by Sheikholeslami *et al.* [36]. The behavior of chemical reaction and non-linear radiation in swirling flow influenced by rough rotating disk was scrutinized by Mustafa *et al.* [37]. Irfan *et al.* [38] presented a new mathematical forming for Maxwell nanomaterial with convective condition. Additionally, the aspects of MHD and heat sink/source are engaged. They indicated that the temperature intensifies for Brownian and thermophoresis parameters. Hamid *et al.* [39] addressed numerically the aspects of activation energy on time-dependent Williamson nanofluid flow with the nanoparticles mass flux condition. They investigated that the heat transport amount over surface cylinder diminished with escalating values of reaction rate parameter. The enactment of nonlinear radiative flow of suspended nanoparticles with melting vertical surface was studied by Mahanthesh *et al.* [40]. They established that the melting and moving parameters declined the drag force.

In recent times, hydrogen-fueled and hydro-carbon homogeneous/heterogeneous micro reactors have been the attention of forceful exertions for an impartially wide-ranging assortment of moveable constructions of energy with established energy compactness considerably sophisticated than those of the advanced Li-ion batteries. The solicitations of micro reactors assortment from catalytic micro reactors recycled for the steam revolutionizing of hydrocarbon fuel in little and high-temperature energy chambers and to micro-scale heat apparatuses, in which a catalytic micro combustor is recycled for straight chemical-to-thermal energy exchange. In furthermost cases, reinforced moral metallic catalysts are engaged owing to their extraordinary biochemical studies on the subject of chemical reaction have attained uninterrupted thoughtfulness from the modern technologists and engineers. The intrinsic way of a chemical reaction happens if two or more reactants yield a product. The aspects of chemical reactions are noteworthy in various developments due to their utilization in numerous techniques like atmospheric flows,

hydrometallurgical diligence, mutilation of crops, fabrication of polymer and porcelains, fog materialization and dispersal. The homogeneous and heterogeneous reactions are two categorization of the chemical processes. This discrepancy is interrelated to the circumstance that whether they arise in liquid substance or transpire in some catalytic exteriors. A homogeneous process occurs consistently in the entire certain phase, whereas the heterogeneous process proceeds in a circumscribed region or inside the phase boundary. The collaboration between the heterogeneous and homogeneous reactions is very problematic containing the fabrication and depletion of reactant sorts at diverse amounts both inside the liquid and on the exteriors catalytic. Apart from in the manifestation of a catalyst, numerous reactions have the aptitude to transfer gradually or not at all. For the exploration of homogeneous-heterogeneous processes on the flow of viscous liquids, Merkin [41] proposed an isothermal relation. This scrutiny exposes that because of the surface retort this utilization is dominant. Further, by considering both sorts of the identical diffusivities, Chaudhry and Merkin [42] conferred the assets of homogeneous-heterogeneous reactions in a viscous liquid. Flow scrutiny of the stagnation region with the stimulus of heterogeneous-homogeneous reactions was explored by Xu [43]. He reported multiple solutions numerically via hysteresis bifurcation approach and showed that the Prandtl number and homogeneous reaction parameter were not the reasons to produce multiple solutions. The MHD flow of a micropolar liquid over a curved stretched surface with heterogeneous-homogeneous reaction was reported by Hayat *et al.* [44]. They noted that the impact of heterogeneous and homogeneous response is quite opposite on the concentration field. In diverse models, a few studies for flow with heterogenous/homogeneous reactions were pointed out via references ([45 − 50]).

Recently, combining energetic liquids with heat transfer have been unique, worthwhile subject owing to their countless methodological and systematic solicitations. With the intention to attain the superiority of the product it is documented that the amount of cooling is noteworthy. For instance, cut-glass foodstuffs, gemstone developing, polymer dispensation, crust of cords, purify- caution of liquefied metals and canvas material, microelectronics, transports, paper productions, copper wires thinning and medical uses (conduction of heat in the muscles and medication targeting) etc. The heat transport mechanism transpires when the temperature of the body or different quantities of body is changed. This procedure has enormous solicitations

in power cohort, heat conduction in nerves, nuclear synthesis and countless industrial arenas. The features of heat transfer around 200 years ago, was first reported by Fourier [51], which is the best heat conduction model to contribute an information to understand the mechanism of heated conversation in numerous circumstances. But, Fourier's law is insufficient owing to the circumstance of the initial disruption that can be controlled straightaway all over the system. Afterwards, Cattaneo [52] established an amendment of Fourier's law for heat transfer in an obstinate form. By insertion of thermal relaxation time aspect to present the thermal inertia, which is recognized as Maxwell–Cattaneo law, he reformed the Fourier's law. By interchanging time derivative with Oldroyd upper convected derivative this notion is additionally improved by Christov [53] and entitled it as Cattaneo-Christov theory for heat flux. For the scrutiny of convective heat transport this model is precise worthwhile. For instance, Tibulle and Zampoli [54] examined the uniqueness of Cattaneo-Christov heat flux model for an incompressible fluid flow. Analytical solution of $3D$ Maxwell fluid flow escorting Cattaneo-Christov theory was investigated by Rubab and Mustafa [55]. The achieved results showed that for thermal relaxation time parameter the penetration depth of temperature is a decline. Cattaneo-Christov heat flux model characteristics in three dimensional Burgers fluid were scrutinized by Khan and Khan [56]. They observed that the temperature field was greater in the instance of Fourier's law, as associated to Cattaneo-Christov model. To see the impact of Cattaneo-Christov model on generalized Burgers fluid, Waqas *et al.* [57] analyzed the characteristics of the heat flux model for generalized Burgers fluid in the existence of time-dependent thermal conductivity. The homotopy analysis method (HAM) has been used for the convergent series solution of the governing equations in this investigation. Moreover, aspects of convection diffusion with fractional Cattaneo-Christov flux were scrutinized by Liu [58]. Combined heat and mass conduction relations with upper-convected Maxwell nanoliquid in the manifestation of the slip velocity were considered by Sui [59]. Cattaneo–Christov double diffusion in Oldroyd-B fluid flow in the rotating frame with variable conductivity was reported by Khan [60]. Mustafa *et al.* [61] scrutinized the theory of upgraded heat flux relation in Maxwell liquids with the aspect of variable conductivity in rotating frame analytically. They pointed out that owing to the insertion of elastic properties the hydrodynamic boundary layer turned out to be thinner. Furthermore, Ali and Sandeep [62] reported numerically, the impact of the improved heat flux theory for radiative

flow of magnetite Casson-ferrofluid. These upshots specified that thermal relaxation parameter efficiently augmented the local Nusselt number and heat transfer enactment is extraordinary towards flow past a wedge when related to flow towards plate/cone. Dogonchi and Ganji [63] investigated the combined features of thermal radiation and MHD for nanofluid between parallel plates by utilizing the theory of Cattaneo–Christov heat flux. They stated that the Nusselt number has revered impact for thermal relaxation and heat source parameters. In outlook of these properties, numerous investigators formerly have scrutinized diverse rheological problems with numerous methods and physical properties were reported in references ([64 − 67]).

Recently, the convective phenomenon has improved noteworthy thoughtfulness of technologists and researchers owing to its proper influence on heat and mass transport structures. It plays an enthusiastic quantity in various built-up problems regarding both metallic and polymers sheets, exchange of heat between efficient heat stowage beds and inaccessibility of thermonuclear pitchers, irrigation systems, diffusion of multifaceted chemicals in waterlogged soil etc. The notion of surface convective boundary condition was instigated by Aziz [68]. He deliberated the viscous fluid flow towards a flat plate with surface convective condition. The flow of an Eyring-Powell liquid with the combined impact of heat and mass convective conditions was scrutinized by Hayat et $al.$ [69]. They noted that the performance of thermal and mass Biot numbers on both the temperature and concentration were analogous. Hayat et $al.$ [70] reported the properties of convective on magnetite flow of Fe_3O_4 nanoparticles towards curved surface. Numerous authors have considered the influence of these conditions in the diverse flow geometries with diverse aspects [71, 72].

In the hurried universal evolution of science and expertise, augmenting the proficiency of energy transfer in addition to tradable energy is pretense novel challenge. Solar energy from side to side insignificant conservational bearing consequently offers a solution. Solar influence is measured an expected tactic of attaining water, heat and voltage from the nature. Solar energy is considered one of the supreme causes of renewable energy which forms energy for billions of years. Although, consuming progressive resource with enhanced assets is a standout among one of the supreme broadly implemented methodologies of heat transfer improvement. Whereas the customary heat transfer fluids, for example engine oil, water or ethylene glycol, have powerless to meet the exceptional necessities such as micro preservation and solid heat

transfer strength. Solar supremacy is measured essential to yield electrical energy and heat from nature. Moreover, the thermal radiative transportation has abundant significance in various manufacturing applications resembling solar power antennas, warming and freezing cavities, and open water tanks and several other engineering and conservational developments. Beside this, radiation from solar energy and the consequential solar energized properties such as breeze and wave supremacy, etc. provide a description for utmost handy renewable energy that is existing in the world. By exhausting the Rosseland estimation, Hossain *et al.* [73] scrutinized natural convective flow by a uniformly heated porous plate with effects of thermal radiation. Numerical exploration on MHD tangent hyperbolic liquid by a stretched surface was reported by Akbar *et al.* [74]. Later on, the radiative flow involving MHD nanofluid by a stretched surface was studied by Akbar *et al.* [75]. Hayat *et al.* [76] analyzed the partial slip mechanism in MHD flow of Cu-water nanofluid due to a rotating disk. Additionally, viscous dissipation and thermal radiation effects are also deliberated. They established that for an escalation in the nanoparticle volume fraction the heat transport rate boosted. The $3D$ radiative flow of Burgers fluid with the influence of the thermophoresis particle was analyzed by Khan and Khan [77]. Heat generation/absorption phenomenon was also carried out in this study. The MHD radiative viscoelastic nanoliquid considering of stagnation region was scrutinized by Farooq *et al.* [78]. Additionally, radiation is taken to be nonlinear in the presence of convective heat transport. It was observed that there is a substantial diminution in the velocity component and its corresponding thickness of the momentum boundary layer with rising values of magnetic parameter. Improvement in the analysis of numerous non-Newtonian liquids related to thermal radiation can be reported in references ([79 − 84]).

The operating liquid heat source or sink structures are precise vigorous in monitoring heat exclusion from nuclear fuel debris, the heat transfer in the regions, underground disposal of radioactive discarded material and exothermic chemical progressions and dissociating liquids in packed-bed vessels. The heat source can arise in the form of a battery or coil. Khan *et al.* [85] studied the impact of nanoparticles on 3D flow of an Oldroyd-B fluid over a stretched surface in the presence of heat source/sink. Again, Khan *et al.* [86] scrutinized the characteristics of nanoparticles for the steady flow of Burgers fluid over a stretched surface by utilizing heat source/sink. They concluded that the impact of heat generation/absorption is quite reverse on

the temperature of Burgers nanoliquid. Moreover, Khan *et al.* [87] investigated the features of chemical processes and heat source/sink for Maxwell fluid. In addition, significant analysis on heat source/sink can be comprehended in the references [88, 89] and numerous explorations therein.

The theory of variable conductivity in heat transport phenomenon has forceful worth in numerous industrial and built-up applications. Undoubtedly variable thermal conductivity is most worthwhile when allied with constant thermal conductivity as realistic conditions claim variable properties. These assets fluctuate with temperature in linear mode for fluid metals from $0°F$ to $400°F$ [90, 91]. The mechanism of heat transportation in heaters, lather isolations, containers, volumetric solar earpieces, porous flames and fibrous etc., is a specimen of the conduction mechanism in which temperature fluctuates and therefore variation in thermal conductivity is high. Aspects of variable conductivity on the Carreau and Eyring liquids with nickel and dust nanoparticles were reported by Upadhya *et al.* [92]. Their study expressed that the amount of heat transfer is advanced in the mixture of the nickel for Eyring-Powell situation when associated with Carreau situation. Hayat *et al.* [93] studied the behavior of variable conductivity on the peristalsis flow of Johnson-Segalman fluid.

Recently, the mixed convection transport of non-Newtonian liquids via thermal and solute stratifications is a subject of abundant scrutiny owing to its widespread manifestation in the engineering and industrial progressions. The heat dismissal into the atmosphere for instance, streams, oceans and ponds; thermal energy storing structures like astrophysical pools etc., are the numerous specimens of such solicitations. Stratification of liquid is a deposition or establishment of layers that happens because of temperature changes, concentration variation or owing to the manifestation of diverse liquids. It is fascinating to scrutinize the impact of double stratification when both heat and mass transfer are existing instantaneously. Moreover, in the manifestation of gravity the density dissimilarities have strategic role in the mixing of heterogeneous liquid and dynamics. For instance, thermal stratification in pools can condense the fraternization of oxygen to the lowest water to become anxious through the achievement of organic progressions. Similarly, the scrutiny of thermal stratification is essential for the solar industry as greater energy competence can be attained with enhanced stratification. The mixed convection thermally stratified flow along a stretched cylinder was scrutinized by Mukhopad-

hyay and Ishak [94]. The properties of chemically reacting flow and mixed convection on nanoliquid towards the moving surface were analyzed by Mahanthesh *et al.* [95]. Imtiaz *et al.* [96] considered the effects of mixed convection on Casson nanofluid due to stretched cylinder. They concluded that for larger Casson liquid and magnetic parameter condensed the liquid flow. Waqas *et al.* [97] explored the mutual effects of thermal and mass stratification on mixed convective Oldroyd-B nanoliquid. They reported that the higher thermal and solutal stratified cause a decline in the temperature and concentration fields, respectively. Moreover, current endeavors on mixed convection as well as double stratifications via diverse thoughtfulness can be referred through references ([98 − 100]).

The mass transport phenomenon with Arrhenius activation energy and chemical reaction has been specified enormously of thoughtfulness owing to its countless uses in simmer down of atomic reacting, compounds invention, geothermal artificial lake and retrieval of thermal lubricant. Activation energy can be precise as the least quantity of energy that is attainable to stimulate particles or molecules to a place wherein they can materialize physical transport or chemical reaction. For a reaction the activation energy can be strong-minded using the Arrhenius equation that states how the rate constant fluctuations in temperature. These are classified by a chemical conversion and one or more products that have diverse effects from the reactants. It is crucial to create the reaction effectual, energy influences, discarded while exploiting the yield and diminishing the quantity of reagents. Mostly, in the mass transport theories with chemical reaction are actually problematic, and it can be analyzed in the exploitation of development and reactant species at numerous rates inside the mass transport of nanofluid. The joint enactment of the Arrhenius activation energy with chemical reaction for radiative flow and heat transport to vertical pipe was reported by Bestman [101]. He acquired an analytical elucidation via perturbation approach. To use the parameters control scheme influence of activation energy thermal extrusion built-up structure proficiency in Carreau nanomaterial was explored by Hsiao [102]. He acquired a greater proficiency thermal energy extrusion structure and endorsed the system's economic proficiency. Mustafa *et al.* [103] addressed the properties of magneto nanofluid with Activation energy and buoyancy influence. They scrutinized that the performance of Brownian motion is quite conflicting to thermophoretic force on nanoparticles concentration. Khan *et al.* [104] numerically considered the aspects of entropy generation and

activation energy with nanoparticles. Their study indicated that the radiative variable intensi-fied the thermal diffusivity and rised the temperature. Zeeshan *et al.* [105] acquired analytical elucidations for Couette-Poiseuille nanofluid flow by performing the aspects of convective and activation energy. They studied that the nanoparticles concentration is directly proportionate to activation energy with chemical reaction. In recent times, influences are fortified by many researchers to scrutinize the aspects of activation energy in diverse models [106, 107].

1.3 Basic Relations of Fluid Mechanics

1.3.1 Conservation Relation of Mass

The mass neither be molded nor destroyed. This phenomenon is termed as mass conservation relation or continuity equation. For time-dependent flow the mass conservation relation can be framed as

$$\frac{\partial \rho_f}{\partial t} + \boldsymbol{\nabla} \cdot \left(\rho_f \mathbf{V} \right) = 0, \tag{1.1}$$

where ρ_f signifies the fluid density, $\mathbf{V}$ the velocity field and t the time.

For the case of an incompressible fluid *i.e.* $\left(\rho_f = \text{constant} \right)$, the relation (1.1) reduces to

$$\boldsymbol{\nabla} \cdot \mathbf{V} = 0. \tag{1.2}$$

1.3.2 Conservation Relation of Linear Momentum

The complete momentum of the system remains conserved. This notion is established from the Newton's second law and acknowledged as conservation relation of momentum. Mathematically,

$$\rho_f \mathbf{a}_i = -\boldsymbol{\nabla} p + \text{div } \boldsymbol{\tau}^* + \rho_f \mathbf{B}. \tag{1.3}$$

Here $\mathbf{a}_i \left(= \frac{\partial \mathbf{V}}{\partial t} + \left(\mathbf{V} \cdot \boldsymbol{\nabla} \right) \mathbf{V} \right)$ represents acceleration vector, in which $\frac{\partial (.)}{\partial t}$ is the time derivative, p the pressure, $\boldsymbol{\tau}^*$ the Cauchy stress tensor and $\mathbf{B}$ the body force per unit mass.

1.3.3   Conservation Relation of Energy

The entire energy of the system remains constant and this notion is follow-on from the first law of thermodynamics. Mathematically,

$$(\rho c)_f \frac{dT}{dt} = \boldsymbol{\tau}^* \cdot \mathbf{L} - \text{div}\,\mathbf{q} - \text{div}\,\mathbf{q}_r, \tag{1.4}$$

where (c_f, T) are the specific heat and temperature of fluid, respectively, $(\mathbf{q}, \mathbf{q}_r)$ the thermal and radiative heat fluxes, respectively, which are characterized by Fourier's and Stefan Boltzman laws, respectively.

Mathematically, the energy flux is termed as

$$\mathbf{q} = -k\boldsymbol{\nabla}T, \tag{1.5}$$

where k represents the thermal conductivity of fluid.

1.3.4   Conservation Relation of Concentration

The entire concentration of the framework under estimation remains unvarying. This thought is established on Fick's second law and defined as

$$\frac{\partial C}{\partial t} + \mathbf{V} \cdot \boldsymbol{\nabla}C = -\boldsymbol{\nabla} \cdot \mathbf{j}, \tag{1.6}$$

where C signifies the fluid concentration, and $\mathbf{j}$ the normal mass flux which is defined by Fick's first law, *i.e.*,

$$\mathbf{j} = -D\boldsymbol{\nabla}C, \tag{1.7}$$

where D defines the mass diffusivity.

Considering the overhead relation the equation of mass transport becomes

$$\frac{\partial C}{\partial t} + \mathbf{V} \cdot \boldsymbol{\nabla}C = D\boldsymbol{\nabla}^2 C. \tag{1.8}$$

1.3.5 Conservation Relation of Energy for Nanofluids

The energy relation with nanoparticles for an incompressible fluid is defined as

$$(\rho c)_f \frac{dT}{dt} = h_p \boldsymbol{\nabla} \cdot \mathbf{j}_p - \operatorname{div} \mathbf{q}, \tag{1.9}$$

where h_p defines the specific enthalpy for nanoparticles and $(\mathbf{q}, \mathbf{j}_p)$ the thermal and diffusivity mass fluxes of nanoparticles, respectively, and are defined by

$$\mathbf{q} = -k\boldsymbol{\nabla}\mathbf{T} + h_p \mathbf{j}_p, \tag{1.10}$$

$$\mathbf{j}_p = -\rho_p D_B \boldsymbol{\nabla}\mathbf{C} - \rho_p D_T \frac{\boldsymbol{\nabla}\mathbf{T}}{T_\infty}, \tag{1.11}$$

in which ρ_p signifies the mass density of nanoparticles and (D_T, D_B) the thermophoretic and Brownian diffusion coefficients, respectively.

Hence, seeing Eqs. (1.10) and (1.11), the nanofluids energy equation (1.9) becomes

$$\frac{dT}{dt} = \frac{k\boldsymbol{\nabla}^2 T}{(\rho c)_f} + \left(\frac{(\rho c)_p}{(\rho c)_f}\right)\left[\frac{\boldsymbol{\nabla}T \cdot \boldsymbol{\nabla}T}{T_\infty} + D_B \boldsymbol{\nabla}C \cdot \boldsymbol{\nabla}T\right]. \tag{1.12}$$

1.3.6 Conservation Relation of Concentration for Nanofluids

The concentration relation with nanoparticles is delineated as

$$\frac{\partial C}{dt} + \mathbf{V} \cdot \boldsymbol{\nabla}C = -\frac{1}{\rho_p}\boldsymbol{\nabla} \cdot \mathbf{j}_p. \tag{1.13}$$

Considering Eq. (1.11), the overhead relation is specified as

$$\frac{\partial C}{dt} + \mathbf{V} \cdot \boldsymbol{\nabla}C = D_B \boldsymbol{\nabla}^2 C + D_T \frac{\boldsymbol{\nabla}^2 \mathbf{T}}{T_\infty}. \tag{1.14}$$

1.4 Generalized Fourier's and Fick's Laws

The energy and concentration relation without nanoparticles are defined as

$$(\rho c)_f \frac{dT}{dt} = -\operatorname{div} \mathbf{q}, \tag{1.15}$$

$$\frac{dC}{dt} = -\operatorname{div} \mathbf{J}, \tag{1.16}$$

The Cattaeno-Christov double diffusion theory which is the generalization of Fourier's and Fick's laws are represented as

$$\mathbf{q} + \lambda_1 \left(\frac{\partial \mathbf{q}}{\partial t} + \mathbf{V}.\boldsymbol{\nabla}\mathbf{q} + (\boldsymbol{\nabla}.\mathbf{V})\,\mathbf{q} - \mathbf{q}.\boldsymbol{\nabla}\mathbf{V} \right) = -k\boldsymbol{\nabla}T, \tag{1.17}$$

$$\mathbf{J} + \lambda_2 \left(\frac{\partial \mathbf{J}}{\partial t} + \mathbf{V}.\boldsymbol{\nabla}\mathbf{J} + (\boldsymbol{\nabla}.\mathbf{V})\,\mathbf{J} - \mathbf{J}.\boldsymbol{\nabla}\mathbf{V} \right) = -D\boldsymbol{\nabla}C, \tag{1.18}$$

where (λ_1, λ_2) are the heat and mass fluxes relaxation times, respectively. For $\lambda_1 = \lambda_2 = 0$, Eqs. (1.17) and (1.18) are condensed to classical Fourier's and Fick's laws, respectively.

1.5 Homogeneous-Heterogeneous Reactions

For cubic autocatalysis homogeneous-heterogeneous chemical reactions where two chemical species are allied in boundary layer flow can be defined as

$$G_1 + 2H_1 \to 3H_1, \quad rate = k_c g_1 h_1^2, \tag{1.19}$$

$$G_1 \to H_1, \quad \text{rate} = k_s g_1. \tag{1.20}$$
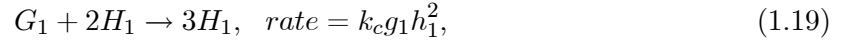
Here (G_1, H_1) signify the chemical species of concentration (g_1, h_1), respectively, and k_j $(j = c, s)$ are the rate constants. For considering isothermal processes and far away from the sheet in the ambient fluid a unvarying concentration g_{1_0} of reactant G_1 is existing and there is no auto catalyst H_1. Under these norms the homogeneous-heterogeneous reaction equations for time-dependent flow are determined as

$$\frac{\partial g_1}{\partial t} + u\frac{\partial g_1}{\partial x} + v\frac{\partial g_1}{\partial y} + w\frac{\partial g_1}{\partial z} = D_{G_1}\frac{\partial^2 g_1}{\partial z^2} - k_c g_1 h_1^2, \tag{1.21}$$

$$\frac{\partial h_1}{\partial t} + u\frac{\partial h_1}{\partial x} + v\frac{\partial h_1}{\partial y} + w\frac{\partial h_1}{\partial z} = D_{H_1}\frac{\partial^2 h_1}{\partial z^2} + k_c g_1 h_1^2. \tag{1.22}$$

For the case of time independent $\left(\frac{\partial(.)}{\partial t} = 0\right)$ overhead equations reduce to

$$u\frac{\partial g_1}{\partial x} + v\frac{\partial g_1}{\partial y} + w\frac{\partial g_1}{\partial z} = D_{G_1}\frac{\partial^2 g_1}{\partial z^2} - k_c g_1 h_1^2, \tag{1.23}$$

$$u\frac{\partial h_1}{\partial x} + v\frac{\partial h_1}{\partial y} + w\frac{\partial h_1}{\partial z} = D_{H_1}\frac{\partial^2 h_1}{\partial z^2} + k_c g_1 h_1^2. \tag{1.24}$$

1.6   The Carreau Rheological Model

This thesis essentially highlights the study of flow and heat transfer properties for three-dimensional Carreau fluid model influenced by bidirectional stretching surface. The Carreau fluid model has the subsequent relation of Cauchy stress tensor $(\boldsymbol{\tau}^*)$.

$$\boldsymbol{\tau}^* = -p\mathbf{I} + \mu(\dot{\gamma})\mathbf{A}_1, \tag{1.25}$$

with

$$\mu(\dot{\gamma}) = (\mu_0 - \mu_\infty)[1 + (\Gamma\dot{\gamma})^2]^{\frac{n-1}{2}} + \mu_\infty, \tag{1.26}$$

here $(p, \mathbf{I})$ denote the pressure and identity tensor, respectively, (μ_0, μ_∞) the zero and the infinity shear-rate viscosities, respectively, (Γ, n) the material time constant and power law exponent, respectively, $\left(\frac{\mu - \mu_\infty}{\mu_0 - \mu_\infty}\right)$ defines the slope in the power law region, $\mathbf{A}_1 = \boldsymbol{\nabla}\mathbf{V} + (\boldsymbol{\nabla}\mathbf{V})^T$ the first Rivlin-Erickson tensor and the shear rate is given by

$$\dot{\gamma} = \sqrt{\frac{1}{2}tr(\mathbf{A}_1^2)}. \tag{1.27}$$

For considering the most practical cases, $\mu_0 >> \mu_\infty$ and μ_∞ is taken to be zero. Consequently, in view of Eq. (1.26), Eq. (1.25) reduces to the following expression

$$\boldsymbol{\tau}^* = -p\mathbf{I} + \mu_0[1 + (\Gamma\dot{\gamma})^2]^{\frac{n-1}{2}}\mathbf{A}_1. \tag{1.28}$$

Note that the power law index range $0 < n < 1$ describes the shear thinning or pseudoplastic fluids and $n > 1$ describes the shear thickening or dilatant fluids in Carreau fluid model.

1.7 Solution Methodologies

To attain the elucidation of differential equations has been a substance of greatest thought-fulness among researchers because numerous real world problems are controlled by differential equations. It has fluctuate problematic to attain the exact elucidations of nonlinear difficulties. Aimed at this trouble different researchers espoused numerous approaches for solutions of nonlinear differential equations. The crucial intention of this thesis is to elucidate the considered governing problems with the support of bvp4c, a Matlab's boundary value solver and the homotopy analysis method (HAM).

1.7.1 Numerical Procedure (bvp4c)

For the elucidation of two-point boundary value problems the Matlab function bvp4c [108] has been utilized. A finite difference collocation scheme has been worked behind this development and make use of 3-stage Labatto IIIa formula. For instance, the BVPs are more problematical when compared to IVPs. In this concerns numerous solver procedures fail for the solutions of unknown parameters. The bvp4c is an effectual method to solve BVPs which is forth order accurate. To disclose the behavior of preferred solution initial guesses are requisite which satisfying the suggested boundary conditions.

1.7.2 Homotopy Analysis Method (HAM)

In 1992, Liao [109] was the first who wished-for the homotopy analysis method (HAM) in attention to elucidate the highly nonlinear differential equations. For both strong/week nonlinear systems this approach is effective. Homotopic method is an uninterrupted deformation or deviation of a function or expression. As allied to other techniques, this method has numerous efficacies, i.e.

1. The homotopic tactic is autonomous of small/great parameters.

2. Assure the convergence of established equations easily.

3. For base function and linear operator, HAM provides remarkable independence.

For numerous non-linear complications this methodology works efficiently for the establishment of series solutions $[110 - 114]$.

Consider a non-linear differential equation

$$\mathcal{N}\left[u\left(\eta\right)\right] = 0. \tag{1.29}$$

Here $\mathcal{N}$ signifies the non-linear operator, u the dependent function which is unknown and η the dependent variable. According to $[109]$ the homotopic equation is

$$(1 - q)\,\mathcal{L}\left[\hat{u}(\eta; q) - u_0(\eta)\right] = q\hbar\mathcal{N}\left[\hat{u}(\eta; q)\right], \tag{1.30}$$

here $(u_0(\eta), \mathcal{L})$ signify the initial guess and auxiliary linear operator, respectively, q $(0 \leq q \leq 1)$ the embedding parameter and $\hbar \neq 0$, the auxiliary parameter.

Moreover, when $q = 0$ and $q = 1$, then the aforestated equation is acknowledged as deformation expression of zeroth order and final solution, respectively.

$$\hat{u}(\eta; 0) - u_0(\eta) = 0, \quad \text{and} \quad \hat{u}(\eta; 1) - u(\eta) = 0. \tag{1.31}$$

The solution $\hat{u}(\eta; q)$ starts from initial guess $(u_0(\eta))$ and goes to the ending solution $(u(\eta))$ with the conversion of q from 0 to 1. For the Taylor series correlated to q, we have

$$\hat{u}(\eta; q) = u_0(\eta) + \sum_{\check{n}=1}^{\infty} u_{\check{n}}(\eta)q^{\check{n}}, \quad u_{\check{n}}(\eta) = \frac{1}{\check{n}!}\frac{\partial^{\check{n}}\hat{u}(\eta; q)}{\partial q^{\check{n}}}\bigg|_{q=0}. \tag{1.32}$$

The equation of $\check{n}$th order is

$$\mathcal{L}\left[u_{\check{n}}(\eta) - u_{\check{n}-1}(\eta)\chi_{\check{n}}\right] = \hbar\mathcal{R}_{\check{n}}\left(u_{\check{n}-1}\right), \tag{1.33}$$

with

$$\mathcal{R}_{\check{n}}\left(u_{\check{n}-1}\right) = \frac{1}{(\check{n}-1)!}\frac{\partial^{\check{n}-1}\hat{u}(\eta; q)}{\partial q^{\check{n}-1}}\bigg|_{q=0}, \tag{1.34}$$

$$\chi_{\check{n}} = \begin{cases} 0, & \check{n} \leq 1, \\ 1, & \check{n} > 1. \end{cases} \tag{1.35}$$

23

By executing a suitable software like MATHEMATICA/MAPLE the solution of equations can be attained. The series will converge at $q = 1$ if appropriate initial approximation, auxiliary variable and auxiliary linear operator are designated properly, thus,

$$\hat{u}(x) = u_0(\eta) + \sum_{\check{n}=1}^{\infty} u_{\check{n}}(\eta). \tag{1.36}$$

1.8 Research Outlines

The notable anxiety of this thesis is to cover the gap in the obtainable prose by giving valuable exertion on the flow, heat and mass transport of three-dimensional Carreau fluid flow influenced by a bidirectional stretching surface. To be sure, formerly there had been no obtainable works in respect of the $3D$ flows of the Carreau rheological model. The most essential contributions are that a mathematical modelling is established and numerical and analytical studies have been worked out. Twelve chapters are reported in this thesis which covers numerous characteristics of Carreau fluid for time independent/dependent flows. It is hoped that this work can help to discover more flow, heat and mass transfer characteristics of the Carreau fluid model. The thesis is organized as follows:

Chapter 1 is a preliminary chapter, which accomplishes the incentive, literature analysis and structure of the thesis.

Chapter 2 confers a new mathematical forming for three-dimensional flow of Carreau fluid due to stretching of surface. Utilizing the standard boundary layer approximations the governing equations of momentum are established. Additionally, numerically (bvp4c) and analytically (HAM) are worked out for the solutions of the equations. A brief discussion of solution methodologies is also provided. The exertion in this chapter is published in *''Results in Physics, 7 (2017) 2692-2704''*.

Chapter 3 is an extension of chapter 2 which scrutinizes the heat and mass transport properties via convective phenomenon in Carreau fluid flow. The Boungiono's model has been utilized which incorporate the stimulus of Brownian and thermophoresis nanoparticles. Moreover, heat sink/source and non linear radiative heat flux are reported. The results are worked out via bvp4c and HAM. For both shear thinning/thickening liquids several tables are structured and graphs are portrayed. The results of this chapter are published in *''The European*

Physical Journal Plus, (2017), doi: 10.1140/epjp/i2017-11803-3".

Chapter 4 visualizes the outcomes of nanoparticles mass flux theory in 3D radiative flow of Carreau nanofluid. The behavior of MHD is also scrutinized. The bvp4c tactic has been executed for the solution of ODEs. The substances of this chapter have been published in *"International Journal of Hydrogen Energy, 42 (2017) 22054-22065"*.

Chapter 5 pictures a numerical considerations of thermal-solutal stratifications and convective conditions in 3D Carreau nanofluid flow. Additionally, the aspect of mixed convection, magnetic field, thermal radiation, heat sink/source are reported. The altered ODEs are tackled via bvp4c approach. The present analysis has been printed in *"Journal of the Brazilian Society of Mechanical Sciences and Engineering, (2018), doi: 10.1007/s40430-018-1429-5"*.

Chapter 6 reports the aspects of 3D Carreau nanofluid for time-dependent flow. The nanoparticles conditions with the properties of variable conductivity and heat sink/source are studied. Practically, nanoparticles condition is more significant because nanoparticles amend the situation accordingly on the boundaries. Suitable conversions alter the PDEs into ODEs and then tackled numerically via bvp4c. The framework of this study has been published in *"Results in Physics, 7 (2017) 3315-3324"*.

Chapter 7 explores the aspects of Arrhenius activation energy and nonlinear mixed convection in 3D unsteady Carreu nanofluid flow. Moreover, thermal radiation, magnetic properties, chemical reaction and convective phenomenon are integrated. Apposite alterations are stimulated to attain the ODEs structure and interpreted via bvp4c scheme. The endorsement of the numerical outcomes is confirmed by associating with HAM technique and former limiting studies. The work stimulated in this chapter has been published in *"Journal of Physics and Chemistry of Solids, 125 (2019) 141-152"*.

Chapter 8 reports the impact of Cattaeno-Christove heat flux theory and homogeneous-heterogeneous reactions on Carreau fluid. The bvp4c approach has been executed to solve the ODEs after appropriate conversions. The graphical verification between bvp4c and HAM as well as the tabular confirmation of these two methods as well as with former works has been established. The present exertion has been published in *''Pramana Journal of Physics, (2018), doi:10.1007/s12043-018-1579-0"*.

Chapter 9 scrutinizes the behavior of Cattaeno-Christov double diffusion on 3D flow of

Carreau fluid. The variable conductivity is also enumerated. The conversions of PDEs into ODEs via apposite alteration are made and then elucidated numerically bvp4c. HAM and bvp4c comparison with earlier exertion is presented. The breakdown reported here has been published in *''Journal of the Brazilian Society of Mechanical Sciences and Engineering, (2018), doi: 10.1007/s40430-018-1498-5''*.

Chapter 10 examines the properties of homogeneous-heterogeneous reactions for time-dependent 3D flow of Carreau fluid. The characteristics of non-linear thermal radiation, magnetic impact and the heat sink/source with convective condition are integrated. The modeled problem is numerically solved through bvp4c. To visualize the properties of influential consideration graphs are depicted and tables are structured. Additionally, HAM and bvp4c assessments are provided to authenticate the present outcomes as well as with previous effort. The substances of this effort have been published in *''Journal of the Brazilian Society of Mechanical Sciences and Engineering, (2018), doi:10.1007/s40430-018-0964-4''*.

Chapter 11 summarizes the exertion executed in this thesis. Moreover, the recommendations are specified for extending this exertion for possible forthcoming research.

Chapter 2

Mathematical Modeling for Three-Dimensional Carreau Fluid Flow with Nonlinear Radiative Heat Flux

The forthright anxiety of this chapter is to establish a new mathematical formulation for three-dimensional Carreau fluid flow. The flow is incompressible and influenced by a bidirectional stretched surface. Additionally, we scrutinized the heat transport properties of the flow field. The Carreau liquid model is the generalization of linear materials which reveal the aspects of shear thinning ($n < 1$) and shear thickening ($n > 1$) liquids. The heat transfer phenomenon is inspected by utilizing the non-linear thermal radiation and convective surface boundary condition. The boundary layer equations of 3D Carreau fluid are established by means of usual boundary layer approximations. The governing set of partial differential equations (PDEs) is rendered into coupled non-linear ordinary differential equations (ODEs) via appropriate transformations. Numerical solutions are computed for the resulting non-linear ODEs by employing an effective numerical scheme namely bvp4c function in Matlab. Features of numerous sundry thermophysical parameters on the liquid velocity, temperature, skin friction and Nusselt number are explored and discussed in detail. The present results reveal that the liquid velocity declines

for shear thinning liquid ($n < 1$) for the larger values of ratio of stretching rates parameter (α) and for shear thickening liquid ($n > 1$) conflicting behavior is detected. It is also remarked that thermal radiation parameter (R_d) is an augmenting function of temperature distribution on both situations. To comprehend the legitimacy of numerical results a comparison between bvp4c results with the analytical results obtained by the homotopy analysis method (HAM) is also made in this study and alleged an admirable agreement. Furthermore, authentication of numerical outcomes is achieved via benchmarking with previously reported limiting cases and we generally found a splendid correlation with these results.

2.1 Development of Physical Model

We considered generalized Newtonian liquid that obeys the rheological features of Carreau fluid model.

2.1.1 Governing Equations

The constitutive equations for ($3D$) steady incompressible flow of Carreau fluid in vectorial form can be written as follows:

$$\rho_f(\mathbf{V}.\boldsymbol{\nabla}) = \boldsymbol{\nabla}.\boldsymbol{\tau}^*, \tag{2.1}$$

For $3D$ steady flow, we seeks the velocity and Cauchy stress tensor given by Eq. (1.28) (cf. Chapter 1) of the form

$$\mathbf{V} = [u(x,y,z), v(x,y,z), w(x,y,z)], \quad \boldsymbol{\tau}^* = \boldsymbol{\tau}^*(x,y,z). \tag{2.2}$$

Now substituting Eq. (2.2) in Eq. (1.27), we have the following expression

$$\dot{\gamma} = \left[\begin{array}{c} 2\left(\frac{\partial u}{\partial x}\right)^2 + 2\left(\frac{\partial v}{\partial y}\right)^2 + 2\left(\frac{\partial w}{\partial z}\right)^2 \\ + \left(\frac{\partial u}{\partial y} + \frac{\partial v}{\partial x}\right)^2 + \left(\frac{\partial u}{\partial z} + \frac{\partial w}{\partial x}\right)^2 + \left(\frac{\partial w}{\partial y} + \frac{\partial v}{\partial z}\right)^2 \end{array} \right]^{\frac{1}{2}}. \tag{2.3}$$

Utilizing Eqs. (2.2) and (2.3) in Eq. (2.1) we have

$$\rho_f\left(u\frac{\partial u}{\partial x} + v\frac{\partial u}{\partial y} + w\frac{\partial u}{\partial z}\right) = -\frac{\partial p}{\partial x} + \frac{\partial \boldsymbol{\tau}^*_{xx}}{\partial x} + \frac{\partial \boldsymbol{\tau}^*_{xy}}{\partial y} + \frac{\partial \boldsymbol{\tau}^*_{xz}}{\partial z}, \tag{2.4}$$

28

$$\rho_f \left(u\frac{\partial v}{\partial x} + v\frac{\partial v}{\partial y} + w\frac{\partial v}{\partial z} \right) = -\frac{\partial p}{\partial y} + \frac{\partial \boldsymbol{\tau}^*_{yx}}{\partial x} + \frac{\partial \boldsymbol{\tau}^*_{yy}}{\partial y} + \frac{\partial \boldsymbol{\tau}^*_{yz}}{\partial z}, \tag{2.5}$$

$$\rho_f \left(u\frac{\partial w}{\partial x} + v\frac{\partial w}{\partial y} + w\frac{\partial w}{\partial z} \right) = -\frac{\partial p}{\partial z} + \frac{\partial \boldsymbol{\tau}^*_{zx}}{\partial x} + \frac{\partial \boldsymbol{\tau}^*_{zy}}{\partial y} + \frac{\partial \boldsymbol{\tau}^*_{zz}}{\partial z}, \tag{2.6}$$

where the stress components are defined to be

$$\boldsymbol{\tau}^*_{xx} = \mu_0[1 + (\Gamma\dot{\gamma})^2]^{\frac{n-1}{2}} \left(2\frac{\partial u}{\partial x} \right), \tag{2.7}$$

$$\boldsymbol{\tau}^*_{yy} = \mu_0[1 + (\Gamma\dot{\gamma})^2]^{\frac{n-1}{2}} \left(2\frac{\partial v}{\partial y} \right), \tag{2.8}$$

$$\boldsymbol{\tau}^*_{zz} = \mu_0[1 + (\Gamma\dot{\gamma})^2]^{\frac{n-1}{2}} \left(2\frac{\partial w}{\partial z} \right), \tag{2.9}$$

$$\boldsymbol{\tau}^*_{yx} = \boldsymbol{\tau}^*_{xy} = \mu_0[1 + (\Gamma\dot{\gamma})^2]^{\frac{n-1}{2}} \left(\frac{\partial u}{\partial y} + \frac{\partial v}{\partial x} \right), \tag{2.10}$$

$$\boldsymbol{\tau}^*_{zy} = \boldsymbol{\tau}^*_{yz} = \mu_0[1 + (\Gamma\dot{\gamma})^2]^{\frac{n-1}{2}} \left(\frac{\partial v}{\partial z} + \frac{\partial w}{\partial y} \right). \tag{2.11}$$

$$\boldsymbol{\tau}^*_{zx} = \boldsymbol{\tau}^*_{xz} = \mu_0[1 + (\Gamma\dot{\gamma})^2]^{\frac{n-1}{2}} \left(\frac{\partial u}{\partial z} + \frac{\partial w}{\partial x} \right), \tag{2.12}$$

Invoking overhead equations into Eqs $(2.4) - (2.6)$, a straightforward calculation yields the following governing equations

$$\rho_f \left(u\frac{\partial u}{\partial x} + v\frac{\partial u}{\partial y} + w\frac{\partial u}{\partial z} \right) = -\frac{\partial p}{\partial x}$$

$$+2\mu_0\frac{\partial}{\partial x}\left[\left(\frac{\partial u}{\partial x}\right) \left(1 + \Gamma^2 \left[\begin{array}{c} 2\left(\frac{\partial u}{\partial x}\right)^2 + 2\left(\frac{\partial v}{\partial y}\right)^2 + 2\left(\frac{\partial w}{\partial z}\right)^2 \\ + \left(\frac{\partial u}{\partial y} + \frac{\partial v}{\partial x}\right)^2 + \left(\frac{\partial u}{\partial z} + \frac{\partial w}{\partial x}\right)^2 + \left(\frac{\partial w}{\partial y} + \frac{\partial v}{\partial z}\right)^2 \end{array} \right]^{\frac{1}{2}} \right) \right]$$

$$+\mu_0\frac{\partial}{\partial y}\left[\left(\frac{\partial v}{\partial x} + \frac{\partial u}{\partial y}\right) \left(1 + \Gamma^2 \left[\begin{array}{c} 2\left(\frac{\partial u}{\partial x}\right)^2 + 2\left(\frac{\partial v}{\partial y}\right)^2 + 2\left(\frac{\partial w}{\partial z}\right)^2 \\ + \left(\frac{\partial u}{\partial y} + \frac{\partial v}{\partial x}\right)^2 + \left(\frac{\partial u}{\partial z} + \frac{\partial w}{\partial x}\right)^2 + \left(\frac{\partial w}{\partial y} + \frac{\partial v}{\partial z}\right)^2 \end{array} \right]^{\frac{1}{2}} \right) \right]$$

$$+\mu_0\frac{\partial}{\partial z}\left[\left(\frac{\partial w}{\partial x} + \frac{\partial u}{\partial z}\right) \left(1 + \Gamma^2 \left[\begin{array}{c} 2\left(\frac{\partial u}{\partial x}\right)^2 + 2\left(\frac{\partial v}{\partial y}\right)^2 + 2\left(\frac{\partial w}{\partial z}\right)^2 \\ + \left(\frac{\partial u}{\partial y} + \frac{\partial v}{\partial x}\right)^2 + \left(\frac{\partial u}{\partial z} + \frac{\partial w}{\partial x}\right)^2 + \left(\frac{\partial w}{\partial y} + \frac{\partial v}{\partial z}\right)^2 \end{array} \right]^{\frac{1}{2}} \right) \right], \tag{2.13}$$

$$\rho_f\left(u\frac{\partial v}{\partial x}+v\frac{\partial v}{\partial y}+w\frac{\partial v}{\partial z}\right)=-\frac{\partial p}{\partial y}$$

$$+\mu_0\frac{\partial}{\partial x}\left[\left(\frac{\partial v}{\partial x}+\frac{\partial u}{\partial y}\right)\left(1+\Gamma^2\left[\begin{array}{c}2\left(\frac{\partial u}{\partial x}\right)^2+2\left(\frac{\partial v}{\partial y}\right)^2+2\left(\frac{\partial w}{\partial z}\right)^2\\+\left(\frac{\partial u}{\partial y}+\frac{\partial v}{\partial x}\right)^2+\left(\frac{\partial u}{\partial z}+\frac{\partial w}{\partial x}\right)^2+\left(\frac{\partial w}{\partial y}+\frac{\partial v}{\partial z}\right)^2\end{array}\right]^{\frac{1}{2}}\right)\right]$$

$$+\mu_0\frac{\partial}{\partial y}\left[\left(2\frac{\partial v}{\partial y}\right)\left(1+\Gamma^2\left[\begin{array}{c}2\left(\frac{\partial u}{\partial x}\right)^2+2\left(\frac{\partial v}{\partial y}\right)^2+2\left(\frac{\partial w}{\partial z}\right)^2\\+\left(\frac{\partial u}{\partial y}+\frac{\partial v}{\partial x}\right)^2+\left(\frac{\partial u}{\partial z}+\frac{\partial w}{\partial x}\right)^2+\left(\frac{\partial w}{\partial y}+\frac{\partial v}{\partial z}\right)^2\end{array}\right]^{\frac{1}{2}}\right)\right]$$

$$+\mu_0\frac{\partial}{\partial z}\left[\left(\frac{\partial w}{\partial y}+\frac{\partial v}{\partial z}\right)\left(1+\Gamma^2\left[\begin{array}{c}2\left(\frac{\partial u}{\partial x}\right)^2+2\left(\frac{\partial v}{\partial y}\right)^2+2\left(\frac{\partial w}{\partial z}\right)^2\\+\left(\frac{\partial u}{\partial y}+\frac{\partial v}{\partial x}\right)^2+\left(\frac{\partial u}{\partial z}+\frac{\partial w}{\partial x}\right)^2+\left(\frac{\partial w}{\partial y}+\frac{\partial v}{\partial z}\right)^2\end{array}\right]^{\frac{1}{2}}\right)\right],\ (2.14)$$

$$\rho_f\left(u\frac{\partial w}{\partial x}+v\frac{\partial w}{\partial y}+w\frac{\partial w}{\partial z}\right)=-\frac{\partial p}{\partial z}$$

$$+\mu_0\frac{\partial}{\partial x}\left[\left(\frac{\partial w}{\partial x}+\frac{\partial u}{\partial z}\right)\left(1+\Gamma^2\left[\begin{array}{c}2\left(\frac{\partial u}{\partial x}\right)^2+2\left(\frac{\partial v}{\partial y}\right)^2+2\left(\frac{\partial w}{\partial z}\right)^2\\+\left(\frac{\partial u}{\partial y}+\frac{\partial v}{\partial x}\right)^2+\left(\frac{\partial u}{\partial z}+\frac{\partial w}{\partial x}\right)^2+\left(\frac{\partial w}{\partial y}+\frac{\partial v}{\partial z}\right)^2\end{array}\right]^{\frac{1}{2}}\right)\right]$$

$$+\mu_0\frac{\partial}{\partial y}\left[\left(\frac{\partial w}{\partial y}+\frac{\partial v}{\partial z}\right)\left(1+\Gamma^2\left[\begin{array}{c}2\left(\frac{\partial u}{\partial x}\right)^2+2\left(\frac{\partial v}{\partial y}\right)^2+2\left(\frac{\partial w}{\partial z}\right)^2\\+\left(\frac{\partial u}{\partial y}+\frac{\partial v}{\partial x}\right)^2+\left(\frac{\partial u}{\partial z}+\frac{\partial w}{\partial x}\right)^2+\left(\frac{\partial w}{\partial y}+\frac{\partial v}{\partial z}\right)^2\end{array}\right]^{\frac{1}{2}}\right)\right]$$

$$+\mu_0\frac{\partial}{\partial z}\left[\left(2\frac{\partial w}{\partial z}\right)\left(1+\Gamma^2\left[\begin{array}{c}2\left(\frac{\partial u}{\partial x}\right)^2+2\left(\frac{\partial v}{\partial y}\right)^2+2\left(\frac{\partial w}{\partial z}\right)^2\\+\left(\frac{\partial u}{\partial y}+\frac{\partial v}{\partial x}\right)^2+\left(\frac{\partial u}{\partial z}+\frac{\partial w}{\partial x}\right)^2+\left(\frac{\partial w}{\partial y}+\frac{\partial v}{\partial z}\right)^2\end{array}\right]^{\frac{1}{2}}\right)\right].\ (2.15)$$

For three-dimensional flow the standard boundary layer estimates *i.e.* x, y, u, v and p are of order 1, whereas the order of z, w and Γ are δ. Consequently, we obtain the following boundary layer equations for the steady 3D flow of Carreau fluid

$$u\frac{\partial u}{\partial x}+v\frac{\partial u}{\partial y}+w\frac{\partial u}{\partial z}=-\frac{1}{\rho_f}\frac{\partial p}{\partial x}+\nu\frac{\partial^2 u}{\partial z^2}\left[1+\Gamma^2\left(\frac{\partial u}{\partial z}\right)^2\right]^{\frac{n-1}{2}}$$

$$+\nu\left(\frac{\partial u}{\partial z}\right)\frac{\partial}{\partial z}\left[1+\Gamma^2\left(\frac{\partial u}{\partial z}\right)^2\right]^{\frac{n-1}{2}},\qquad (2.16)$$

$$u\frac{\partial v}{\partial x} + v\frac{\partial v}{\partial y} + w\frac{\partial v}{\partial z} = -\frac{1}{\rho_f}\frac{\partial p}{\partial y} + \nu\frac{\partial^2 v}{\partial z^2}\left[1 + \Gamma^2\left(\frac{\partial v}{\partial z}\right)^2\right]^{\frac{n-1}{2}}$$

$$+\nu\left(\frac{\partial v}{\partial z}\right)\frac{\partial}{\partial z}\left[1 + \Gamma^2\left(\frac{\partial v}{\partial z}\right)^2\right]^{\frac{n-1}{2}}, \tag{2.17}$$

$$0 = -\frac{1}{\rho_f}\frac{\partial p}{\partial z}, \tag{2.18}$$

where $\nu\left(=\frac{\mu_0}{\rho_f}\right)$ is the kinematic viscosity.

2.2   Description of the Problem

Let report the steady $3D$ flow of a Carreau fluid persuaded by a bidirectional stretched surface. The sheet is stretched with linear velocities $u = ax$ and $v = by$, where a and b are positive constants relating to stretching speed. The $x-$ and $y-$axes are concentrated along the continuous stretching sheet, z the coordinate restrained perpendicular to it and the flow existence restricted in the domain $z > 0$ as depicted in figure **2.1**. Additionally, the hot liquid below the sheet with temperature T_f consumed to reform the temperature of the sheet by convective heat transfer approach, which brings a heat conversion coefficient h_f. Also consequence of viscous dissipation is deserted.

Execution of the overhead assumptions in attention the governing equations for Carreau fluid are
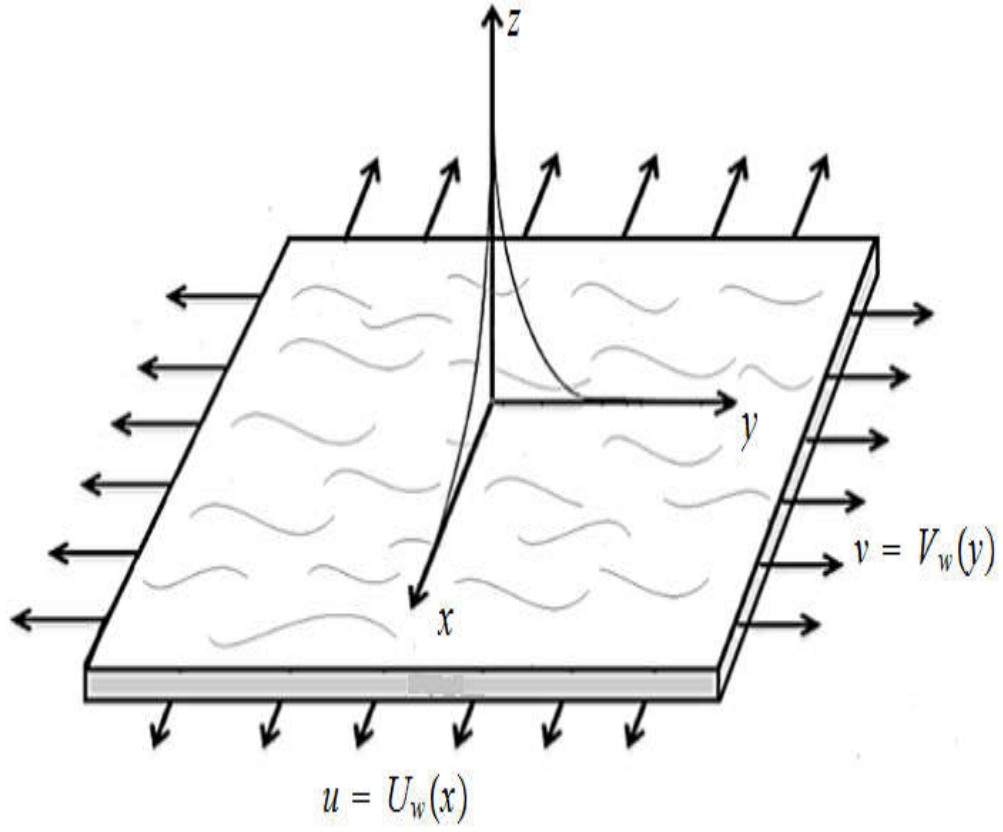
Figure 2.1: Flow configuration and coordinates system.

$$\frac{\partial u}{\partial x} + \frac{\partial v}{\partial y} + \frac{\partial w}{\partial z} = 0, \tag{2.19}$$

$$u\frac{\partial u}{\partial x} + v\frac{\partial u}{\partial y} + w\frac{\partial u}{\partial z} = \nu\frac{\partial^2 u}{\partial z^2}\left[1 + \Gamma^2\left(\frac{\partial u}{\partial z}\right)^2\right]^{\frac{n-1}{2}}$$
$$+\nu(n-1)\Gamma^2\frac{\partial u}{\partial z}\left[1 + \Gamma^2\left(\frac{\partial u}{\partial z}\right)^2\right]^{\frac{n-3}{2}}, \tag{2.20}$$

$$u\frac{\partial v}{\partial x} + v\frac{\partial v}{\partial y} + w\frac{\partial v}{\partial z} = \nu\frac{\partial^2 v}{\partial z^2}\left[1 + \Gamma^2\left(\frac{\partial v}{\partial z}\right)^2\right]^{\frac{n-1}{2}}$$

$$+\nu(n-1)\Gamma^2\frac{\partial v}{\partial z}\left[1 + \Gamma^2\left(\frac{\partial v}{\partial z}\right)^2\right]^{\frac{n-3}{2}}, \tag{2.21}$$

$$u\frac{\partial T}{\partial x} + v\frac{\partial T}{\partial y} + w\frac{\partial T}{\partial z} = \alpha_1\frac{\partial^2 T}{\partial z^2} - \frac{1}{(\rho c)_f}\frac{\partial q_r}{\partial z}. \tag{2.22}$$

in which α_1 denotes the thermal diffusivity.

The resultant boundary conditions are

$$u = U_w(x) = ax, \quad v = V_w(y) = by, \quad w = 0, \quad -k\frac{\partial T}{\partial z} = h_f[T_f - T] \quad \text{at} \quad z = 0, \tag{2.23}$$

$$u \to 0, \quad v \to 0, \quad T \to T_\infty \quad \text{as} \quad z \to \infty. \tag{2.24}$$

On the behalf of non-linear radiation, we employ the Rosseland approximation, the radiative heat flux q_r is simplified as

$$q_r = -\frac{4\sigma^*}{3k^*}\frac{\partial T^4}{\partial z} = -\frac{16\sigma^* T^3}{3k^*}\frac{\partial^2 T}{\partial z^2}, \tag{2.25}$$

in which (σ^*, k^*) are the Stefan Boltzmann constant and mean absorption coefficient.

Using the above expression in Eq. (2.22) we have the following resultant energy equation

$$u\frac{\partial T}{\partial x} + v\frac{\partial T}{\partial y} + w\frac{\partial T}{\partial z} = \alpha_1\frac{\partial^2 T}{\partial z^2} + \frac{16\sigma^*}{3k^*(\rho c_f)}\frac{\partial}{\partial z}\left(T^3\frac{\partial^2 T}{\partial z^2}\right). \tag{2.26}$$

2.2.1 Appropriate Conversions

Let we define

$$u = axf'(\eta), \quad v = ayg'(\eta), \quad w = -\sqrt{a\nu}[f(\eta) + g(\eta)],$$

$$\theta(\eta) = \frac{T - T_\infty}{T_f - T_\infty}, \quad \eta = z\sqrt{\frac{a}{\nu}}. \tag{2.27}$$

By employing the above conversions, the incompressibility condition (2.19) is substantiated identically and Eqs. (2.20), (2.21) and (2.26) with boundary conditions (2.23) and (2.24) are

condensed into the subsequent form

$$f'''[1 + We_1^2 f''^2]^{\frac{n-3}{2}}[1 + nWe_1^2 f''^2] - f'^2 + f''(f + g) = 0, \tag{2.28}$$

$$g'''[1 + We_2^2 g''^2]^{\frac{n-3}{2}}[1 + nWe_2^2 g''^2] - g'^2 + g''(f + g) = 0, \tag{2.29}$$

$$\frac{d}{d\eta}[\{1 + R_d(1 + (\theta_f - 1)\theta)^3\}\theta'] + \Pr(f + g)\theta' = 0, \tag{2.30}$$

$$f(0) = 0, \quad g(0) = 0, \quad f'(0) = 1, \quad g'(0) = \alpha, \quad \theta'(0) = -\gamma_1[1 - \theta(0)], \tag{2.31}$$

$$f' \to 0, \quad g' \to 0, \quad \theta \to 0 \quad \text{as} \quad \eta \to \infty. \tag{2.32}$$

In the above equations, $We_1 \left(= \sqrt{\frac{\Gamma^2 a^3 x^2}{\nu}}\right)$ and $We_2 \left(= \sqrt{\frac{\Gamma^2 a^3 y^2}{\nu}}\right)$ are the local Weissenberg numbers, $R_d \left(= \frac{16\sigma^* T_\infty^3}{3k^* k}\right)$ the radiation parameter, $\theta_f \left(= \frac{T_f}{T_\infty}\right)$ the ratio of liquid temperature to the ambient temperature, $\Pr \left(= \frac{\nu}{\alpha_1}\right)$ the Prandtl number, $\alpha \left(= \frac{b}{a}\right)$ the ratio of stretching rates parameter and $\gamma_1 = \left(\frac{h_f}{k}\sqrt{\frac{\nu}{a}}\right)$ the Biot number.

It is exposed that for $\alpha = 0$ reduces the equation of momentum into two dimensional case ($g = 0$), i.e.,

$$f'''[1 + We_1^2 f''^2]^{\frac{n-3}{2}}[1 + nWe_1^2 f''^2] - f'^2 + f''f = 0. \tag{2.33}$$

Furthermore, it is noted that for $n = 1$ or $We_1 = 0$ the above equation reduces to Newtonian fluid.

2.3   Engineering and Industrial Quantities of Interest

The essential physical quantities of foremost interests are (C_{fx}, C_{fy}) the local skin friction coefficients and (Nu_x) the local Nusselt number.

2.3.1 The Skin Friction Coefficients

As C_{fx} and C_{fy} are influential boundary layer features which are the dimensionless shear rate at the wall i.e. $(z = 0)$ along the $x-$ and $y-$ directions, respectively. Thus

$$C_{fx} = \frac{\tau_{xz}}{\frac{1}{2}\rho U_w^2} \quad \text{and} \quad C_{fy} = \frac{\tau_{yz}}{\frac{1}{2}\rho U_w^2}. \tag{2.34}$$

The dimensionless form of the above expressions can be written as

$$\tfrac{1}{2}C_{fx}\,\mathrm{Re}_x^{\frac{1}{2}} = f''(0)[1 + We_1^2 f''^2]^{\frac{n-1}{2}}, \tag{2.35}$$

$$\tfrac{1}{2}C_{fy}\left(\tfrac{U_w}{V_w}\right)\mathrm{Re}_x^{\frac{1}{2}} = g''(0)[1 + We_2^2 g''^2]^{\frac{n-1}{2}}. \tag{2.36}$$

2.3.2 The Local Nusselt Number

Since Nu_x gives the rate of heat transfer at the wall and is defined as

$$Nu_x = -\frac{x}{(T_f - T_\infty)}\left(\frac{\partial T}{\partial z}\right)\bigg|_{z=0} + \frac{x q_r}{k\,(T_f - T_\infty)}. \tag{2.37}$$

The dimensionless variable, we have

$$\mathrm{Re}_x^{-\frac{1}{2}}Nu_x = -[1 + R_d\{1 + (\theta_f - 1)\theta(0)\}^3]\theta'\,(0)\,, \tag{2.38}$$

in which $\mathrm{Re}_x = \frac{U_w(x)x}{\nu}$ is the local Reynolds number.

2.4 Solution Methodologies

2.4.1 Numerical Scheme

The computation of numerical scheme is established for nonlinear ODEs $(2.28) - (2.30)$ with boundary conditions (2.31) and (2.32) via bvp4c procedure. To achieve this objective, we modify Eqs. $(2.28) - (2.32)$ into first order differential structures as follows:

$$f = y_1, \quad f' = y_2, \quad f'' = y_3, \quad f''' = yy_1, \tag{2.39}$$

$$g = y_4, \quad g' = y_5, \quad g'' = y_6, \quad g''' = yy_2, \tag{2.40}$$

$$\theta = y_7, \quad \theta' = y_8, \quad \theta'' = yy_3, \tag{2.41}$$

$$yy_1 = \frac{-(y_1+y_4)y_3+y_2^2}{A_1}, \quad A_1 = \left(1 + nWe_1^2 y_3^2\right) * \left(1 + We_1^2 y_3^2\right)^{\frac{n-3}{2}}, \tag{2.42}$$

$$yy_2 = \frac{-(y_1+y_4)y_6+y_5^2}{A_2}, \quad A_2 = \left(1 + nWe_2^2 y_6^2\right) * \left(1 + We_2^2 y_6^2\right)^{\frac{n-3}{2}}, \tag{2.43}$$

$$A_3 = \left(1 + R_d(1 + (\theta_f - 1)y_7)^3\right), \tag{2.44}$$

$$y_1(0) = 0, \quad y_2(0) = 1, \quad y_2(\infty) = 0, \tag{2.45}$$

$$y_4(0) = 0, \quad y_5(0) = \alpha, \quad y_5(\infty) = 0, \tag{2.46}$$

$$y_8(0) + \gamma_1(1 - y_7(0)) = 0, \quad y_7(\infty) = 0. \tag{2.47}$$

2.4.2 Homotopy Aanalysis Method (HAM)

The ODEs $(2.27) - (2.29)$ with boundary conditions (2.30) are solved analytically, by utilizing the homotopic algorithm (HAM). The $f_0(\eta)$, $g_0(\eta)$ and $\theta_0(\eta)$ are initial guesses and $\mathcal{L}_f$, $\mathcal{L}_g$, and $\mathcal{L}_\theta$ are the auxiliary linear operators which are given below:

$$f_0(\eta) = 1 - e^{-\eta}, \qquad g_0(\eta) = \alpha\left[1 - e^{-\eta}\right], \qquad \theta_0(\eta) = \frac{\gamma_1}{1 + \gamma_1} e^{-\eta}, \tag{2.48}$$

$$\mathcal{L}_f[f(\eta)] = \left(\frac{d^3}{d\eta^3} - \frac{d}{d\eta}\right)f, \quad \mathcal{L}_g[g(\eta)] = \left(\frac{d^3}{d\eta^3} - \frac{d}{d\eta}\right)g, \quad \mathcal{L}_\theta[\theta(\eta)] = \left(\frac{d^2}{d\eta^2} - 1\right)\theta. \tag{2.49}$$

The overhead operators satisfying the following properties

$$\mathcal{L}_f\left[C_1^* + C_2^* e^{\eta} + C_3^* \exp e^{-\eta}\right] = 0, \tag{2.50}$$

$$\mathcal{L}_g\left[C_4^* + C_5^* e^{\eta} + C_6^* \exp e^{-\eta}\right] = 0, \tag{2.51}$$

$$\mathcal{L}_\theta\left[C_7^* e^{\eta} + C_8^* \exp e^{-\eta}\right] = 0, \tag{2.52}$$

here C_j^* $(j = 1 - 8)$ are the constant values.

36

The deformation problems of zeroth-order

The zeroth order deformation problems are defined as follows:

$$(1-q)\,\mathcal{L}_f\left[\hat{f}\left(\eta,q\right)-f_0\left(\eta\right)\right]-q\hbar_f\mathcal{N}_f\left[\hat{f}\left(\eta,q\right),\hat{g}\left(\eta,q\right),\hat{\theta}\left(\eta,q\right),\hat{\phi}\left(\eta,q\right)\right]=0, \qquad (2.53)$$

$$(1-q)\,\mathcal{L}_g\left[\hat{g}\left(\eta,q\right)-g_0\left(\eta\right)\right]-q\hbar_g\mathcal{N}_g\left[\hat{f}\left(\eta,q\right),\hat{g}\left(\eta,q\right),\hat{\theta}\left(\eta,q\right),\hat{\phi}\left(\eta,q\right)\right]=0, \qquad (2.54)$$

$$(1-q)\,\mathcal{L}_\theta\left[\hat{\theta}\left(\eta,q\right)-\theta_0\left(\eta\right)\right]-q\hbar_\theta\mathcal{N}_\theta\left[\hat{f}\left(\eta,q\right),\hat{g}\left(\eta,q\right),\hat{\theta}\left(\eta,q\right),\hat{\phi}\left(\eta,q\right)\right]=0, \qquad (2.55)$$

$$\hat{f}\left(0,q\right)=0,\qquad \left.\frac{\partial\hat{f}\left(\eta,q\right)}{\partial\eta}\right|_{\eta=0}=1,\qquad \left.\frac{\partial\hat{f}\left(\eta,q\right)}{\partial\eta}\right|_{\eta\to\infty}=0, \qquad (2.56)$$

$$\hat{g}\left(0,q\right)=0,\qquad \left.\frac{\partial\hat{g}\left(\eta,q\right)}{\partial\eta}\right|_{\eta=0}=\alpha,\qquad \left.\frac{\partial\hat{g}\left(\eta,q\right)}{\partial\eta}\right|_{\eta\to\infty}=0, \qquad (2.57)$$

$$\hat{\theta}'(0,q)=-\gamma_1[1-\hat{\theta}(0,q)],\qquad \left.\hat{\theta}\left(\eta,q\right)\right|_{\eta\to\infty}=0. \qquad (2.58)$$

The non-linear operators $\mathcal{N}_f$, $\mathcal{N}_g$, and $\mathcal{N}_\theta$ are

$$\begin{aligned}\mathcal{N}_f\left[\hat{f}\left(\eta;q\right),\hat{g}\left(\eta;q\right),\hat{\theta}\left(\eta;q\right)\right] &= \left[\left(1+We_1^2\frac{\partial^2\hat{f}(\eta,q)}{\partial\eta^2}\right)^{\frac{n-3}{2}}\left(1+nWe_1^2\frac{\partial^2\hat{f}(\eta,q)}{\partial\eta^2}\right)\right]\frac{\partial^3\hat{f}(\eta,q)}{\partial\eta^3}\\ &\quad +\left(\frac{\partial^2\hat{f}(\eta,q)}{\partial\eta^2}\right)\left(\hat{f}+\hat{g}\right)-\left(\frac{\partial\hat{f}(\eta,q)}{\partial\eta}\right)^2,\end{aligned} \qquad (2.59)$$

$$\begin{aligned}\mathcal{N}_g\left[\hat{f}\left(\eta;q\right),\hat{g}\left(\eta;q\right),\hat{\theta}\left(\eta;q\right)\right] &= \left(1+We_2^2\frac{\partial^2\hat{g}(\eta,q)}{\partial\eta^2}\right)^{\frac{n-3}{2}}\left(1+nWe_2^2\frac{\partial^2\hat{g}(\eta,q)}{\partial\eta^2}\right)\frac{\partial^3\hat{g}(\eta,q)}{\partial\eta^3}\\ &\quad -\left(\frac{\partial\hat{g}(\eta,q)}{\partial\eta}\right)^2+\frac{\partial^2\hat{g}(\eta,q)}{\partial\eta^2}\left(\hat{f}+\hat{g}\right),\end{aligned} \qquad (2.60)$$

$$\mathcal{N}_\theta\left[\hat{f}\left(\eta;q\right),\hat{g}\left(\eta;q\right),\hat{\theta}\left(\eta;q\right)\right]=\frac{\partial}{\partial\eta}\left[\{1+R_d\left(1+(\theta_f-1)\theta\right)^3\}\frac{\partial^2\hat{\theta}(\eta,q)}{\partial\eta^2}\right]+\Pr\left(\hat{f}+\hat{g}\right)\frac{\partial\hat{\theta}(\eta,q)}{\partial\eta}, \qquad (2.61)$$

For $q=0$ and $q=1$, we have

$$\hat{f}(\eta;0)=f_0(\eta),\quad \hat{f}(\eta;1)=f(\eta), \qquad (2.62)$$

37

$$\hat{g}(\eta; 0) = g_0(\eta), \quad \hat{g}(\eta; 1) = g(\eta), \tag{2.63}$$

$$\hat{\theta}(\eta; 0) = \theta_0(\eta), \quad \hat{\theta}(\eta; 1) = \theta(\eta), \tag{2.64}$$

Note that $f_0(\eta)$, $g_0(\eta)$ and $\theta_0(\eta)$ approach $f(\eta)$, $g(\eta)$ and $\theta(\eta)$, respectively, when q has variation from 0 to 1. According to Taylor series, we have

$$\hat{f}(\eta, q) = f_0(\eta) + \sum_{\check{n}=1}^{\infty} f_{\check{n}}(\eta) q^{\check{n}}, \quad f_{\check{n}}(\eta) = \frac{1}{\check{n}!} \frac{\partial^{\check{n}} f(\eta, q)}{\partial q^{\check{n}}} \bigg|_{q=0}, \tag{2.65}$$

$$\hat{g}(\eta, q) = g_0(\eta) + \sum_{\check{n}=1}^{\infty} g_{\check{n}}(\eta) q^{\check{n}}, \quad g_{\check{n}}(\eta) = \frac{1}{\check{n}!} \frac{\partial^{\check{n}} g(\eta, q)}{\partial q^{\check{n}}} \bigg|_{q=0}, \tag{2.66}$$

$$\hat{\theta}(\eta, q) = \theta_0(\eta) + \sum_{\check{n}=1}^{\infty} \theta_{\check{n}}(\eta) q^{\check{n}}, \quad \theta_{\check{n}}(\eta) = \frac{1}{\check{n}!} \frac{\partial^{\check{n}} \theta(\eta, q)}{\partial q^{\check{n}}} \bigg|_{q=0}, \tag{2.67}$$

The value of $\hbar_f$, $\hbar_g$ and $\hbar_\theta$ are preferred in such a tactic that the series $(2.64) - (2.66)$ are convergent at $q = 1$ and hence

$$f(\eta) = f_0(\eta) + \sum_{\check{n}=1}^{\infty} f_{\check{n}}(\eta), \tag{2.68}$$

$$g(\eta) = g_0(\eta) + \sum_{\check{n}=1}^{\infty} g_{\check{n}}(\eta), \tag{2.69}$$

$$\theta(\eta) = \theta_0(\eta) + \sum_{\check{n}=1}^{\infty} \theta_{\check{n}}(\eta). \tag{2.70}$$

The deformation problems of $\check{n}^{th}$ order

The deformation problems of $\check{n}^{th}$ order are of the form

$$\mathcal{L}_f [f_{\check{n}}(\eta) - \chi_{\check{n}} f_{\check{n}-1}(\eta)] - \hbar_f \mathcal{R}_{\check{n}}^f(\eta) = 0, \tag{2.71}$$

$$\mathcal{L}_g [g_{\check{n}}(\eta) - \chi_{\check{n}} g_{\check{n}-1}(\eta)] - \hbar_g \mathcal{R}_{\check{n}}^g(\eta) = 0, \tag{2.72}$$

$$\mathcal{L}_\theta [\theta_{\check{n}}(\eta) - \chi_{\check{n}} \theta_{\check{n}-1}(\eta)] - \hbar_\theta \mathcal{R}_{\check{n}}^\theta(\eta) = 0, \tag{2.73}$$

$$f_{\check{n}}(0) = 0, \qquad \left.\frac{\partial f_{\check{n}}(\eta)}{\partial \eta}\right|_{\eta=0} = 0, \qquad \left.\frac{\partial f_{\check{n}}(\eta)}{\partial \eta}\right|_{\eta\to\infty} = 0, \tag{2.74}$$

$$g_{\check{n}}(0) = 0, \qquad \left.\frac{\partial g_{\check{n}}(\eta)}{\partial \eta}\right|_{\eta=0} = 0, \qquad \left.\frac{\partial g_{\check{n}}(\eta)}{\partial \eta}\right|_{\eta\to\infty} = 0, \tag{2.75}$$

$$\theta'_{\check{n}}(0) - \gamma_1\theta_{\check{n}}(0) = \theta_{\check{n}}(\infty) = 0, \tag{2.76}$$

where

$$\chi_{\check{n}} = \begin{cases} 0; & \check{n} \leqslant 1, \\ 1; & \check{n} > 1. \end{cases} \tag{2.77}$$

$$\mathcal{R}^f_{\check{n}}(\eta) = \sum_{\check{i}=0}^{\check{n}-1} f''_{\check{n}-1-\check{i}}(f_{\check{i}} + g_{\check{i}}) - \sum_{\check{i}=0}^{\check{n}-1} f'_{\check{n}-1-\check{i}}f'_{\check{i}} + \varphi_f(\eta), \tag{2.78}$$

$$\mathcal{R}^g_{\check{n}}(\eta) = \sum_{\check{i}=0}^{\check{n}-1} g''_{\check{n}-1-\check{i}}(f_{\check{i}} + g_{\check{i}}) - \sum_{\check{i}=0}^{\check{n}-1} g'_{\check{n}-1-\check{i}}g'_{\check{i}} + \varphi_g(\eta), \tag{2.79}$$

$$\begin{aligned}
\mathcal{R}^\theta_{\check{n}}(\eta) &= (1 + R_d)\theta''_{\check{n}-1}(\eta) + R_d(\theta_f - 1)^3 \sum_{\check{i}=0}^{\check{n}-1} \theta_{\check{n}-1-\check{i}} \sum_{l=0}^{\check{i}} \theta_{\check{i}-l} \sum_{j=0}^{l} \theta_{l-j}\theta''_j \\
&\quad + 3R_d(\theta_f - 1)^2 \sum_{\check{i}=0}^{\check{n}-1} \theta_{\check{n}-1-\check{i}} \sum_{l=0}^{\check{i}} \theta_{\check{i}-l}\theta''_l + 3R_d(\theta_f - 1) \sum_{\check{i}=0}^{\check{n}-1} \theta_{\check{n}-1-\check{i}}\theta''_{\check{i}} \\
&\quad + 3R_d(\theta_f - 1) \sum_{k=0}^{\check{n}-1} \theta'_{\check{n}-1-\check{i}}\theta'_{\check{i}} + 6R_d(\theta_f - 1)^2 \sum_{\check{i}=0}^{\check{n}-1} \theta_{\check{n}-1-\check{i}} \sum_{l=0}^{\check{i}} \theta'_{\check{i}-l}\theta'_l \\
&\quad + 3R_d(\theta_f - 1)^3 \sum_{\check{i}=0}^{\check{n}-1} \theta_{\check{n}-1-\check{i}} \sum_{l=0}^{\check{i}} \theta_{\check{i}-l} \sum_{j=0}^{l} \theta'_{l-j}\theta'_j \\
&\quad + \Pr \sum_{\check{i}=0}^{\check{n}-1} (f_{\check{n}-1-\check{i}} + g_{\check{n}-1-\check{i}}) \theta'_{\check{i}},
\end{aligned} \tag{2.80}$$

where

$$\varphi_f(\eta) = \begin{cases} = f'''_{\check{n}-1}, & n = 1, \\ = f'''_{\check{n}-1} + 3We_1^2 \sum_{\check{i}=0}^{\check{n}-1} f'''_{\check{n}-1-\check{i}} \sum_{l=0}^{\check{i}} f''_{\check{i}-l}\, f''_l, & n = 3, \end{cases} \tag{2.81}$$

$$\varphi_g(\eta) = \begin{cases} = g'''_{\check{n}-1}, & n = 1, \\ = g'''_{\check{n}-1} + 3We_2^2 \sum_{\check{i}=0}^{\check{n}-1} g'''_{\check{n}-1-\check{i}} \sum_{l=0}^{\check{i}} g''_{\check{i}-l}\, g''_l, & n = 3, \end{cases} \tag{2.82}$$

The general solutions are

$$f_{\check{n}}(\eta) = f_{\check{n}}^*(\eta) + C_1^* + C_2^* e^{\eta} + C_3^* e^{-\eta}, \tag{2.83}$$

$$g_{\check{n}}(\eta) = g_{\check{n}}^*(\eta) + C_4^* + C_5^* e^{\eta} + C_6^* e^{-\eta}, \tag{2.84}$$

$$\theta_{\check{n}}(\eta) = \theta_{\check{n}}^*(\eta) + C_7^* e^{\eta} + C_8^* e^{-\eta}, \tag{2.85}$$

where $f_{\check{n}}^*$, $g_{\check{n}}^*$ and $\theta_{\check{n}}^*$ denote the particular solutions and the constants C_j^* $(j = 1 - 8)$ can be attained by utilizing Eqs. $(2.74) - (2.76)$. They are given by

$$C_3^* = \left.\frac{\partial f^*(\eta)}{\partial \eta}\right|_{\eta=0}, \; C_1^* = -C_3^* - f^*(0), \; C_6^* = \left.\frac{\partial g^*(\eta)}{\partial \eta}\right|_{\eta=0}, \; C_4^* = -C_6^* - g^*(0),$$

$$C_8^* = \frac{1}{1+\gamma_1}\left[\left.\frac{\partial \theta^*(\eta)}{\partial \eta}\right|_{\eta=0} - \gamma_1 \theta^*(0)\right],$$

$$C_2^* = C_5^* = C_7^* = 0. \tag{2.86}$$

2.5 Graphical Illustration and Analysis

This fragment is intensive to explore the impact of numerous corporal parameters on the velocities $f'(\eta)$ and $g'(\eta)$ and temperature $\theta(\eta)$ fields. The combined set of Eqs. $(2.27) - (2.29)$ with boundary conditions (2.30) are elucidated numerically by means of the bvp4c technique. Graphs are strategized for the values of distinct flow parameter like the local Weissenberg numbers (We_1, We_2), velocity ratio parameter (α), non-linear radiation parameter (R_d), temperature ratio parameter (θ_f), Prandtl number (Pr) and thermal Biot number (γ_1). Moreover, the results for the skin-friction coefficients $\left(\frac{1}{2}C_{fx}\mathrm{Re}_x^{\frac{1}{2}}, \frac{1}{2}C_{fy}\left(\frac{U_w}{V_w}\right)\mathrm{Re}_x^{\frac{1}{2}}\right)$ and local Nusselt number $\left(\mathrm{Re}_x^{-\frac{1}{2}}Nu_x\right)$ are also tabulated and deliberated in details.

Figures 2.2(a − d) are strategic to perceive the behavior of local Weissenberg number (We_1) on velocity components $f'(\eta)$ and $g'(\eta)$ for the instance of $(n < 1)$ and $(n > 1)$. From these sketches, it is established that intensifying values of We_1 decline the velocity component $f'(\eta)$ for shear thinning circumstance, whereas an opposed behavior is identified for $g'(\eta)$. Correspondingly, instead of this, it is also distinguished that for shear thickening fluid the increase in value of We_1 augments the fluid velocity $f'(\eta)$ and its related thickener of boundary

40

layer and it diminishes the fluid velocity $g'(\eta)$ for enlarging values of We_1 as displayed in **figures 2.2(b)** and **2.2(d)**. Physically, We_1 is the relation of relaxation time of the fluid and a certain process in which time growths the viscosity of liquid. Subsequently, there is a decline in the liquid velocity. Moreover, the boundary layer thickness is thinner for escalating values of We_1 for $n = 0.5$, while it augments for $n = 1.5$. **Figures 2.3(a − d)** are schemed to recognize the performance of local Weissenberg number (We_2) on $f'(\eta)$ and $g'(\eta)$, for $n = 0.5$ and $n = 1.5$. From these plots quite opposed behaviors are identified for the augmented value of We_2. An increase in the value of We_2 enhances the velocity component $f'(\eta)$ and declines the velocity component $g'(\eta)$ for shear thinning liquid. While, differing behavior is being noted for shear thickening liquid. **Figures 2.4(a − d)** are plotted to scrutinize the effects of the ratio of stretching rates (α) for $(n = 0.5)$ and $(n = 1.5)$ on $f'(\eta)$ and $g'(\eta)$, respectively. It is illustrated from these graphs that the velocity component $f'(\eta)$ and associated momentum boundary layer thickness decline for the augmented value of α while the inverse trend is observed for $g'(\eta)$. Physically, α is the relation of stretching in $y-$direction to the stretching in $x-$direction. As we enhance α the velocity in $y-$direction boosts up when compared with the velocity in $x-$direction.

The impact of local Weissenberg numbers (We_1, We_2) on $\theta(\eta)$ is demonstrated through **figures 2.5(a − d)**. It is clear from these sketches that the higher values of We_1 augment the temperature and associated thermal boundary layer thickness for $(n < 1)$ and opposite behavior is observed for $(n > 1)$. The results are more pronounced for the shear thickening liquid. Physically, We_1 and We_2 are the ratio of viscous to the elastic forces, so intensifying values of We_1 cause an augmentation in the liquid viscosity. Therefore, flow befits more resistive and consequently, $\theta(\eta)$ enhances for $n < 1$ and for $n > 1$ behavior is quite reversed. The impact of radiation parameter (R_d) and temperature ratio parameters (θ_f) on $\theta(\eta)$ for both circumstances, i.e., $(n < 1)$ and $(n > 1)$ is depicted via **figures 2.6(a, b)** and **2.7(a, b)**. These figures expose that the advanced assessment of the radiation and temperature ratio parameters have the tendency to augment both the temperature and allied thermal boundary layer thickness. **Figures 2.7(a, b)** spectacle that for the amassed values of θ_f, the fluid temperature (T_f) is greater than the ambient temperature (T_∞), which raises the thermal state of the fluid and the outcome is intensification of $\theta(\eta)$. Moreover, these figures clue to the decision that the

41

temperature and thermal boundary layer thickness are accumulative functions of R_d and θ_f for both cases. **Figures 2.8(a, b)** and **2.9(a, b)** depict the discrepancy of the Biot number (γ_1) and Prandtl number (Pr) on the heat process for shear thinning and shear thickening fluids. It is noticed from these sketches that the γ_1 is an intensifying function of $\theta(\eta)$ for the growing value of γ_1. By physical point of assessment the advance values of γ_1 intensify the heat transfer amount which clues higher temperature and its thermal boundary layer thickness pointedly enhanced. Furthermore, the influence of Prandtl number (Pr) is relatively opposing on $\theta(\eta)$. An escalation in Pr resembles to a reduction in thermal diffusivity which thus, arises difference in the thermal features and diminutions the fluid temperature and its allied thermal boundary layer thickness. The structure of $\theta(\eta)$ for diverse values of the ratio of stretching rates parameter (α) is established through **figures 2.10(a, b)**. It is probable from these drafts that $\theta(\eta)$ diminishes for improving the values of α for both $(n < 1)$ and $(n > 1)$. An amplification in α resembles that the velocity in $x - direction$ clues than the velocity in $y - direction$, because of the particles collision boosts which as an outcome diminishes the temperature of Carreau liquid.

2.5.1 Graphical Comparison between bvp4c and HAM

From **figures 2.11(a, b)** to **2.14(a, b)**, it is enthusiastic that the displayed plots of $f'(\eta)$, $g'(\eta)$ and $\theta(\eta)$ reveal a tremendous graphical settlement of the bvp4c technique with the homotopy analysis method (HAM).

2.5.2 Tabular Representations

Tables 2.1 and **2.2** are established for numerical values of $\left(\frac{1}{2} C_{fx} \operatorname{Re}_x^{\frac{1}{2}}, \; \frac{1}{2} \left(\frac{U_w}{V_w} \right) C_{fy} \operatorname{Re}_x^{\frac{1}{2}} \right)$ and $\left(\operatorname{Re}_x^{-\frac{1}{2}} N u_x \right)$ for controlling parameter. The wall temperature gradient is improved for liquid in both situations *i.e.*, $(n = 0.5, 1.5)$ for the augmented values of R_d and γ_1. Therefore, it consequences in the increase of the heat transfer coefficient.

2.5.3 Confirmation of Numerical Outcomes

Tables 2.3 and **2.4** present the comparison of two dissimilar techniques, namely the homotopy analysis method (HAM) and bvp4c for different values of ratio of stretching rates parameter (α) with homotopy perturbation method (HPM) [115], exact solutions [115] and homotopy analysis method (HAM) [116]. From these tables, a tremendous agreement is renowned in a limiting sense. Additionally, the influence of We_1, We_2 and α on $\left(\frac{1}{2}C_{fx}\operatorname{Re}_x^{\frac{1}{2}}, \ \frac{1}{2}\left(\frac{U_w}{V_w}\right)C_{fy}\operatorname{Re}_x^{\frac{1}{2}} \right)$ is addressed numerically (bvp4c) and analytically (HAM) through **Table 2.5** with excellent agreement. **Table 2.6** numerically (bvp4c) and analytically (HAM) revealed the effects of R_d, θ_f, γ_1 and Pr on $\left(\operatorname{Re}_x^{-\frac{1}{2}} Nu_x \right)$. Here both the techniques are remarkable in agreement.
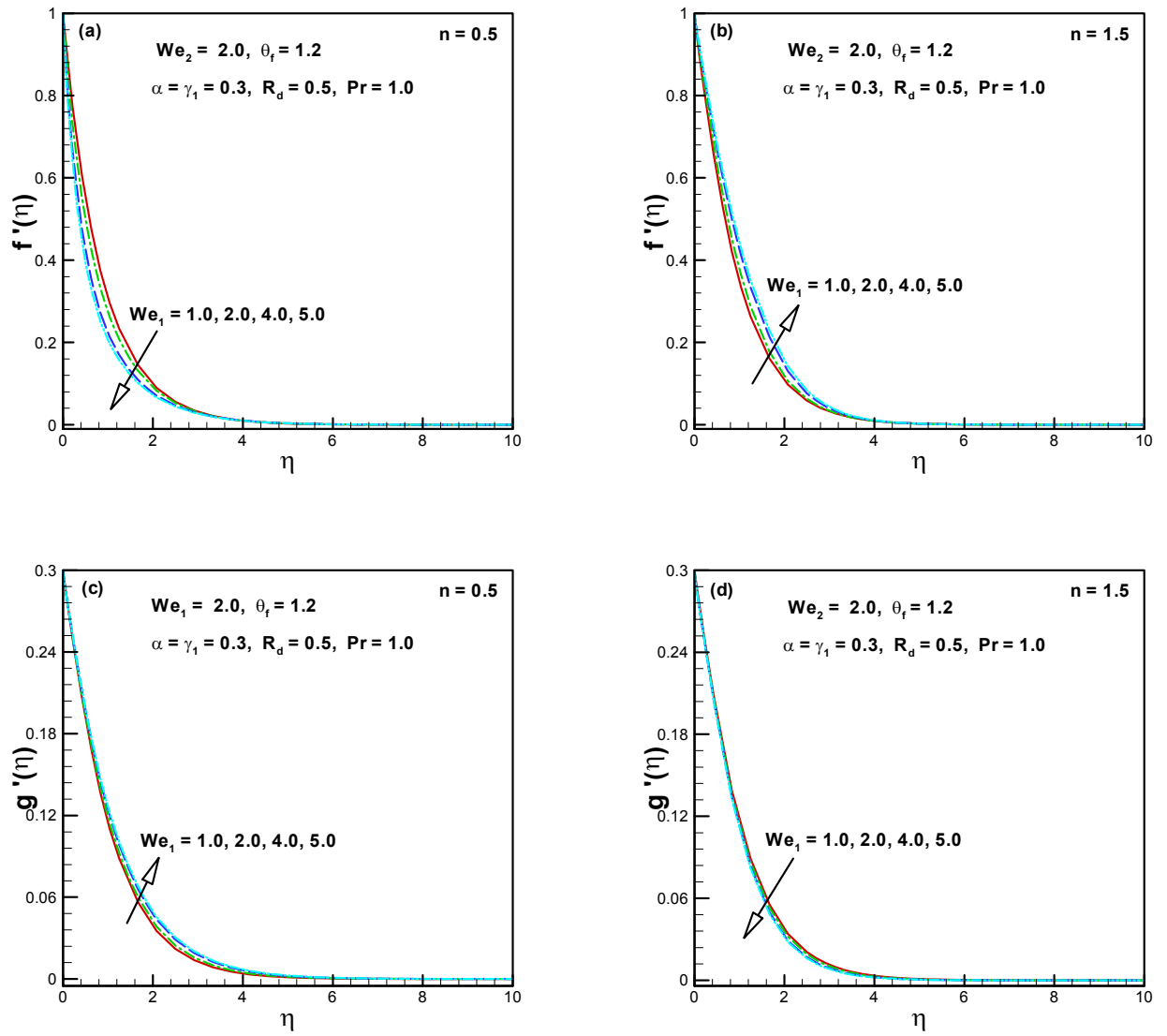
Figure 2.2(a − d): Influence of We_1 on $f'(\eta)$ and $g'(\eta)$.
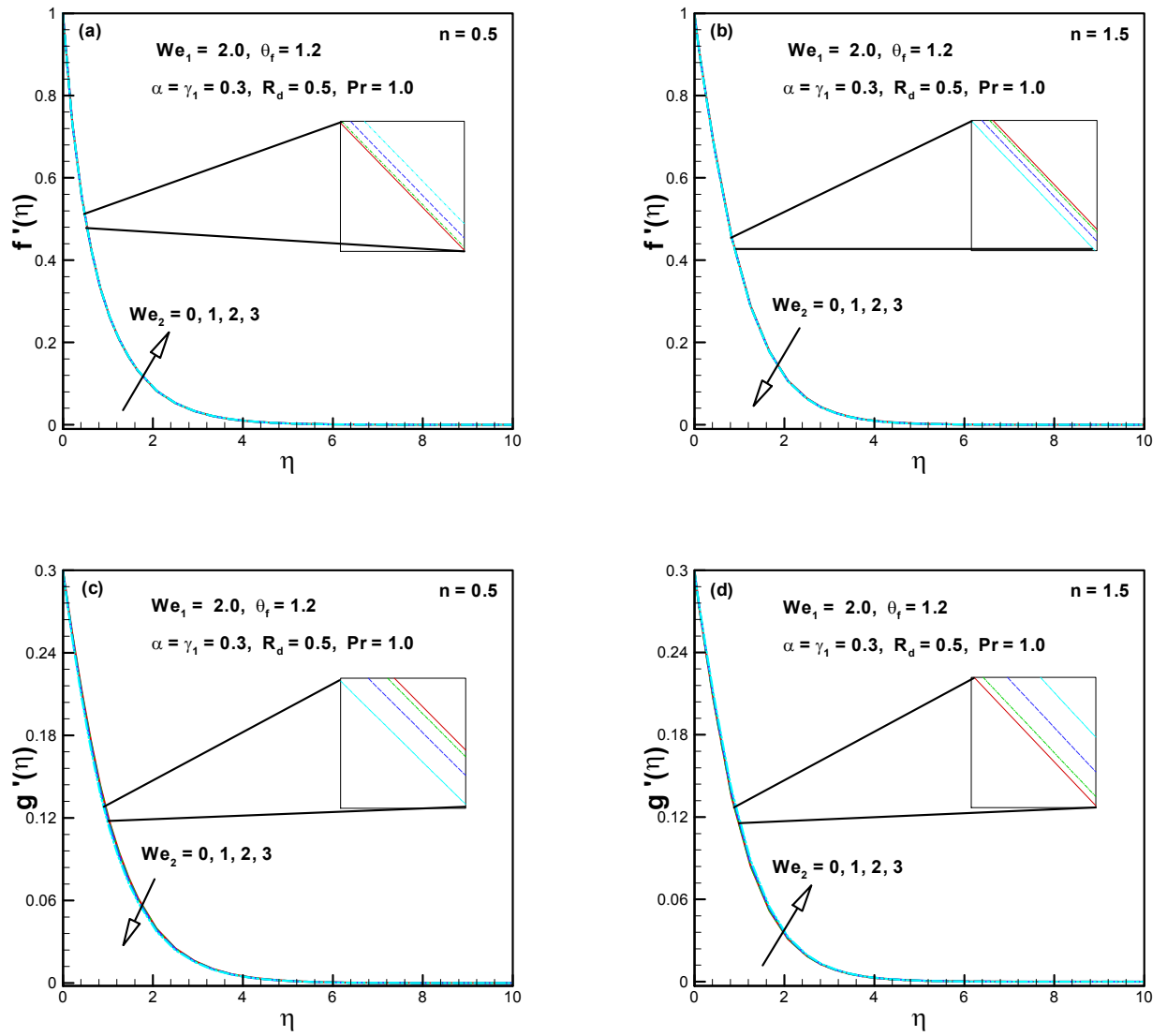
Figure 2.3(a − d): Influence of We_2 on $f'(\eta)$ and $g'(\eta)$.
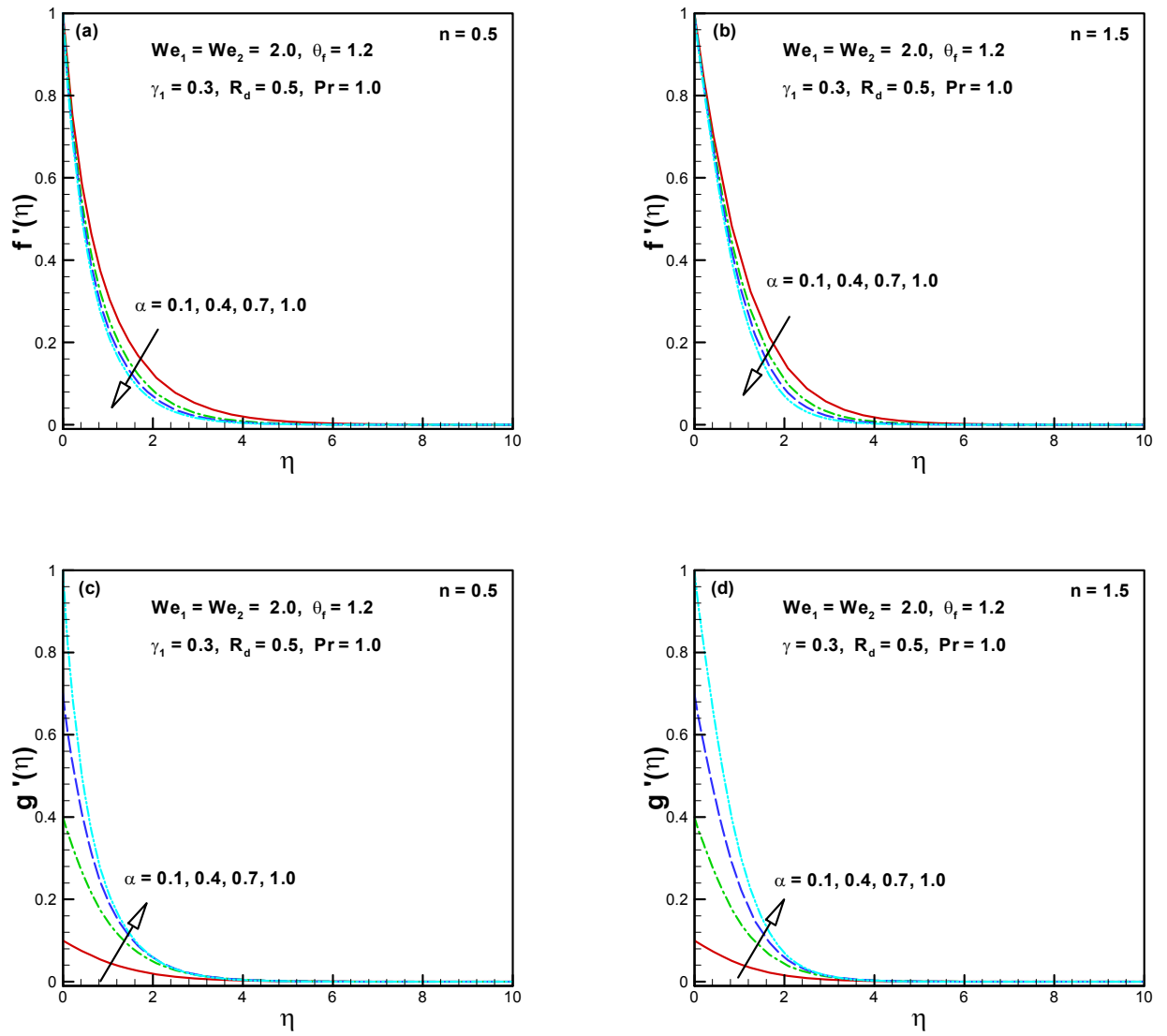
Figure 2.4(a − d): Influence of α on $f'(\eta)$ and $g'(\eta)$.
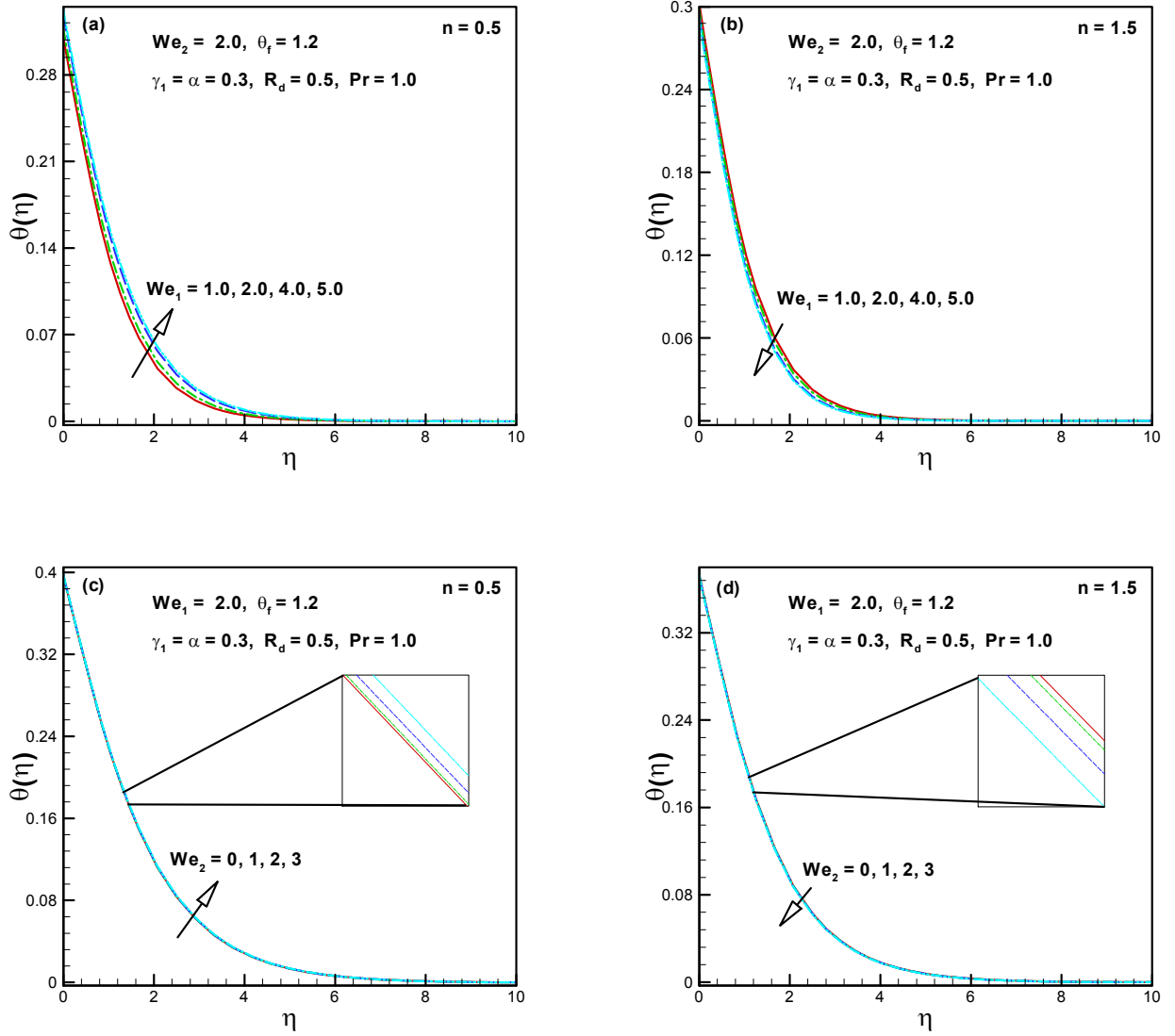
Figure 2.5(**a** − **d**): Influence of We_1 and We_2 on $\theta(\eta)$.
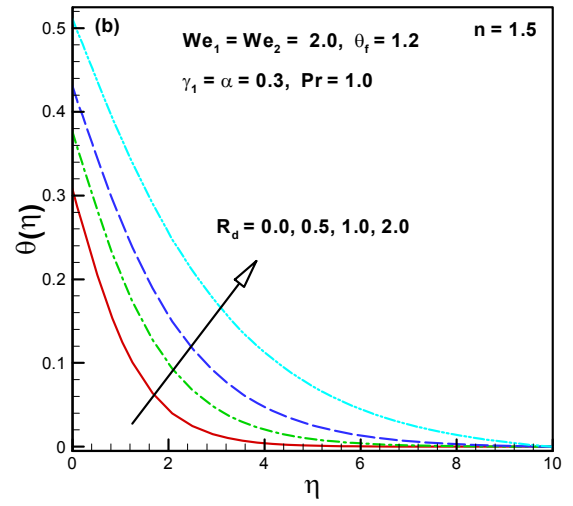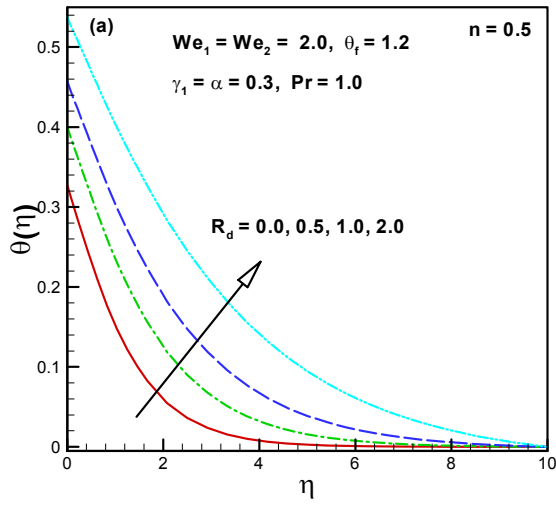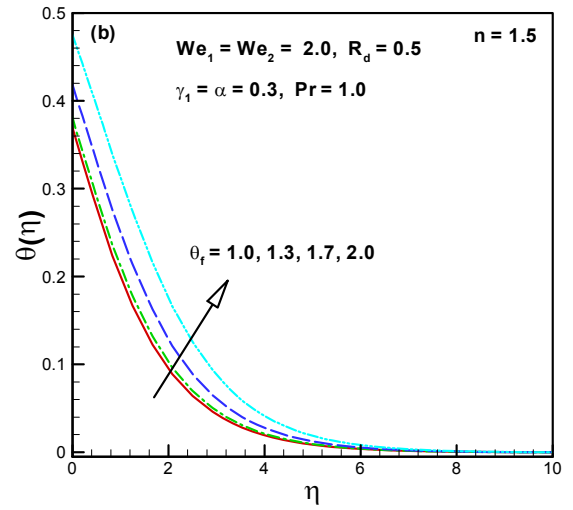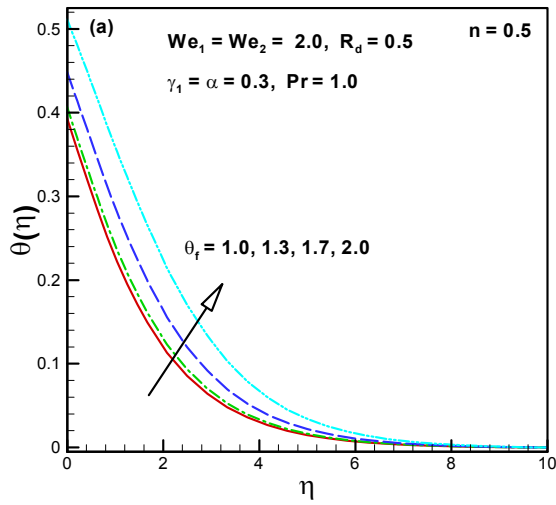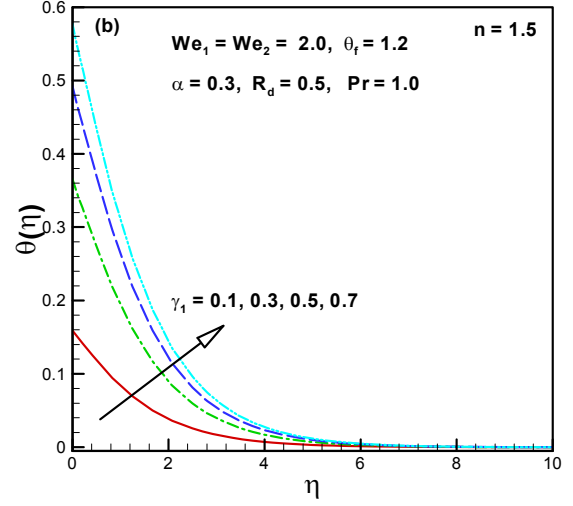
Figure 2.6(a, b): Influence of R_d on $\theta(\eta)$.

Figure 2.7(a, b): Influence of θ_f on $\theta(\eta)$.
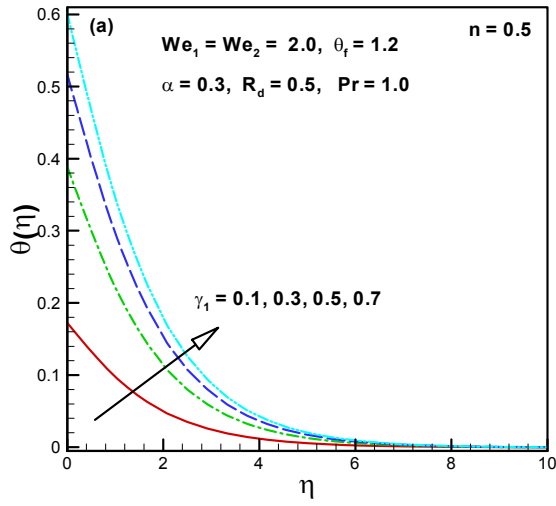
Figure 2.8(a, b): Influence of γ_1 on $\theta(\eta)$.

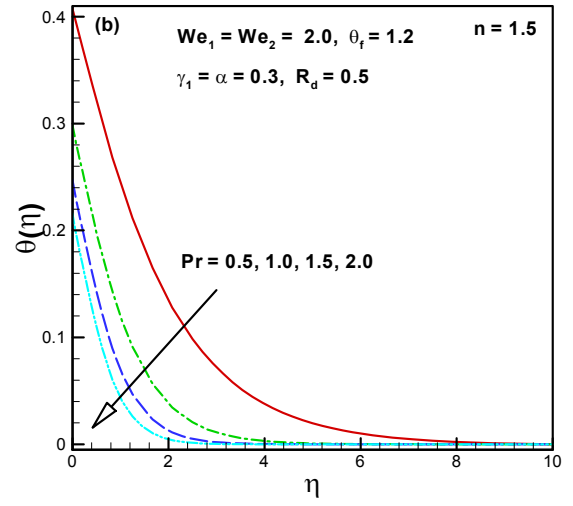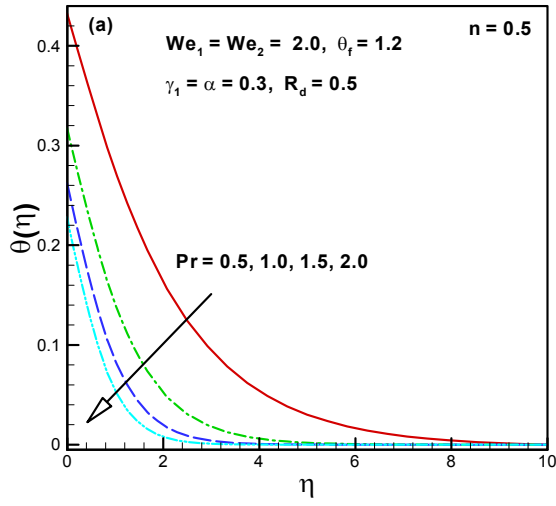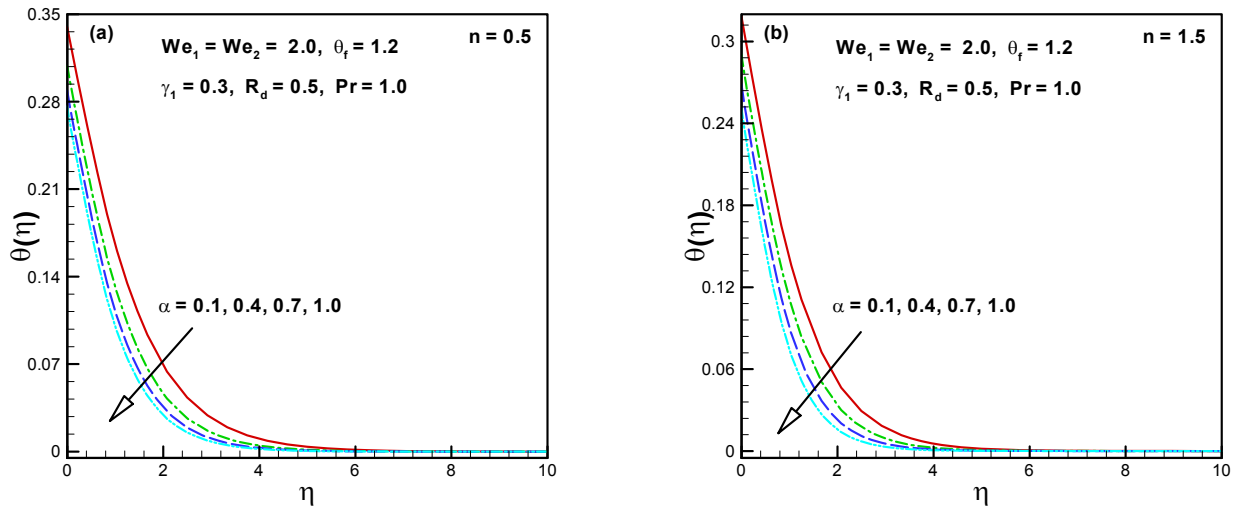**Figure 2.9(a, b):** Influence of Pr on $\theta(\eta)$.

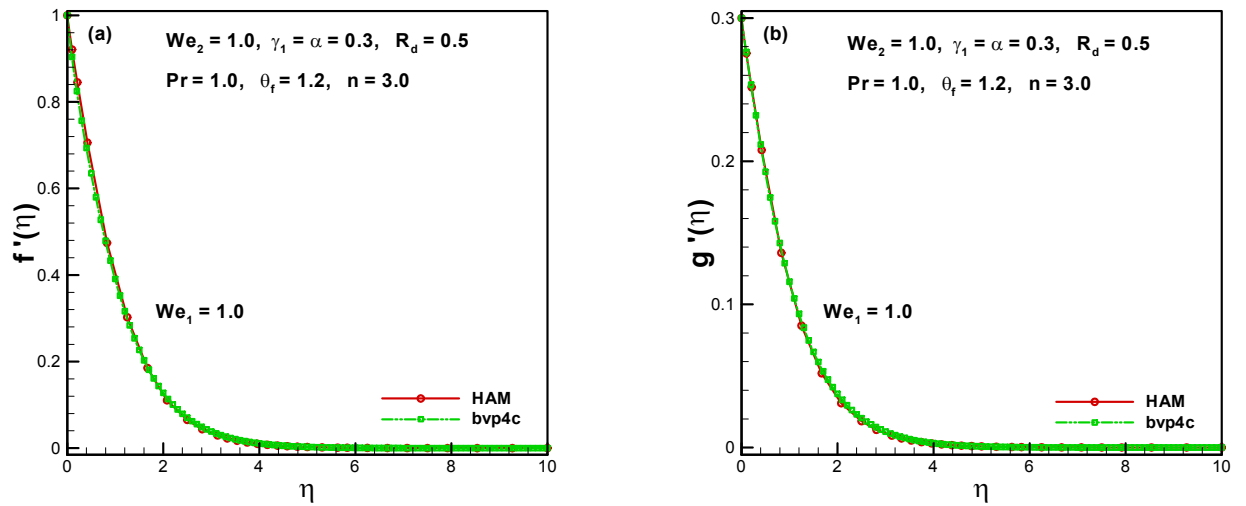**Figure 2.10(a, b):** Influence of α on $\theta(\eta)$.

Figure 2.11(a, b): Graphical assessment between bvp4c and HAM for We_1 on $f'(\eta)$ and $g'(\eta)$.
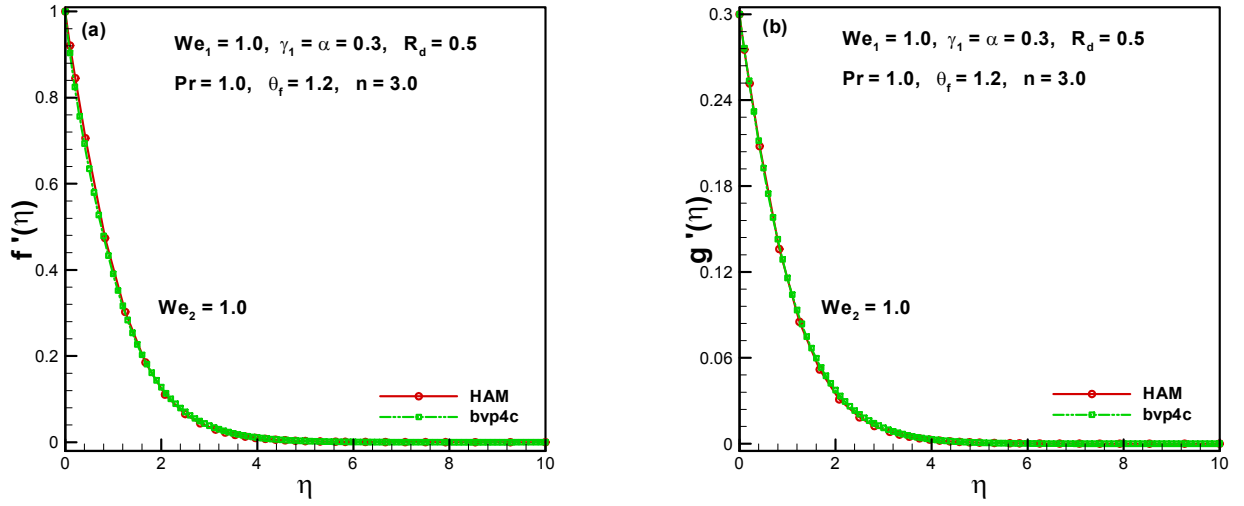
Figure 2.12(a, b): Graphical assessment between bvp4c and HAM for We_2 on $f'(\eta)$ and $g'(\eta)$.
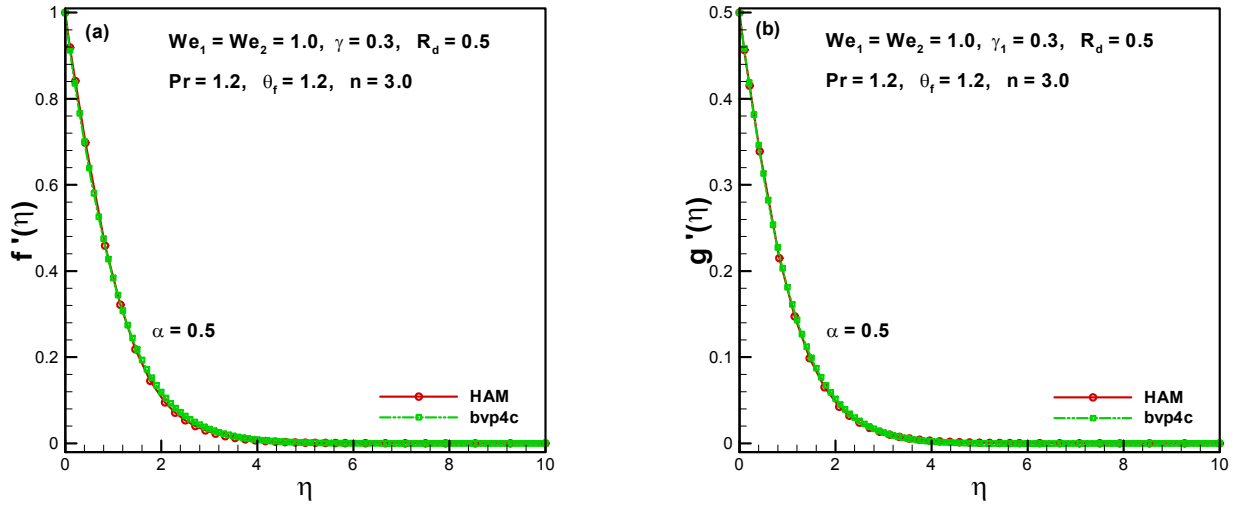

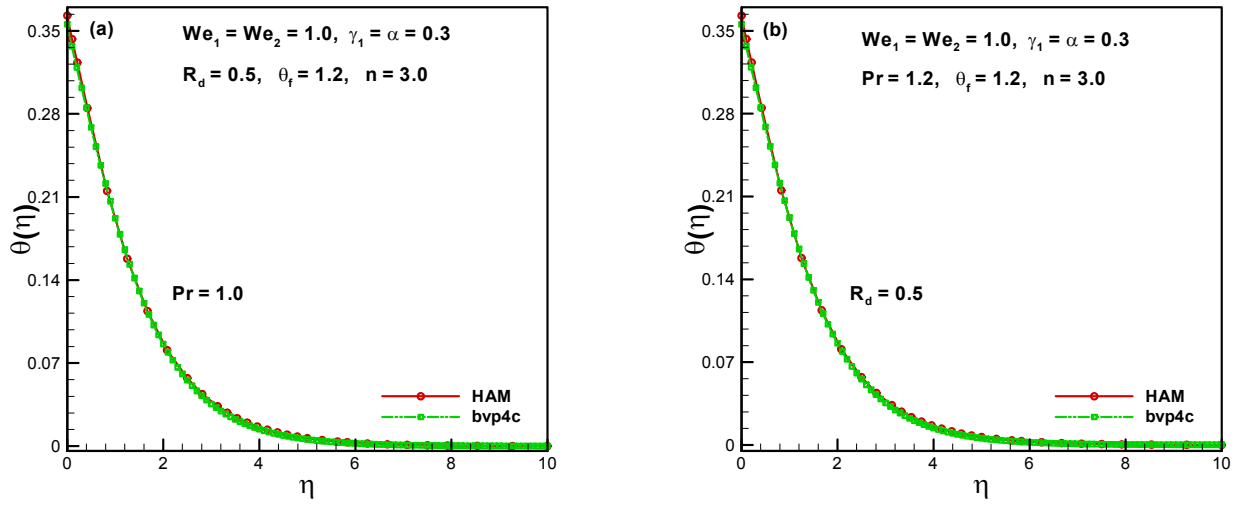**Figure 2.13(a, b):** Graphical assessment between bvp4c and HAM for α on $f'(\eta)$ and $g'(\eta)$.

Figure 2.14(a, b): Graphical assessment between bvp4c and HAM for Pr and R_d on $\theta(\eta)$.

Table 2.1: Outcomes of $\left(\frac{1}{2}C_{fx}\operatorname{Re}_x^{\frac{1}{2}}, \frac{1}{2}\left(\frac{U_w}{V_w}\right)C_{fy}\operatorname{Re}_x^{\frac{1}{2}}\right)$ for different parameters when $R_d = 0.5$, $\theta_f = 1.2$, $\gamma_1 = 0.3$ and $\operatorname{Pr} = 1.0$ are fixed.

We_1	We_2	α	$\frac{1}{2}C_{fx}\operatorname{Re}_x^{\frac{1}{2}}$		$\frac{1}{2}\left(\frac{U_w}{V_w}\right)C_{fy}\operatorname{Re}_x^{\frac{1}{2}}$	
			$n = 0.5$	$n = 1.5$	$n = 0.5$	$n = 1.5$
2.0	3.0	0.3	-1.581674	-3.344919	-0.255535	-0.345016
3.0			-1.856803	-5.271657	-0.250302	-0.350016
4.0			-2.073570	-7.485905	-0.246271	-0.353936
5.0			-2.253414	-9.936722	-0.343069	-0.357096
2.0	4.0		-1.580164	-3.350012	-0.270037	-0.406513
	5.0		-1.578454	-3.354100	-0.286856	-0.476625
	6.0		-1.576657	-3.358029	-0.304832	-0.553578
	3.0	0.5	-1.647423	-3.594553	-0.577434	-1.013007
		0.8	-1.728708	-3.986363	-1.379147	-3.485158
		1.0	-1.775024	-4.258813	-2.114502	-6.702600

Table 2.2: Outcomes of $\left(\mathrm{Re}_x^{-\frac{1}{2}} Nu_x\right)$ for different parameters R_d, θ_f, γ_1 and Pr when $We_1 = We_2 = 2.0$ and $\alpha = 0.3$ are fixed.

R_d	θ_f	γ_1	Pr	$\mathrm{Re}_x^{-\frac{1}{2}} Nu_x$	
				$n = 0.5$	$n = 1.5$
0.5	1.2	0.3	1.0	0.294477	0.304676
1.0				0.372689	0.388123
1.5				0.441783	0.462292
2.0				0.504335	0.529242
0.5	1.5			0.325703	0.335816
	1.7			0.352423	0.362326
	2.0			0.404464	0.413952
	1.2	0.5		0.394499	0.413634
		0.7		0.460224	0.486964
		1.0		0.524613	0.560187
		0.3	1.3	0.313658	0.322535
			1.7	0.331121	0.338646
			2.0	0.340662	0.347414

Table 2.3: A comparison of $-f''(0)$ for numerous values of α when $We_1 = We_2 = 0$ and $n = 1$.

α	Ariel(HPM) [115]	Ariel(Exact) [115]	Hayat *et al.* [116]	Present (HAM)	Present (bvp4c)
0	1	1	1	1	1
0.1	1.017027	1.020264	1.020260	1.020263	1.020264
0.2	1.034587	1.039497	1.039495	1.039496	1.039497
0.3	1.057470	1.057956	1.057955	1.057956	1.057956
0.4	1.070529	1.075788	1.075788	1.075787	1.075788
0.5	1.088662	1.093095	1.093095	1.093095	1.093095
0.6	1.106797	1.109946	1.109947	1.109946	1.109946
0.7	1.124882	1.126397	1.126398	1.126396	1.126397
0.8	1.142879	1.142488	1.142489	1.142489	1.142488
0.9	1.160762	1.158253	1.158254	1.158252	1.158253
1.0	1.178511	1.17372	1.173721	1.173720	1.173720

Table 2.4: A comparison of $-g''(0)$ for numerous values of α when $We_1 = We_2 = 0$ and $n = 1$.

α			$-g''(0)$		
	Ariel(HPM) [115]	Ariel(Exact) [115]	Hayat *et al.* [116]	Present (HAM)	Present (bvp4c)
0	0.0	0.0	0.0	0.0	0.0
0.1	0.070399	0.066847	0.066847	0.066848	0.0668485
0.2	0.158231	0.148737	0.148737	0.148737	0.1487382
0.3	0.254347	0.243360	0.243359	0.243360	0.2433607
0.4	0.360599	0.349209	0.349209	0.349208	0.3492087
0.5	0.476290	0.465205	0.465205	0.465207	0.4652046
0.6	0.600833	0.590529	0.590529	0.590528	0.5905229
0.7	0.733730	0.724532	0.724532	0.724530	0.7245312
0.8	0.874551	0.866683	0.866683	0.866682	0.8666822
0.9	1.022922	1.016539	1.016540	1.016540	1.016538
1.0	1.178511	1.173721	1.173722	1.173721	1.173720

Table 2.5: A comparison of $\left(\frac{1}{2}C_{fx}\,\mathrm{Re}_x^{\frac{1}{2}}, \frac{1}{2}\left(\frac{U_w}{V_w}\right)C_{fy}\,\mathrm{Re}_x^{\frac{1}{2}}\right)$ between bvp4c and HAM for different parameters when $R_d = 0.5$, $\theta_f = \gamma_1 = 0.3$, $\mathrm{Pr} = 0.7$ and $n = 3$ are fixed.

We_1	We_2	α	$\frac{1}{2}C_{fx}\,\mathrm{Re}_x^{\frac{1}{2}}$		$\frac{1}{2}\left(\frac{U_w}{V_w}\right)C_{fy}\,\mathrm{Re}_x^{\frac{1}{2}}$	
			HAM	bvp4c	HAM	bvp4c
0.1	0.1	0.3	-1.06140	-1.061402	-0.243538	-0.2435388
0.2			-1.07126	-1.071256	-0.243930	-0.2439302
0.3			-1.08638	-1.086387	-0.244524	-0.2445312
0.4			-1.10543	-1.105454	-0.245261	-0.2452684
0.1	0.0		-1.06140	-1.061396	-0.243497	-0.2434975
	0.2		-1.06142	-1.061421	-0.243662	-0.2436622
	0.3		-1.06145	-1.061452	-0.243866	-0.2438667
	0.1	0.4	-1.07942	-1.079422	-0.349508	-0.3495075
		0.5	-1.09693	-1.096927	-0.465711	-0.4657115
		0.6	-1.11399	-1.113986	-0.591380	-0.5913799

Table 2.6: A comparison of $\left(\mathrm{Re}_x^{-\frac{1}{2}} Nu_x\right)$ between bvp4c and HAM for different parameters when $We_1 = We_2 = 0.1$, $\alpha = 0.3$ and $n = 3$ are fixed.

R_d	θ_f	γ_1	Pr	$\mathrm{Re}_x^{-\frac{1}{2}} Nu_x$ HAM	bvp4c
0.5	0.3	0.3	0.7	0.219951	0.219914
0.6				0.224867	0.224881
0.7				0.229686	0.229695
0.8				0.234365	0.234373
0.5	0.0			0.210419	0.210411
	0.5			0.228013	0.228010
	1.0			0.256641	0.256622
	0.3	0.5		0.282772	0.282752
		0.7		0.324442	0.324437
		1.0		0.366528	0.366523
		0.3	1.0	0.245430	0.245432
			1.3	0.263400	0.263400
			1.5	0.272786	0.272796

Chapter 3

Influence of Convective Conditions in 3D Carreau Nanofluid Flow

This chapter reports a mathematical relation for 3D forced convective heat and mass transfer mechanisms of Carreau nanoliquid over a bidirectional stretched surface. Additionally, the features of heat source/sink and non-linear thermal radiation are considered. The governing non-linear PDEs are established and altered into a set of non-linear ODEs by utilizing the suitable conversion. A numerical approach, namely bvp4c is adopted to resolve the resultant equations. The achieved outcomes are schemed and conferred in detail for somatic parameters. It is realized that amassed values of Brownian motion parameter (N_b) lead to enhance the temperature of Carreau nanoliquid while quite conflicting behavior is being noticed for the concentration of Carreau nanoliquid. Moreover, it is also noted that the influence of heat source $(\delta > 0)$ is relatively antithesis to heat sink $(\delta < 0)$ parameter. However an analogous impact is being identified for thermal Biot number (γ_1) on temperature and the concentration Biot number (γ_2) on concentration of Carreau nanoliquid for shear thinning/thickening liquids. Additionally, an assessment between analytical technique, the homotopy analysis method (HAM) and numerical scheme bvp4c is presented graphically, as well as in tabular form. From these comparisons we initiate a splendid communication with these results.

3.1 Description of the Problem

Here we scrutinize the steady 3D forced convective flow of a Carreau nanofluid over a bidirectional stretched surface. The aspects of Brownian motion and thermophoresis particles are also occupied in this description. The flow is influenced by stretching the surface in two adjacent x and y directions with linear velocities $(u, v) = (ax, by)$ respectively, where a and b are positive constants and the fluid conquers the region $z > 0$. The heat transfer mechanism is also considered subject to nonlinear thermal radiation and heat generation/absorption.

Under these norms the existing flow problem of a Carreau nanofluid can be written as

$$\frac{\partial u}{\partial x} + \frac{\partial v}{\partial y} + \frac{\partial w}{\partial z} = 0, \tag{3.1}$$

$$u\frac{\partial u}{\partial x} + v\frac{\partial u}{\partial y} + w\frac{\partial u}{\partial z} = \nu\frac{\partial^2 u}{\partial z^2}\left[1 + \Gamma^2\left(\frac{\partial u}{\partial z}\right)^2\right]^{\frac{n-1}{2}}$$
$$+ \nu(n-1)\Gamma^2\left(\frac{\partial u}{\partial z}\right)^2\frac{\partial^2 u}{\partial z^2}\left[1 + \Gamma^2\left(\frac{\partial u}{\partial z}\right)^2\right]^{\frac{n-3}{2}}, \tag{3.2}$$

$$u\frac{\partial v}{\partial x} + v\frac{\partial v}{\partial y} + w\frac{\partial v}{\partial z} = \nu\frac{\partial^2 v}{\partial z^2}\left[1 + \Gamma^2\left(\frac{\partial v}{\partial z}\right)^2\right]^{\frac{n-1}{2}}$$
$$+ \nu(n-1)\Gamma^2\left(\frac{\partial v}{\partial z}\right)^2\frac{\partial^2 v}{\partial z^2}\left[1 + \Gamma^2\left(\frac{\partial v}{\partial z}\right)^2\right]^{\frac{n-3}{2}}, \tag{3.3}$$

$$u\frac{\partial T}{\partial x} + v\frac{\partial T}{\partial y} + w\frac{\partial T}{\partial z} = \alpha_1\frac{\partial^2 T}{\partial z^2} + \tau\left[D_B\frac{\partial C}{\partial z}\frac{\partial T}{\partial z} + \frac{D_T}{T_\infty}\left(\frac{\partial T}{\partial z}\right)^2\right]$$
$$- \frac{1}{(\rho c)_f}\frac{\partial q_r}{\partial z} + \frac{Q_0}{(\rho c)_f}(T - T_\infty), \tag{3.4}$$

$$u\frac{\partial C}{\partial x} + v\frac{\partial C}{\partial y} + w\frac{\partial C}{\partial z} = D_B\frac{\partial^2 C}{\partial z^2} + \frac{D_T}{T_\infty}\frac{\partial^2 T}{\partial z^2}. \tag{3.5}$$

The esulting boundary conditions of flow problem are

$$u = ax, \quad v = by, \quad w = 0, \quad -k\frac{\partial T}{\partial z} = h_f[T_f - T], \quad -D_B\frac{\partial C}{\partial z} = h_m[C_f - C] \quad \text{at} \quad z = 0, \quad (3.6)$$

$$u \to 0, \quad v \to 0, \quad T \to T_\infty, \quad C \to C_\infty \quad \text{as} \quad z \to \infty. \quad (3.7)$$

Here C is the volume friction of nanoliquid, τ the effective heat capacity of nanoparticles to heat capacity of the base liquid ratio, (D_B, D_T) the Brownian and thermal diffusion coefficients, respectively, C_∞ the ambient concentration of the nanoliquid, Q_0 the heat source/sink coefficient, h_m wall mass transport coefficient and C_f the liquid concentration near to the surface.

3.1.1 Appropriate Conversions

Let we consider

$$\phi = \frac{C - C_\infty}{C_f - C_\infty}. \quad (3.8)$$

In the perception of overhead conversion and Eq. (2.27) (cf. Chapter 2), the condition of incompressibility (3.1) is automatically satisfied and Eqs. $(3.2) - (3.7)$ reduce to

$$f'''[1 + We_1^2 f''^2]^{\frac{n-3}{2}}[1 + nWe_1^2 f''^2] - f'^2 + f''(f + g) = 0, \quad (3.9)$$

$$g'''[1 + We_2^2 g''^2]^{\frac{n-3}{2}}[1 + nWe_2^2 g''^2] - g'^2 + g''(f + g) = 0, \quad (3.10)$$

$$\frac{d}{d\eta}[\{1 + R_d(1 + (\theta_f - 1)\theta)^3\}\theta'] + \Pr(f + g)\theta' + \Pr[N_b\theta'\phi' + N_t\theta'^2] + \Pr\delta\theta] = 0, \quad (3.11)$$

$$\phi'' + \Pr Le(f + g)\phi' + \left(\frac{N_t}{N_b}\right)\theta'' = 0, \quad (3.12)$$

$$f(0) = 0, \quad g(0) = 0, \quad f'(0) = 1, \quad g'(0) = \alpha,$$

$$\theta'(0) = -\gamma_1(1 - \theta(0)), \quad \phi'(0) = -\gamma_2(1 - \phi(0)), \quad (3.13)$$

$$f' \to 0, \quad g' \to 0, \quad \theta \to 0, \quad \phi \to 0 \quad \text{as} \quad \eta \to \infty. \quad (3.14)$$

Here $N_b\left(= \frac{\tau D_B(C_f - C_\infty)}{\nu}\right)$ is the Brownian motion parameter, $N_t\left(= \frac{\tau D_T(T_f - T_\infty)}{\nu T_\infty}\right)$ the thermophoresis parameter, $\delta\left(= \frac{Q_0}{a(\rho c)_f}\right)$ the heat source ($\delta > 0$) and heat sink ($\delta < 0$) parameter,

$Le \left(= \frac{\alpha_1}{D_B} \right)$ the Lewis number and $\gamma_2 \left(= \frac{h_m}{D_B} \sqrt{\frac{\nu}{a}} \right)$ the mass Biot number. Moreover, We_1, We_2, R_d, θ_f, γ_1 and α are the dimensionless parameters and are same as defined in chapter 2.

3.2 Engineering and Industrial Quantities of Interest

From the industrial and engineering point of view, the essential quantities of physical interest are the skin friction coefficients, heat and mass transfer coefficients which may be defined by the subsequent expressions.

3.2.1 The Skin Friction Coefficients

It is defined as

$$C_{fx} = \frac{\tau_{xz}}{\frac{1}{2}\rho_f U_w^2}, \quad C_{fy} = \frac{\tau_{yz}}{\frac{1}{2}\rho_f U_w^2}, \tag{3.15}$$

and in dimensionless form

$$\frac{1}{2}C_{fx} \operatorname{Re}_x^{\frac{1}{2}} = f''(0)[1 + We_1^2 f''^2(0)]^{\frac{n-1}{2}}, \tag{3.16}$$

$$\frac{1}{2}\left(\frac{U_w}{V_w}\right)C_{fy} \operatorname{Re}_x^{\frac{1}{2}} = g''(0)[1 + We_2^2 g''^2(0)]^{\frac{n-1}{2}}. \tag{3.17}$$

3.2.2 The Local Nusselt and Sherwood Numbers

These are defined as

$$Nu_x = -\frac{x}{(T_f - T_\infty)} \left.\frac{\partial T}{\partial z}\right|_{z=0} + \frac{xq_r}{k(T_f - T_\infty)}, \quad Sh_x = -\frac{x}{(C_f - C_\infty)} \left.\frac{\partial C}{\partial z}\right|_{z=0}, \tag{3.18}$$

and the above quantities in the dimensionless expression are

$$\operatorname{Re}_x^{-\frac{1}{2}} Nu_x = -[1 + R_d\{1 + (\theta_f - 1)\theta(0)\}^3]\theta'(0), \quad \operatorname{Re}_x^{-\frac{1}{2}} Sh_x = -\phi'(0). \tag{3.19}$$

3.3 Graphical Illustration and Analysis

To report the influence of various inferential parameters on the temperature field $\theta(\eta)$ and concentration field $\phi(\eta)$ of Carreau nanoliquid this part is focused. A set of combined nonlinear ODEs (3.9) to (3.14) are interpreted numerically by employing bvp4v technique. For the values of diverse flow parameters graphs are depicted. Furthermore, the outcomes for the local Nusselt number $\left(\mathrm{Re}_x^{-\frac{1}{2}} Nu_x\right)$ and Sherwood number $\left(\mathrm{Re}_x^{-\frac{1}{2}} Sh_x\right)$ are tabularized and discussed.

Figures 3.1(a, b) and **3.2(a, b)** are portrayed to visualize the performance of Brownian motion (N_b) and thermophoresis (N_t) parameters on nanoliquid temperature $\theta(\eta)$ for shear thinning/thickening liquids. From these plots it is detected that both are augmenting functions of temperature of Carreau liquid for rising value of N_b and N_t. Physically, N_b depends on the unsystematic motion of nanoparticles in the Carreau liquid. When N_b is augmented the unsystematic gesture of the particles intensifies which exaggerates the velocity of the nanoparticles. Hence, $\theta(\eta)$ augments. Moreover, N_t is directly proportional to the difference of temperature between the wall and the reference temperature. In the flow domain of the particulate structure, there is temperature gradient in hotter regions which causes small elements inclined to isolated quicker. Consequently, the surface temperature of the nanoliquid and its thickness of boundary layer are enhanced. Additionally, growing values of N_t physically means that the smallest nanoparticles are pulled away from the warm surface to the cold surface. Therefore, the higher number of small nanoparticles is dragged away from the warm surface due to which concentration of the nanoliquid decline. **Figures 3.3(a, b)** and **3.4(a, b)** are plotted to determine the features of thermal radiation parameter (R_d) and temperature ratio parameter (θ_f) on $\theta(\eta)$ for $(n = 0.5)$ and $(n = 1.5)$. It is noted that the temperature and its related thickness of boundary layer enhance for the augmented values of R_d and θ_f in both instances. The increasing values of R_d formed much heat in working liquid which consequences augment $\theta(\eta)$. **Figures 3.5(a, b)** and **3.6(a, b)** clarify the properties of heat sink/source parameter (δ) on the nanoparticles $\theta(\eta)$. From these sketches it is established that the temperature of Carreau nanoliquid and associated thermal boundary layer thickness decline when we rise the values of $\delta < 0$; however, the conflicting circumstance is being remarked for $\delta > 0$. Apparently in $\delta > 0$ phenomenon provides much heat to the liquid that corresponds to an increase in $\theta(\eta)$ for both $(n < 1)$ and $(n > 1)$. The influence of increasing values of the thermal Biot number (γ_1) for

shear thinning/thickening liquids on $\theta(\eta)$ is portrayed in **figure 3.7(a, b)**. We can perceive from these designs that augmenting behavior for enhancing values of γ_1 on $\theta(\eta)$ is detected. Due to increase in γ_1 the convection of the surface rises and as a result an enhancement in the liquid temperature and its allied thickness of the boundary layer occur.

Figures 3.8(a, b) and **3.9(a, b)** are delineated to interpret the aspects of N_b and N_t, respectively on $\phi(\eta)$. These displays reported that the concentration of the Carreau nanoliquid and associated concentration boundary layer thickness diminish for the larger values of N_b. But, the higher N_t leads to an augmentation in $\phi(\eta)$ for both situations $(n < 1)$ and $(n > 1)$. The influence of higher values of the concentration Biot number (γ_2) and Lewis number (Le) on $\phi(\eta)$ depicts the conflicting impacts which are expressed in **figures 3.10(a, b)** and **3.11(a, b)**. An increase in γ_2 enhances the concentration of Carreau liquid, while it declines for Le. From the physical point of assessment Le is the inversely amount to the Brownian diffusion coefficient (D_B) owing to which a magnification in Le produces a decline in diffusion coefficient and hence, $\phi(\eta)$ decays.

3.3.1 Graphical Comparison between bvp4c and HAM

Figures 3.12(a, b) and **3.13(a, b)** are depicted to scrutinize the legitimacy of current results on $\theta(\eta)$ through graphical illustrations and reveal a remarkable settlement of the bvp4c scheme with homotopy analysis method (HAM).

3.3.2 Tabular Representations

The convergence of different flow parameters on local Nusselt $\left(\mathrm{Re}_x^{-\frac{1}{2}} Nu_x \right)$ and local Sherwood $\left(\mathrm{Re}_x^{-\frac{1}{2}} Sh_x \right)$ for both $(n = 0.5,\ 1.5)$ are reported in **Table 3.1**. The heat and mass transport rates decline for intensifying values of N_b for both situations $(n < 1)$ and $(n < 1)$ in **Table 3.1**, while the influence of amassed values of γ_2 on $Nu_x \mathrm{Re}_x^{-\frac{1}{2}}$ is quite reverse to $Sh_x \mathrm{Re}_x^{-\frac{1}{2}}$.

3.3.3 Confirmation of Numerical Outcomes

Table 3.2 is organized for $\left(\mathrm{Re}_x^{-\frac{1}{2}} Nu_x \right)$ and $\left(\mathrm{Re}_x^{-\frac{1}{2}} Sh_x \right)$ of two different schemes numerically (bvp4c) and analytically (HAM). In this table a tremendous agreement is established between

both techniques. Additionally, the validity of the numerical and analytical results are also presented by assessment with former related prose and remarked an excellent settlement in **Tables 3.3** and **3**.**4**.
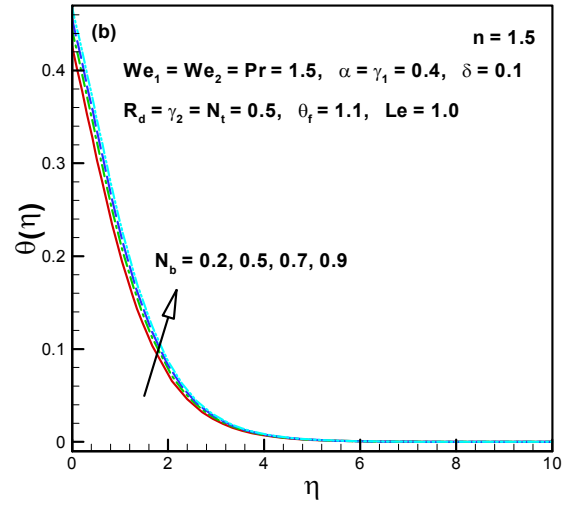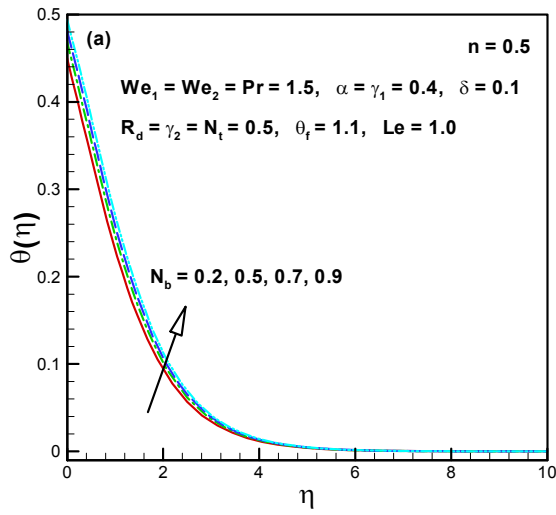
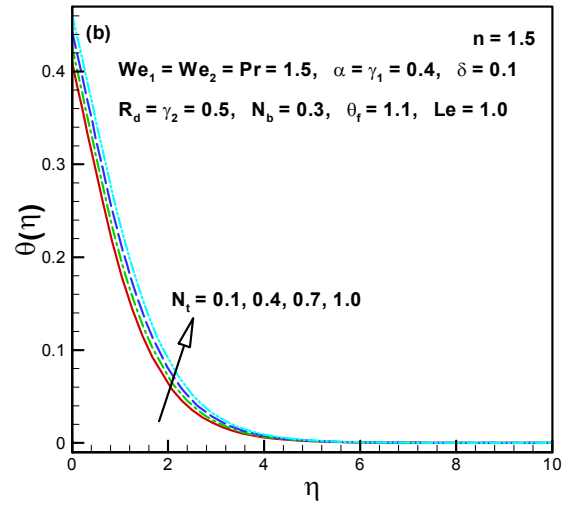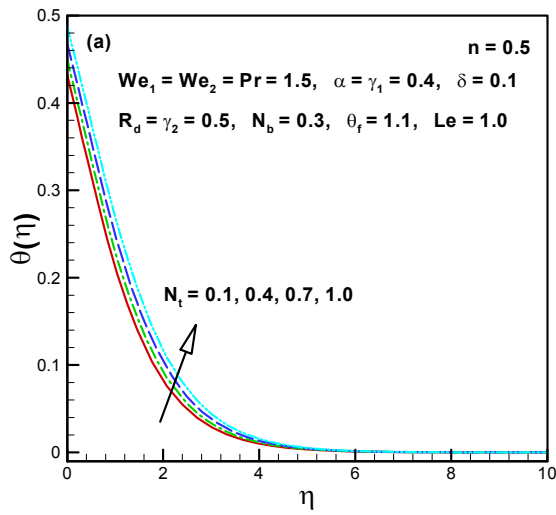**Figure 3.1(a, b):** Influence of N_b on $\theta(\eta)$.

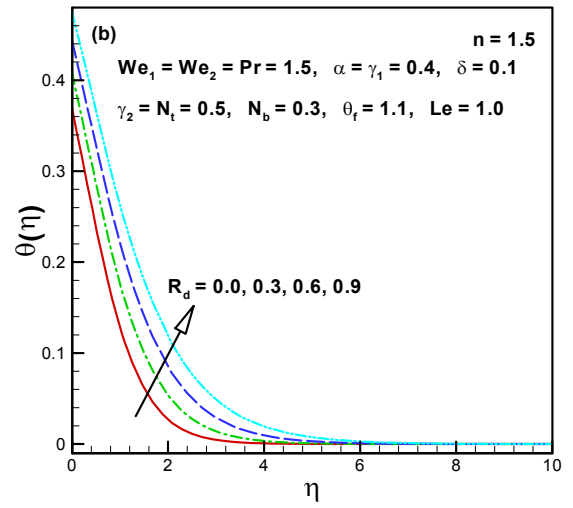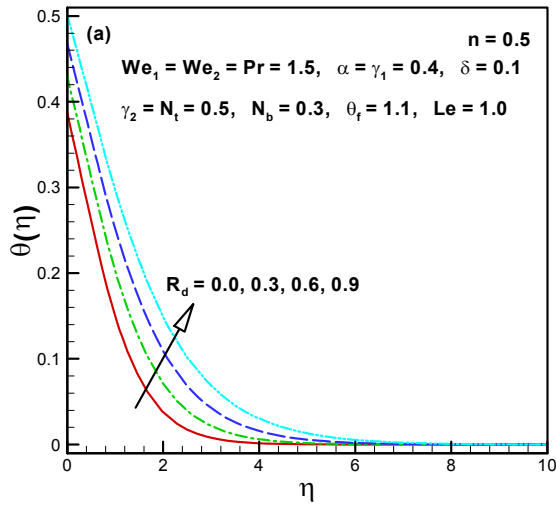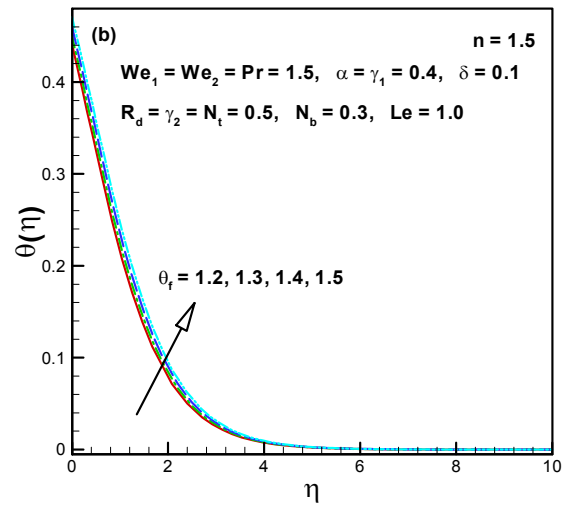**Figure 3.2(a, b):** Influence of N_t on $\theta(\eta)$.
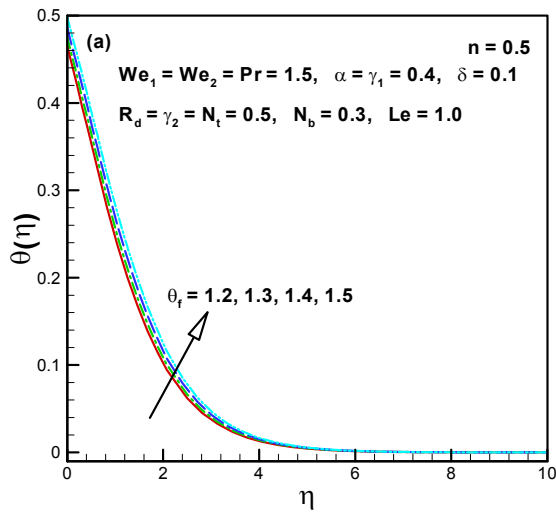
Figure 3.3(a, b): Influence of R_d on $\theta(\eta)$.
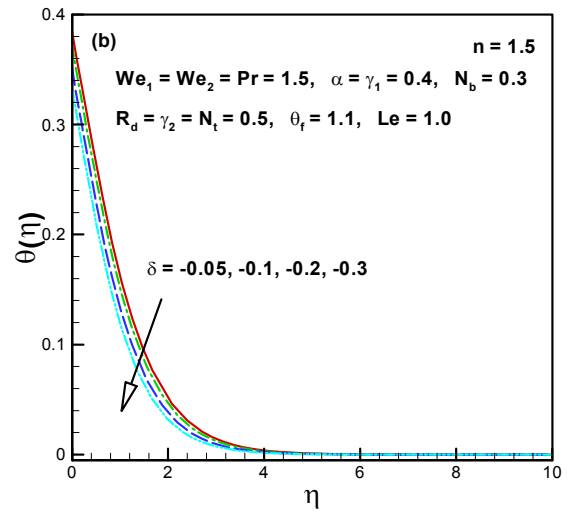

Figure 3.4(a, b): Influence of θ_f on $\theta(\eta)$.

67
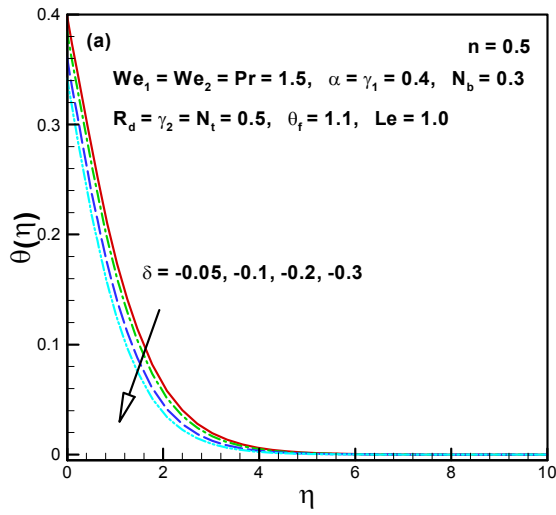
Figure 3.5(a, b): Influence of $\delta < 0$ on $\theta(\eta)$.

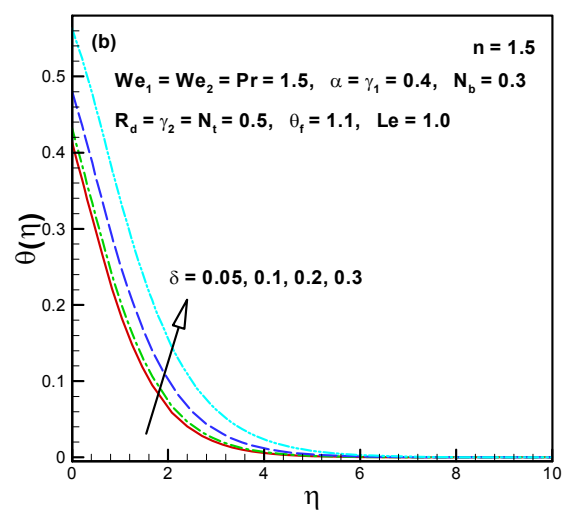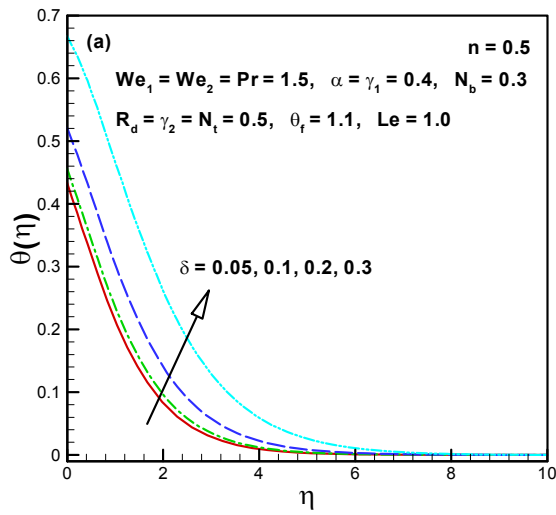**Figure 3.6(a, b):** Influence of $\delta > 0$ on $\theta(\eta)$.
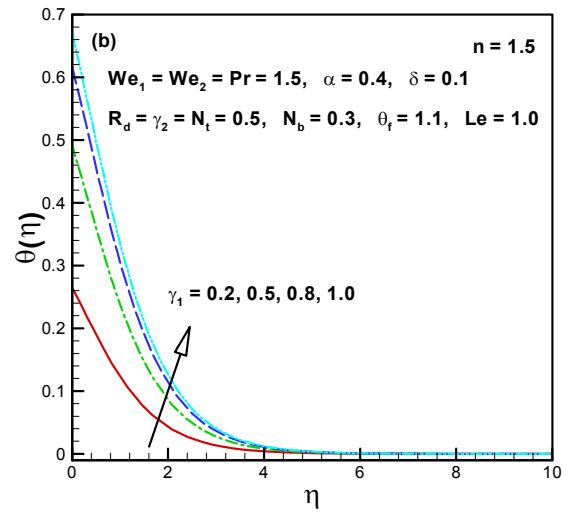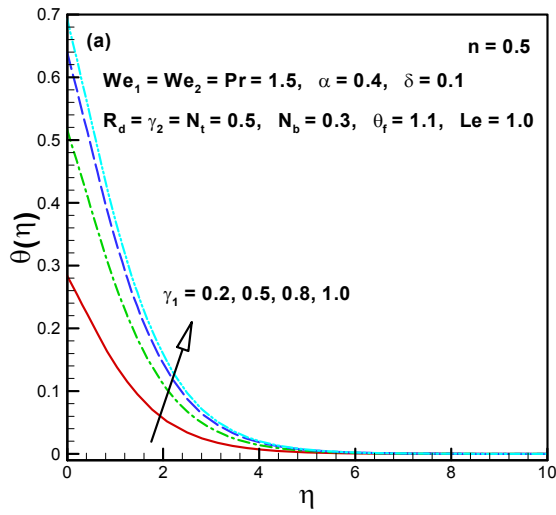
Figure 3.7(a, b): Influence of γ_1 on $\theta(\eta)$.
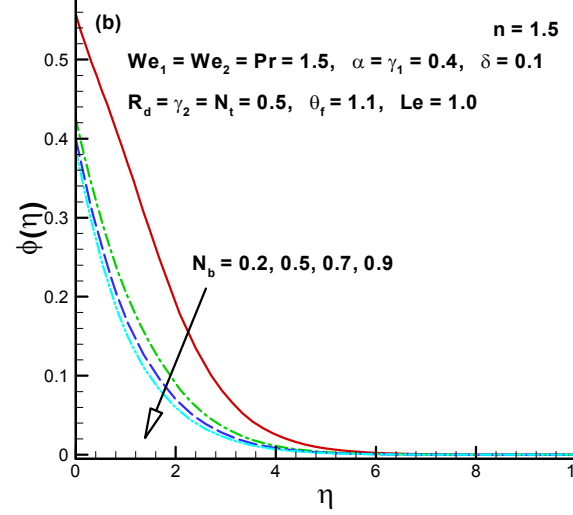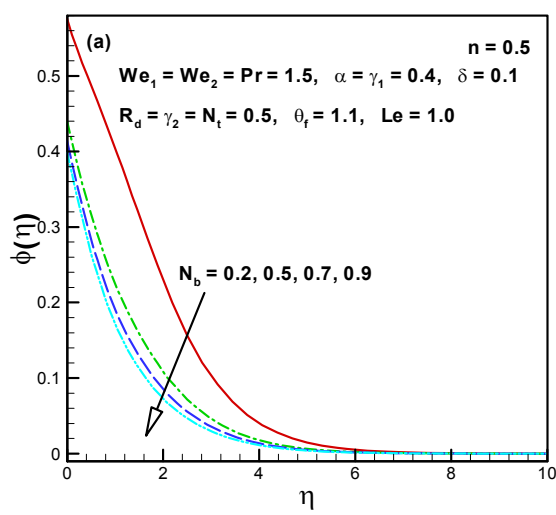
Figure 3.8(a, b): Influence of N_b on $\phi(\eta)$.
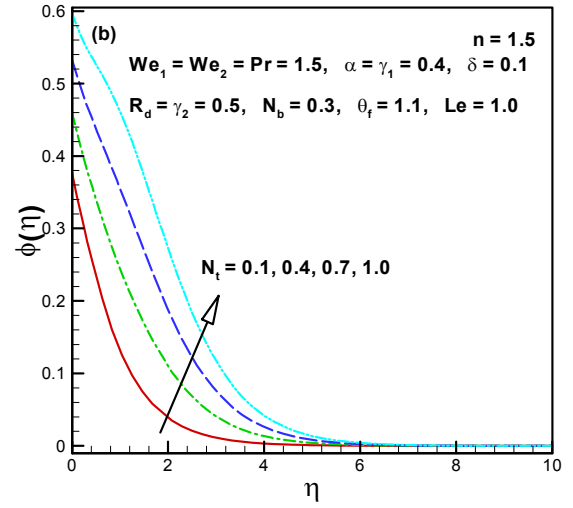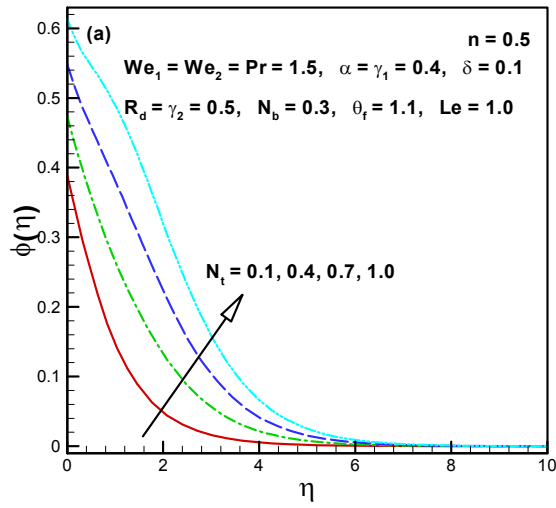
Figure 3.9(**a**, **b**): Influence of N_t on $\phi(\eta)$.
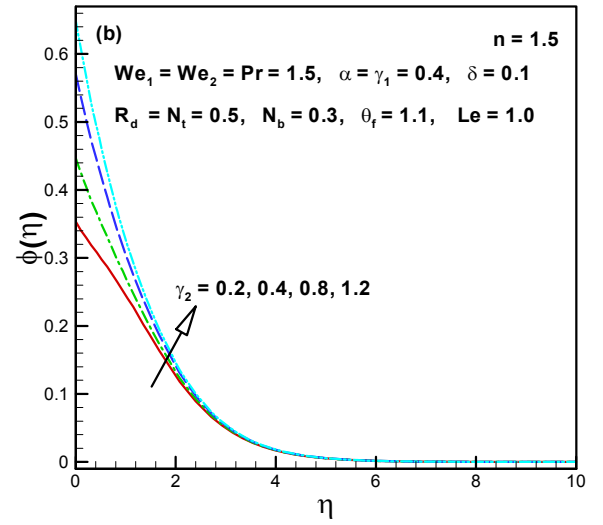
Figure 3.10(**a**, **b**): Influence of γ_2 on $\phi(\eta)$.

Figure 3.11(a, b): Influence of Le on $\phi(\eta)$.

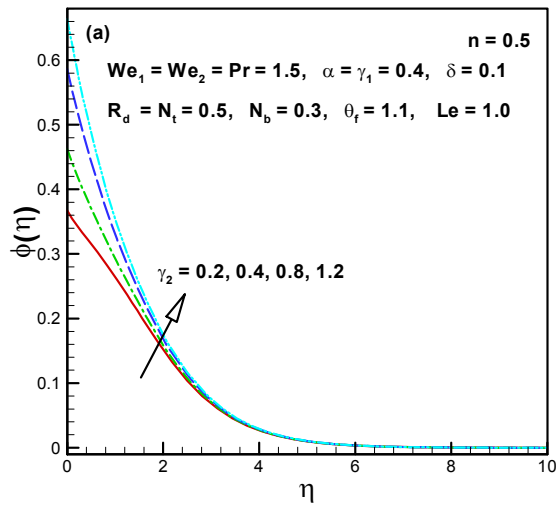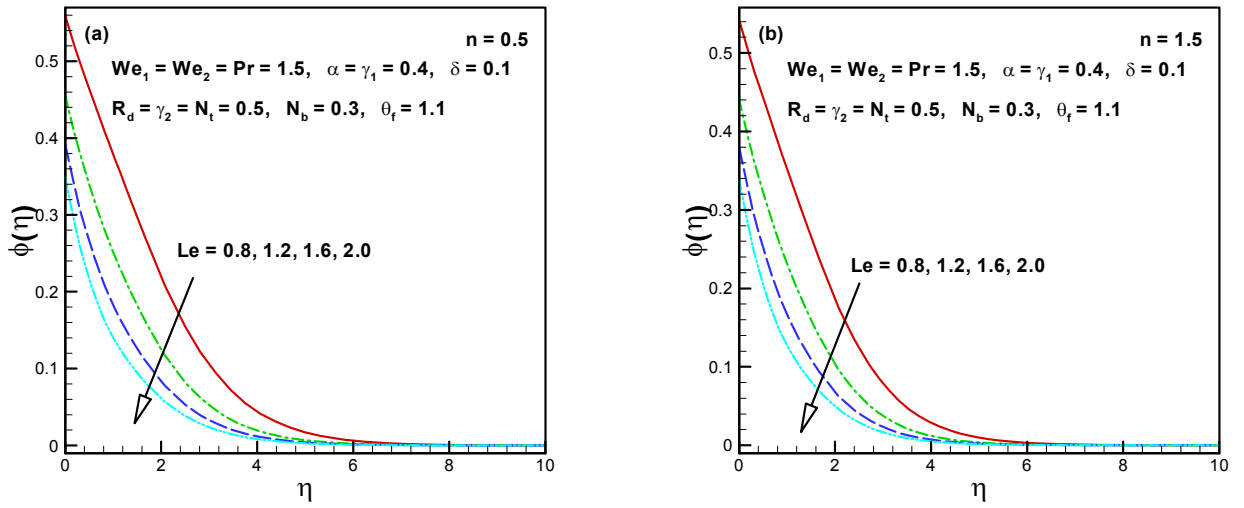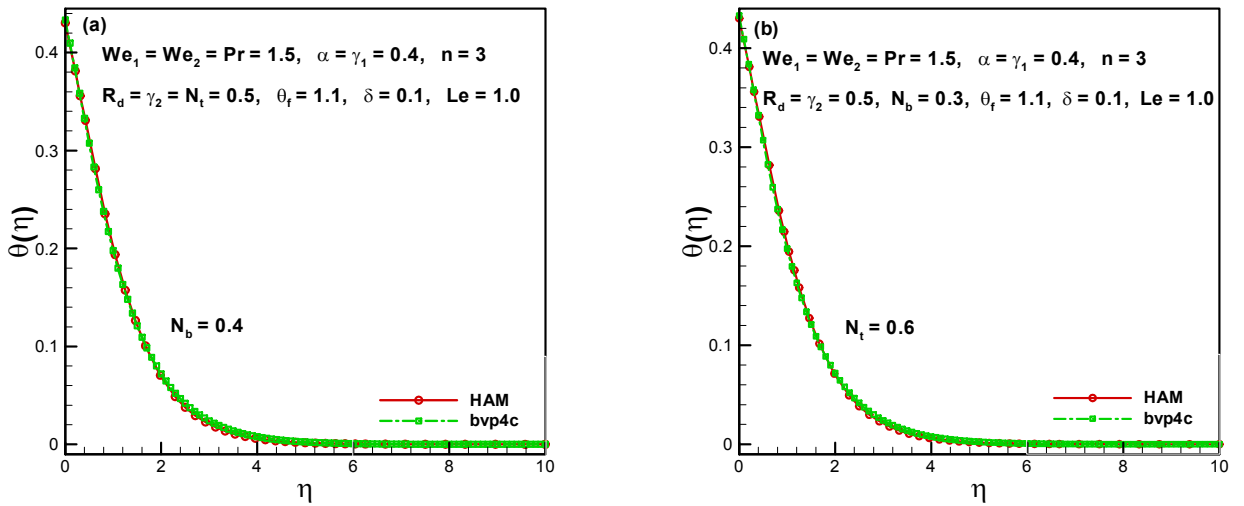**Figure 3.12(a, b):** Graphical assessment between bvp4c and HAM for N_b and N_t on $\theta(\eta)$.
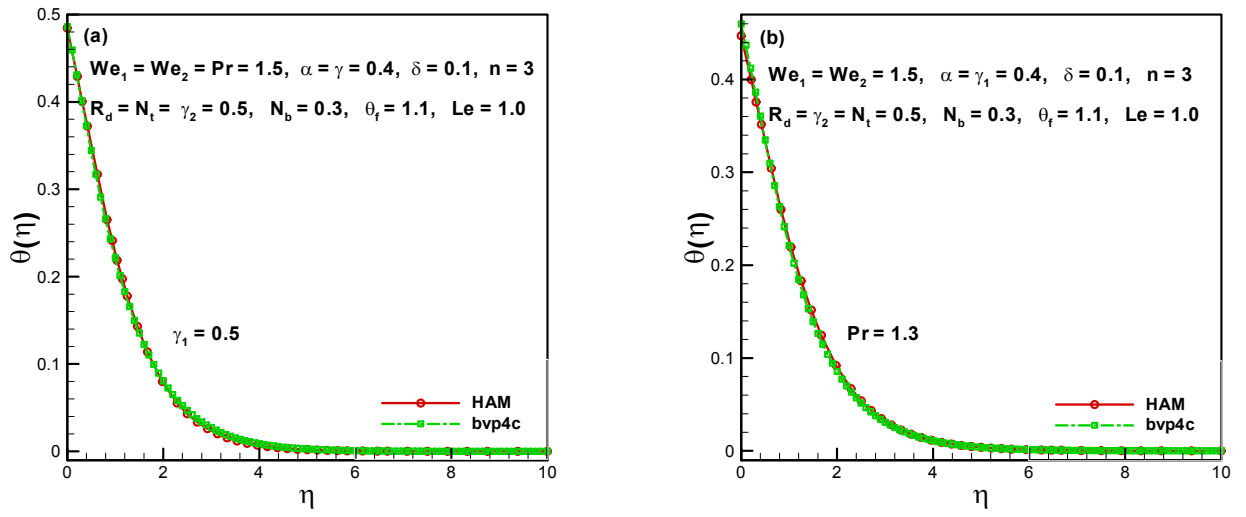
Figure 3.13(a, b): Graphical assessment between bvp4c and HAM for γ_1 and Pr on $\theta(\eta)$.

Table 3.1: Outcomes of $\left(\mathrm{Re}_x^{-\frac{1}{2}} Nu_x, \ \mathrm{Re}_x^{-\frac{1}{2}} Sh_x\right)$ for different parameters when $We_1 = We_2 = 1.5,\ \alpha = \gamma_1 = 0.4,\ R_d = 0.5,\ \theta_f = 1.1$ are fixed.

N_t	N_b	δ	Pr	γ_2	Le	$\mathrm{Re}_x^{-\frac{1}{2}} Nu_x$		$\mathrm{Re}_x^{-\frac{1}{2}} Sh_x$	
						$n = 0.5$	$n = 1.5$	$n = 0.5$	$n = 1.5$
0.5	0.3	0.1	1.5	0.5	1.0	0.341960	0.355985	0.249964	0.257590
0.6						0.338322	0.352647	0.237525	0.245339
0.7						0.334630	0.349260	0.225651	0.233611
0.8						0.330883	0.345823	0.214344	0.222408
0.5	0.4					0.338260	0.352554	0.268821	0.275984
	0.5					0.334526	0.349089	0.280138	0.287025
	0.6					0.330758	0.345591	0.287685	0.294387
	0.3	0.0				0.366450	0.376012	0.239956	0.249322
		0.2				0.303074	0.327126	0.264898	0.268906
		0.3				0.213655	0.277479	0.296008	0.287032
		0.1	1.2			0.318472	0.334126	0.227834	0.235484
			1.4			0.334979	0.349493	0.243130	0.250807
			1.6			0.348263	0.361847	0.256325	0.263875
			1.5	0.7		0.340017	0.354120	0.307357	0.317713
				0.9		0.338491	0.352645	0.351684	0.365050
				1.0		0.337845	0.352018	0.370532	0.385135
				0.5	0.8	0.342023	0.356046	0.220321	0.228760
					1.1	0.342000	0.356019	0.261808	0.269075
					1.3	0.342155	0.356154	0.281407	0.288046

Table 3.2: A comparison of $\left(\mathrm{Re}_x^{-\frac{1}{2}} Nu_x\right)$ and $\left(\mathrm{Re}_x^{-\frac{1}{2}} Sh_x\right)$ between bvp4c and HAM for different parameters when $We_1 = We_2 = R_d = 0.5$, $\alpha = 0.4$, $\theta_f = 1.1$, $\delta = 0.1$ and $n = 3$ are fixed.

N_t	N_b	Pr	γ_1	γ_2	Le	$\mathrm{Re}_x^{-\frac{1}{2}} Nu_x$		$\mathrm{Re}_x^{-\frac{1}{2}} Sh_x$	
						bvp4c	HAM	bvp4c	HAM
0.2	0.3	1.5	0.3	0.3	1.0	0.305948	0.305959	0.209633	0.209637
0.3						0.304038	0.304044	0.201220	0.201222
0.4						0.302094	0.302103	0.193054	0.193052
0.5						0.300115	0.300122	0.185130	0.185111
0.2	0.1					0.309066	0.309069	0.173196	0.173163
	0.2					0.307515	0.307514	0.200523	0.200517
	0.4					0.304366	0.304366	0.214189	0.214189
	0.3	1.4				0.301094	0.301095	0.206679	0.206681
		1.7				0.314283	0.314288	0.214797	0.214788
		2.0				0.324258	0.324252	0.221128	0.221090
		1.5	0.1			0.130296	0.130298	0.219452	0.219449
			0.2			0.229213	0.229214	0.213837	0.213841
			0.4			0.366754	0.366757	0.206396	0.206392
			0.3	0.2		0.307140	0.307149	0.151935	0.151942
				0.4		0.304926	0.304945	0.258768	0.258776
				0.5		0.304040	0.304052	0.301115	0.301111
				0.3	0.7	0.305733	0.305746	0.190679	0.190708
					0.8	0.305794	0.305800	0.198174	0.198188
					1.2	0.218066	0.218049	0.306115	0.306117

Table 3.3: A comparison of $-f''(0)$ in limiting sense when $We_1 = We_2 = 0$ and $n = 1$ are fixed.

α	$-f''(0)$			
	Wang [117]	Liu and Anderson [118]	Present (bvp4c)	Present (HAM)
0.0	1	1	1	1
0.25	1.048813	1.048813	1.0488130	1.0488131
0.50	1.093097	1.093096	1.0930954	1.0930943
0.75	1.134485	1.134486	1.1344854	1.1344858
1.0	1.173720	1.173721	1.1737199	1.1737201

Table 3.4: A comparison of $-g''(0)$ in limiting sense when $We_1 = We_2 = 0$ and $n = 1$ are fixed.

α	$-g''(0)$			
	Wang [117]	Liu and Anderson [118]	Present(bvp4c)	Present (HAM)
0.0	0	0	0	0
0.25	0.194564	0.194565	0.1945652	0.1945617
0.50	0.465205	0.465206	0.4652058	0.4652047
0.75	0.794622	0.794619	0.7946180	0.7946184
1.0	1.173720	1.173721	1.1737199	1.1737201

Chapter 4

Influence of Thermal Radiation on Magnetohydrodynamic 3D Flow of Carreau Nanofluid

This chapter investigates 3D radiative flow of a magneto Carreau nanofluid over a bidirectional stretched surface. Additionally, the aspect of the nanoparticles mass flux condition is occupied. Practically, this recently recommended approach is more realistic where we assume that the nanoparticle flux is zero and nanoparticle fraction adjusts itself on the boundaries accordingly. With this convincing and revised relation, the features of Buongiorno's relation on 3D Carreau liquid can be applied in a more effective way. The appropriate transformations are employed to alter the PDEs into ODEs and then tackled numerically by employing bvp4c scheme. The numerous consequence of scheming parameters on the velocity components, temperature and concentration fields is portrayed graphically and deliberated in detail. The numerical outcomes for local skin friction coefficients and the wall temperature gradient for nanoliquid are intended and presented through tables. The outcomes conveyed here manifest that the impact of Brownian motion parameter on the rate of heat transfer for nanoliquids becomes negligible for the recently recommended revised relation. It is notable that the magnetic parameter (M) is a diminishing function to the velocity components $f'(\eta)$ and $g'(\eta)$, while it enhances the temperature of Carreau liquid for both shear thinning/thickening liquids. Moreover, it is noted

that the influence of the Brownian motion (N_b) and thermophoresis parameter (N_t) on the concentration of the Carreau nanofluid is quite opposite. For authentication of the present relation, the achieved results are distinguished with earlier research works in specific cases and marvelous agreement has been noted.

4.1 Description of the Problem

Consider the steady 3D flow of an electrical conducting forced convective Carreau nanofluid over a bidirectional stretched surface. The flow is persuaded owing to stretching surface in two horizontal $x-$and $y-$directions with velocity $u = ax$ and $v = by$, respectively, where a and b are stretching rates and the fluid flow occupies the region in the domain $z > 0$. The magnetic field of strength (B_0) is imposed parallel to $z-axis$. The notion of induced magnetic and electric fields are insignificant considered here when compared to the applied magnetic field. This postulation is effective only for the insignificant magnetic Reynolds number. Moreover, the temperature of the nanoliquid at the surface T_w is superior than temperature of nanoliquid distant from the stretched surface. The Carreau nanoliquid relation in view of overhead declared assumptions are given below:

$$\frac{\partial u}{\partial x} + \frac{\partial v}{\partial y} + \frac{\partial w}{\partial z} = 0, \tag{4.1}$$

$$u\frac{\partial u}{\partial x} + v\frac{\partial u}{\partial y} + w\frac{\partial u}{\partial z} = \nu\frac{\partial^2 u}{\partial z^2}\left[1 + \Gamma^2\left(\frac{\partial u}{\partial z}\right)^2\right]^{\frac{n-1}{2}}$$
$$+\nu(n-1)\Gamma^2\frac{\partial u}{\partial z}\left[1 + \Gamma^2\left(\frac{\partial u}{\partial z}\right)^2\right]^{\frac{n-3}{2}} - \frac{\sigma B_0^2}{\rho_f}u, \tag{4.2}$$

$$u\frac{\partial v}{\partial x} + v\frac{\partial v}{\partial y} + w\frac{\partial v}{\partial z} = \nu\frac{\partial^2 v}{\partial z^2}\left[1 + \Gamma^2\left(\frac{\partial v}{\partial z}\right)^2\right]^{\frac{n-1}{2}}$$
$$+\nu(n-1)\Gamma^2\frac{\partial v}{\partial z}\left[1 + \Gamma^2\left(\frac{\partial v}{\partial z}\right)^2\right]^{\frac{n-3}{2}} - \frac{\sigma B_0^2}{\rho_f}v, \tag{4.3}$$

$$u\frac{\partial T}{\partial x} + v\frac{\partial T}{\partial y} + w\frac{\partial T}{\partial z} = \alpha_1\frac{\partial^2 T}{\partial z^2} + \tau\left[D_B\frac{\partial C}{\partial z}\frac{\partial T}{\partial z} + \frac{D_T}{T_\infty}\left(\frac{\partial T}{\partial z}\right)^2\right] - \frac{1}{(\rho c)_f}\frac{\partial q_r}{\partial z}, \tag{4.4}$$

$$u\frac{\partial C}{\partial x} + v\frac{\partial C}{\partial y} + w\frac{\partial C}{\partial z} = D_B\frac{\partial^2 C}{\partial z^2} + \frac{D_T}{T_\infty}\frac{\partial^2 T}{\partial z^2}. \tag{4.5}$$

The boundary conditions of the existing flow problems are

$$u = U_w(x) = ax, \quad v = V_w(y) = by, \quad w = 0,$$

$$T = T_w, \quad D_B\frac{\partial C}{\partial z} + \frac{D_T}{T_\infty}\frac{\partial T}{\partial z} = 0 \quad \text{at} \quad z = 0, \tag{4.6}$$

$$u \to 0, \quad v \to 0, \quad T \to T_\infty, \quad C \to C_\infty \quad \text{as} \quad z \to \infty. \tag{4.7}$$

Here σ is the electrical conductivity.

4.1.1 Appropriate Conversions

In view of dimensionless transformation variables

$$\theta(\eta) = \frac{T - T_\infty}{T_w - T_\infty}, \quad \phi = \frac{C - C_\infty}{C_\infty}. \tag{4.8}$$

and Eq. (2.27) (cf. Chapter 2), the incompressibility condition is automatically satisfied and Eqs. $(4.2) - (4.7)$ yield

$$f'''[1 + We_1^2 f''^2]^{\frac{n-3}{2}}[1 + nWe_1^2 f''^2] - f'^2 + f''(f + g) - M^2 f' = 0, \tag{4.9}$$

$$g'''[1 + We_2^2 g''^2]^{\frac{n-3}{2}}[1 + nWe_2^2 g''^2] - g'^2 + g''(f + g) - M^2 g' = 0, \tag{4.10}$$

$$(1 + R_d)\theta'' + \Pr(f + g)\theta' + \Pr[N_b\theta'\phi' + N_t\theta'^2] = 0, \tag{4.11}$$

$$\phi'' + \Pr Le(f + g)\phi' + \left(\frac{N_t}{N_b}\right)\theta'' = 0, \tag{4.12}$$

$$f(0) = 0, \quad g(0) = 0, \quad f'(0) = 1, \quad g'(0) = \alpha,$$

$$\theta(0) = 1, \quad N_b\phi'(0) + N_t\theta'(0) = 0, \tag{4.13}$$

$$f' \to 0, \quad g' \to 0, \quad \theta \to 0 \quad \phi \to 0 \quad \text{as} \quad \eta \to \infty. \tag{4.14}$$

Here, $M \left(= \sqrt{\frac{\sigma B_0^2}{\rho_f a}} \right)$ reports the magnetic parameter, $N_b \left(\frac{\tau D_B C_\infty}{\nu} \right)$ the Brownian motion parameter and $N_t \left(= \frac{D_T (T_w - T_\infty)}{\nu T_\infty} \right)$ the thermophoresis parameter.

4.2 Engineering and Industrial Quantities of Interest

From the physical point of view, the quantities of industrial and engineering interest in materials processing are the skin friction coefficients and heat transfer coefficient which may be defined below.

4.2.1 The Skin Friction Coefficients

Let

$$C_{fx} = \frac{\tau_{xz}}{\frac{1}{2}\rho U_w^2} \quad \text{and} \quad C_{fy} = \frac{\tau_{yz}}{\frac{1}{2}\rho U_w^2}, \tag{4.15}$$

and the dimensionless quantities of above expressions

$$\frac{1}{2} C_{fx} \operatorname{Re}_x^{\frac{1}{2}} = f''(0)[1 + We_1^2 f''^2]^{\frac{n-1}{2}}, \tag{4.16}$$

$$\frac{1}{2} \left(\frac{U_w}{V_w} \right) C_{fy} \operatorname{Re}_x^{\frac{1}{2}} = g''(0)[1 + We_2^2 g''^2]^{\frac{n-1}{2}}, \tag{4.17}$$

4.2.2 The local Nusselt number

Let

$$Nu_x = - \frac{x}{(T_w - T_\infty)} \left. \frac{\partial T}{\partial z} \right|_{z=0} + \frac{x q_r}{k (T_w - T_\infty)}, \tag{4.18}$$

and in the dimensionless variable is

$$\operatorname{Re}_x^{-\frac{1}{2}} Nu_x = - (1 + R_d) \theta'(0). \tag{4.19}$$

4.3 Graphical Illustration and Analysis

The foremost attention here is to inspect the features of nanoparticles mass flux theory for 3D magnetohydrodynamic (MHD) flow of Carreau nanofluid over a bidirectional stretching surface. Widespread numerical computation, namely, bvp4c has been worked out for the exploration of

the influential parameters on the velocity components $f'(\eta)$ and $g'(\eta)$, temperature $\theta(\eta)$ and concentrations $\phi(\eta)$ fields. The graphs are portrayed and the discrepancy of the local skin friction coefficients $\left(\frac{1}{2}C_{fx}\operatorname{Re}_x^{\frac{1}{2}}, \ \frac{1}{2}\left(\frac{U_w}{V_w}\right)C_{fy}\operatorname{Re}_x^{\frac{1}{2}}\right)$ and the local Nusselt number $\left(\operatorname{Re}_x^{-\frac{1}{2}}Nu_x\right)$ are reported in tabular arrangement and deliberated in detail.

Figures 4.1(a − d) are plotted to visualize the characteristics of magnetic parameter (M) on the nanoliquid velocity components $f'(\eta)$ and $g'(\eta)$ for shear thinning and shear thickening liquids. We perceived a diminishing behavior in the nanoliquid velocity profiles and associated momentum boundary layer thickness with growing values of M. Physically, this happens because of fact that the Lorentz force boosts up for higher values of M which yields much struggle to the fluid. Therefore, the complicity between the nanoparticles intensifies. This phenomenon reduces the associated momentum boundary layer. Therefore, the velocities of the nanoliquid decline.

Figures 4.2(a − d) demonstrate the impact of local Weissenberg number (We_1) on the nanoliquid temperature $\theta(\eta)$ and concentrations $\phi(\eta)$ profiles. It is manifest from these figures that the nanoliquid temperature and concentration profiles enhance with the augmented values of We_1 for $(n = 0.5)$ while the reverse trend is observed for the $(n = 1.5)$. Noticeably, We_1 is the relation of viscous to the elastic forces, so strengthening in the values of We_1 reasons an amplification in the liquid viscosity. This consequence augments the temperature of Carreau liquid for $(n < 1)$ and reverse trend is detected for $(n > 1)$. The properties of nanoliquid temperature and concentration profiles for distinct values of the ratio of stretching rates parameter (α) are presented through **figures 4.3(a − d)**. It is estimated from these sketches that $\theta(\eta)$ and $\phi(\eta)$ decline with the boosted values of α for shear thinning and shear thickening liquids. The augmented values of α the nanoliquid velocity in $y − direction$ leads, then the nanoliquid velocity in $x − direction$ owing to the collision of the particles which result in a reduction in the concentration field and concentration thickness of the boundary layer. **Figures 4.4(a − d)** spectacle the impact of magnetic parameter (M) on the nanoliquid temperature and concentration profiles for both $(n = 0.5).$and $(n = 1.5)$. The nanoliquid temperature and concentration profiles decay when M intensified. Physically, this is owing to the fact that the Lorentz force is a resistive force which opposes the liquid motion due to which nanoliquid temperature profile enhances. **Figures 4.5(a − d)** are drafted to deliberate the variations in the nanoliquid tem-

perature and concentration distributions under the influence of the radiation parameter (R_d). It can be reported from these sketches that the nanoliquid $\theta(\eta)$ and $\phi(\eta)$ enhance for higher R_d. Physically, by strengthening the R_d offers more heat to the nanoliquid and subsequently, the thickness of the thermal boundary layer is intensified. Thus, the radiation plays a key role in boosting the rate of heat transfer of the nanoliquid. **Figures 4.6(a − d)** are sketched to interpret the aspects of thermophoresis parameter (N_t) on the nanoliquid temperature $\theta(\eta)$ and concentration $\phi(\eta)$ distributions. Here, the temperature and concentration of the nanoliquid across the thickness of boundary layer rise with intensifying values of N_t. Physically, this is because of the fact that the difference between the temperature of wall (T_w) and the reference temperature (T_∞) rise which intensify the nanoliquid temperature field. Moreover, in the flow domain of the particulate structure, there is a temperature gradient in hotter regions which causes small elements incline to isolated quicker. Consequently, the surface temperature of the nanoliquid and its thickness of boundary layer enhance. Additionally, growing values of N_t physically means that the small nanoparticles are pulled away from the warm surface to the cold surface. Therefore, the higher number of small nanoparticles is dragged away from the warm surface due to which concentration of the nanoliquid declines. **Figures 4.7(a − d)** demonstrate the domination of Prandtl number (Pr) on the nanoliquid temperature and concentration distributions. From these graphs we found that boosting values of Pr decline the temperature and concentration distributions. The greater Pr has lesser thermal diffusivity. Hence, the temperature of the nanoliquid and the thermal boundary layer increase and decline $\theta(\eta)$ when Pr is enlarged. **Figures 4.8(a, b)** and **4.9(a, b)** are drafted to deliberate the variations in the nanoliquid temperature and concentration distributions under the influence of the Brownian motion (N_b) and Lewis number (Le), respectively. Here a fall in the nanoliquid temperature and concentration profiles for the rising value of N_b and Le is noted. In fact, Le is inversely proportional to the Brownian diffusion coefficient (D_B). Here $\phi(\eta)$ falloffs owing to small diffusivity influence when Le intensifies.

4.3.1 Tabular Representations

The value of $\left(\frac{1}{2}C_{fx}\operatorname{Re}_x^{\frac{1}{2}}, \frac{1}{2}\left(\frac{U_w}{V_w}\right)C_{fy}\operatorname{Re}_x^{\frac{1}{2}} \right)$ and $\left(\operatorname{Re}_x^{-\frac{1}{2}}Nu_x \right)$ of Carreau nanoliquid at the boundary of the stretched sheet are presented by **Tables 4.1** and **4.2**. By keeping the other

nonlinear material parameters fixed. An enhancement in M and α correspond to an improvement in $\left(\frac{1}{2} C_{fx} \operatorname{Re}_x^{\frac{1}{2}}, \; \frac{1}{2} \left(\frac{U_w}{V_w} \right) C_{fy} \operatorname{Re}_x^{\frac{1}{2}} \right)$. Additionally, it appears from **Table 4.2** that the magnitude of rate of heat transfer of nanoliquid enlarged with increasing values of Pr and R_d; however, N_t and Le have reverse trend.

4.3.2 Confirmation of Numerical Outcomes

Tables 4.3, **4.4** and **4.5** depict an assessment of the numerical values for the velocity gradients $(-f''(0), \; -g''(0))$ and Nusselt number $\left(-\theta'(0) \right)$ with formerly existing outcomes for different values of α. These tables initiated a tremendous settlement of the existent outcomes with present ones. This demonstrates the legitimacy of the current analysis along with the admirable precision of numerically (bvp4c) and analytically (HAM).
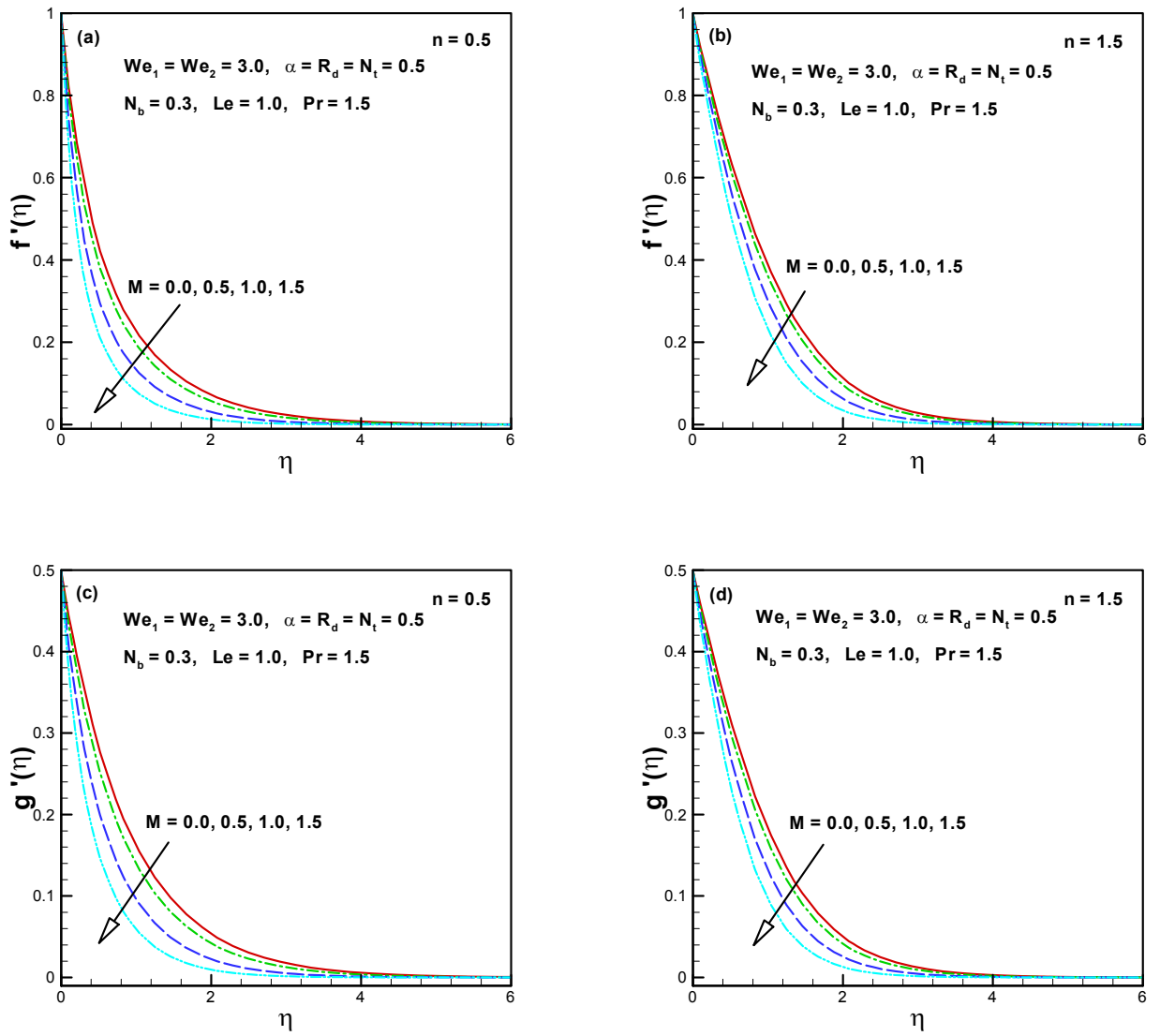
Figure 4.1(a − d): Influence of M on $f'(\eta)$ and $g'(\eta)$.
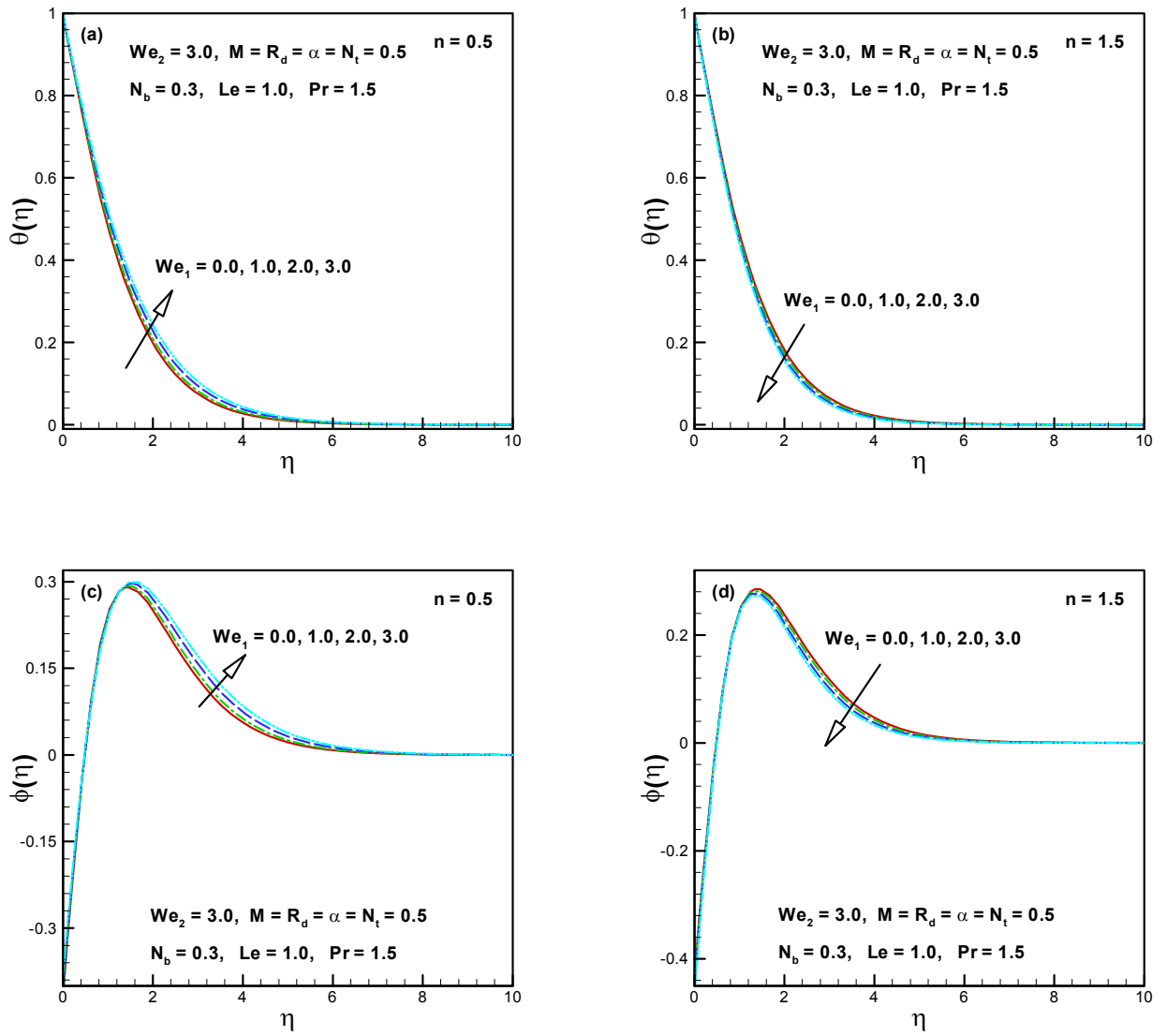
Figure 4.2(a − d): Influence of We_1 on $\theta(\eta)$ and $\phi(\eta)$.

Figure 4.3(a − d): Influence of α on $\theta(\eta)$ and $\phi(\eta)$.

Figure 4.4(a − d): Influence of M on $\theta(\eta)$ and $\phi(\eta)$..

Figure 4.5(a − d): Influence of R_d on $\theta(\eta)$ and $\phi(\eta)$..
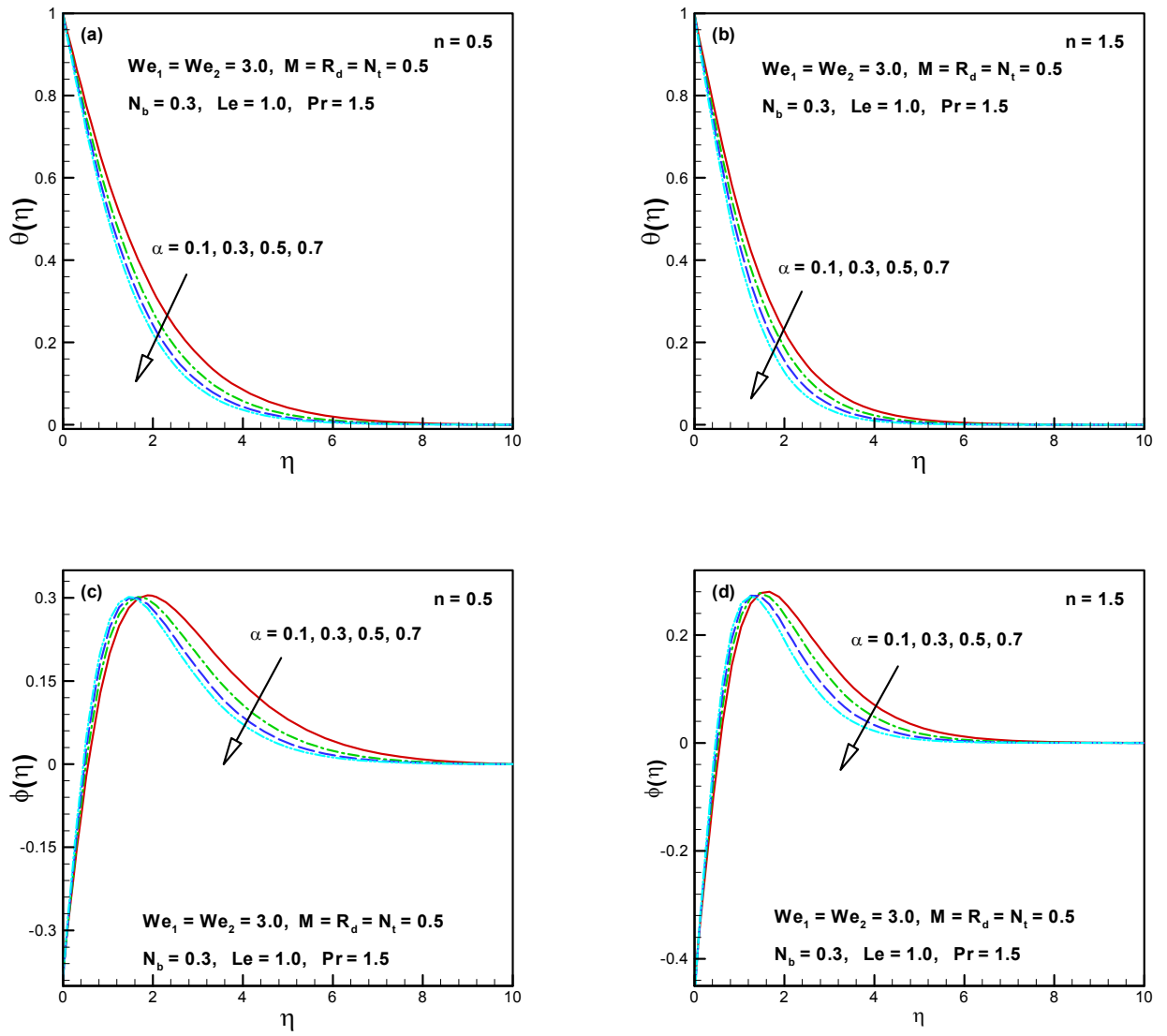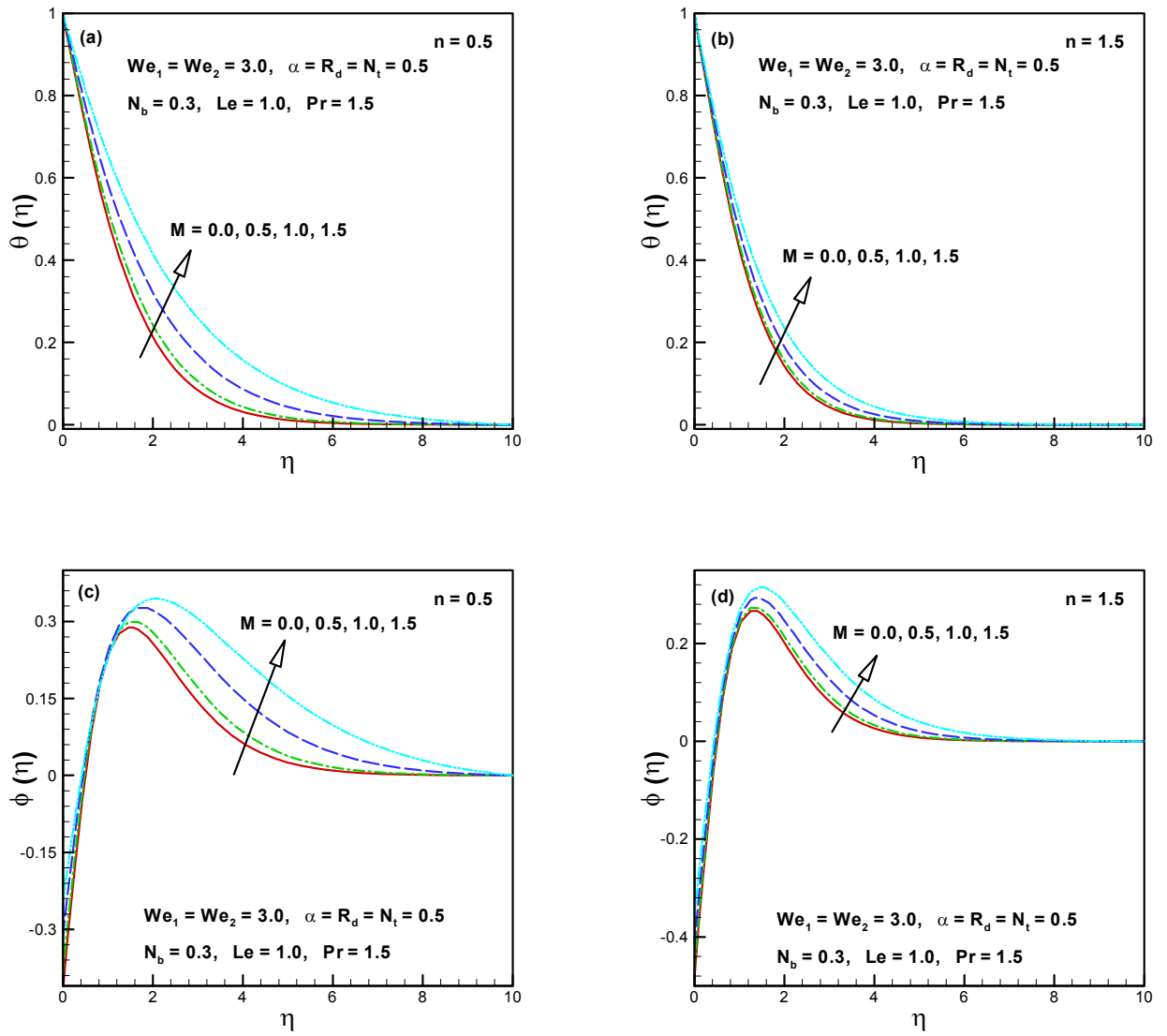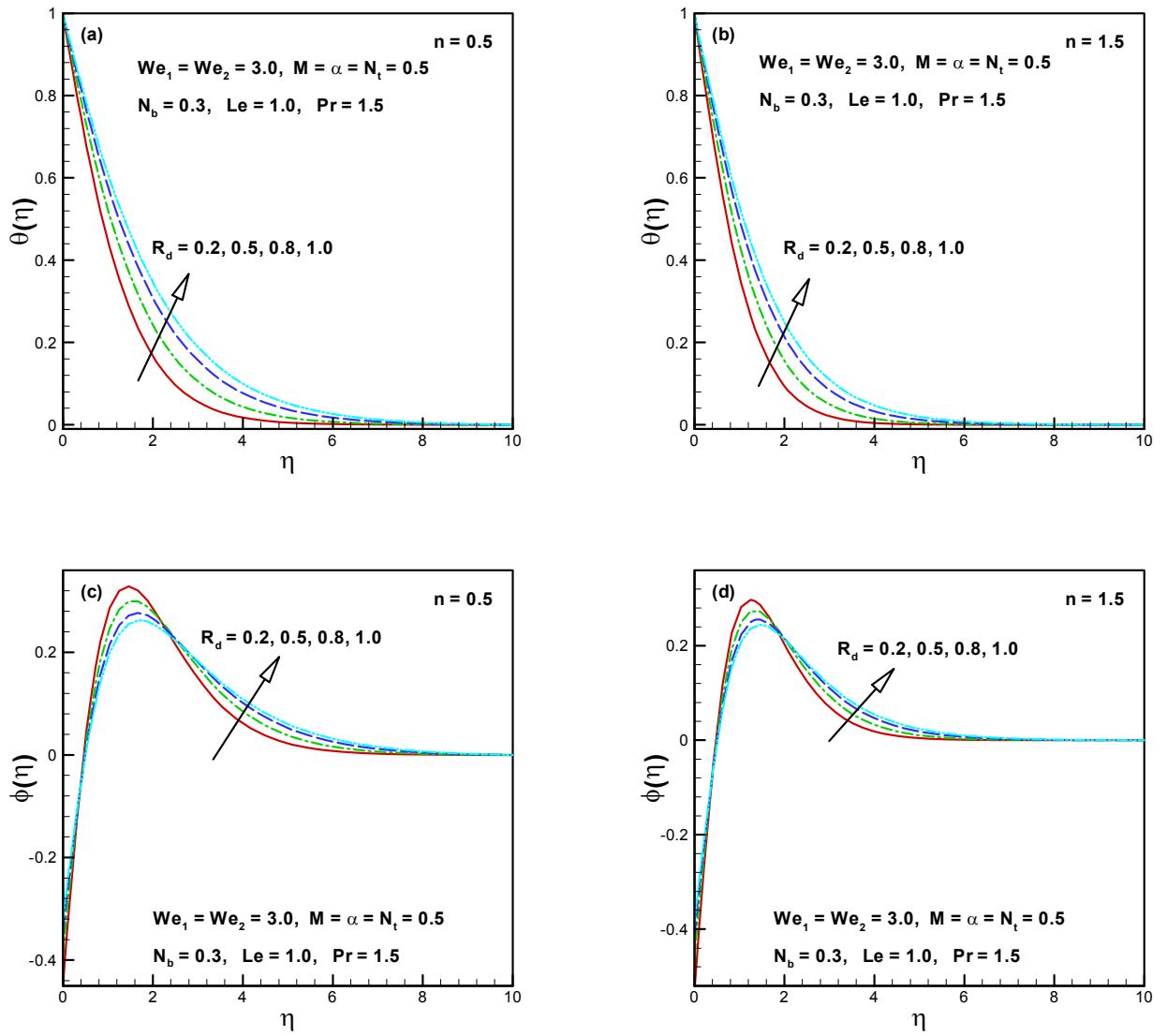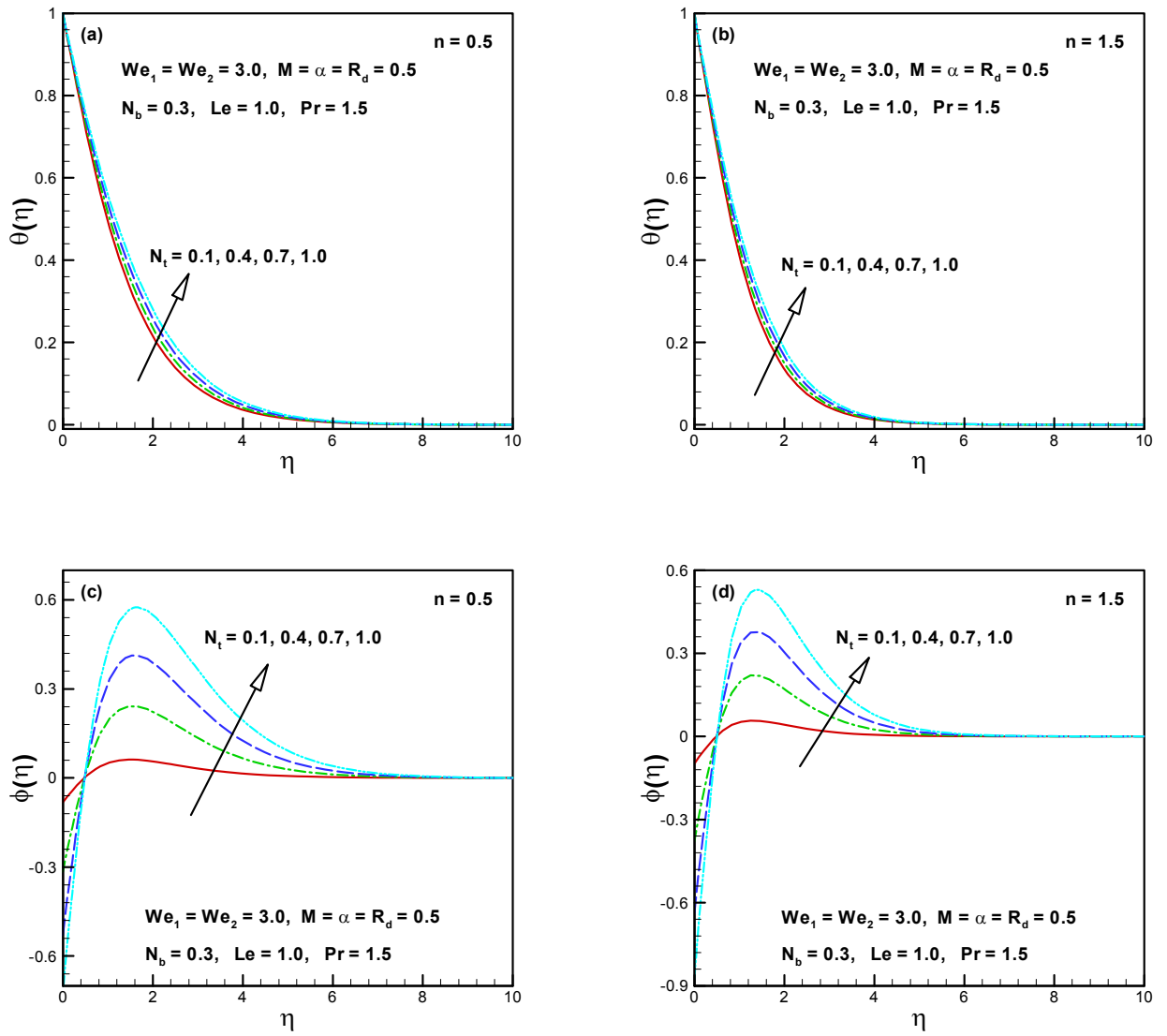
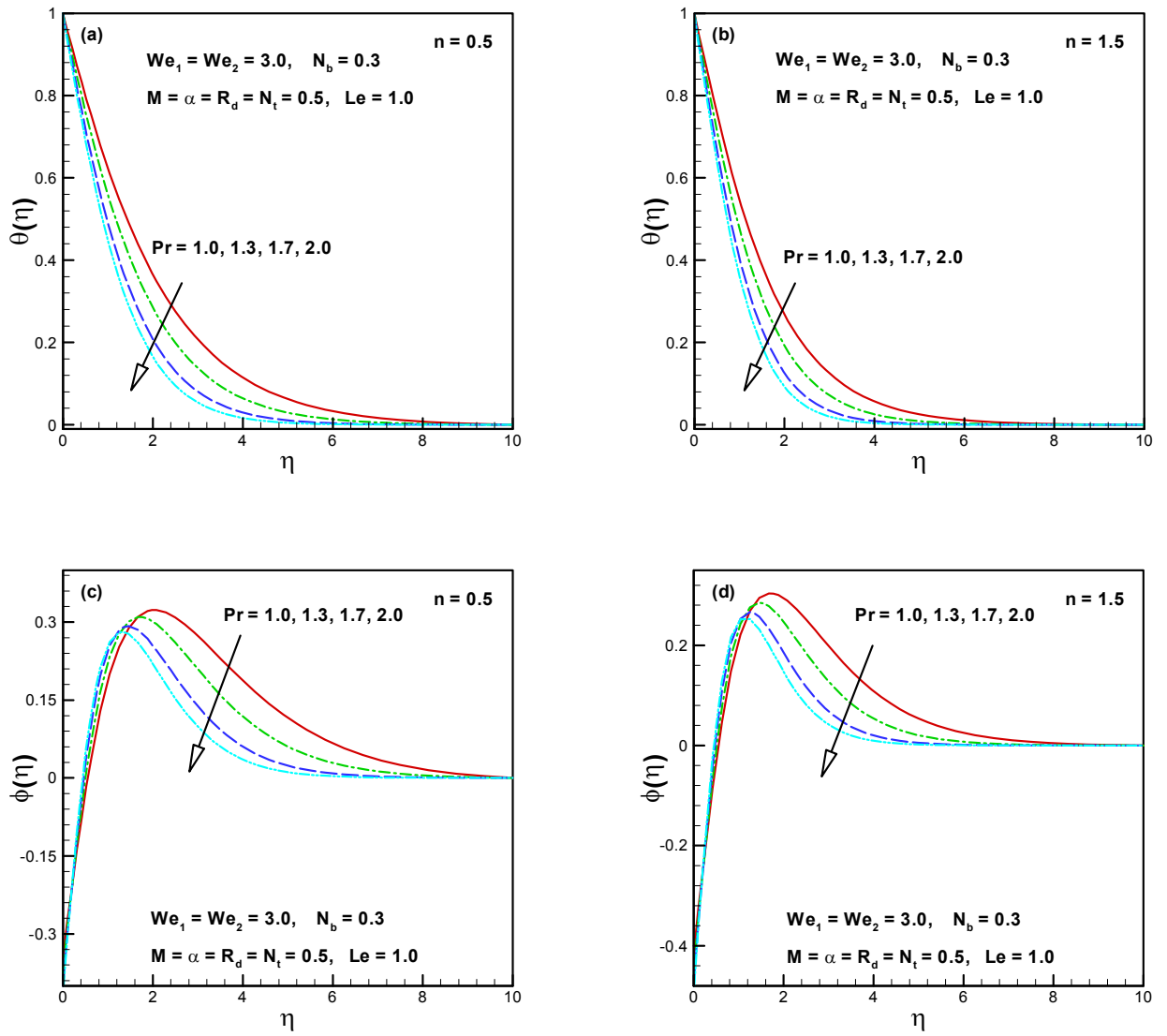**Figure 4.6(a − d):** Influence of N_t on $\theta(\eta)$ and $\phi(\eta)$.

Figure 4.7(a − d): Influence of Pr on $\theta(\eta)$ and $\phi(\eta)$.
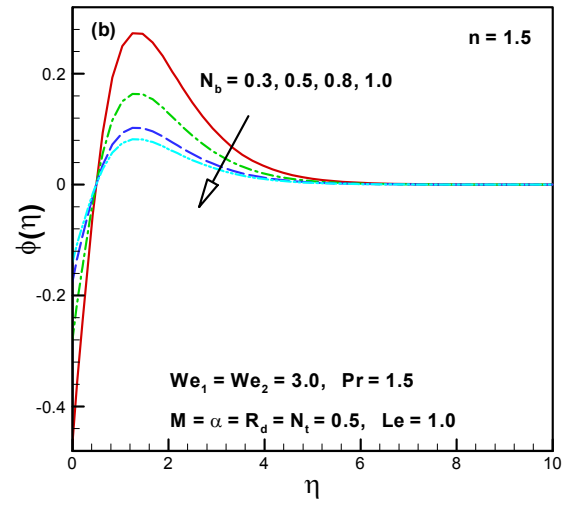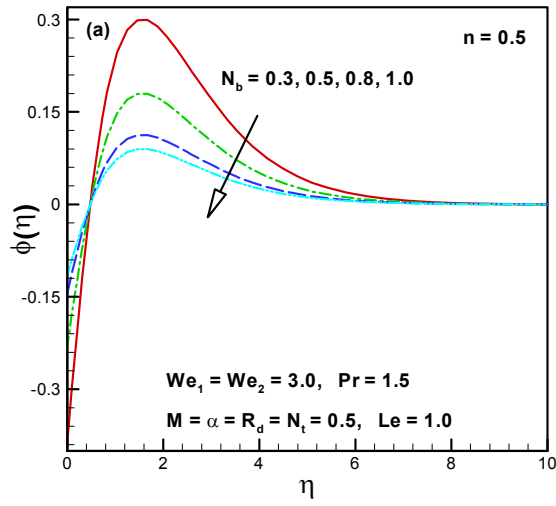
Figure 4.8(a − d): Influence of N_b on $\phi(\eta)$.
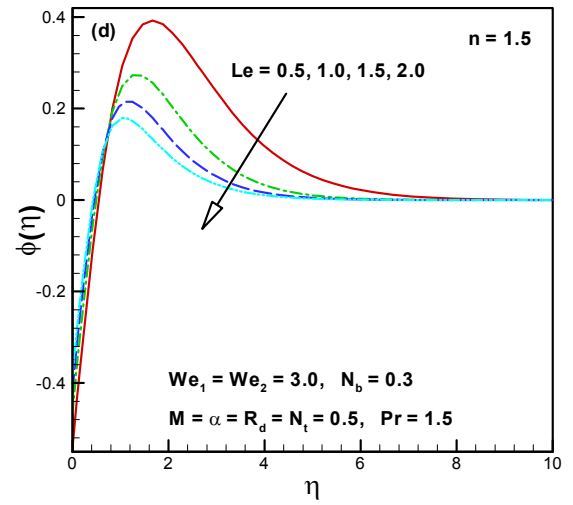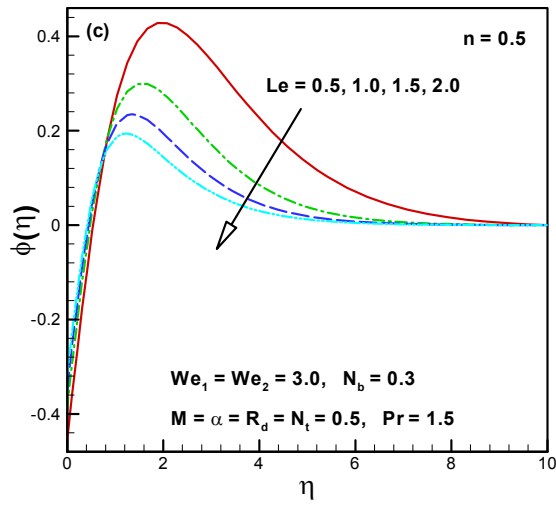
Figure 4.9(a − d): Influence of Le on $\phi(\eta)$.

Table 4.1: Outcomes of $\left(\frac{1}{2}C_{fx}\operatorname{Re}_x^{\frac{1}{2}}, \frac{1}{2}C_{fy}\left(\frac{U_w}{V_w}\right)\operatorname{Re}_x^{\frac{1}{2}}\right)$ for different values of α and M when $We_1 = We_2 = 2.0$ are fixed.

M	α	$\frac{1}{2}C_{fx}\operatorname{Re}_x^{\frac{1}{2}}$		$\frac{1}{2}C_{fy}\left(\frac{U_w}{V_w}\right)\operatorname{Re}_x^{\frac{1}{2}}$	
		$n = 0.5$	$n = 1.5$	$n = 0.5$	$n = 1.5$
0.5	0.5	-1.896547	-4.321695	-0.6051041	-0.9147802
1.0		-2.570714	-6.655255	-0.8570421	-1.4181890
1.5		-3.555854	-10.821100	-1.2354530	-2.2880650
2.0		-4.755225	-17.073510	-1.7073990	-3.5625300
0.5	0.6	-1.926160	-4.445858	-0.8136476	-1.3608700
	0.8	-1.980438	-4.700804	-1.3470240	-2.7344020
	1.0	-2.029327	-4.964101	-2.0293270	-4.9641010

Table 4.2: Outcomes of $\left(\mathrm{Re}_x^{-\frac{1}{2}} Nu_x\right)$ for different values of the R_d, Pr, N_t and Le when $We_1 = We_2 = 2.0$, $N_b = 0.3$ and $M = \alpha = 0.5$ are fixed.

R_d	Pr	N_t	Le	$\mathrm{Re}_x^{-\frac{1}{2}} Nu_x$	
				$n = 0.5$	$n = 1.5$
0.5	0.7	0.5	1.0	0.544664	0.622229
0.8				0.572512	0.654022
1.2				0.607435	0.691702
1.5				0.633160	0.718299
0.5	1.0			0.699751	0.794837
	1.5			0.914065	1.026980
	2.0			1.086800	1.211240
	0.7	0.8		0.529463	0.605695
		1.0		0.519503	0.594830
		1.3		0.504833	0.578781
		0.5	1.5	0.539958	0.617056
			2.0	0.536784	0.613523
			2.5	0.534456	0.610905

Table 4.3: A comparison of $-f''(0)$ between bvp4c and HAM for numerous values of α in limiting cases when $We_1 = We_2 = M = 0$ and $n = 1$.

α	$-f''(0)$			
	Ariel(HPM) [115]	Ariel(Exact) [115]	Present(bvp4c)	Present(HAM)
0	1	1	1	1
0.1	1.017027	1.020264	1.020264	1.020264
0.2	1.034587	1.039497	1.039497	1.039495
0.3	1.057470	1.057956	1.057956	1.057955
0.4	1.070529	1.075788	1.075788	1.075785
0.5	1.088662	1.093095	1.093095	1.093092
0.6	1.106797	1.109946	1.109946	1.109944
0.7	1.124882	1.126397	1.126397	1.126395
0.8	1.142879	1.142488	1.142488	1.142488
0.9	1.160762	1.158253	1.158253	1.158254
1.0	1.178511	1.17372	1.173720	1.173721

Table 4.4: A comparison values of $-g''(0)$ between bvp4c and HAM for numerous values of α in limiting cases when $We_1 = We_2 = M = 0$ and $n = 1$.

α	$-g''(0)$			
	Ariel(HPM) [115]	Ariel(Exact) [115]	Present(bvp4c)	Present(HAM)
0	0.0	0.0	0.0	0.0
0.1	0.070399	0.066847	0.0668485	0.0668484
0.2	0.158231	0.148737	0.1487382	0.1487384
0.3	0.254347	0.243360	0.2433607	0.2433605
0.4	0.360599	0.349209	0.3492087	0.3492087
0.5	0.476290	0.465205	0.4652046	0.4652045
0.6	0.600833	0.590529	0.5905229	0.5905227
0.7	0.733730	0.724532	0.7245312	0.7245310
0.8	0.874551	0.866683	0.8666822	0.8666821
0.9	1.022922	1.016539	1.0165380	1.0165360
1.0	1.178511	1.173721	1.1737200	1.1737210

Table 4.5: A comparison of $\theta'(0)$ between bvp4c and HAM for numerous values of α in limiting cases when $We_1 = We_2 = R = N_t = N_b = 0$ and $n = 1$.

α	$\theta'(0)$			
	Liu and Anderson [118]	Munir *et al.* [119]	Present(bvp4c)	Present(HAM)
0.25	-0.665933	-0.665939	-0.665933	-0.665926
0.50	-0.735334	-0.735336	-0.735335	-0.735332
0.75	-0.796472	-0.796472	-0.796473	-0.796471

Chapter 5

Effect of Thermal-Solutal Stratifications in 3D Flow of Carreau Nanofluid

The notable intention of the current chapter is to explore the features of combined convective and stratifications by utilizing Brownian and thermophrosis nanoparticles in 3D mixed convection flow of magnetite Carreau fluid influenced by stretched surface. The heat transport phenomenon is also betrothed in the manifestation of thermal radiation and the heat sink/source. By means of compatible alterations to rehabilitate the structure of non-linear PDEs into non-linear ODEs. To identify the behavior of numerous somatic parameters, numerically bvp4c tactic has been worked out to elucidate the governing ODEs. The graphical depiction is delineated and tables are organized for diverse physical parameters of Carreau nanofluid. It is scrutinized that the impact of induced magnetic parameter on both the velocity components is analogous and it diminish both the velocities for shear thinning/thickening liquids. Moreover, the present outcomes reported that the mixed convection and thermal stratification parameters decline the liquid temperature and allied thickness of the thermal boundary layer for both shear thickening/thinning liquids.

5.1 Description of the Problem

We scrutinize the steady 3D mixed convection flow of a Carreau magnetite-nanofluid over a bidirectional stretched surface. The influence of combined stratification and convective conditions are engaged in heat and mass transfer phenomena. Additionally, thermal radiation and the heat sink/source are deliberated. The flow is persuaded by stretching the surface in two nearby $x-$ and $y-$ directions with linear velocities $(u, v) = (ax, by)$ respectively, where $a, b > 0$ and the fluid overcomes the region $z > 0$. Furthermore, it is also supposed that the electric and magnetic fields are inconsequential when we equated with applied magnetic field (as depicted in figure 5.1). This notion is only effective when the magnetic Reynolds number is inconsequential.

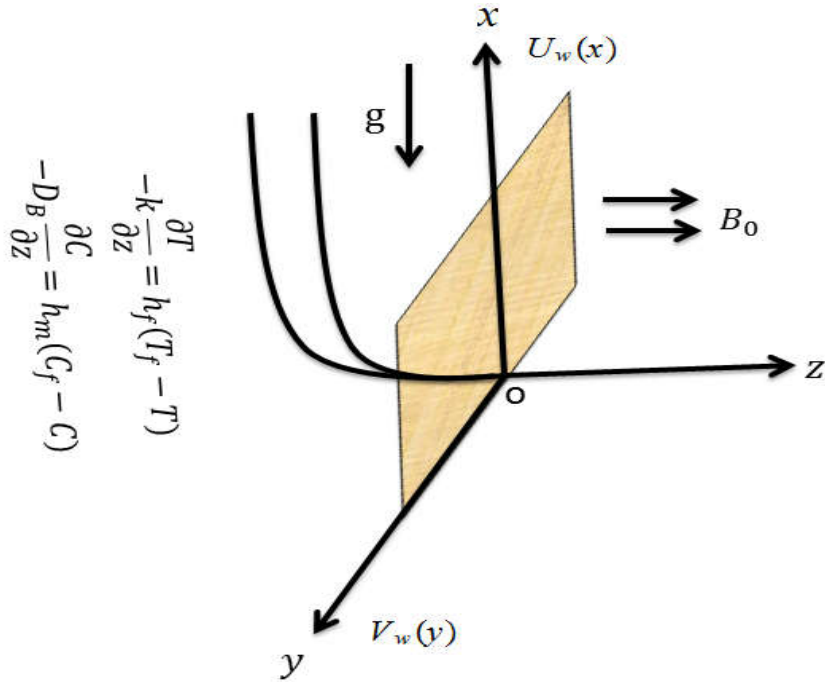Under these attentions the governing problem of magnetite Carreau nanofluid is

Figure 5.1: Flow configuration and coordinates system.

$$\frac{\partial u}{\partial x} + \frac{\partial v}{\partial y} + \frac{\partial w}{\partial z} = 0, \tag{5.1}$$

$$u\frac{\partial u}{\partial x} + v\frac{\partial u}{\partial y} + w\frac{\partial u}{\partial z} = \nu\frac{\partial^2 u}{\partial z^2}\left[1 + \Gamma^2\left(\frac{\partial u}{\partial z}\right)^2\right]^{\frac{n-1}{2}}$$
$$+ \nu(n-1)\Gamma^2\left(\frac{\partial u}{\partial z}\right)^2\frac{\partial^2 u}{\partial z^2}\left[1 + \Gamma^2\left(\frac{\partial u}{\partial z}\right)^2\right]^{\frac{n-3}{2}}$$
$$- \frac{\sigma B_0^2}{\rho_f}u + g[\beta_T(T - T_\infty) + \beta_C(C - C_\infty)], \tag{5.2}$$

$$u\frac{\partial v}{\partial x} + v\frac{\partial v}{\partial y} + w\frac{\partial v}{\partial z} = \nu\frac{\partial^2 v}{\partial z^2}\left[1 + \Gamma^2\left(\frac{\partial v}{\partial z}\right)^2\right]^{\frac{n-1}{2}}$$
$$+ \nu(n-1)\Gamma^2\left(\frac{\partial v}{\partial z}\right)^2\frac{\partial^2 v}{\partial z^2}\left[1 + \Gamma^2\left(\frac{\partial v}{\partial z}\right)^2\right]^{\frac{n-3}{2}} - \frac{\sigma B_0^2}{\rho_f}v, \tag{5.3}$$

$$u\frac{\partial T}{\partial x} + v\frac{\partial T}{\partial y} + w\frac{\partial T}{\partial z} = \alpha_1\frac{\partial^2 T}{\partial z^2} + \tau\left[D_B\frac{\partial C}{\partial z}\frac{\partial T}{\partial z} + \frac{D_T}{T_\infty}\left(\frac{\partial T}{\partial z}\right)^2\right]$$
$$- \frac{1}{(\rho c)_f}\frac{\partial q_r}{\partial z} + \frac{Q_0}{(\rho c)_f}(T - T_\infty), \tag{5.4}$$

$$u\frac{\partial C}{\partial x} + v\frac{\partial C}{\partial y} + w\frac{\partial C}{\partial z} = D_B\frac{\partial^2 C}{\partial z^2} + \frac{D_T}{T_\infty}\frac{\partial^2 T}{\partial z^2}. \tag{5.5}$$

Subject to the boundary conditions

$$\begin{aligned}
u &= U_w(x) = ax, \quad v = V_w(y) = by, \quad w = 0, \\
-k\frac{\partial T}{\partial z} &= h_f[T_f - T], \quad -D_B\frac{\partial C}{\partial z} = h_m[C_f - C] \quad \text{at} \quad z = 0, \tag{5.6} \\
u &\to 0, \quad v \to 0, \quad T \to T_\infty, \quad C \to C_\infty \quad \text{as} \quad z \to \infty. \tag{5.7}
\end{aligned}$$

Here g is the gravitational acceleration, (β_T, β_C) the coefficients of thermal and concentration expansion respectively, $(T_f, C_f) = (T_0 + dx, C_0 + ex)$ the heated liquid temperature and concentration, respectively, $(T_\infty, C_\infty) = (T_0 + d_1x, C_0 + e_1x)$ the ambient temperature and concentration, respectively, in which (T_0, C_0) the reference temperature and concentration re-

spectively and (d, d_1, e, e_1) the dimensionless constants.

5.1.1 Appropriate Conversions

Let we introduce

$$\theta\left(\eta\right) = \frac{T - T_\infty}{T_f - T_0}, \quad \phi = \frac{C - C_\infty}{C_f - C_0}. \tag{5.8}$$

In vision of overhead conversions and Eq. (2.27) (cf. Chapter 2), Eq. (5.1) satisfied automatically and Eqs. (5.2) − (5.7) reduced to the following ODEs

$$f'''[1 + We_1^2 f''^2]^{\frac{n-3}{2}}[1 + nWe_1^2 f''^2] - f'^2 + f''(f + g) - M^2 f' + \lambda^*(\theta + N^*\phi) = 0, \tag{5.9}$$

$$g'''[1 + We_2^2 g''^2]^{\frac{n-3}{2}}[1 + nWe_2^2 g''^2] - g'^2 + g''(f + g) - M^2 g' = 0, \tag{5.10}$$

$$(1 + R_d)\,\theta'' + \Pr(f + g)\theta' - \Pr f'\theta - \Pr S_1 f' + \Pr[N_b\theta'\phi' + N_t\theta'^2 + \delta\theta] = 0, \tag{5.11}$$

$$\phi'' + \Pr Le(f + g)\phi' - \Pr Le f'\phi - \Pr Le S_2 f' + \left(\frac{N_t}{N_b}\right)\theta'' = 0, \tag{5.12}$$

with BCs

$$f(0) = 0, \quad g(0) = 0, \quad f'(0) = 1, \quad g'(0) = \alpha,$$

$$\theta'(0) = -\gamma_1(1 - S_1 - \theta(0)), \quad \phi'(0) = -\gamma_2(1 - S_2 - \phi(0)), \tag{5.13}$$

$$f' \to 0, \quad g' \to 0, \quad \theta \to 0, \quad \phi \to 0 \quad \text{as} \quad \eta \to \infty. \tag{5.14}$$

Here $\lambda^*\left(= \frac{g\beta_T d}{a^2}\right)$ is the mixed convection parameter, $N^*\left(= \frac{\beta_C e}{\beta_T d}\right)$ the buoyancy ratio parameter ratio parameter, $N_b\left(= \frac{\tau D_B(C_f - C_0)}{\nu}\right)$ the Brownian motion parameter, $N_t\left(= \frac{D_T(T_f - T_0)}{\nu T_\infty}\right)$ the thermophoresis parameter and $(S_1, S_2)\left(= \frac{d_1}{d}, \frac{e_1}{e}\right)$ the thermal and mass stratification parameters, respectively.

5.2 Engineering and Industrial Quantities of Interest

From the industrial and engineering point of view, the essential quantities of physical interest are the skin friction coefficients, heat and mass transport rates which may be defined by the subsequent relations. These quantities in non-dimensional forms are given as:

$$\frac{1}{2} C_{fx} \operatorname{Re}_x^{\frac{1}{2}} = f''(0)[1 + We_1^2 f''^2(0)]^{\frac{n-1}{2}}, \tag{5.15}$$

$$\frac{1}{2} \left(\frac{U_w}{V_w}\right) C_{fy} \operatorname{Re}_x^{\frac{1}{2}} = g''(0)[1 + We_2^2 g''^2(0)]^{\frac{n-1}{2}}. \tag{5.16}$$

$$\operatorname{Re}_x^{-\frac{1}{2}} Nu_x = \frac{-(1 + R_d)\theta'(0)}{1 - S_1}, \quad \operatorname{Re}_x^{-\frac{1}{2}} Sh_x = -\left(\frac{1}{1 - S_2}\right)\phi'(0). \tag{5.17}$$

5.3 Graphical Illustration and Analysis

The notable objective here is to disclose the structure of numerous parameters on mixed convection stratified flow of magnetite Carreau nanofluid subject to convectives phenomena. The heat transport mechanism is also considered in manifestation of the heat sink/source and thermal radiation. For this persistence, graphs are planned and tables are structured for diverse parameters and discussed in facts.

To envision the impact of magnetic parameter (M) on velocity components $f'(\eta)$ and $g'(\eta)$ for both cases $(n < 1)$ and $(n > 1)$, **figures 5.2(a − d)** are strategized. It is noted that both the liquid velocities decline for enhancing values of M for shear thinning/thickening cases. This occurs because of the circumstance that the outcome of strong magnetic field contributes resistance to flow in both $x-$ and $y-$directions which intensify the Lorentz force in $z-$direction. Therefore, the flow in both the directions, which decays the liquid velocities. The stimulus of mixed convection (λ^*) and buoyancy ratio (N^*) on velocity components for $(n < 1)$ and $(n > 1)$ are schemed in **figures 5.3(a − d)** and **5.4(a − d)**. It is noteworthy to note that when values of λ^* and N^* intensify, the liquid velocity $f'(\eta)$ increases. Physically, augmented values of λ^* reason a forceful buoyancy force which clues the escalation of velocity field $f'(\eta)$. Similarly, the concentration buoyancy strength boost up for the increase in N^* which consequences the decline of velocity $g'(\eta)$. Moreover, it is reported that both the velocity components decay for augmenting values of λ^* and N^* for both $(n < 1)$ and $(n > 1)$ as displayed in **figures 5.3(c, d)** and **5.4(c, d)**. Hence, we can say from these strategies that the impact of these flow parameters λ^* and N^* are entirely conflicting for velocity components $f'(\eta)$ and $g'(\eta)$.

100

Figures **5.5(a, b)** and **5.6(a, b)** are intended to visualize the enactment of mixed convection parameter (λ^*) and buoyancy ratio parameter (N^*) for shear thickening/thinning cases on nanoliquid temperature field $\theta(\eta)$. From these structures it is scrutinized that both λ^* and N^* are retreating functions of temperature distribution $\theta(\eta)$. For higher values of λ^* and N^* display thinner thickness of the thermal boundary layer and low temperature on Carreau nanofluid. The enhancing values of λ^* relate to stronger buoyancy force because mixed convection parameter depends on buoyancy force. Hence, owing to stronger buoyancy force is the reason for the decline in temperature and its allied thickness of the boundary layer. Furthermore, analogous enactment is being detected for the progressive values of N^*. **Figures 5.7(a, b)** and **5.8(a, b)** expose the tendency of thermal Biot number (γ_1) and stratification parameter (S_1), respectively, for $(n = 0.5$ and $1.5)$ on Carreau liquid temperature field. Here scrutinized that quite conflicting tendency is being famed for growing value of γ_1 and S_1. When values of γ_1 intensify the temperature field enhances; however, the temperature of Carreau fluid is declining function of S_1. Physically, enlarging the values of γ_1 arise the heat transfer amount which is responsible to enhance $\theta(\eta)$. Moreover, the difference between the sheet and ambient liquid temperature is condensed with intensified values of S_1. Therefore, the temperature field decays for S_1 as shown in **figure 5.8(a, b)**. The nanoparticles display a strategic role in the enhancement of heat transfer features in Carreau fluid. For this persistence, **figures 5.9(a, b)** and **5.10(a, b)** are designed for both $(n < 1$ and $n > 1)$. These drafts scrutinized that N_b and N_t are both boosting the liquid temperature and thermal thickness of the boundary layer. Intensification in N_b enriches the accidental gesture of liquid particles because of this aspect the additional heat is formed which rises $\theta(\eta)$. From **figure 5.9(a, b)**, it is reported that the higher N_t also enhances the liquid temperature. As, thermophoresis is a mechanism wherein minor elements are dragged away from the hot to the cold surface. Therefore, enormous quantity of nanoparticles is relocated away from the intense surface which increases the temperature of the liquid. The characteristic of thermal radiation (R_d) for $(n = 0.5$ and $1.5)$ is exposed in **figure 5.11(a, b)** on nanoliquid temperature field. There is an enhancement in both the liquid temperature and thermal thickness of boundary layer for higher values of R_d. The heat flux from the sheet intensifies for larger R_d which rise $\theta(\eta)$. Moreover, the coefficient of means absorption decays for enhancing values of R_d which is blamable for the enrichment of $\theta(\eta)$.

An intensification in nanoparticles concentration Biot number (γ_2) and stratification parameter (S_2) on concentration field $\phi(\eta)$ for shear thinning/thickening parameters are exposed in **figures 5.12(a, b)** and **5.13(a, b)**. These strategies spectacles opposing tendency for higher values of γ_2 and S_2. An increase in γ_2 enhances the concentration of nanoliquid; however, it declines for S_2. The higher values of γ_2 relate to advance mass transfer coefficient and thus, the concentration field arises. On the other hand, it is inspected that when S_2 enhances, the difference between surface and reference nanoparticles reduces and the outcomes the declination of $\phi(\eta)$.

5.3.1 Tabular Representations

Tables 5.1 and **5.2** are established to visualize the tendency of the involved parameters on the local skin friction coefficients $\left(\frac{1}{2} C_{fx} \operatorname{Re}_x^{\frac{1}{2}}, \ \frac{1}{2} \left(\frac{U_w}{V_w} \right) C_{fy} \operatorname{Re}_x^{\frac{1}{2}} \right)$, local Nusselt number $\left(\operatorname{Re}_x^{-\frac{1}{2}} Nu_x \right)$ and local Sherwood number $\left(\operatorname{Re}_x^{-\frac{1}{2}} Sh_x \right)$ for both shear thinning/thickening liquids. From **Table 5.1** it is fascinating to note that by increasing the value of M, S_1 and S_2 rises $\left(\frac{1}{2} C_{fx} \operatorname{Re}_x^{\frac{1}{2}} \right)$, while it declines for enhancing value of λ^*, N^*, γ_1 and γ_2 for both $(n < 1)$ and $(n > 1)$. It is also reported that $\left(\frac{1}{2} \left(\frac{U_w}{V_w} \right) C_{fy} \operatorname{Re}_x^{\frac{1}{2}} \right)$ enhances for M, λ^*, N^*, γ_1 and γ_2 whereas conflicting behavior is being identified for S_1 and S_2. From **Table 5.2**, the rate of heat transfer $\left(\operatorname{Re}_x^{-\frac{1}{2}} Nu_x \right)$, enhanced for λ^*, N^*, γ_1, S_1 and S_2 and declined for M and γ_2. Moreover, the mass transfer rate $\left(\operatorname{Re}_x^{-\frac{1}{2}} Sh_x \right)$ for shear thinning/thickening liquids diminished for the progressive values of λ^*, N^* and S_1 while increasing for M, γ_1 and γ_2.

5.3.2 Confirmation of Numerical Outcomes

For the endorsement of numerical upshots of $-f''(0)$ and $-g''(0)$ with former related prose for diverse values of α, **Tables 5.3** and **5.4** are organized. It is reported that intensifying values of α is to enhance the magnitude of $-f''(0)$ and $-g''(0)$. From these tables a noteworthy feature is being noted with earlier studies.
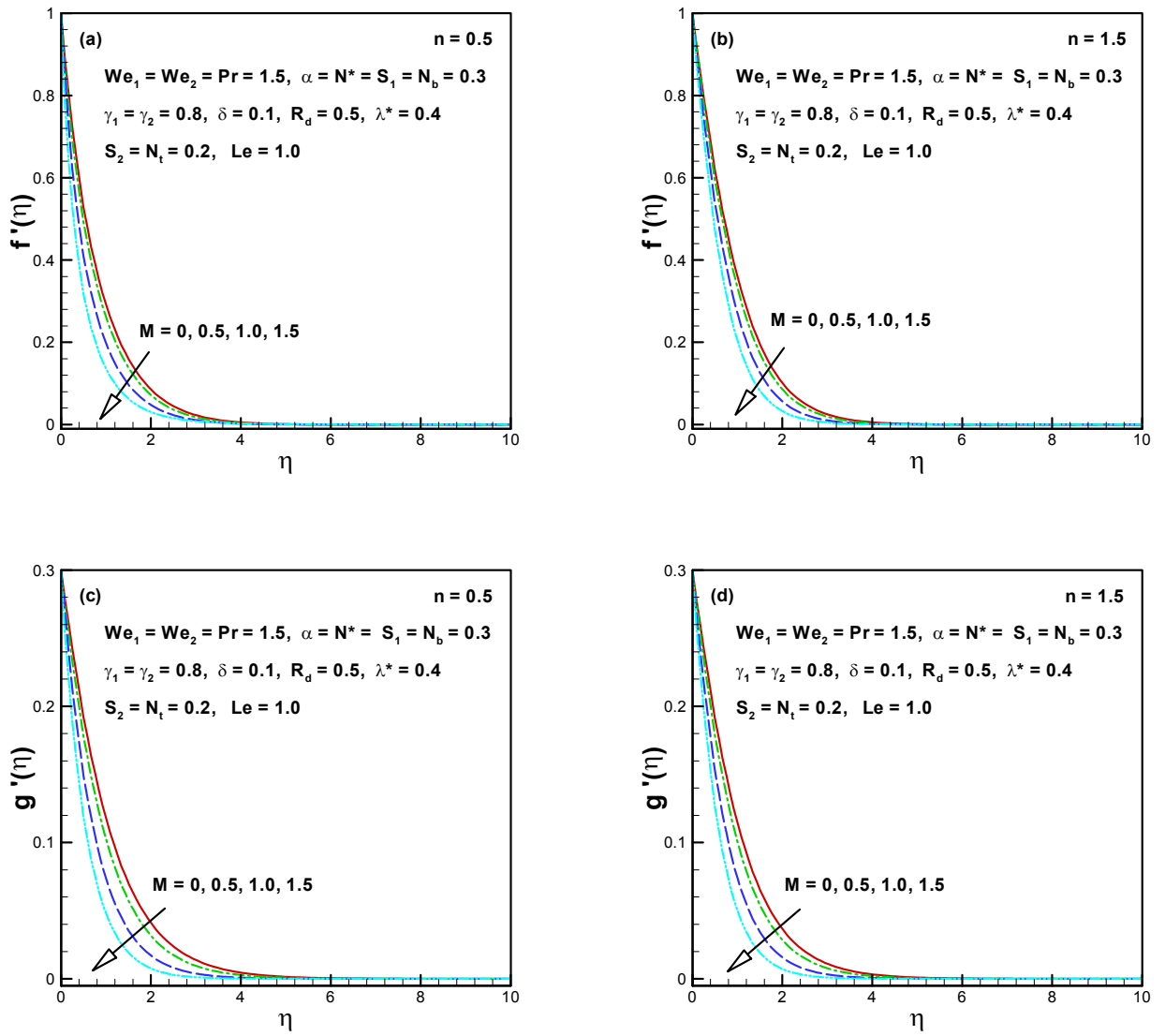
(a) n = 0.5

We$_1$ = We$_2$ = Pr = 1.5, α = N* = S$_1$ = N$_b$ = 0.3

γ_1 = γ_2 = 0.8, δ = 0.1, R$_d$ = 0.5, λ* = 0.4

S$_2$ = N$_t$ = 0.2, Le = 1.0

M = 0, 0.5, 1.0, 1.5

(b) n = 1.5

We$_1$ = We$_2$ = Pr = 1.5, α = N* = S$_1$ = N$_b$ = 0.3

γ_1 = γ_2 = 0.8, δ = 0.1, R$_d$ = 0.5, λ* = 0.4

S$_2$ = N$_t$ = 0.2, Le = 1.0

M = 0, 0.5, 1.0, 1.5

(c) n = 0.5

We$_1$ = We$_2$ = Pr = 1.5, α = N* = S$_1$ = N$_b$ = 0.3

γ_1 = γ_2 = 0.8, δ = 0.1, R$_d$ = 0.5, λ* = 0.4

S$_2$ = N$_t$ = 0.2, Le = 1.0

M = 0, 0.5, 1.0, 1.5

(d) n = 1.5

We$_1$ = We$_2$ = Pr = 1.5, α = N* = S$_1$ = N$_b$ = 0.3

γ_1 = γ_2 = 0.8, δ = 0.1, R$_d$ = 0.5, λ* = 0.4

S$_2$ = N$_t$ = 0.2, Le = 1.0

M = 0, 0.5, 1.0, 1.5

Figure 5.2(a − d): Influence of M on $f'(\eta)$ and $g'(\eta)$.
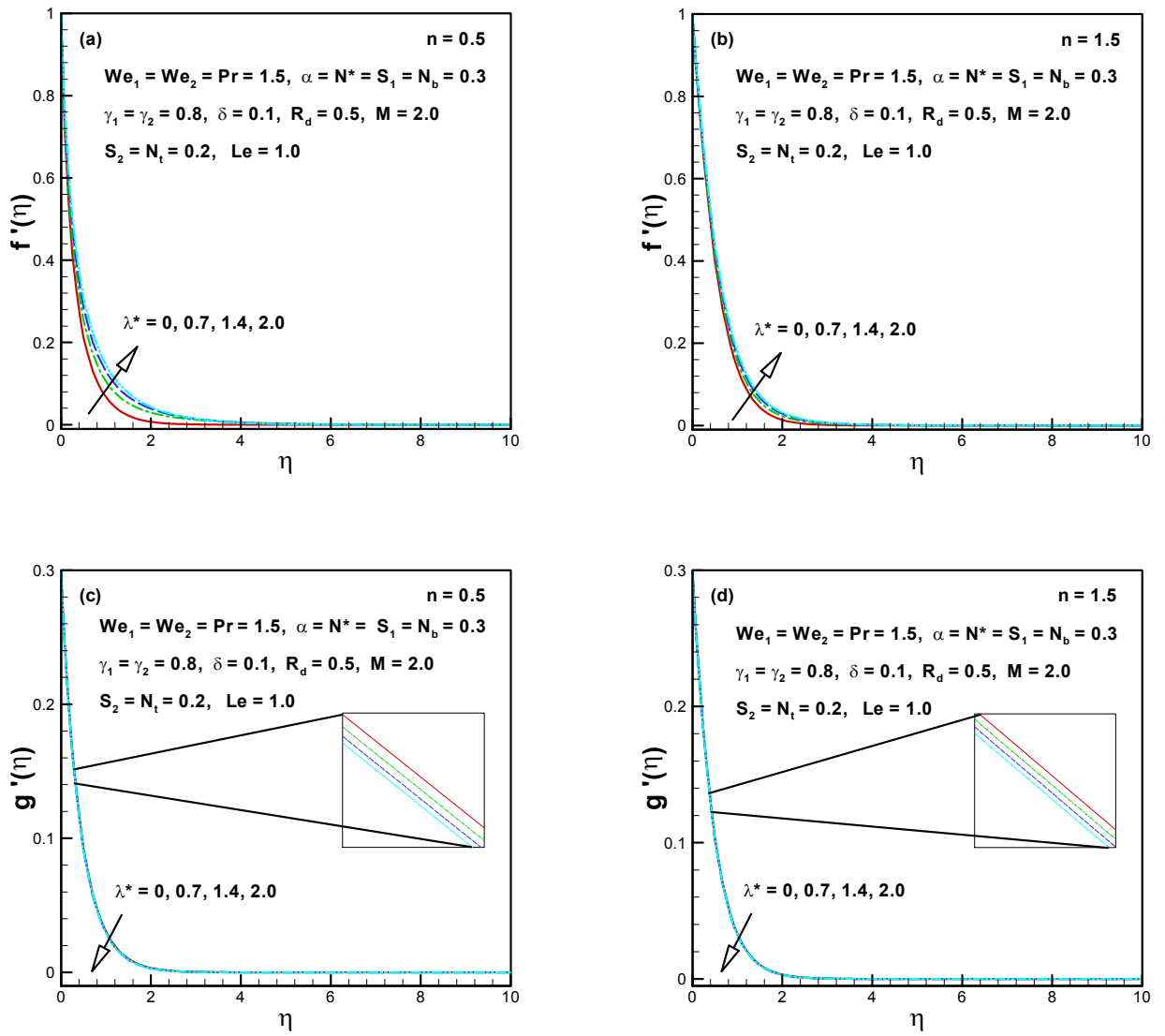
Figure 5.3(a − d): Influence of λ^* on $f'(\eta)$ and $g'(\eta)$.
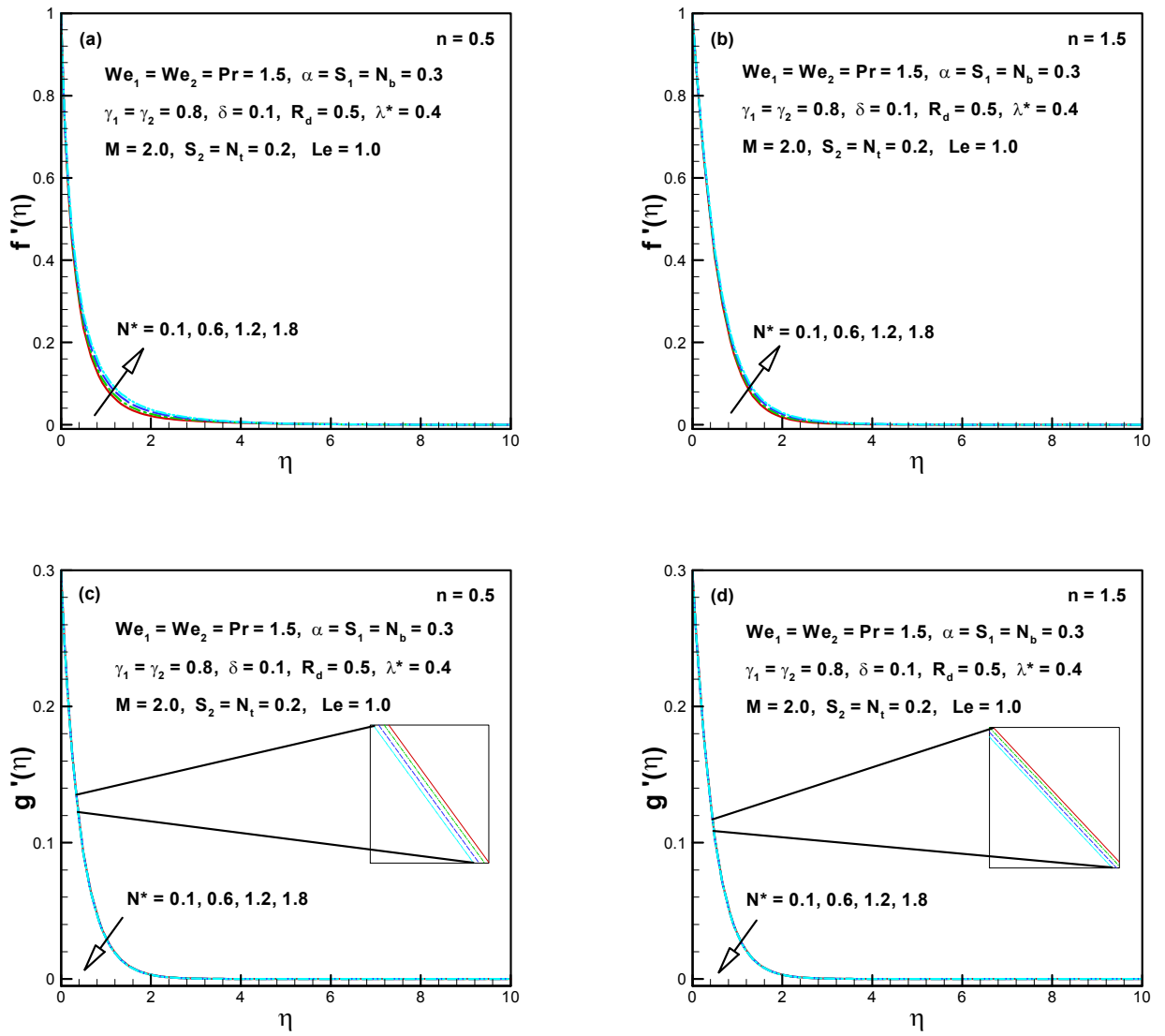
Figure 5.**4(a − d)**: Influence of N^* on $f'(\eta)$ and $g'(\eta)$.
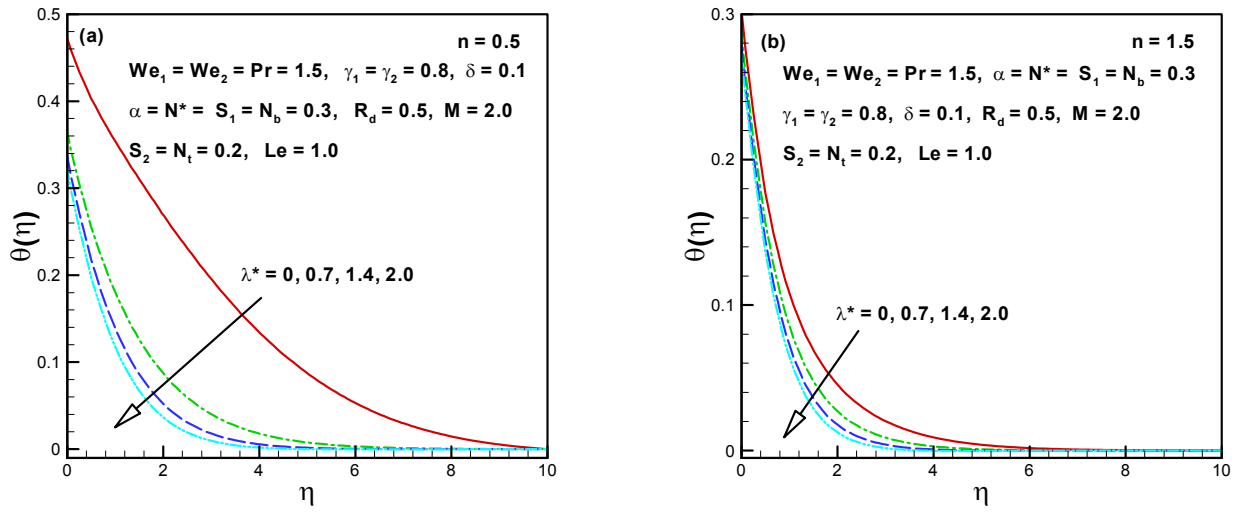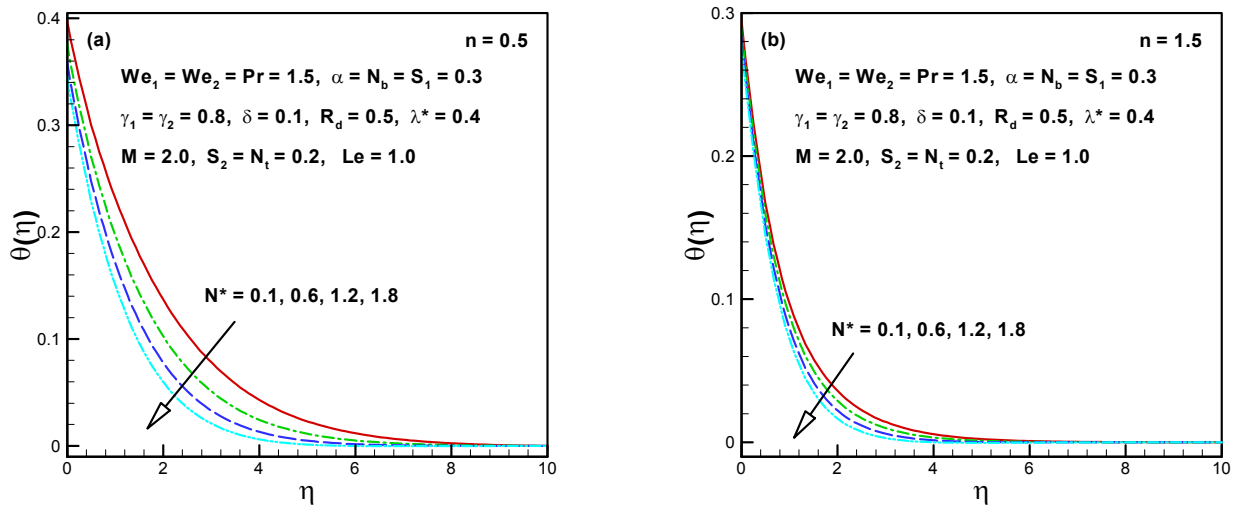
Figure 5.5(a, b): Influence of λ^* on $\theta(\eta)$.

Figure 5.6(a, b): Influence of N^* on $\theta(\eta)$.

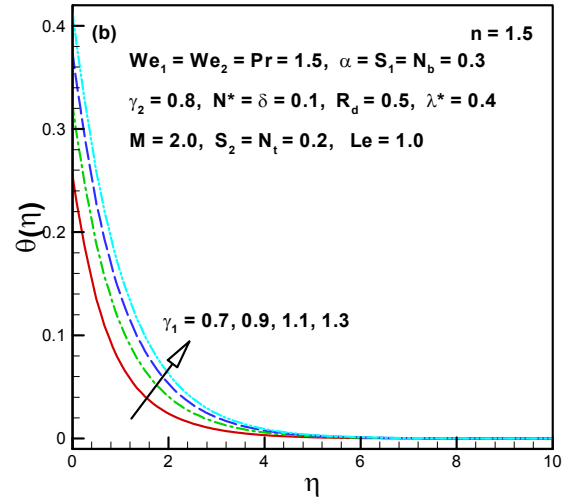**Figure 5.7(a, b)**: Influence of γ_1 on $\theta(\eta)$.
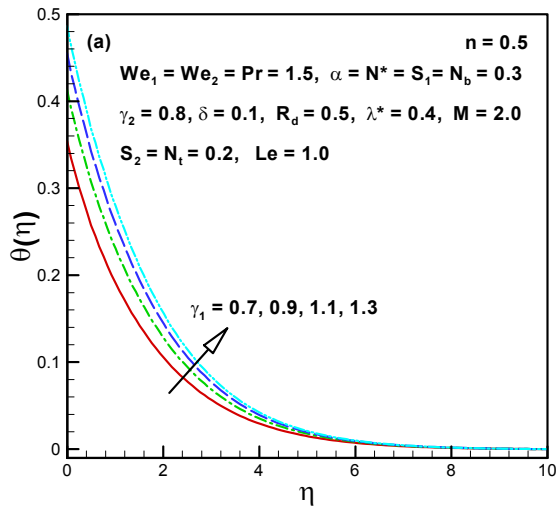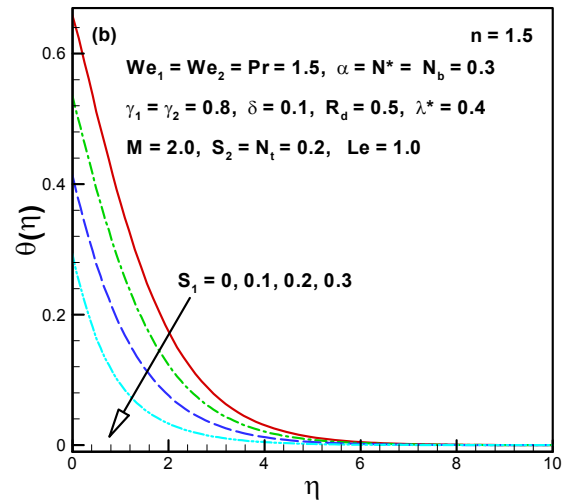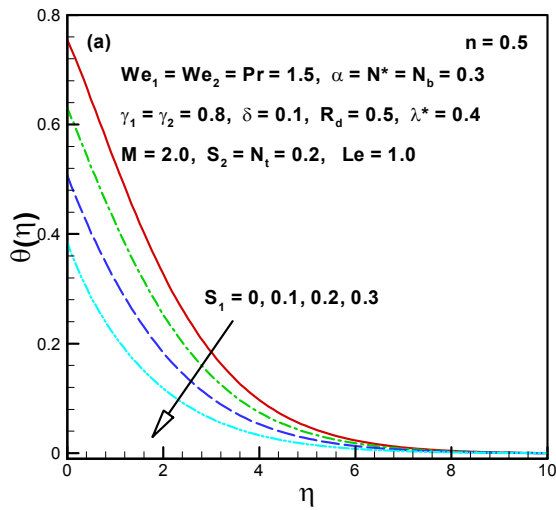

Figure 5.8(a, b): Influence of S_1 on $\theta(\eta)$.
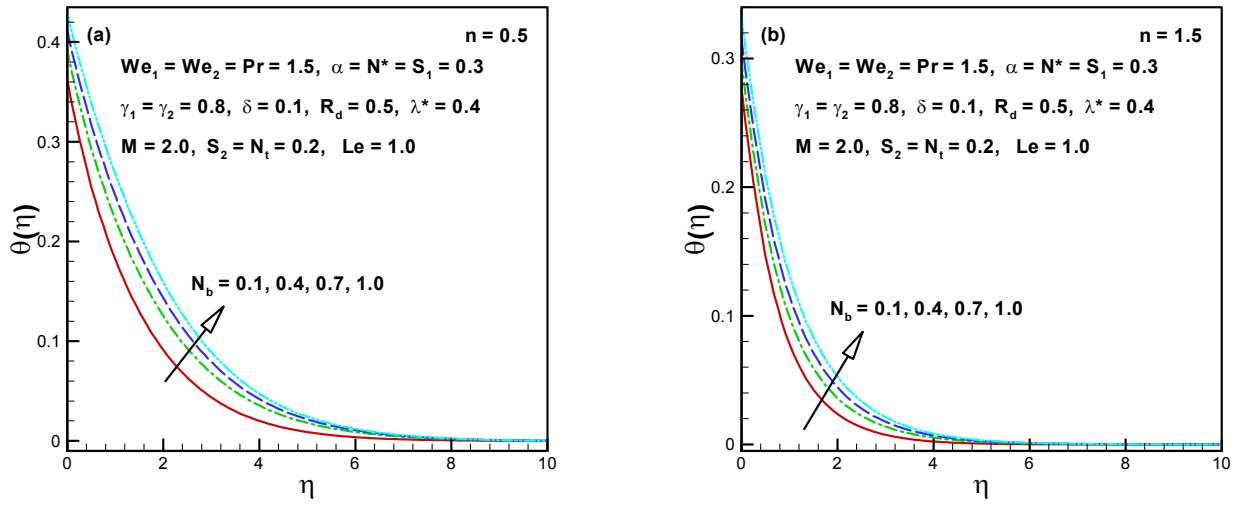
Figure 5.9(a, b): Influence of N_b on $\theta(\eta)$.
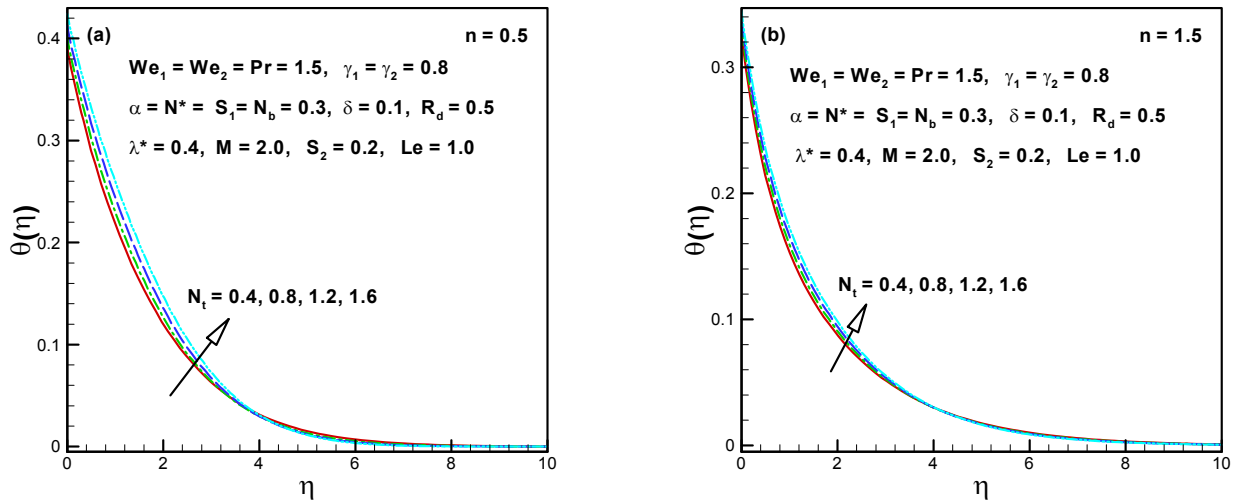

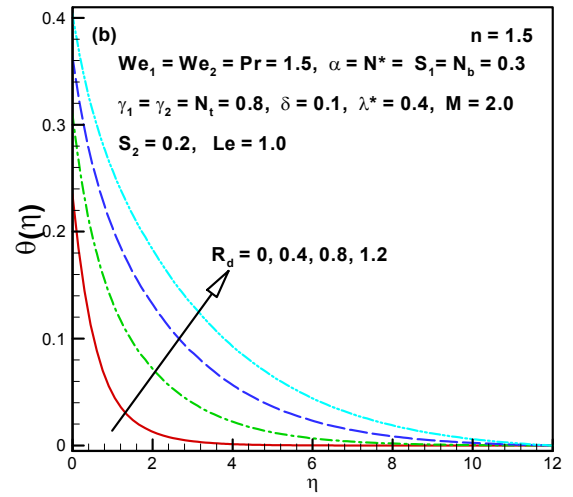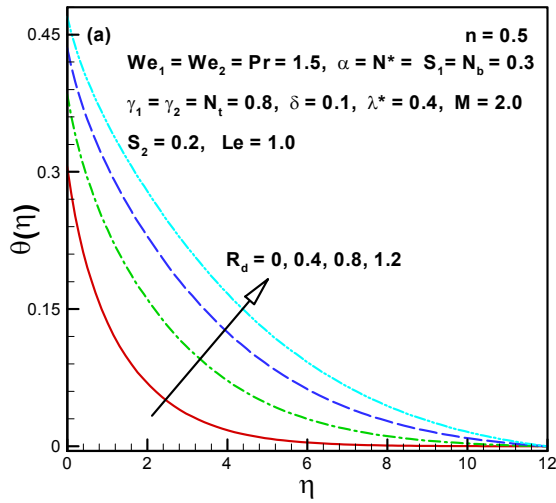**Figure 5.10(a, b):** Influence of N_t on $\theta(\eta)$.

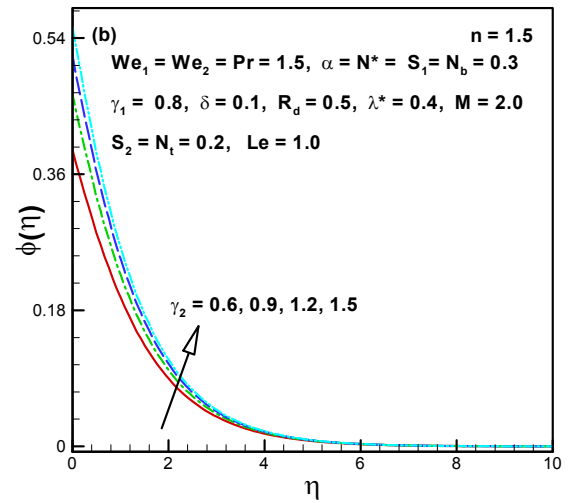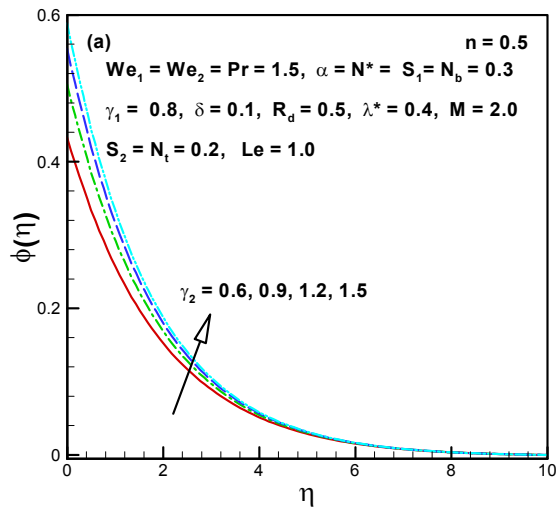**Figure 5.11(a, b)**: Influence of R_d on $\theta(\eta)$.

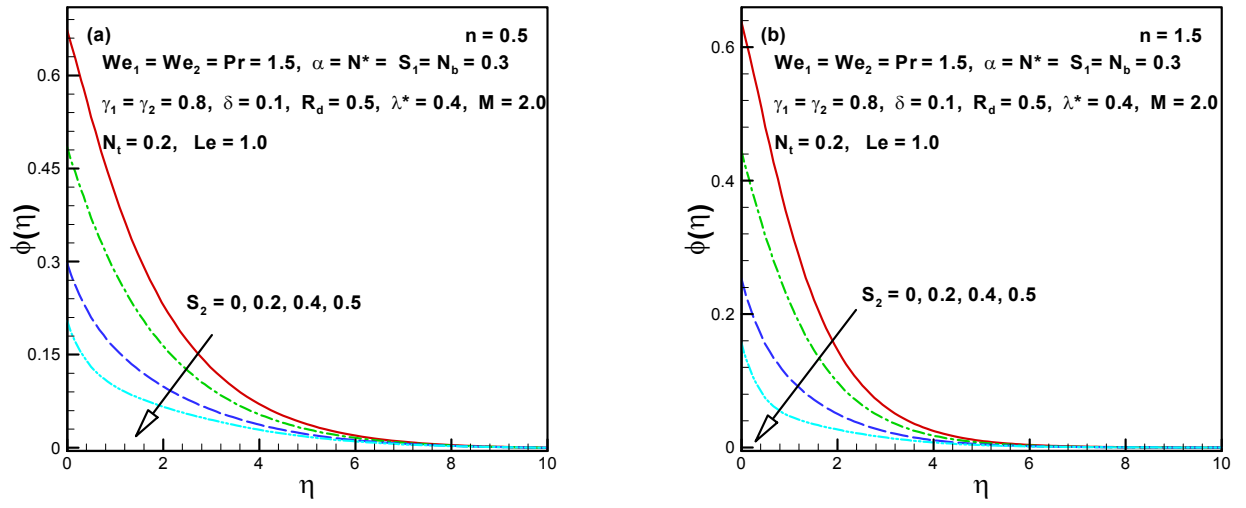**Figure 5.12(a, b)**: Influence of γ_2 on $\phi(\eta)$.

Figure 5.13(a, b): Influence of S_2 on $\phi(\eta)$.

Table 5.1: Outcomes of $\left(\frac{1}{2}C_{fx}\operatorname{Re}_x^{\frac{1}{2}}, \frac{1}{2}\left(\frac{U_w}{V_w}\right)C_{fy}\operatorname{Re}_x^{\frac{1}{2}}\right)$ when $We_1 = We_2 = \Pr = 1.5$, $\delta = 0.1$, $N_t = 0.2$, $\alpha = N_b = 0.3$, $R_d = 0.5$, and $Le = 1.0$ are fixed.

M	λ^*	N^*	S_1	γ_1	S_2	γ_2	$\frac{1}{2}C_{fx}\operatorname{Re}_x^{\frac{1}{2}}$		$\frac{1}{2}\left(\frac{U_w}{V_w}\right)C_{fy}\operatorname{Re}_x^{\frac{1}{2}}$	
							$n=0.5$	$n=1.5$	$n=0.5$	$n=1.5$
0.4	0.4	0.3	0.3	0.8	0.2	0.8	-1.460721	-2.702463	-0.2739822	-0.3101425
0.7							-1.718577	-3.357890	-0.3290915	-0.3808131
1.0							-2.100599	-4.412760	-0.4035425	-0.4832473
1.3							-2.587644	-5.905137	-0.4925378	-0.6152006
0.4	0.1						-1.532698	-2.812340	-0.2730782	-0.3099244
	0.6						-1.414603	-2.628506	-0.2745703	-0.3103278
	1.2						-1.285444	-2.410590	-0.2762105	-0.3109680
	0.4	0.2					-1.470707	-2.720519	-0.2738206	-0.3100615
		0.4					-1.450823	-2.684511	-0.2741418	-0.3102233
		0.6					-1.431282	-2.648912	-0.2744551	-0.3103841
		0.3	0.0				-1.333852	-2.409828	-0.2774695	-0.3128348
			0.1				-1.376357	-2.507028	-0.2762919	-0.3119151
			0.2				-1.418661	-2.604599	-0.2751290	-0.3110178
			0.3	0.3			-1.547184	-2.883712	-0.2720473	-0.3088822
				0.5			-1.504591	-2.795352	-0.2730074	-0.3094936
				0.7			-1.473393	-2.729474	-0.2737020	-0.3099532
				0.8	0.0		-1.439437	-2.653593	-0.2744843	-0.3105191
					0.1		-1.450078	-2.678001	-0.2742330	-0.3103304
					0.3		-1.471366	-2.726980	-0.2737319	-0.3099554
					0.2	0.2	-1.482257	-2.745890	-0.2735980	-0.3098986
						0.4	-1.473374	-2.728128	-0.2737565	-0.3099981
						0.6	-1.466377	-2.714009	-0.2738814	-0.3100774

Table 5.2: Outcomes of $\left(\mathrm{Re}_x^{-\frac{1}{2}} Nu_x\right)$ and $\left(\mathrm{Re}_x^{-\frac{1}{2}} Sh_x\right)$ when $We_1 = We_2 = \mathrm{Pr} = 1.5$, $\delta = 0.1$, $N_t = 0.2$, $\alpha = N_b = 0.3$, $R_d = 0.5$, and $Le = 1.0$ are fixed.

M	λ^*	N^*	S_1	γ_1	S_2	γ_2	$\mathrm{Re}_x^{-\frac{1}{2}} Nu_x$		$\mathrm{Re}_x^{-\frac{1}{2}} Sh_x$	
							$n = 0.5$	$n = 1.5$	$n = 0.5$	$n = 1.5$
0.4	0.4	0.3	0.3	0.8	0.2	0.8	0.7907507	0.8222056	0.2984109	0.2754751
0.7							0.7703503	0.8096584	0.3132862	0.2846241
1.0							0.7409110	0.7923285	0.3347524	0.2972605
1.3							0.7040871	0.7716916	0.3616032	0.3123082
0.4	0.1						0.7884971	0.8230341	0.3000542	0.2748710
	0.6						0.7924613	0.8220249	0.2971637	0.2756068
	1.2						0.7974830	0.8223095	0.2935020	0.2753994
	0.4	0.2					0.7901262	0.8220475	0.2988663	0.2755904
		0.4					0.7913636	0.8223643	0.2979641	0.2753593
		0.6					0.792556	0.8226835	0.2970945	0.2751266
		0.3	0.0				0.6340343	0.6523905	0.5895476	0.5704266
			0.1				0.6759248	0.6974054	0.4913205	0.4711825
			0.2				0.7268688	0.7525559	0.3942760	0.3728701
			0.3	0.3			0.4199406	0.4312493	0.0584489	0.0364596
				0.5			0.5999854	0.6201335	0.1750171	0.1515109
				0.7			0.7350988	0.7630746	0.2624176	0.2391045
				0.8	0.0		0.7900713	0.8206323	0.2391251	0.2212978
					0.1		0.7904104	0.8214178	0.2654748	0.2453774
					0.3		0.7910923	0.8229956	0.3407564	0.3141703
					0.2	0.2	0.7977195	0.8300549	0.2933295	0.2697516
						0.4	0.7948675	0.8268635	0.2954091	0.2720787
						0.6	0.7925988	0.8242934	0.2970633	0.2739527

Table 5.3: A comparison of $-f''(0)$ between bvp4c and HAM in limiting sense when $We_1 = We_2 = M = \lambda^* = N^* = 0$ and $n = 1$ are fixed.

α	Wang [117]	Liu and Anderson [118]	$-f''(0)$ cf. Chapter 3 Table 3.3 (bvp4c)	cf. Chapter 3 Table 3.3 (HAM)	Present bvp4c
0.0	1	1	1	1	1
0.25	1.048813	1.048813	1.0488130	1.0488131	1.0488113
0.50	1.093097	1.093096	1.0930954	1.0930943	1.0930949
0.75	1.134485	1.134486	1.1344854	1.1344858	1.1344856
1.0	1.173720	1.173721	1.1737199	1.1737201	1.1737208

Table 5.4: A comparison values of $-g''(0)$ between bvp4c and HAM in limiting sense when $We_1 = We_2 = M = \lambda^* = N^* = 0$ and $n = 1$ are fixed.

α	Wang [117]	Liu and Anderson [118]	$-g''(0)$ cf. Chapter 3 Table 3.4 (bvp4c)	cf. Chapter 3 Table 3.4 (HAM)	Present (bvp4c)
0.0	0	0	0	0	0
0.25	0.194564	0.194565	0.1945652	0.1945617	0.19456397
0.50	0.465205	0.465206	0.4652058	0.4652047	0.46520490
0.75	0.794622	0.794619	0.7946180	0.7946184	0.79461824
1.0	1.173720	1.173721	1.1737199	1.1737201	1.17372080

Chapter 6

Impact of Variable Thermal Conductivity in 3D Unsteady flow of Carreau Nanofluid

This chapter reports unsteady 3D forced convective flow of Carreau nanofluid over a bidirectional stretched surface. Heat transfer phenomenon of Carreau nanofluid is inspected through the variable thermal conductivity and heat generation/absorption. Furthermore, this chapter presents a more convincing approach for heat and mass transfer phenomena of nanoliquid by utilizing new mass flux condition. Practically, zero mass flux condition is more adequate because here we assume nanoparticle amends itself accordingly on the boundary. Now the features of Buongiorno's relation for Carreau nanofluid can be applied in a more efficient way. The appropriate transformations are employed to alter the PDEs into ODEs and then tackled numerically by employing bvp4c scheme. The numerous consequence of scheming parameters on the Carreau nanoliquid velocity components, temperature and concentration fields is portrayed graphically and deliberated in detail. The numerical outcomes for local skin friction and the wall temperature gradient for Carreau nanoliquid are intended and reported through tables. The outcomes conveyed here manifest that the impact of Brownian motion parameter N_b on the rate of heat transfer for nanoliquids has become negligible for the recently recommended revised relation. Additionally, for authentication of the present relation, the achieved results

are distinguished with earlier research works in specific cases and marvelous agreement has been noted.

6.1 Description of the Problem

Here we report unsteady 3D flow of Carreau nanofluid over a bidirectional stretched surface. The flow is persuaded owing to stretching surface in two horizontal $x-$and $y-$directions with velocities $U_w(x,t)$ and $V_w(y,t)$, respectively, where a and b are stretching rates and the nanofluid flow that occupies the region in the domain $z > 0$. Characteristics of heat transfer mechanism are inspected in view of heat source/sink and variable thermal conductivity. Features of nanoparticles are taken considering Brownian motion and thermophoresis. Temperature of the nanoliquid at the surface T_w is superior than temperature of nanoliquid distant from the stretched surface.

The Carreau nanoliquid equations in view of overhead declared assumptions are given below:

$$\frac{\partial u}{\partial x} + \frac{\partial v}{\partial y} + \frac{\partial w}{\partial z} = 0, \tag{6.1}$$

$$\frac{\partial u}{\partial t} + u\frac{\partial u}{\partial x} + v\frac{\partial u}{\partial y} + w\frac{\partial u}{\partial z} = \nu\frac{\partial^2 u}{\partial z^2}\left[1 + \Gamma^2\left(\frac{\partial u}{\partial z}\right)^2\right]^{\frac{n-1}{2}}$$
$$+ \nu(n-1)\Gamma^2\left(\frac{\partial u}{\partial z}\right)^2\left(\frac{\partial^2 u}{\partial z^2}\right)\left[1 + \Gamma^2\left(\frac{\partial u}{\partial z}\right)^2\right]^{\frac{n-3}{2}}, \tag{6.2}$$

$$\frac{\partial v}{\partial t} + u\frac{\partial v}{\partial x} + v\frac{\partial v}{\partial y} + w\frac{\partial v}{\partial z} = \nu\frac{\partial^2 v}{\partial z^2}\left[1 + \Gamma^2\left(\frac{\partial v}{\partial z}\right)^2\right]^{\frac{n-1}{2}}$$
$$+ \nu(n-1)\Gamma^2\left(\frac{\partial v}{\partial z}\right)^2\left(\frac{\partial^2 v}{\partial z^2}\right)\left[1 + \Gamma^2\left(\frac{\partial v}{\partial z}\right)^2\right]^{\frac{n-3}{2}}, \tag{6.3}$$

$$\frac{\partial T}{\partial t} + u\frac{\partial T}{\partial x} + v\frac{\partial T}{\partial y} + w\frac{\partial T}{\partial z} = \frac{1}{(\rho c)_f}\frac{\partial}{\partial z}\left(K(T)\frac{\partial^2 T}{\partial z^2}\right)$$
$$+ \tau\left[D_B\frac{\partial C}{\partial z}\frac{\partial T}{\partial z} + \frac{D_T}{T_\infty}\left(\frac{\partial T}{\partial z}\right)^2\right] + \frac{Q_0}{(\rho c)_f}(T - T_\infty), \tag{6.4}$$

$$\frac{\partial C}{\partial t} + u\frac{\partial C}{\partial x} + v\frac{\partial C}{\partial y} + w\frac{\partial C}{\partial z} = D_B\frac{\partial^2 C}{\partial z^2} + \frac{D_T}{T_\infty}\frac{\partial^2 T}{\partial z^2}. \tag{6.5}$$

The following appropriate boundary conditions are imposed at the stretched surface and in the freestream

$$u = U_w = \frac{ax}{1-\beta t}, \quad v = V_w = \frac{by}{1-\beta t}, \quad w = 0, \quad T = T_w(x,t)$$

$$D_B \frac{\partial C}{\partial z} + \frac{D_T}{T_\infty} \frac{\partial T}{\partial z} = 0 \quad \text{at} \quad z = 0, \tag{6.6}$$

$$u \to 0, \quad v \to 0, \quad T \to T_\infty, \quad C \to C_\infty \quad \text{as} \quad z \to \infty. \tag{6.7}$$

Here $K(T)$ is the variable thermal conductivity. Furthermore, temperature of the nanofluid at the surface $T_w(x,t)$ and variable thermal conductivity $K(T)$ are given by the following expressions

$$T_w(x,t) = T_\infty + \frac{T_0 a x^2}{(1-\beta t)^{\frac{3}{2}}}, \quad K(T) = k_\infty \left[1 + \varepsilon \left(\frac{T - T_\infty}{\Delta T}\right)\right], \tag{6.8}$$

where (k_∞, ε) are the thermal conductivity of the nanoliquid far away from the stretched surface and ε the thermal conductivity parameter, respectively, T_0 the the positive reference temperature of the nanoliquid and ΔT represents the liquid temperature difference between the stretched surface and far away from the surface.

6.1.1 Appropriate Conversions

In view of non-dimensionless transformation variables

$$u = \left(\frac{ax}{1-\beta t}\right) f'(\eta), \quad v = \left(\frac{ay}{1-\beta t}\right) g'(\eta), \quad w = -\sqrt{\frac{a\nu}{(1-\beta t)}}[f(\eta) + g(\eta)],$$

$$\theta(\eta) = \frac{T - T_\infty}{T_w - T_\infty}, \quad \phi = \frac{C - C_\infty}{C_\infty}, \quad \eta = z\sqrt{\frac{a}{\nu(1-\beta t)}}, \tag{6.9}$$

and Eq. (6.8), the Eq. (6.1) is satisfied automatically and Eqs. (6.2) − (6.7) yield

$$f'''[1 + We_1^2 f''^2]^{\frac{n-3}{2}}[1 + nWe_1^2 f''^2] - S\left(f' + \frac{1}{2}\eta f''\right) - f'^2 + f''(f + g) = 0, \tag{6.10}$$

$$g'''[1 + We_2^2 g''^2]^{\frac{n-3}{2}}[1 + nWe_2^2 g''^2] - S\left(g' + \frac{1}{2}\eta g''\right) - g'^2 + g''(f + g) = 0, \tag{6.11}$$

116

$$(1 + \varepsilon\theta)\,\theta'' + \varepsilon\theta'^2 + \Pr(f + g)\theta' - 2\Pr f'\theta - \Pr\tfrac{S}{2}\left(3\theta + \eta\theta'\right)$$

$$+ \Pr N_b\theta'\phi' + \Pr N_t\theta'^2 + \Pr\delta\theta = 0, \tag{6.12}$$

$$\phi'' + \Pr Le(f + g)\phi' - \Pr S\left(\phi + \frac{1}{2}\eta\phi'\right) + \left(\frac{N_t}{N_b}\right)\theta'' = 0 \tag{6.13}$$

$$f(0) = 0, \quad g(0) = 0, \quad f'(0) = 1, \quad g'(0) = \alpha,$$

$$\theta(0) = 1, \quad N_b\phi'(0) + N_t\theta'(0) = 0, \tag{6.14}$$

$$f' \to 0, \quad g' \to 0, \quad \theta \to 0 \quad \phi \to 0 \quad \text{as} \quad \eta \to \infty. \tag{6.15}$$

In the above equations, $S\left(= \frac{\beta}{a}\right)$ is the unsteadiness parameter, and $\delta\left(= \frac{Q_0(1-\beta t)}{a(\rho c)_f}\right)$ the heat sink/source parameter.

6.2   Engineering and Industrial Quantities of Interest

From the physical point of view, the quantities of industrial and engineering interest in materials processing are the skin friction coefficients and heat transfer rate which may be defined in dimensionless forms

$$\tfrac{1}{2}C_{fx}\,\mathrm{Re}_x^{\frac{1}{2}} = f''(0)[1 + We_1^2 f''^2(0)]^{\frac{n-1}{2}}, \tag{6.16}$$

$$\tfrac{1}{2}\left(\frac{U_w}{V_w}\right)C_{fy}\,\mathrm{Re}_x^{\frac{1}{2}} = g''(0)[1 + We_2^2 g''^2(0)]^{\frac{n-1}{2}}, \tag{6.17}$$

and

$$\mathrm{Re}_x^{-\frac{1}{2}}\,Nu_x = -\theta'(0). \tag{6.18}$$

6.3   Graphical Illustration and Analysis

The main theme of this section is to scrutinize the impact of variable thermal conductivity and heat source/sink in unsteady 3D flow of Carreau nanofluid over a bidirectional stretching surface. Widespread numerical computation namely, bvp4c has been reported for the exploration of scheming parameters on the velocity components, temperature and concentration fields. The graphs are portrayed and the discrepancy of the local skin friction coefficients and the local

Nusselt number is established in tabular arrangement and deliberated in details.

Figures 6.1(a − d) are sketched to visualize the features of the unsteadiness parameter (S) on the nanoliquid velocity components $f'(\eta)$ and $g'(\eta)$ for shear thinning and shear thickening liquids. The diminishing behavior in velocity components and associated momentum boundary layer thickness with enhanced values of S is being acknowledged. Physically, S is inversely proportional to the stretching rate of the nanoliquid along x−direction. When the values of is S intensified the stretching rate along x−direction decline due to which the velocity of the nanoliquid is diminished.

Figures 6.2(a − d) are drafted to deliberate the variations in the nanoliquid temperature $\theta(\eta)$ and concentration $\phi(\eta)$ distributions under the influence of the unsteadiness parameter (S). It can be perceived from these sketches that the nanoliquid temperature and concentration distributions are declined for intensifying values of S. Physically, by strengthening the value of S reduces the velocity of the nanoliquid along x−direction due to which kinetic energy of the nanoliquid decreases. Therefore, the temperature of the nanoliquid declines. **Figures 6.3(a − d)** demonstrate the impact of heat source parameter $(\delta > 0)$ on the nanoliquid temperature and concentration profiles. It is manifest from these figures that the nanoliquid temperature and concentration profiles enhance with the augmented values of $\delta > 0$ for shear thinning liquid and shear thickening liquids. As heat transfer mechanism contributes additional heat to the liquid that resembles to an intensification in the nanoliquid temperature and the thickness of thermal boundary layer. **Figures 6.4(a − d)** demonstrate the domination of the thermal conductivity parameter (ε) on the nanoliquid temperature and concentration distributions. From these graphs it is established that boosting values of ε enhance the temperature and concentration distributions. Physically, the thermal conductivity of the Carreau nanoliquids enhances when ε increases due to which temperature of the nanoliquids boosts up. **Figures 6.5(a − d)** are sketched to interpret the features of thermophoresis parameter (N_t) on nanoliquid temperature and concentration distributions. It is reported that the temperature and concentration of the nanoliquid across the thickness of boundary layer rise with the emergent values of N_t. Physically, this is because of the statistic that the difference between the temperature of wall and the reference temperature rises which intensify the nanoliquid temperature field. Moreover, in the flow domain of the particulate structure there is a temperature gradient in hotter regions which

causes the smallest elements incline to isolated quicker. Consequently, the surface temperature of the nanoliquid and its thickness of boundary layer enhance. Additionally, growing values of N_t physically means that the small nanoparticles are pulled away from the warm surface to the cold surface. Therefore, the higher number of small nanoparticles are dragged away from the warm surface due to which concentration of the nanoliquid declines.

6.3.1 Tabular Representations

The coefficients of skin friction $\left(\frac{1}{2} C_{fx} \operatorname{Re}_x^{\frac{1}{2}}, \ \frac{1}{2} \left(\frac{U_w}{V_w} \right) C_{fy} \operatorname{Re}_x^{\frac{1}{2}} \right)$ and heat transport rate $\left(\operatorname{Re}_x^{-\frac{1}{2}} Nu_x \right)$ of nanoliquid at the boundary of the stretched sheet are presented through **Tables 6.1** and **6.2**. By keeping the other nonlinear material parameters fixed, an augmentation in S and α corresponds an enhancement in the magnitude of $\frac{1}{2} C_{fx} \operatorname{Re}_x^{\frac{1}{2}}, \ \frac{1}{2} \left(\frac{U_w}{V_w} \right) C_{fy} \operatorname{Re}_x^{\frac{1}{2}}$. Moreover, it appears from **Table 6.2** that heat transport quantity $\operatorname{Re}_x^{-\frac{1}{2}} Nu_x$ of nanoliquid augment with amassed values of S and Pr; however, the opposite tendency is pragmatic for the ε, N_t and $\delta > 0$ for both shear thinning/thickening liquids. Furthermore, the numerical values of $\operatorname{Re}_x^{-\frac{1}{2}} Nu_x$ for $(n = 0.5, 1.5$ and $3)$ wide-ranging of Pr is depicted through **Table 6.3**. It is also noted that amassed values of Pr enhance the heat transport amount in all circumstances.

6.3.2 Confirmation of Numerical Outcomes

For the legitimacy of our outcomes, a comparison **Table 6.4** is structured in a limiting case i.e., in case of 2D flow. **Tables 6.5** and **6.6** contemporary the assessment of numerically scheme bvp4c with homotopy perturbation method (HPM) [115], exact solutions [115], homotopy analysis method (HAM) (cf. Chapter 2) and bvp4c (cf. Chapter 2) for distinct values of α. A remarkable assertion is distinguished in a limiting sense from these tables.
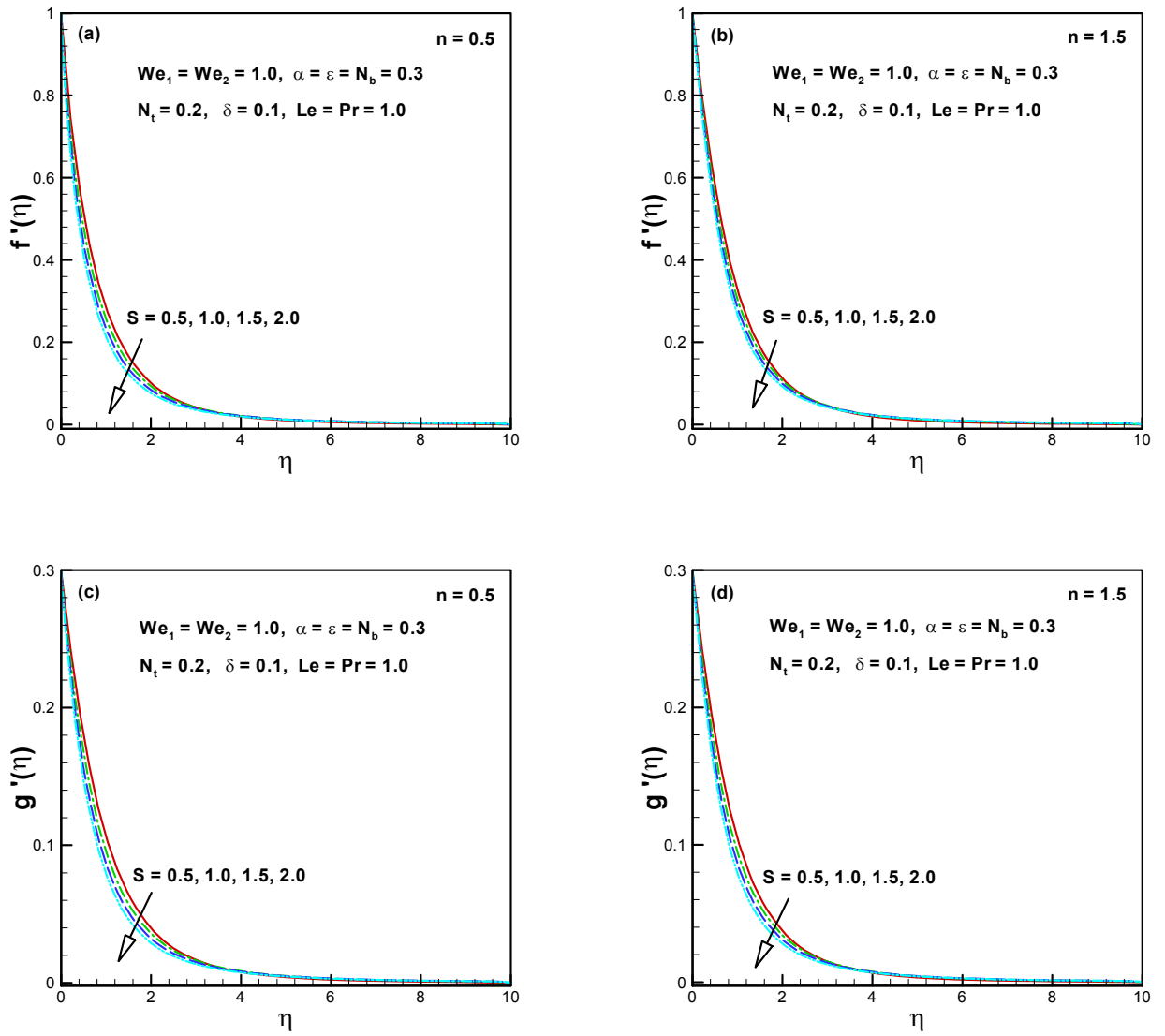
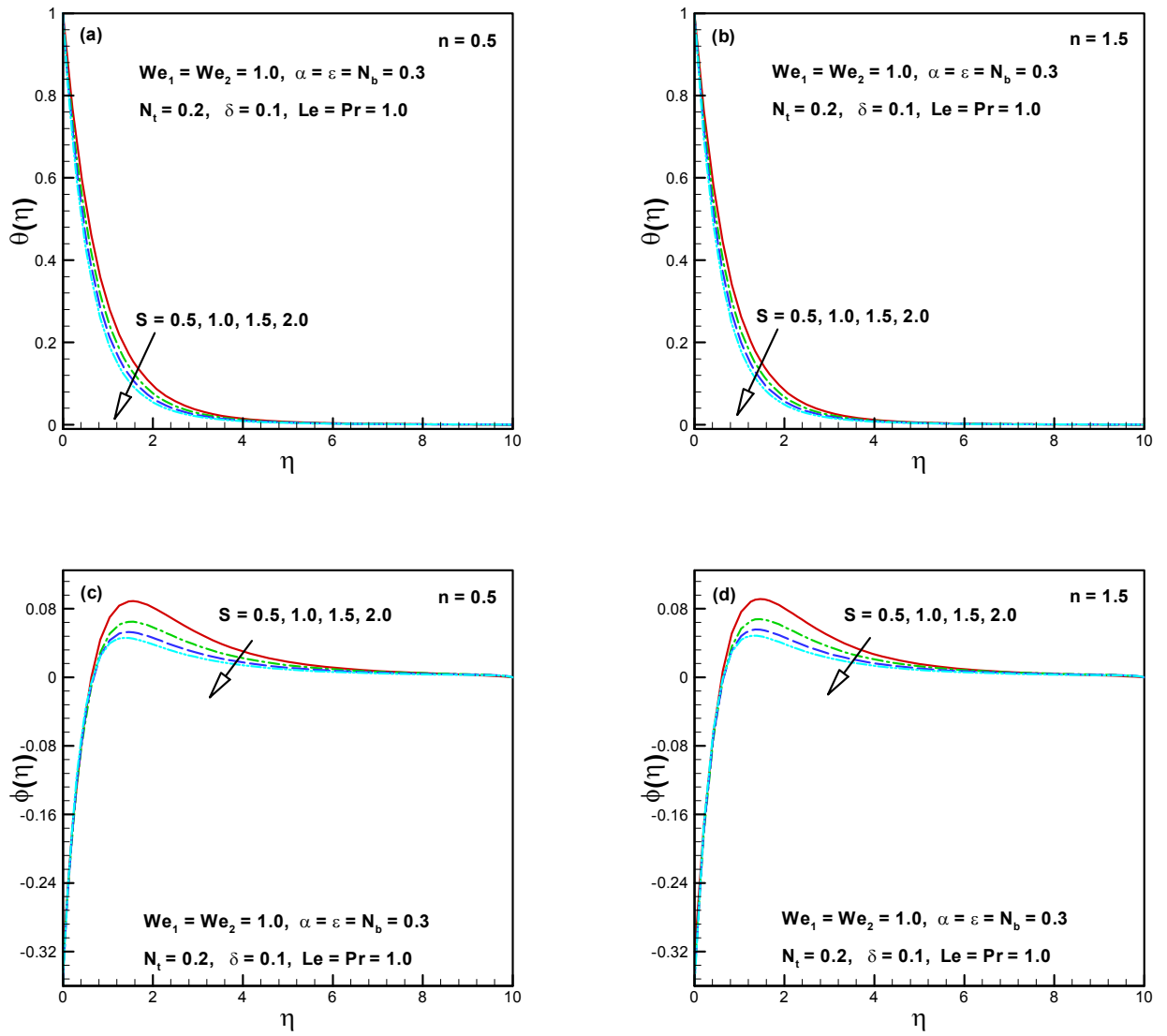**Figure 6.1(a − d):** Influence of S on $f'(\eta)$ and $g'(\eta)$.

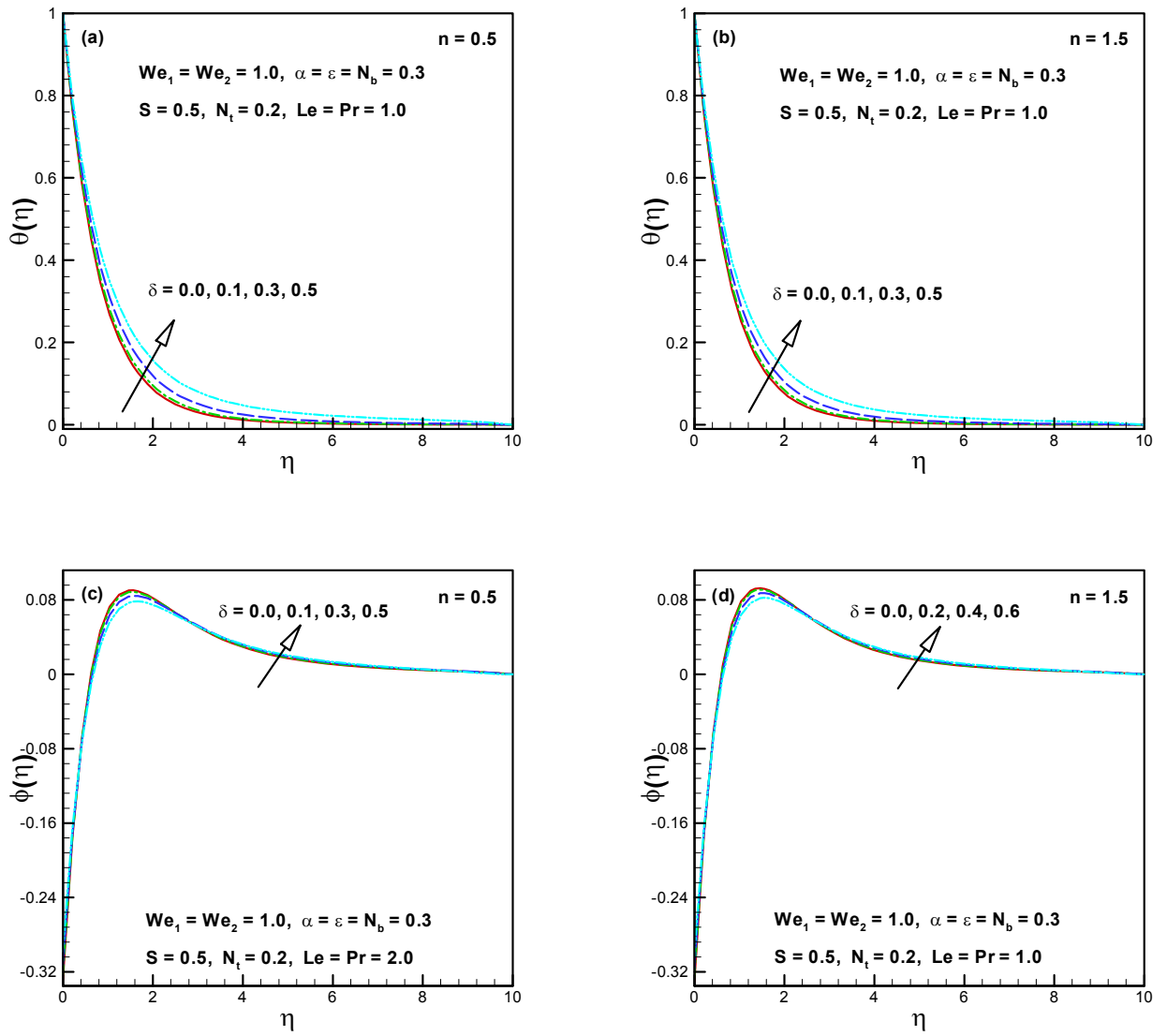**Figure 6.2(a − d)**: Influence of S on $\theta(\eta)$ and $\phi(\eta)$.

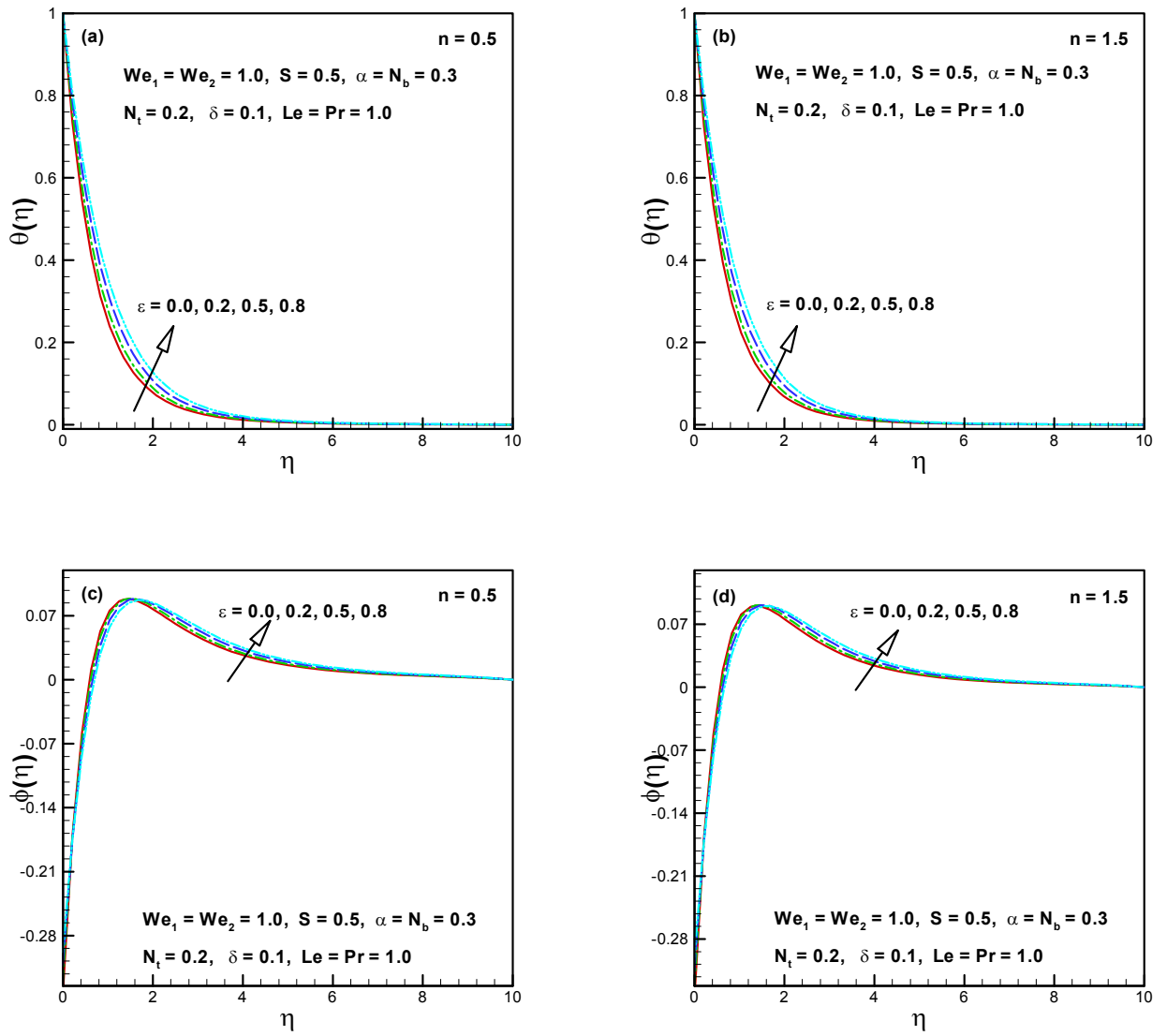**Figure 6.3(a − d)**: Influence of $\delta > 0$ on $\theta(\eta)$ and $\phi(\eta)$.

Figure 6.4(**a** − **d**): Influence of ε on $\theta(\eta)$ and $\phi(\eta)$.
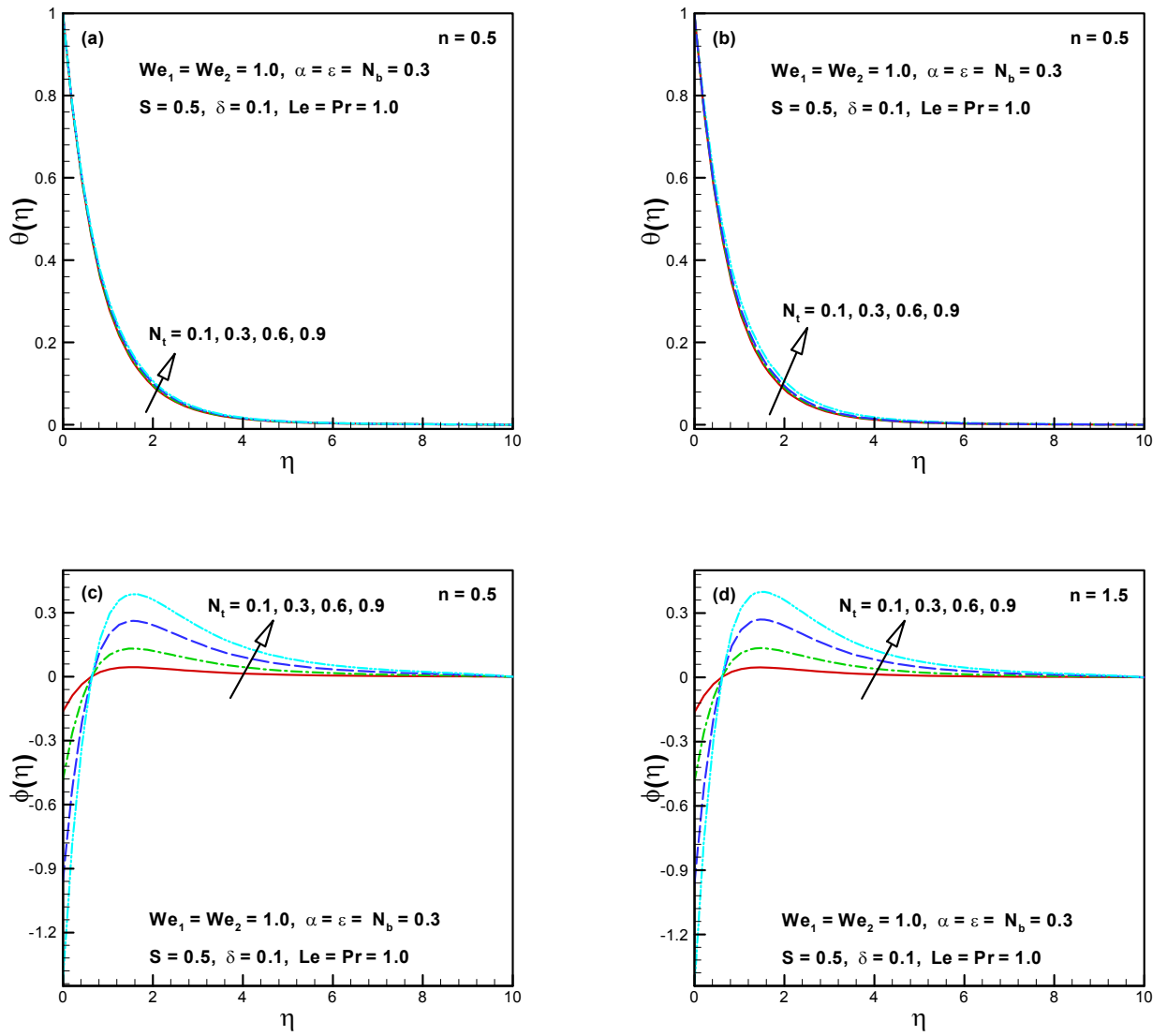
Figure 6.5(a − d): Influence of N_t on $\theta(\eta)$ and $\phi(\eta)$.

Table 6.1: Outcomes of $\left(\frac{1}{2}C_{fx}\operatorname{Re}_{x}^{\frac{1}{2}}, \frac{1}{2}C_{fy}\left(\frac{U_w}{V_w}\right)\operatorname{Re}_{x}^{\frac{1}{2}}\right)$ for We_1, We_2, S and α.

We_1	We_2	S	α	$\frac{1}{2}C_{fx}\operatorname{Re}_{x}^{\frac{1}{2}}$		$\frac{1}{2}C_{fy}\left(\frac{U_w}{V_w}\right)\operatorname{Re}_{x}^{\frac{1}{2}}$	
				$n=0.5$	$n=1.5$	$n=0.5$	$n=1.5$
1.0	1.0	0.5	0.3	-1.495932	-2.275974	-0.3014584	-0.3224466
1.5				-1.735959	-3.240193	-0.2992882	-0.3238545
2.0				-1.953110	-4.360016	-0.2973149	-0.3250810
2.5				-2.139428	-5.604837	-0.2956285	-0.3261349
1.0	1.5			-1.495648	-2.276565	-0.3074282	-0.3473583
	2.0			-1.495263	-2.277291	-0.3156383	-0.3796407
	2.5			-1.494790	-2.278095	-0.3258926	-0.4178941
	1.0	0.7		-1.597571	-2.473501	-0.3239701	-0.3481788
		0.9		-1.698759	-2.674949	-0.3456479	-0.3734159
		1.1		-1.799172	-2.879372	-0.3664994	-0.3981124
		0.5	0.5	-1.540941	-2.374278	-0.5729707	-0.6737814
			0.7	-1.583640	-2.474459	-0.9220556	-1.2239450
			1.0	-1.642297	-2.629779	-1.6422970	-2.6297790

Table 6.2: Outcomes of $\left(\mathrm{Re}_x^{-\frac{1}{2}} Nu_x\right)$ for S, ε, Pr, N_t and δ when $N_b = 0.3$ and $Le = 1.0$ are fixed.

S	ε	Pr	N_t	δ	$\mathrm{Re}_x^{-\frac{1}{2}} Nu_x$	
					$n = 0.5$	$n = 1.5$
0.5	0.3	1.0	0.2	0.1	1.26096	1.29885
0.7					1.32981	1.36747
0.9					1.39482	1.43240
1.1					1.45670	1.49430
0.5	0.5				1.14343	1.17857
	0.8				1.01115	1.04311
	1.0				0.94252	0.97278
	0.3	1.3			1.46421	1.50558
		1.6			1.64507	1.68907
		2.0			1.86106	1.90771
		1.0	0.4		1.25338	1.29116
			0.6		1.24591	1.28359
			0.8		1.23855	1.27613
			0.2	0.2	1.22654	1.26605
				0.3	1.19030	1.23167
				0.4	1.15174	1.19533

Table 6.3: Outcomes of $\left(\mathrm{Re}_x^{-\frac{1}{2}} Nu_x \right)$ for Pr when $We_1 = We_2 = 2.0$, $S = 0.5$, $\alpha = \epsilon = N_b = 0.3$, $N_t = 0.2$ and $Le = 1.0$ are fixed.

| Pr | $\mathrm{Re}_x^{-\frac{1}{2}} Nu_x$ | | |
	$n = 0.5$	$n = 1.5$	$n = 3.0$
0.8	1.07517	1.1593	1.20571
1.1	1.29391	1.38825	1.43679
1.4	1.48539	1.58709	1.63678
1.7	1.65749	1.76481	1.81518
2.0	1.81489	1.92667	1.97746
2.5	2.05234	2.16985	2.22106
3.0	2.26599	2.38783	2.43926
3.5	2.46131	2.58663	2.63818
4.0	2.64194	2.77004	2.82165
5.0	2.96863	3.10102	3.15265
6.0	3.25964	3.39514	3.44671
7.0	3.52319	3.66105	3.71252
8.0	3.76469	3.90438	3.95573
9.0	3.98798	4.12910	4.18031
10	4.19585	4.33811	4.38915

Table 6.4: A comparison of $f''(0)$ for S when $We_1 = We_2 = \alpha = 0$ and $n = 1$.

| | $f''(0)$ | | |
S	Sharidan *et al.* [120]	Chamkha *et al.* [121]	Present(bvp4c)
0.8	-1.261042	-1.261512	-1.261044
1.2	-1.377722	-1.378052	-1.3777280
2.0	-1.587362	-	-1.587371

Table 6.5: A comparison of $-f''(0)$ for α when $We_1 = We_2 = S = 0$ and $n = 1$.

			$-f''(0)$		
α	Ariel [115]	Ariel [115]	[cf. Chapter 2]	[cf. Chapter 2]	Present
	(HPM)	(Exact)	Table 2.3 (HAM)	Table 2.3 (bvp4c)	(bvp4c)
0	1	1	1	1	1
0.1	1.017027	1.020264	1.020263	1.020264	1.020264
0.2	1.034587	1.039497	1.039496	1.039497	1.039497
0.3	1.057470	1.057956	1.057956	1.057956	1.057956
0.4	1.070529	1.075788	1.075787	1.075788	1.075789
0.5	1.088662	1.093095	1.093095	1.093095	1.093095
0.6	1.106797	1.109946	1.109946	1.109946	1.109947
0.7	1.124882	1.126397	1.126396	1.126397	1.126398
0.8	1.142879	1.142488	1.142489	1.142488	1.142489
0.9	1.160762	1.158253	1.158252	1.158253	1.158254
1.0	1.178511	1.17372	1.173720	1.173720	1.173721

Table 6.6: A comparison of $-g''(0)$ for α when $We_1 = We_2 = S = 0$ and $n = 1$.

α	Ariel [115] (HPM)	Ariel [115] (Exact)	[cf. Chapter 2] Table 2.3(HAM)	[cf. Chapter 2] Table 2.3 (bvp4c)	Present (bvp4c)
			$-g''(0)$		
0	0.0	0.0	0.0	0.0	0.0
0.1	0.070399	0.066847	0.066848	0.0668485	0.06684873
0.2	0.158231	0.148737	0.148737	0.1487382	0.14873860
0.3	0.254347	0.243360	0.243360	0.2433607	0.2433613
0.4	0.360599	0.349209	0.349208	0.3492087	0.3492100
0.5	0.476290	0.465205	0.465207	0.4652046	0.4652060
0.6	0.600833	0.590529	0.590528	0.5905229	0.5905299
0.7	0.733730	0.724532	0.724530	0.7245312	0.7245326
0.8	0.874551	0.866683	0.866682	0.8666822	0.8666836
0.9	1.022922	1.016539	1.016540	1.016538	1.0165390
1.0	1.178511	1.173721	1.173721	1.173720	1.173721

Chapter 7

Influence of Arrhenius Activation Energy in 3D Chemically Reactive Flow of Unsteady Carreau Nanofluid

The forthright intention of this chapter is to scrutinize the up-to-date advances in nanoparticles by utilizing the properties of nonlinear mixed convection and binary chemical reaction with Arrhenius activation energy in time-dependent Carreau fluid flow. The energy and concentration terminologies contain Brownian and thermophoresis nanoparticles. The silent features of magnetohydrodynamic (MHD), non-uniform heat sink/source and thermal radiation are being presented. Additionally, heat and mass transport phenomena are manifest by convective conditions. Apposite conversions are executed to acquire the essential nonlinear ordinary differential equations (ODEs) structure and elucidated numerically via bvp4c. Graphs are portrayed and tables are structured to scrutinize the behavior of diverse influential variables. As of graphical consequences, it is scrutinized that the fluid velocities enhance for an intensification in the power law exponent. These outcomes reported that on the temperature field, thermal Biot number, radiation and Brownian motion parameters indicate analogous performance and intensify the temperature of Carreau fluid. Furthermore, augmenting performance is being established for activation energy and thermophrosis parameters; however, the behavior is quite antithesis for fitting rate constant.

7.1 Description of the Problem

Let us scrutinize unsteady 3D magnetohydrodynamic (MHD) convective flow of a Carreau nanofluid in the presence of suspended nanoparticles influenced by a bidirectional stretching surface. The flow is induced by a stretching surface in two nearby $x-$ and $y-$ directions with velocities $(u, v) = \left(\frac{ax}{1-\beta t}, \frac{by}{1-\beta t}\right)$, respectively, where $a, b > 0$ and the fluid occupies the region $z > 0$. The structure of non-uniform heat sink/source with nonlinear mechanism of thermal radiation and mixed convection are also integrated. Furthermore, concentration equation deals with the impact of Arrhenius activation energy with the binary chemical reaction. In this clarification the Brownian and thermophoresis nanoparticles are also engaged. This chapter also pretends that the electric and induced magnetic fields are insignificant when equated with applied magnetic field. This concept is only effective when the magnetic Reynolds number is very small.

These attentions leads to the following equations of Carreau nanofluid:

$$\frac{\partial u}{\partial x} + \frac{\partial v}{\partial y} + \frac{\partial w}{\partial z} = 0, \tag{7.1}$$

$$\frac{\partial u}{\partial t} + u\frac{\partial u}{\partial x} + v\frac{\partial u}{\partial y} + w\frac{\partial u}{\partial z} = \nu\frac{\partial^2 u}{\partial z^2}\left[1 + \Gamma^2\left(\frac{\partial u}{\partial z}\right)^2\right]^{\frac{n-1}{2}}$$
$$+ \nu(n-1)\Gamma^2\left(\frac{\partial u}{\partial z}\right)^2\frac{\partial^2 u}{\partial z^2}\left[1 + \Gamma^2\left(\frac{\partial u}{\partial z}\right)^2\right]^{\frac{n-3}{2}} - \frac{\sigma B^2(t)}{\rho_f}u$$
$$+ g[\beta_T(T - T_\infty) + \beta_T^*(T - T_\infty)^2 + \beta_C(C - C_\infty) + \beta_C^*(C - C_\infty)^2], \tag{7.2}$$

$$\frac{\partial v}{\partial t} + u\frac{\partial v}{\partial x} + v\frac{\partial v}{\partial y} + w\frac{\partial v}{\partial z} = \nu\frac{\partial^2 v}{\partial z^2}\left[1 + \Gamma^2\left(\frac{\partial v}{\partial z}\right)^2\right]^{\frac{n-1}{2}}$$
$$+ \nu(n-1)\Gamma^2\left(\frac{\partial v}{\partial z}\right)^2\frac{\partial^2 v}{\partial z^2}\left[1 + \Gamma^2\left(\frac{\partial v}{\partial z}\right)^2\right]^{\frac{n-3}{2}} - \frac{\sigma B^2(t)}{\rho_f}v, \tag{7.3}$$

$$\frac{\partial T}{\partial t} + u\frac{\partial T}{\partial x} + v\frac{\partial T}{\partial y} + w\frac{\partial T}{\partial z} = \alpha_1\frac{\partial^2 T}{\partial z^2} + \tau\left[D_B\frac{\partial C}{\partial z}\frac{\partial T}{\partial z} + \frac{D_T}{T_\infty}\left(\frac{\partial T}{\partial z}\right)^2\right] - \frac{1}{(\rho c)_f}\frac{\partial q_r}{\partial z} + Q''', \tag{7.4}$$

$$\frac{\partial C}{\partial t} + u\frac{\partial C}{\partial x} + v\frac{\partial C}{\partial y} + w\frac{\partial C}{\partial z} = D_B\frac{\partial^2 C}{\partial z^2} + \frac{D_T}{T_\infty}\frac{\partial^2 T}{\partial z^2} - k_r^2(C - C_\infty)\left(\frac{T}{T_\infty}\right)^m\exp\left(-\frac{E^*}{K^*T}\right). \tag{7.5}$$

Subject to the boundary conditions

$$u = U_w(x,t) = \frac{ax}{1-\beta t}, \quad v = V_w(y,t) = \frac{by}{1-\beta t}, \quad w = 0,$$

$$-k\frac{\partial T}{\partial z} = h_f[T_f - T], \quad -D_B\frac{\partial C}{\partial z} = h_m[C_f - C] \quad \text{at} \quad z = 0, \tag{7.6}$$

$$u \to 0, \quad v \to 0, \quad T \to T_\infty, \quad C \to C_\infty \quad \text{as} \quad z \to \infty. \tag{7.7}$$

Here (β_T, β_c^*) are the nonlinear thermal and concentration expansions respectively, m the fitted rate constant $(-1 < m < 1)$, k_r the reaction rate, E^* the activation energy, $\kappa = 8.61 \times 10^5 eV/K$ the Boltzmann constant and whole expression $k_r^2 \left(\frac{T}{T_\infty}\right)^m \exp\left(-\frac{E^*}{\kappa T}\right)$ is entitled as modified Arrhenius equation.

The expression of non-uniform heat sink/source Q''' is defined as

$$Q''' = \frac{kU_w(x,t)}{x\nu}\left[h(T_f - T_\infty)f' + h^*(T - T_\infty)\right]. \tag{7.8}$$

Here (h, h^*) are the space and temperature dependent heat sink/source coefficients, respectively. Additionally, $(h, h^*) > 0$ relate to internal heat source and $(h, h^*) < 0$ internal heat sink parameters.

7.1.1 Appropriate Conversions

Let us define the following quantities

$$\theta(\eta) = \frac{T - T_\infty}{T_f - T_\infty}, \quad \phi = \frac{C - C_\infty}{C_f - C_\infty}. \tag{7.9}$$

The overhead conversions and Eq. (6.9) (cf. Chapter 6) satisfy Eq. (7.1) automatically and Eqs. (7.2) − (7.7) with Eq. (7.8) are reduced to the following ODEs

$$f'''[1 + We_1^2 f''^2]^{\frac{n-3}{2}}[1 + nWe_1^2 f''^2] - f'^2 + f''(f + g)$$
$$-S\left(f' + \frac{\eta}{2}f''\right) - M^2 f' + \lambda^*(1 + \xi_t\theta)\theta + \lambda^* N^*(1 + \xi_c\phi)\phi = 0, \tag{7.10}$$

$$g'''[1 + We_2^2 g''^2]^{\frac{n-3}{2}}[1 + nWe_2^2 g''^2] - g'^2 + g''(f + g) - S\left(g' + \frac{\eta}{2}g''\right) - M^2 g' = 0, \tag{7.11}$$

$$(1 + R_d)\theta'' + \Pr(f + g)\theta' - \Pr S\left(\theta + \frac{\eta}{2}\theta'\right) + \Pr[N_b\theta'\phi' + N_t\theta'^2] + \delta\theta + \delta^* f' = 0, \tag{7.12}$$

132

$$\phi'' + \Pr Le(f+g)\phi' + \left(\frac{N_t}{N_b}\right)\theta'' - \Pr S\left(\phi + \frac{\eta}{2}\phi'\right)$$
$$- \Pr Le\Lambda(1+\Lambda^*\theta)^m\phi\exp\left[\frac{-E}{1+\Lambda^*\theta}\right] = 0, \tag{7.13}$$

with BCs

$$f(0) = 0, \quad g(0) = 0, \quad f'(0) = 1, \quad g'(0) = \alpha,$$
$$\theta'(0) = -\gamma_1(1-\theta(0)), \quad \phi'(0) = -\gamma_2(1-\phi(0)), \tag{7.14}$$
$$f' \to 0, \quad g' \to 0, \quad \theta \to 0 \quad \phi \to 0 \quad \text{as} \quad \eta \to \infty. \tag{7.15}$$

In the above expressions, $\lambda^*\left(=\frac{g\beta_T(T_f-T_\infty)}{aU_w(x,t)}\right)$ is the mixed convection parameter, $N^*\left(=\frac{\beta_C(C_f-C_\infty)}{\beta_T(T_f-T_\infty)}\right)$ the buoyancy ratio parameter, $\xi_t\left(=\frac{\beta_T^*(T_f-T_\infty)}{\beta_T}\right)$ and $\xi_c\left(=\frac{\beta_C^*(C_f-C_\infty)}{\beta_C}\right)$ the nonlinear convection parameters due to temperature and concentration, $\gamma_i\left(=\frac{h_f}{k}\sqrt{\frac{\nu(1-\beta t)}{a}}, \frac{h_m}{D_B}\sqrt{\frac{\nu(1-\beta t)}{a}}\right)$ $i=1,2$, are the thermal and concentration Biot numbers, $\Lambda\left(=\frac{k_r^2(1-\beta t)}{a}\right)$ the reaction rate parameter, $\Lambda^*\left(=\frac{T_f-T_\infty}{T_\infty}\right)$ the temperature difference parameter, and $E\left(=\frac{E^*}{\kappa T_\infty}\right)$ the activation energy parameter respectively.

7.2 Engineering and Industrial Quantities of Interest

The notable quantities of physical concern are the local skin friction coefficients (C_{fx}, C_{fy}), heat and mass transfer rates (Nu_x, Sh_x) and are defined in the following dimensionless variables:

$$\frac{1}{2}\operatorname{Re}_x^{\frac{1}{2}} C_{fx} = f''(0)[1+We_1^2f''^2(0)]^{\frac{n-1}{2}},$$
$$\frac{1}{2}\left(\frac{U_w}{V_w}\right)\operatorname{Re}_x^{\frac{1}{2}} C_{fy} = g''(0)[1+We_2^2g''^2(0)]^{\frac{n-1}{2}}, \tag{7.16}$$

and

$$\operatorname{Re}_x^{-\frac{1}{2}} Nu_x = -\left(1+R_d\right)\theta'(0), \quad \operatorname{Re}_x^{-\frac{1}{2}} Sh_x = -\phi'(0). \tag{7.17}$$

7.3 Graphical Illustration and Analysis

The framework of this section is to scrutinize the properties of Arrhenius activation energy with binary chemical reaction in 3D Carreau nanofluid flow subject to nonlinear phenomena of mixed convection and radiation. Additionally, MHD, non-uniform heat sink/source and convective conditions are involved. The bvp4c scheme has been executed to elucidate the present ODEs. The inducement of numerous parameters on velocities $f'(\eta)$ and $g'(\eta)$, temperature $\theta(\eta)$ and concentration $\phi(\eta)$ are portrayed and discussed.

The physical enactment of power-law exponent (n) for both shear thinning/thinking fluids $(n = 0.5$ and $1.5)$ on fluid velocities $f'(\eta)$ and $g'(\eta)$ are presented in **figures 7.1(a − d)**. These strategies display augmenting performance for larger values of n. It is also reported that the thickness of the momentum boundary layer and fluid velocities exaggerate when the values of n enhance. **Figures 7.2(a − d)** portray the properties of mixed convection parameter (λ^*) on the velocities of Carreau fluid for shear thinning/thickening fluids. In fact, from these schemes the larger λ^* intensifies the liquid velocity $f'(\eta)$ for both $(n < 1$ and $n > 1)$. This arises owing to the fact that a strong buoyancy force appears which specifies the intensification of velocity field $f'(\eta)$ for both situations. Furthermore, differing tendency is being established for velocity field $g'(\eta)$ for boosting value of λ^*. The higher value of λ^* causes the decline of $g'(\eta)$ and its allied thickness of the layer as exposed in **figures 7.2(c)** and **7.2(d)**.

Figures 7.3(a, b) and **7.4(a, b)** are envisioned to picture the performance of nonlinear convection parameter (ξ_t) and magnetic parameter (M) on temperature field $\theta(\eta)$ for the cases $n < 1$ and $n > 1$. The portrayal of these designs, specifies diverse behavior for both ξ_t and M. Intensifying values of ξ_t not only diminish the temperature of Carreau nanoliquid but, also the allied thermal thickness of layer falloff. This mechanism relates to stronger buoyancy force, since ξ_t be influenced by buoyancy force. Therefore, in consequence of this buoyancy force the Carreau liquid temperature decays. Similarly, M intensifies the temperature field for both circumstances. Physically, by reason of higher M enriches the Lorentz force and form additional struggle to the fluid gesture and the energy is converted into heat. This fact causes to the enhancing of $\theta(\eta)$. **Figures 7.5(a, b)** and **7.6(a, b)** expose the enhancing trend for $(n = 0.5)$ and $(n = 1.5)$ cases for increasing values of Brownian (N_b) and thermophrosis (N_t) nanoparticles on $\theta(\eta)$. These nanoparticles spectacles a forceful part of the enrichment of heat

transport properties of Carreau fluid. At this instant, outcomes indicate that N_b and N_t raise the temperature and thermal thickness of the boundary layer. As, thermophoretic potency is exaggerated by the temperature gradient, the heated particles dragged away from hot to cold surface which enhances $\theta(\eta)$. Consequently, vast amount of nanoparticles is transferred away from the intense surface which intensify the temperature of Carreau liquid. Hence, the analogous performance ensued for both parameters in both circumstances in these plots. To disclose the enactment of thermal Biot (γ_1) and thermal radiation (R_d) parameters for two different values of n ($n = 0.5$ and $n = 1.5$) **figures 7.7(a, b)** and **7.8(a, b)** are exposed. It is scrutinized that the intensifying values of γ_1 and R_d present analogous impact and enhance both the temperature and thermal layer thickness of Carreau fluid. Physically, an increasing value of γ_1 intensifies the heat transport quantity which boosts $\theta(\eta)$. Additionally, **figures 7.8(a, b)** indicate that higher values of R_d formed significant heat throughout radiation processes in functioning liquid which intensifies $\theta(\eta)$.

Figures 7.9(a, b) and **7.10(a, b)** capture the portrayal of Brownian (N_b) and thermophrosis (N_t) nanoparticles on concentration $\phi(\eta)$ scattering for shear thinning/thickening liquids. These presentations indicate that both the thickness of concentration boundary layer and concentration of Carreau nanofluid are diminishing functions of N_b; however, for N_t conflicting drift is being reported in both instances. The larger values of N_b intensify the nanoparticles transport rate with different velocities in arbitrary direction owing to the Brownian influence. Consequently, higher N_b corresponds to a reduction in $\theta(\eta)$ for $n = 0.5$ and 1.5. Additionally, the liquid thermal conductivity in the existence of nanoparticles intensifies. The rise in N_t contributes higher liquid thermal conductivity which spectacles the higher concentration as seen in **figures 7.10(a, b)**. Thus, the performance is thoroughly conflicting for both parameters on concentration scattering. The aspects of reaction rate (Λ) and temperature difference (Λ^*) parameters for concentration of Carreau nanofluid with shear thinning/thickening properties are reported via **figures 7.11(a, b)** and **7.12(a, b)**. There is a diminishing trend being acknowledged for both considerations. As we improve the value of Λ the destructive amount of chemical reaction also rises. It is used to dismiss or separate the liquid specie more efficiently. When the destructive chemical reaction parameter is enlarged then a reduction in the nanoparticle concentration field is detected. Similarly, larger Λ^* displays that the thickness of concentration as

well as the concentration field decay for $n = 0.5$ and 1.5. To scrutinize the consequence of shear thinning/thickening liquids for fitted rate constant (m) and activation energy parameter (E) on concentration field, **figures 7.13(a, b)** and **7.14(a, b)** are drafted. A dissimilar enactment is noted for these schemes. The enhancing value of these parameters causes a decline in the concentration field for m but it enhances for E. The larger m spectacles an increase in nanoparticle concentration for $n = 0.5$ and 1.5 as fitted rate constant is intensifying. Additionally, physically advanced values of E falling-off the modified Arrhenius function which ultimately stimulates the generative chemical reaction quantity. Thus, the concentration of Carreau fluid augments.

7.3.1 Tabular Representations

Tables 7.1 and **7.2** are structured for the intensifying value of influential parameters on local skin friction coefficients $\left(\frac{1}{2} \mathrm{Re}_x^{\frac{1}{2}} C_{fx}, \ \frac{1}{2} \left(\frac{U_w}{V_w} \right) \mathrm{Re}_x^{\frac{1}{2}} C_{fy} \right)$, heat and mass transfer amount $\left(\mathrm{Re}_x^{-\frac{1}{2}} Nu_x, \ \mathrm{Re}_x^{-\frac{1}{2}} Sh_x \right)$ on Carreau nanofluid for $n < 1$ and $n > 1$. From these tables, outcomes acknowledge that the $\left(\frac{1}{2} \mathrm{Re}_x^{\frac{1}{2}} C_{fx} \right)$ intensifies for S, M and m; however, it falloffs for λ^*, N_t, N_b and E. Instead of this, $\left(\frac{1}{2} \left(\frac{U_w}{V_w} \right) \mathrm{Re}_x^{\frac{1}{2}} C_{fy} \right)$ exhibits boosting enactment for S, M, λ^*, N_t, N_b and E but for m its falloff for both cases *i.e.*, $n = 0.5$ and 1.5. The heat transport amount for S, λ^*, m have conflicting tendency when we compare with M, N_t, N_b and E. Moreover, the mass transport amount diminishes for S, M, N_t and E and intensify for λ^*, N_b and m for both values of $n = 0.5$ and 1.5.

7.3.2 Confirmation of Numerical Outcomes

For the endorsement of numerical upshots, **Tables (7.3) to (7.5)** are documented. **Table 7.3** is the assessment table of $-f''(0)$ in the restrictive sense while **Tables 7.4** and **7.5** are the estimated value of local skin friction coefficients $\left(\frac{1}{2} \mathrm{Re}_x^{\frac{1}{2}} C_{fx}, \ \frac{1}{2} \left(\frac{U_w}{V_w} \right) \mathrm{Re}_x^{\frac{1}{2}} C_{fy} \right)$ for both values of $n = 0.5$ and $n = 1.5$ with those of (cf. Chapter 6). From both these tables, a remarkable agreement is being reported with earlier obtainable fictions.
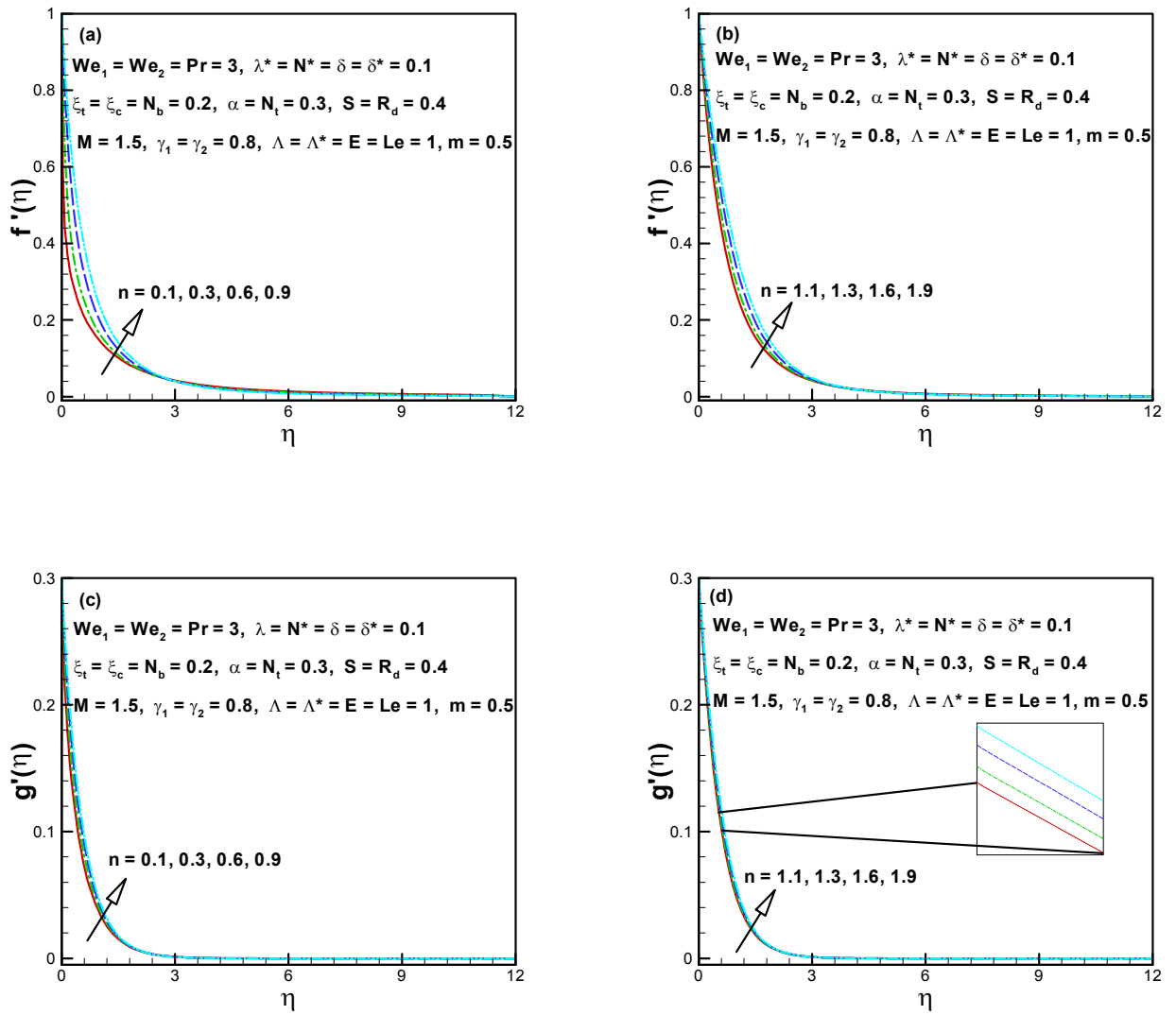
(a)

$We_1 = We_2 = Pr = 3, \ \lambda^* = N^* = \delta = \delta^* = 0.1$

$\xi_t = \xi_c = N_b = 0.2, \ \alpha = N_t = 0.3, \ S = R_d = 0.4$

$M = 1.5, \ \gamma_1 = \gamma_2 = 0.8, \ \Lambda = \Lambda^* = E = Le = 1, \ m = 0.5$

$n = 0.1, 0.3, 0.6, 0.9$

(b)

$We_1 = We_2 = Pr = 3, \ \lambda^* = N^* = \delta = \delta^* = 0.1$

$\xi_t = \xi_c = N_b = 0.2, \ \alpha = N_t = 0.3, \ S = R_d = 0.4$

$M = 1.5, \ \gamma_1 = \gamma_2 = 0.8, \ \Lambda = \Lambda^* = E = Le = 1, \ m = 0.5$

$n = 1.1, 1.3, 1.6, 1.9$

(c)

$We_1 = We_2 = Pr = 3, \ \lambda = N^* = \delta = \delta^* = 0.1$

$\xi_t = \xi_c = N_b = 0.2, \ \alpha = N_t = 0.3, \ S = R_d = 0.4$

$M = 1.5, \ \gamma_1 = \gamma_2 = 0.8, \ \Lambda = \Lambda^* = E = Le = 1, \ m = 0.5$

$n = 0.1, 0.3, 0.6, 0.9$

(d)

$We_1 = We_2 = Pr = 3, \ \lambda^* = N^* = \delta = \delta^* = 0.1$

$\xi_t = \xi_c = N_b = 0.2, \ \alpha = N_t = 0.3, \ S = R_d = 0.4$

$M = 1.5, \ \gamma_1 = \gamma_2 = 0.8, \ \Lambda = \Lambda^* = E = Le = 1, \ m = 0.5$

$n = 1.1, 1.3, 1.6, 1.9$

Figure 7.1(a − d): Influence of n on $f'(\eta)$ and $g'(\eta)$.
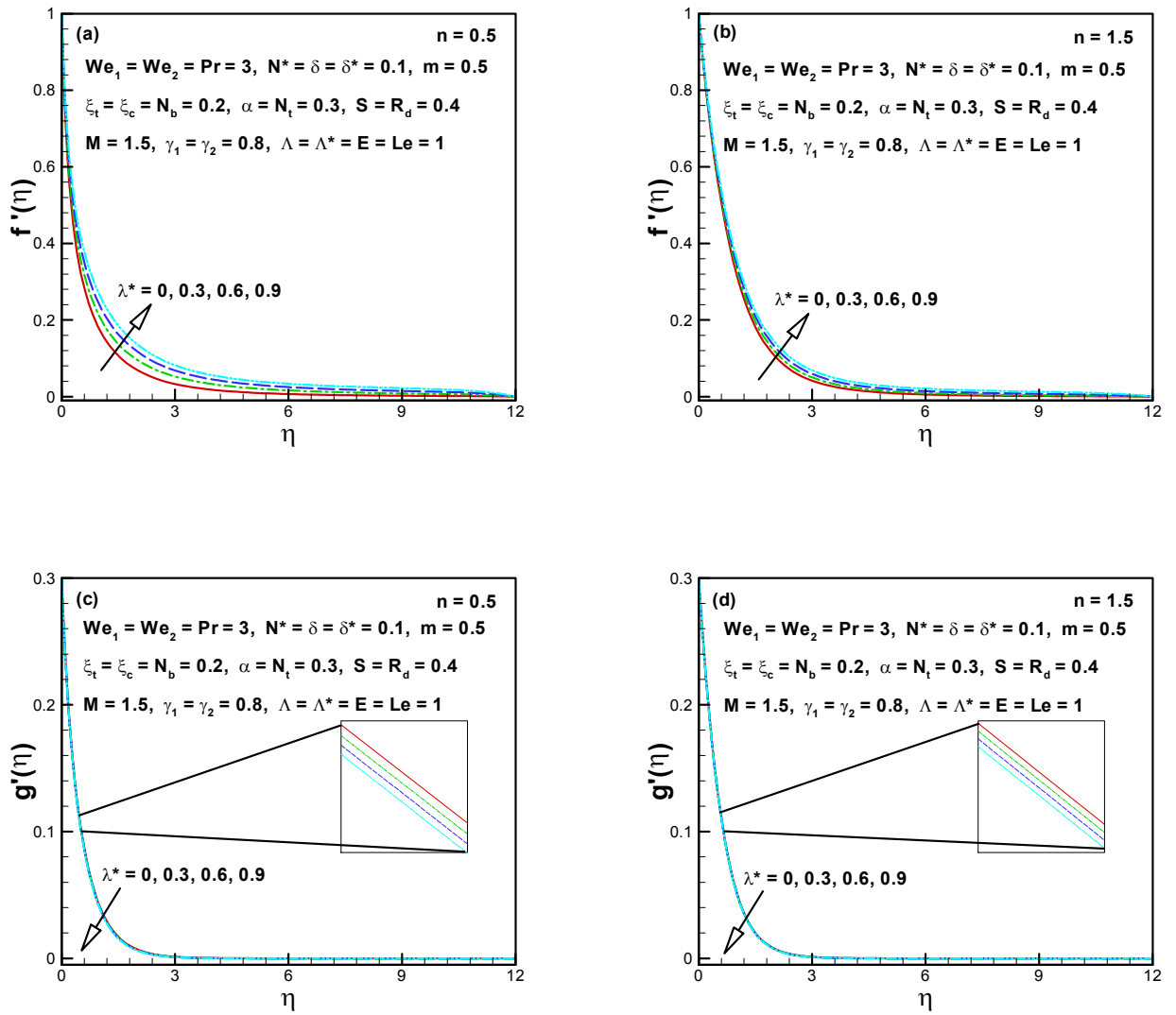
Figure 7.2(a − d): Influence of λ^* on $f'(\eta)$ and $g'(\eta)$.
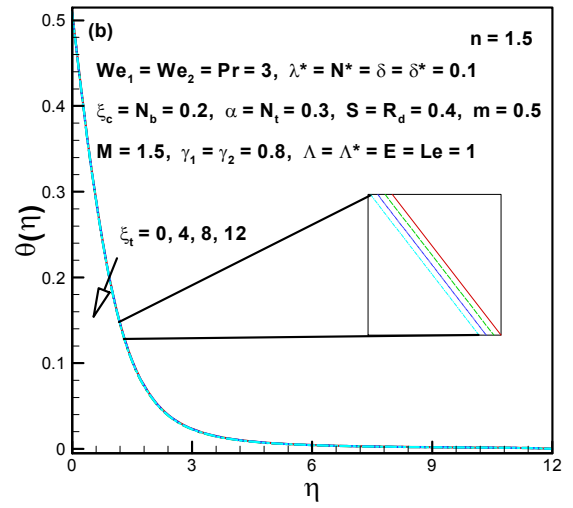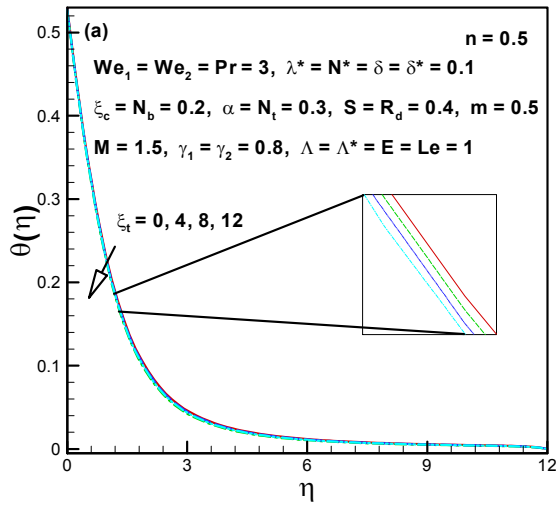
Figure 7.3(a, d): Influence of ξ_t on $\theta(\eta)$.
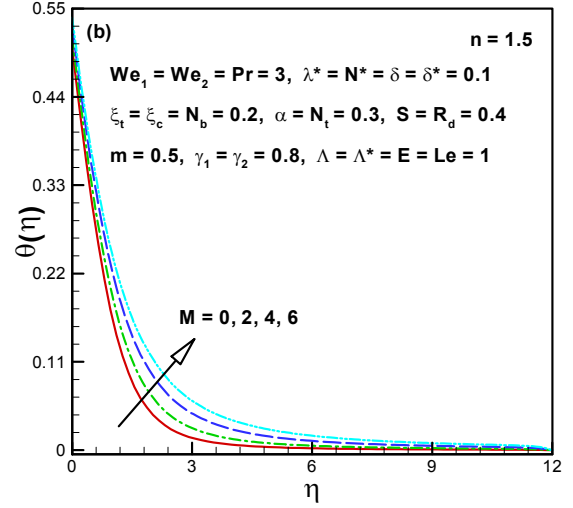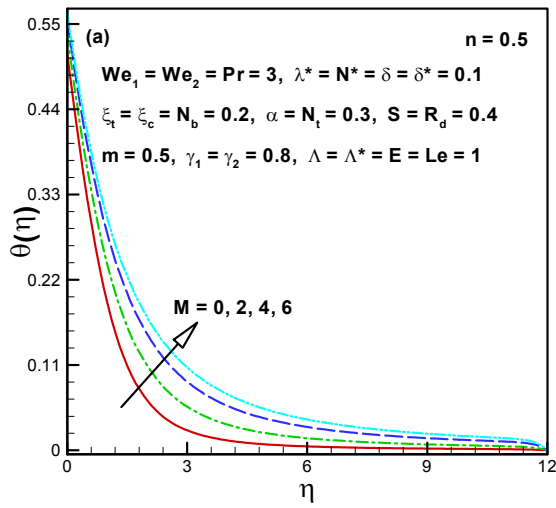
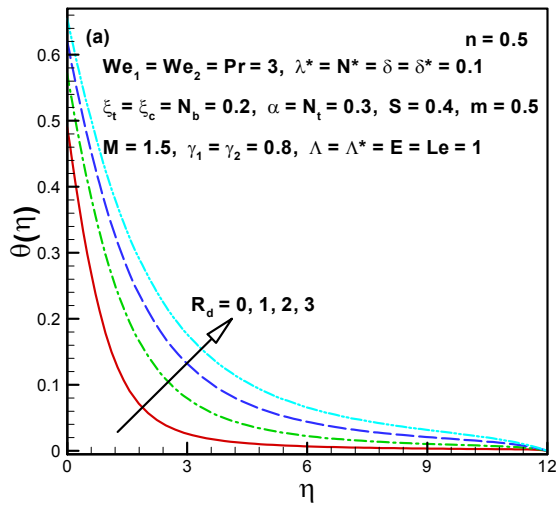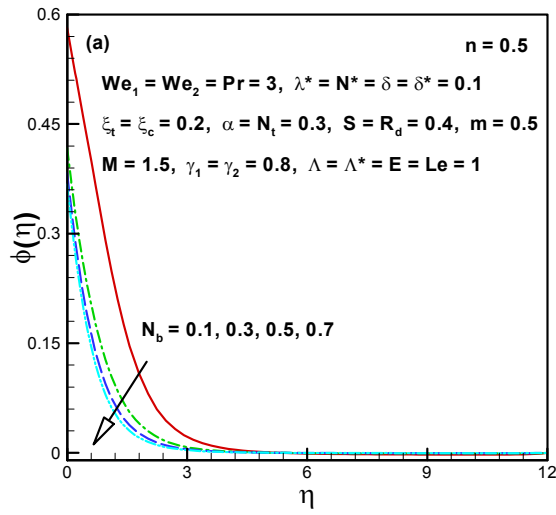**Figure 7.4(a, b):** Influence of M on $\theta(\eta)$.
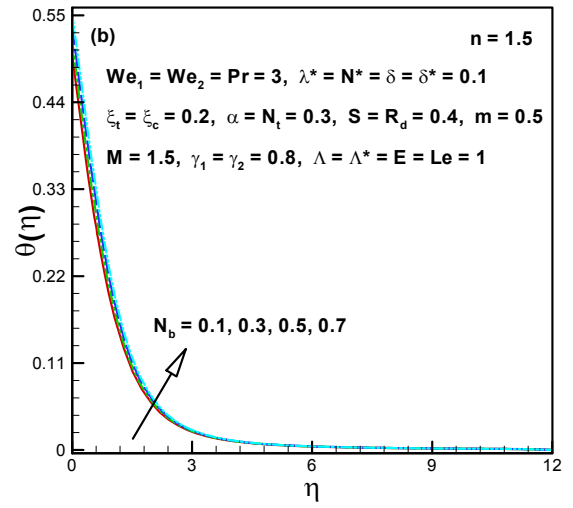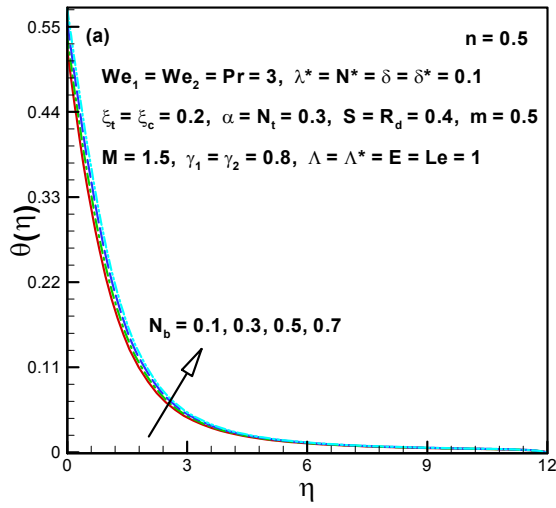
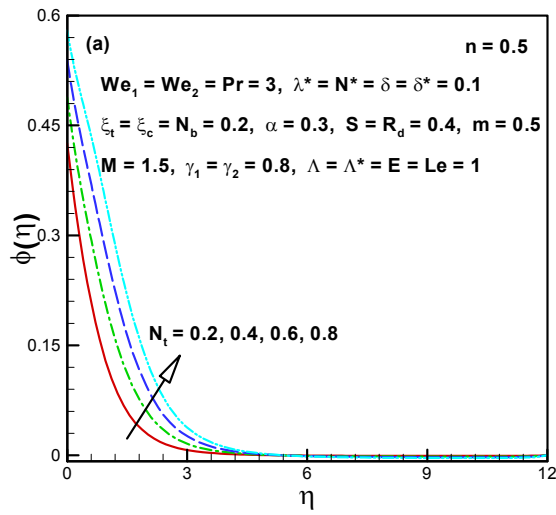**Figure 7.5(a, b):** Influence of N_b on $\theta(\eta)$.
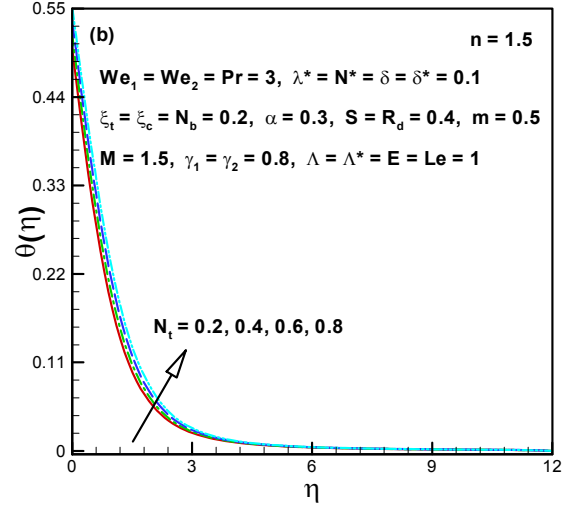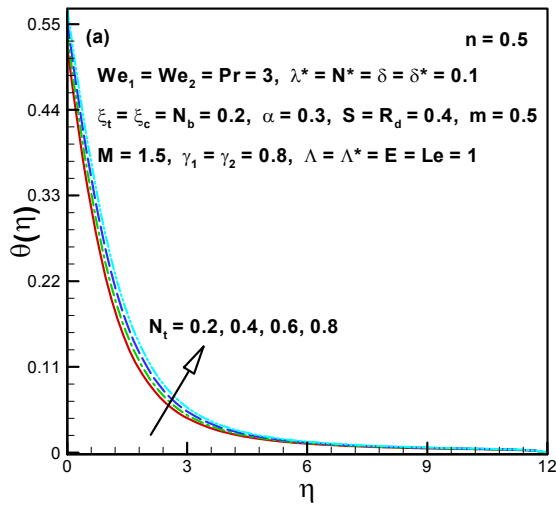
Figure 7.6(a, b): Influence of N_t on $\theta(\eta)$.
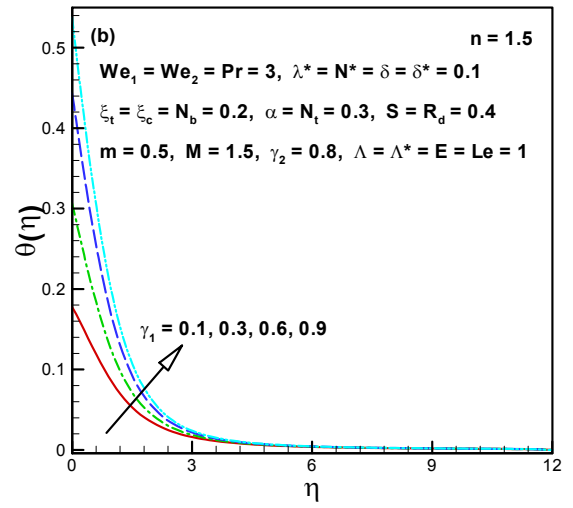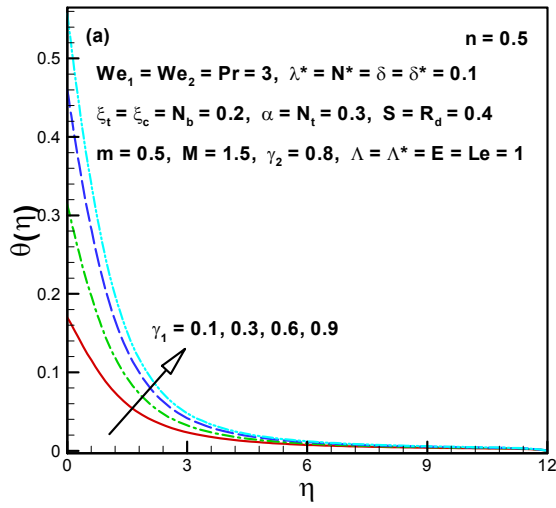
Figure 7.7(a, b): Influence of γ_1 on $\theta(\eta)$.
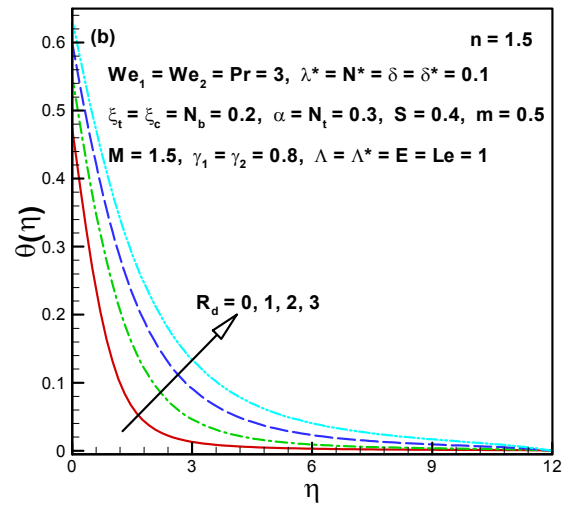
Figure 7.8(a, b): Influence of R_d on $\theta(\eta)$.
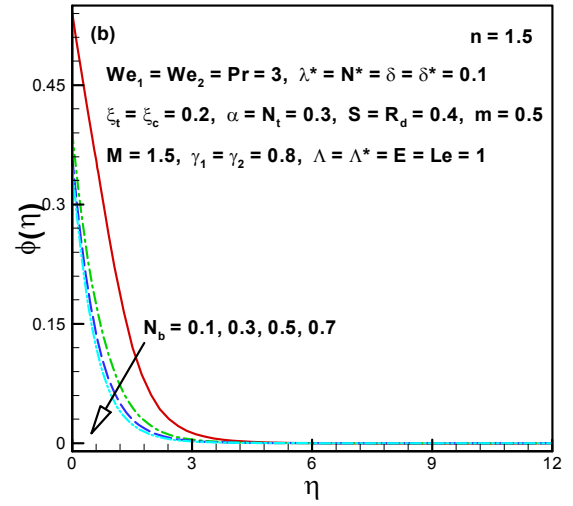
Figure 7.9(a, b): Influence of N_b on $\phi(\eta)$.
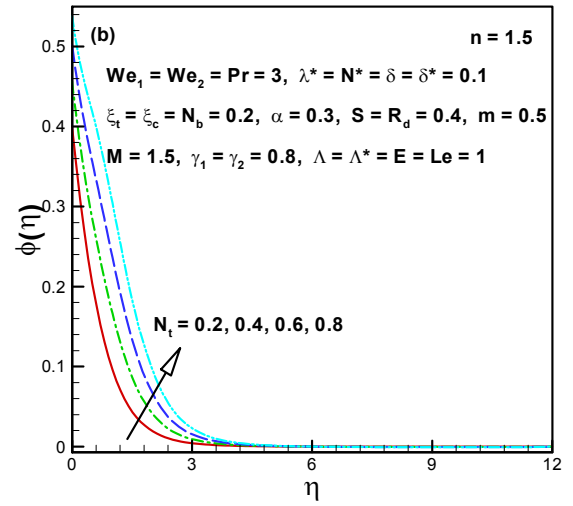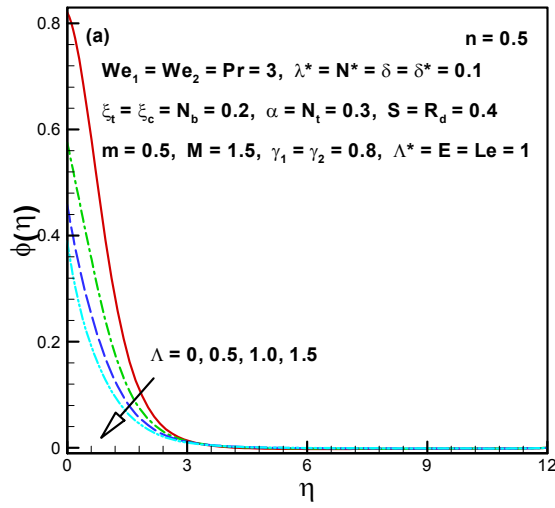

Figure 7.10(a, b): Influence of N_t on $\phi(\eta)$.
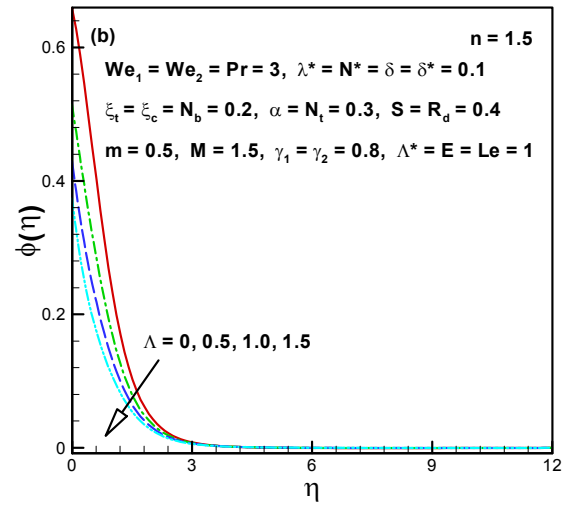
Figure 7.11(a, b): Influence of Λ on $\phi(\eta)$.
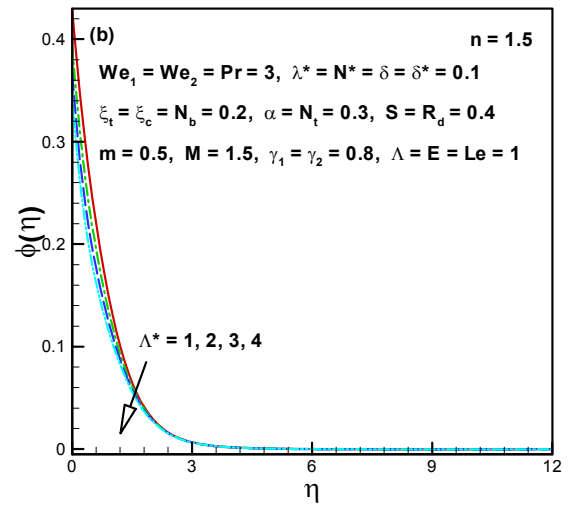
Figure 7.12(a, b): Influence of Λ^* on $\phi(\eta)$.
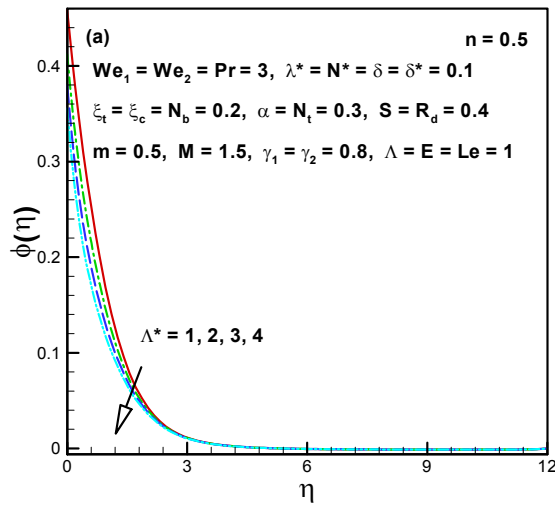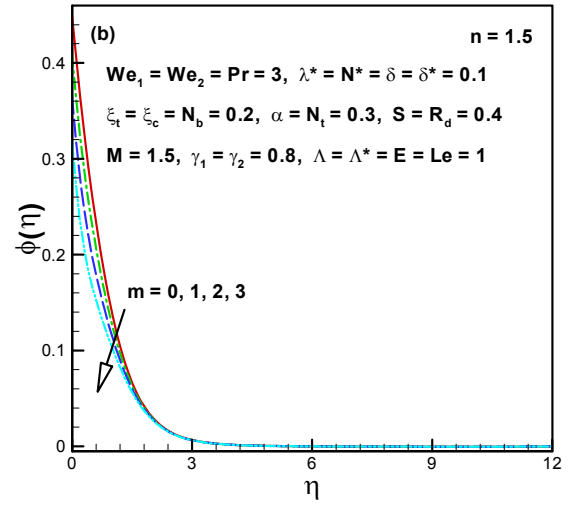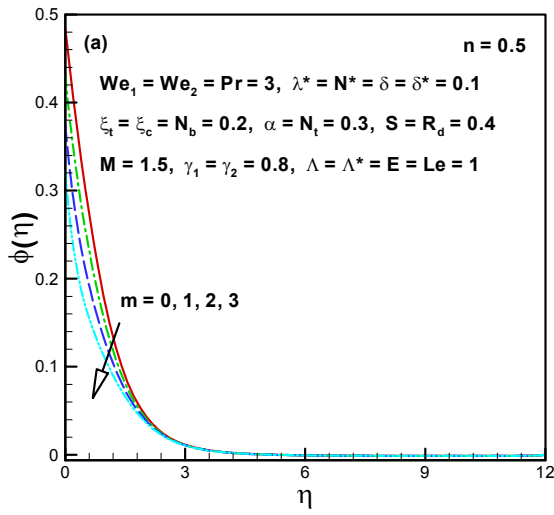
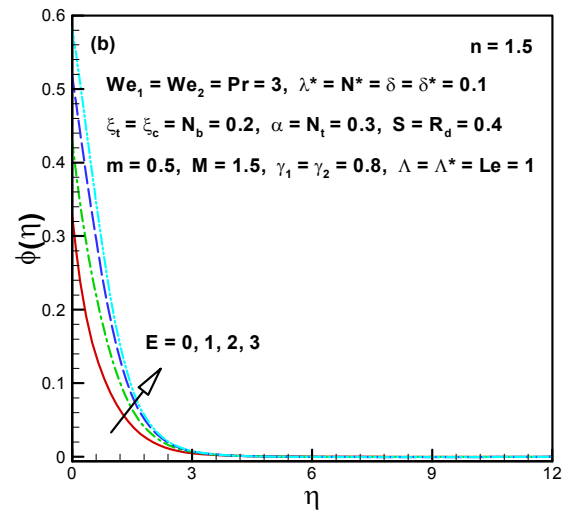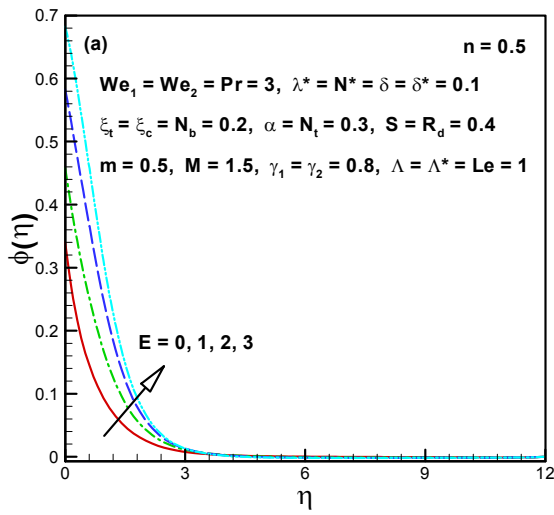**Figure 7.13(a, b)**: Influence of m on $\phi(\eta)$.

Figure 7.14(a, b): Influence of E on $\phi(\eta)$.

Table 7.1: Outcomes of $\left(\frac{1}{2}C_{fx}\,\mathrm{Re}_x^{\frac{1}{2}},\ \frac{1}{2}\left(\frac{U_w}{V_w}\right)C_{fy}\,\mathrm{Re}_x^{\frac{1}{2}}\right)$ when $We_1 = We_2 = \mathrm{Pr} = 3.0$, $N^* = \delta = \delta^* = 0.1$, $\xi_c = \xi_t = 0.2$, $\alpha = 0.3$, $R_d = 0.4$, $\gamma_1 = \gamma_2 = 0.8$, and $\Lambda = \Lambda^* = Le = 1.0$ are fixed.

S	M	λ^*	N_t	N_b	m	E	$\frac{1}{2}C_{fx}\,\mathrm{Re}_x^{\frac{1}{2}}$		$\frac{1}{2}\left(\frac{U_w}{V_w}\right)C_{fy}\,\mathrm{Re}_x^{\frac{1}{2}}$	
							$n=0.5$	$n=1.5$	$n=0.5$	$n=1.5$
0.2	0.5	0.1	0.3	0.2	0.5	1.0	-2.12086	-6.42904	-0.339987	-0.490901
0.3							-2.21382	-6.78915	-0.354492	-0.515325
0.4							-2.30607	-7.15928	-0.369073	-0.540188
0.5							-2.39711	-7.53779	-0.383708	-0.565455
0.2	0.2						-1.96905	-5.77391	-0.292578	-0.412462
	0.6						-2.19941	-6.77972	-0.363443	-0.531575
	1.0						-2.64142	-8.90320	-0.489244	-0.766933
	0.5	0.0					-2.21547	-6.71371	-0.338410	-0.490016
		0.2					-2.02931	-6.15185	-0.341502	-0.491784
		0.3					-1.94046	-5.88197	-0.342970	-0.492666
		0.1	0.1				-2.12763	-6.45158	-0.339838	-0.490813
			0.2				-2.12426	-6.44045	-0.339911	-0.490856
			0.4				-2.11741	-6.41734	-0.340065	-0.490949
			0.3	0.1			-2.12111	-6.42784	-0.340000	-0.490917
				0.4			-2.11742	-6.41957	-0.340040	-0.490925
				0.5			-2.11539	-6.41357	-0.340075	-0.490943
				0.2	0.0		-2.12048	-6.42800	-0.339994	-0.490905
					0.3		-2.12070	-6.42861	-0.339990	-0.490903
					0.6		-2.12094	-6.42926	-0.339985	-0.490901
					0.5	0.2	-2.12226	-6.43366	-0.339956	-0.490883
						0.4	-2.12191	-6.43247	-0.339964	-0.490888
						0.6	-2.12156	-6.43130	-0.339972	-0.490892

Table 7.2: Outcomes of $\left(\mathrm{Re}_x^{-\frac{1}{2}} Nu_x, \ \mathrm{Re}_x^{-\frac{1}{2}} Sh_x\right)$ when $We_1 = We_2 = \mathrm{Pr} = 3.0$, $N^* = \delta = \delta^* = 0.1$, $\xi_c = \xi_t = 0.2$, $\alpha = 0.3$, $R_d = 0.4$, $\gamma_1 = \gamma_2 = 0.8$, and $\Lambda = \Lambda^* = Le = 1.0$ are fixed.

S	M	λ^*	N_t	N_b	m	E	$\mathrm{Re}_x^{-\frac{1}{2}} Nu_x$		$\mathrm{Re}_x^{-\frac{1}{2}} Sh_x$	
							$n = 0.5$	$n = 1.5$	$n = 0.5$	$n = 1.5$
0.2	0.5	0.1	0.3	0.2	0.5	1.0	0.503349	0.526309	0.535465	0.539490
0.3							0.531448	0.548969	0.531497	0.536941
0.4							0.556993	0.570018	0.528702	0.535095
0.5							0.579895	0.589424	0.526957	0.533911
0.2	0.2						0.508541	0.528719	0.535482	0.539688
	0.6						0.500854	0.525164	0.535456	0.539393
	1.0						0.488371	0.519507	0.535433	0.538903
	0.5	0.0					0.502150	0.526205	0.535062	0.539333
		0.2					0.504403	0.526407	0.535860	0.539648
		0.3					0.505309	0.526495	0.536256	0.539806
		0.1	0.1				0.528223	0.550041	0.552856	0.557868
			0.2				0.515843	0.538258	0.542804	0.547344
			0.4				0.490760	0.514209	0.530732	0.534242
			0.3	0.1			0.514184	0.536627	0.495155	0.498329
				0.4			0.481625	0.505501	0.556079	0.560472
				0.5			0.470746	0.495032	0.560378	0.564822
				0.2	0.0		0.502827	0.525839	0.525102	0.530586
					0.3		0.503133	0.526115	0.531222	0.535836
					0.6		0.50346	0.526410	0.537634	0.541364
					0.5	0.2	0.504308	0.527326	0.574254	0.576156
						0.4	0.504052	0.527058	0.564432	0.566675
						0.6	0.503805	0.526800	0.554635	0.557343

Table 7.3: A comparison of $-f''(0)$ for S when $We_1 = We_2 = M = \lambda^* = N^* = \xi_c = \xi_t = 0$ and $n = 1$.

S	Sharidan *et al.* [120]	Chamkha *et al.* [121]	cf. Chapter 6 Table 6.4 (bvp4c)	Present (bvp4c)
0.8	-1.261042	-1.261512	-1.261044	-1.2610433
1.2	-1.377722	-1.378052	-1.377728	-1.3777257
2.0	-1.587362	-	-1.587371	-1.5873714

Table 7.4: A comparison of $\left(\frac{1}{2} C_{fx} \operatorname{Re}_x^{\frac{1}{2}} \right)$ when $M = \lambda^* = N^* = \xi_c = \xi_t = 0$.

We_1	We_2	S	α	$\frac{1}{2}C_{fx}\operatorname{Re}_x^{\frac{1}{2}}$ cf. Chapter 6 Table 6.5 (bvp4c) $n = 0.5$	$n = 1.5$	$\frac{1}{2}C_{fx}\operatorname{Re}_x^{\frac{1}{2}}$ Present (bvp4c) $n = 0.5$	$n = 1.5$
1.0	1.0	0.5	0.3	-1.495932	-2.275974	-1.4959297	-2.2759716
1.5				-1.735959	-3.240193	-1.7359481	-3.2401889
2.0				-1.953110	-4.360016	-1.9531051	-4.3600111
2.5				-2.139428	-5.604837	-2.1394249	-5.6048323
1.0	1.5			-1.495648	-2.276565	-1.4956459	-2.2765631
	2.0			-1.495263	-2.277291	-1.4952613	-2.2772888
	2.5			-1.494790	-2.278095	-1.4947885	-2.2780928
	1.0	0.7		-1.597571	-2.473501	-1.5975519	-2.4735003
		0.9		-1.698759	-2.674949	-1.6987548	-2.6749507
		1.1		-1.799172	-2.879372	-1.7991637	-2.8793713
		0.5	0.5	-1.540941	-2.374278	-1.5409627	-2.3742755
			0.7	-1.583640	-2.474459	-1.5836865	-2.4744540
			1.0	-1.642297	-2.629779	-1.6423871	-2.6297725

Table 7.5: A comparison of $\left(\frac{1}{2} \left(\frac{U_w}{V_w} \right) C_{fy} \operatorname{Re}_x^{\frac{1}{2}} \right)$ when $M = \lambda^* = N^* = \xi_c = \xi_t = 0$.

| We_1	We_2	S	α	$\frac{1}{2} \left(\frac{U_w}{V_w} \right) C_{fy} \operatorname{Re}_x^{\frac{1}{2}}$ cf. Chapter 6 Table 6.4 (bvp4c)		$\frac{1}{2} \left(\frac{U_w}{V_w} \right) C_{fy} \operatorname{Re}_x^{\frac{1}{2}}$ Present (bvp4c)	
				$n = 0.5$	$n = 1.5$	$n = 0.5$	$n = 1.5$
1.0	1.0	0.5	0.3	-0.3014584	-0.3224466	-0.30145875	-0.32244680
1.5				-0.2992882	-0.3238545	-0.29928831	-0.32385468
2.0				-0.2973149	-0.3250801	-0.29731498	-0.32508109
2.5				-0.2956285	-0.3261349	-0.29562848	-0.32613498
1.0	1.5			-0.3074282	-0.3473583	-0.30742884	-0.34735831
	2.0			-0.3156383	-0.3796407	-0.31563951	-0.37964054
	2.5			-0.3258926	-0.4178941	-0.32589468	-0.41789377
	1.0	0.7		-0.3239701	-0.3481788	-0.32397045	-0.34817952
		0.9		-0.3456479	-0.3734159	-0.34564809	-0.37341649
		1.1		-0.3664994	-0.3981124	-0.36649962	-0.39811393
		0.5	0.5	-0.5729707	-0.6737814	-0.57297368	-0.67378130
			0.7	-0.9220556	-1.2239450	-0.92206906	-1.22394310
			1.0	-1.6422970	-2.6297790	-1.64238710	-2.62977250

Chapter 8

Homogeneous-Heterogenous Reactions in 3D Flow of Carreau Fluid with Cattaneo Christov Heat Flux

This chapter communicates the consideration of 3D Carreau liquid flow under the impact of homogeneous/heterogeneous chemical reactions over a stretched surface. Moreover, heat transfer aspect is reported in vision of an improved heat flux relation. This phenomenon is established upon the theory of Cattaneo–Christov heat flux relation that contributes by the thermal relaxation. On exploitation of apposite transformations a system of nonlinear ODEs is attained and then elucidated numerically by means of bvp4c scheme. The description of temperature and concentration fields equivalent to the frequent somatic parameters are graphically scrutinized. Our analysis carries that the concentration of the Carreau liquid declines as the heterogenous-homogeneous reaction parameters intensify. Furthermore, it is notable that for shear thinning $(n < 1)$ liquid, the influence of local Weissenberg numbers is absolutely conflicted as compared with the instance of shear thickening $(n > 1)$ liquid. Additionally, validation of numerical results is done via benchmarking with previously stated limiting cases and initiated a superb correspondence with these outcomes.

8.1 Description of the Problem

Consider the steady, 3D incompressible Carreau fluid flow over a bidirectional stretched surface. The sheet is stretched with linear velocities $u = ax$ and $v = by$, respectively, in which $a, b > 0$ are taken as constants and flow occupies the domain $z > 0$. The heat transfer phenomenon is established in the presence of an improved heat conduction relation. Additionally, the influences of heterogeneous-homogeneous reactions are occupied in the present flow analysis. Homogeneous reaction for cubic autocatalysis can be termed as

$$G_1 + 2H_1 \rightarrow 3H_1, \quad \text{rate} = k_c g_1 h_1^2, \tag{8.1}$$
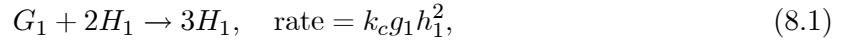
whereas on the catalyst surface, the isothermal reaction of the first-order is of the form

$$G_1 \rightarrow H_1, \quad \text{rate} = k_s g_1, \tag{8.2}$$

where the chemical species (G_1, H_1) have the concentration (g_1, h_1) and rate constants (k_c, k_s), respectively. Moreover, assumed that both are isothermal processes for reactant G_1 there is a uniform concentration g_{1_0}, while there is no autocatalyst H_1.

Under these considerations, the governing flow problem with boundary conditions is written as

$$\frac{\partial u}{\partial x} + \frac{\partial v}{\partial y} + \frac{\partial w}{\partial z} = 0, \tag{8.3}$$

$$u\frac{\partial u}{\partial x} + v\frac{\partial u}{\partial y} + w\frac{\partial u}{\partial z} = \nu\frac{\partial^2 u}{\partial z^2}\left[1 + \Gamma^2\left(\frac{\partial u}{\partial z}\right)^2\right]^{\frac{n-1}{2}}$$
$$+ \nu(n-1)\Gamma^2\frac{\partial u}{\partial z}\left[1 + \Gamma^2\left(\frac{\partial u}{\partial z}\right)^2\right]^{\frac{n-3}{2}}, \tag{8.4}$$

$$u\frac{\partial v}{\partial x} + v\frac{\partial v}{\partial y} + w\frac{\partial v}{\partial z} = \nu\frac{\partial^2 v}{\partial z^2}\left[1 + \Gamma^2\left(\frac{\partial v}{\partial z}\right)^2\right]^{\frac{n-1}{2}}$$
$$+ \nu(n-1)\Gamma^2\frac{\partial v}{\partial z}\left[1 + \Gamma^2\left(\frac{\partial v}{\partial z}\right)^2\right]^{\frac{n-3}{2}}, \tag{8.5}$$

$$u\frac{\partial T}{\partial x} + v\frac{\partial T}{\partial y} + w\frac{\partial T}{\partial z} = \alpha_1 \frac{\partial^2 T}{\partial z^2}$$

$$+\lambda_1 \left[\begin{array}{c} u^2\frac{\partial^2 T}{\partial x^2} + v^2\frac{\partial^2 T}{\partial y^2} + w^2\frac{\partial^2 T}{\partial z^2} + 2uv\frac{\partial^2 T}{\partial x\partial y} \\ +2vw\frac{\partial^2 T}{\partial y\partial z} + 2uw\frac{\partial^2 T}{\partial x\partial z} + \left(u\frac{\partial u}{\partial x} + v\frac{\partial u}{\partial y} + w\frac{\partial u}{\partial z}\right)\frac{\partial T}{\partial x} \\ + \left(u\frac{\partial v}{\partial x} + v\frac{\partial v}{\partial y} + w\frac{\partial v}{\partial z}\right)\frac{\partial T}{\partial y} + \left(u\frac{\partial w}{\partial x} + v\frac{\partial w}{\partial y} + w\frac{\partial w}{\partial z}\right)\frac{\partial T}{\partial z} \end{array} \right], \tag{8.6}$$

$$u\frac{\partial g_1}{\partial x} + v\frac{\partial g_1}{\partial y} + w\frac{\partial g_1}{\partial z} = D_{G_1}\frac{\partial^2 g_1}{\partial z^2} - k_c g_1 h_1^2, \tag{8.7}$$

$$u\frac{\partial h_1}{\partial x} + v\frac{\partial h_1}{\partial y} + w\frac{\partial h_1}{\partial z} = D_{H_1}\frac{\partial^2 h_1}{\partial z^2} + k_c g_1 h_1^2, \tag{8.8}$$

$$u = U_w(x) = ax, \quad v = V_w(y) = by, \quad w = 0,$$

$$T = T_w, \quad D_{G_1}\frac{\partial g_1}{\partial z} = k_s g_1, \quad D_{H_1}\frac{\partial h_1}{\partial z} = -k_s g_1 \quad \text{at} \quad z = 0, \tag{8.9}$$

$$u \to 0, \quad v \to 0, \quad T \to T_\infty, \quad g_1 \to g_{1_0}, \quad h_1 \to 0 \quad \text{as} \quad z \to \infty, \tag{8.10}$$

where λ_1 is the thermal relaxation time and (D_{G_1}, D_{H_1}) the coefficients of diffusion species of G_1 and H_1, respectively.

8.1.1 Appropriate Conversions

We define the following applicable conversions

$$\theta(\eta) = \frac{T - T_\infty}{T_w - T_\infty}, \quad g_1 = g_{1_0}l(\eta), \quad h_1 = h_{1_0}r(\eta), \quad \eta = z\sqrt{\frac{a}{\nu}}. \tag{8.11}$$

In view of overhead conversions and Eq. (2.27) (cf. Chapter 2), Eqs. (8.4) − (8.10) yield

$$f'''[1 + We_1^2 f''^2]^{\frac{n-3}{2}}[1 + nWe_1^2 f''^2] - f'^2 + f''(f + g) = 0, \tag{8.12}$$

$$g'''[1 + We_2^2 g''^2]^{\frac{n-3}{2}}[1 + nWe_2^2 g''^2] - g'^2 + g''(f + g) = 0, \tag{8.13}$$

$$\theta'' + \Pr(f + g)\theta' - \Pr\beta_1[(f + g)(f' + g')\theta' - (f + g)^2\theta''] = 0, \tag{8.14}$$

$$\frac{1}{Sc}l'' + (f + g)l' - k_1 lr^2 = 0, \tag{8.15}$$

$$\frac{\lambda_c}{Sc}r'' + (f+g)r' + k_1 lr^2 = 0, \tag{8.16}$$

$$f(0) = 0, \quad g(0) = 0, \quad f'(0) = 1, \quad g'(0) = \alpha, \quad \theta(0) = 1, \tag{8.17}$$

$$l'(0) = k_2 l(0), \quad \lambda_c r'(0) = -k_2 l(0), \tag{8.18}$$

$$f' \to 0, \quad g' \to 0, \quad \theta \to 0, \tag{8.19}$$

$$l \to 1, \quad r \to 0 \quad \text{as} \quad \eta \to \infty. \tag{8.20}$$

Here, $\beta_1 \left(= \lambda_1 a\right)$ indicates the thermal relaxation time parameter, $Sc \left(= \frac{\nu}{D_G}\right)$ the Schmidt number, $\lambda_c \left(= \frac{D_{H_1}}{D_{G_1}}\right)$ the diffusion coefficient ratio and (k_2, k_1) the measures the strength of heterogeneous-homogeneous processes.

In physical circumstances, the D_{G_1} and D_{H_1} the diffusion coefficients are taken to be equal i.e., $\lambda_c = 1$, which will provide as:

$$l(\eta) + r(\eta) = 1. \tag{8.21}$$

Thus, Eqs. (8.15), (8.16), (8.18) and (8.20) yield

$$\frac{1}{Sc}l'' + (f+g)l' - k_1(1-l)^2 l = 0, \tag{8.22}$$

$$l'(0) = k_2 l(0), \quad l \to 1 \quad \text{as } \eta \to \infty. \tag{8.23}$$

8.2   Engineering and Industrial Quantities of Interest

The essential features of flow is the coefficient of skin friction (C_{fx}, C_{fy}) which are demarcated as

$$C_{fx} = \frac{\tau_{xz}}{\frac{1}{2}\rho U_w^2} \quad \text{and} \quad C_{fy} = \frac{\tau_{yz}}{\frac{1}{2}\rho U_w^2}, \tag{8.24}$$

and in the dimensionless representations, we have

$$\frac{1}{2}C_{fx}\,\mathrm{Re}_x^{\frac{1}{2}} = f''(0)[1 + We_1^2 f''^2]^{\frac{n-1}{2}}, \tag{8.25}$$

$$\frac{1}{2}\left(\frac{U_w}{V_w}\right)C_{fy}\,\mathrm{Re}_x^{\frac{1}{2}} = g''(0)[1 + We_2^2 g''^2]^{\frac{n-1}{2}}, \tag{8.26}$$

8.3 Graphical Illustration and Analysis

This section is predominantly emphases to interpret the somatic features of heterogeneous-homogeneous reactions in $3D$ Carreau fluid flow past a stretched sheet by utilizing the non-Fourier's heat conduction relation. The set of Eqs. $(8.12) - (8.14)$ and (8.22) with boundary restrictions $(8.17), (8.19)$ and (8.23) are established and resolved via bvp4c scheme. The core purpose of the following discussion is to fetch out the influences of scheming parameters such as We_1, We_2, α, Pr, β_1, k_1, k_2 and Sc on the temperature $\theta(\eta)$ and concentration $l(\eta)$ fields in both circumstances $(n < 1)$ and $(n > 1)$, (i.e., shear thinning/thickening). Additionally, the numerical and analytical outcomes in comparison of former existing prose are presented for some descriptive value of α and Pr.

Figures 8.1(a, b) and **8.2(a, b)** are portrayed to visualize the impact of the thermal relaxation parameter (β_1) and Prandtl number (Pr) on the temperature $\theta(\eta)$ of Carreau liquid for both shear thinning/thickening liquids, respectively. These plots acknowledged that the liquid temperature in addition to the thickness of thermal boundary layer spectacles a diminishing behavior for enhancing values of Pr and β_1 for $(n < 1)$ and $(n > 1)$. Physically, this happens because of the fact that for larger value of β_1, the liquid material needs extra time for heat transfer to its adjacent elements which raises the temperature gradient and hence, declines the temperature distribution. Moreover, the instance of Fourier's law in association with the Cattaneo-Christov heat flux model the temperature profile is higher for $\beta_1 = 0$.

Figures 8.3(a, b) and **8.4(a, b)** are sketched to interpret the features of the local Weissenberg numbers (We_1, We_2) on concentration field $l(\eta)$ of Carreau liquid for higher We_1 and We_2, respectively. These results exhibit that with the enlargement of We_1 and We_2, the concentration distribution intensifies, whereas the thickness of concentration boundary layer reduces for shear thinning liquid. Instead of shear thickening liquid moderately conflicting behavior is identified for the increasing values of We_1 and We_2 on $l(\eta)$. The impact of the growing value of the ratio of stretching rates parameter (α) and the Schmidt number (Sc) on concentration of Carreau fluid for the both instances $(n < 1)$ and $(n > 1)$ is clarified via **figures 8.5(a, b)** and **8.6(a, b)**, respectively. From these sketches the analogous behaviors for the emergent value of α and Sc for the circumstances of shear thinning/thickening liquids are perceived. Uplifting the values of α and Sc enhance the concentration of Carreau liquid while its allied thickness of con-

centration boundary layer reduces. For physical point of vision, advance value of α, stretching beside the $y-$direction growths which reasons the escalation of the concentration of Carreau liquid. Moreover, as Sc is the relation of the viscous diffusion rate to the molecular diffusion rate, higher value of Sc resembles the greater viscous diffusion rate, which is fit to intensify the liquid concentration. **Figures 8.7$(\mathbf{a}, \mathbf{b})$** and **8.8$(\mathbf{a}, \mathbf{b})$**, respectively, explore the properties of homogeneous and heterogeneous reaction parameters (k_1, k_2) for the shear thinning and shear thickening situations on the concentration scattering. The concentration field moderates for both conditions $(n < 1)$ and $(n > 1)$ for increasing values of k_1 and k_2; however, the thickness of concentration boundary layer assembled for larger k_1 and k_2. Physically, from **figures 8.7$(\mathbf{a}, \mathbf{b})$**, this is owing to the circumstance that the reactants are consumed throughout the homogeneous reaction which reasons the decline of the concentration distribution. Instead, one can noticed from **figures 8.8$(\mathbf{a}, \mathbf{b})$** that the advance value of k_2 outcomes in the decline of $l(\eta)$. This coincides with the overall physical behavior of homogeneous k_1 and heterogeneous k_2 reactions.

8.3.1 Graphical Comparison between bvp4c and HAM

Figures 8.9$(\mathbf{a}, \mathbf{b})$ depict the impact of Pr and β_1 for two dissimilar schemes, namely the homotopy analysis method (HAM) and bvp4c approach. From these plots a brilliant agreement is initiated amongst both techniques.

8.3.2 Confirmation of Numerical Outcomes

The authenticity of the numerical consequence are also established by assessment with the analytical outcomes achieved by the HAM as shown in **Tables 8.1** to **8.3**. Moreover, these results are compared with former available prose as an exceptional instance of the problem and outstanding settlement is noticed. The discrepancy of the Nusselt number for different values of Pr is presented through **Table 8.4**. A comparison between analytical technique (HAM) and the numerical scheme (bvp4c) with some former prose is also presented in this table. Consequently, these tables assured that the present outcomes are very accurate.
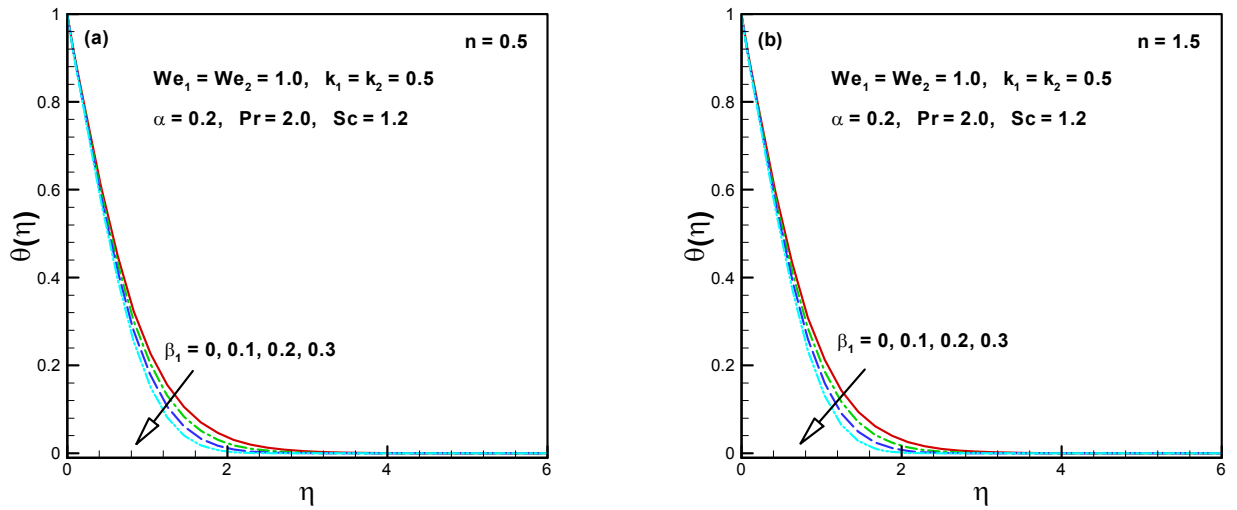
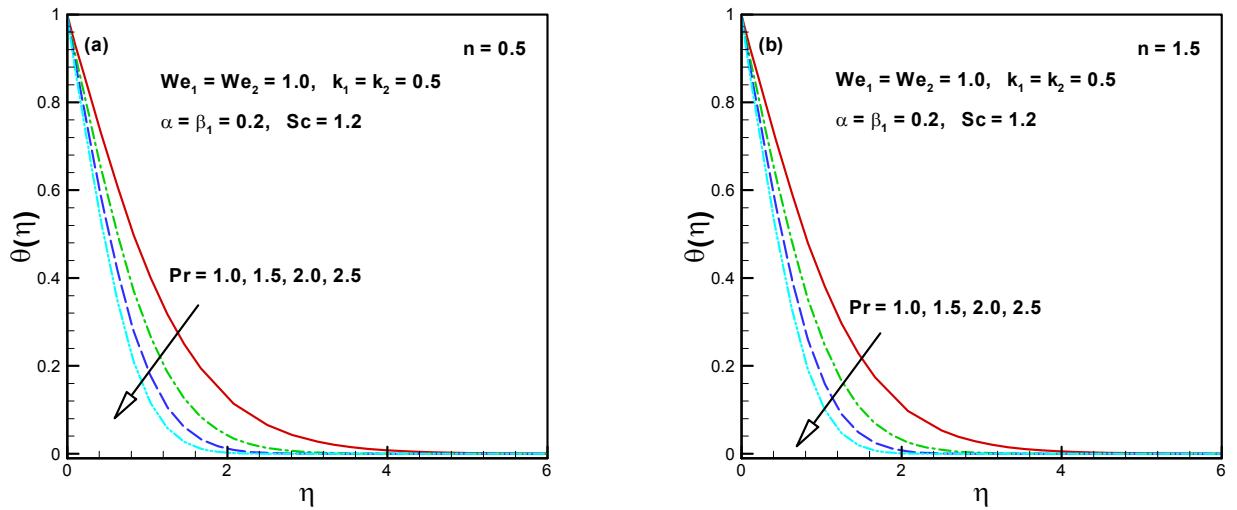**Figure 8.1(a, b):** Influence of β_1 on $\theta(\eta)$.

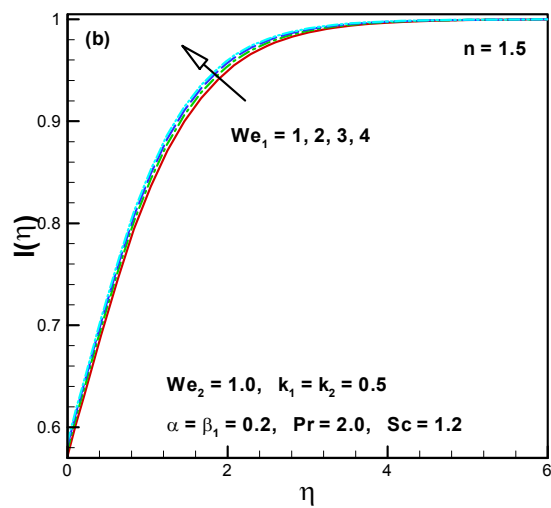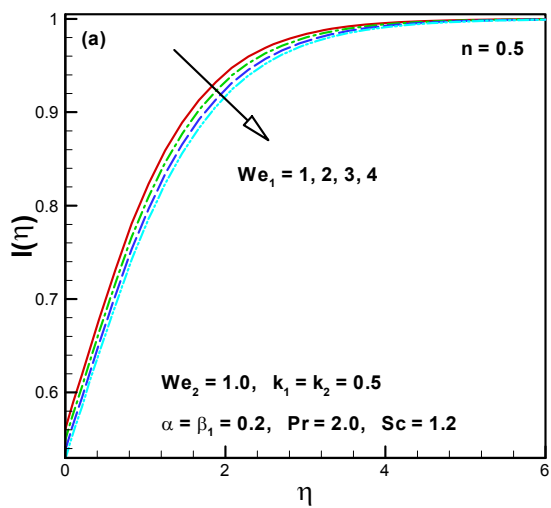**Figure 8.2(a, b):** Influence of Pr on $\theta(\eta)$.
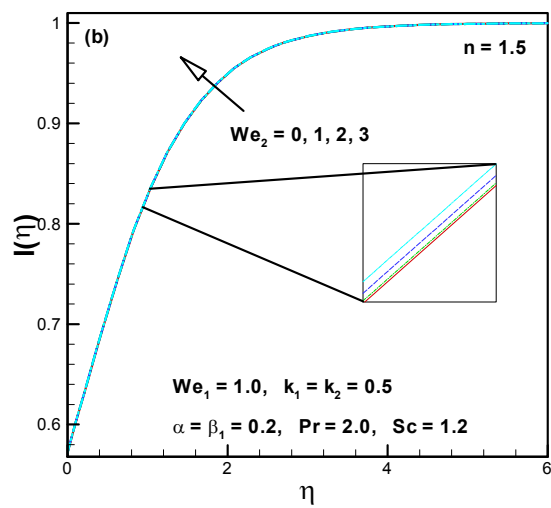
155
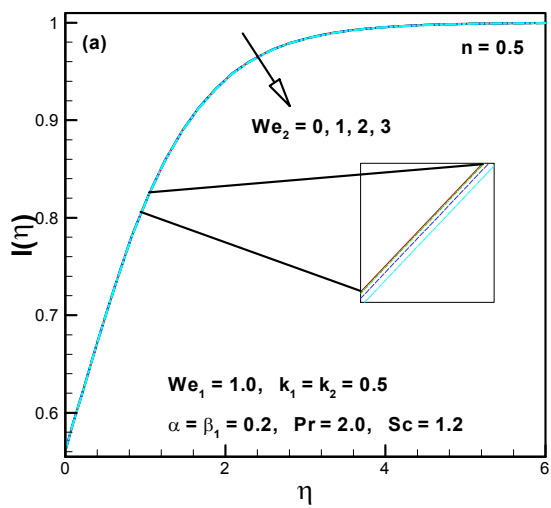
Figure 8.3(a, b): Influence of We_1 on $l(\eta)$.

Figure 8.4(a, b): Influence of We_1 on $l(\eta)$.
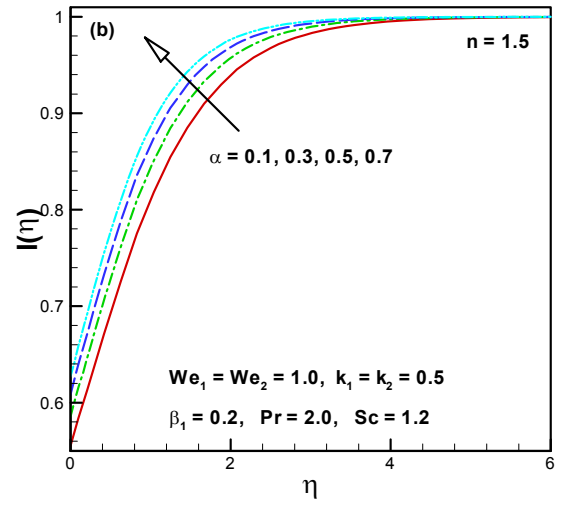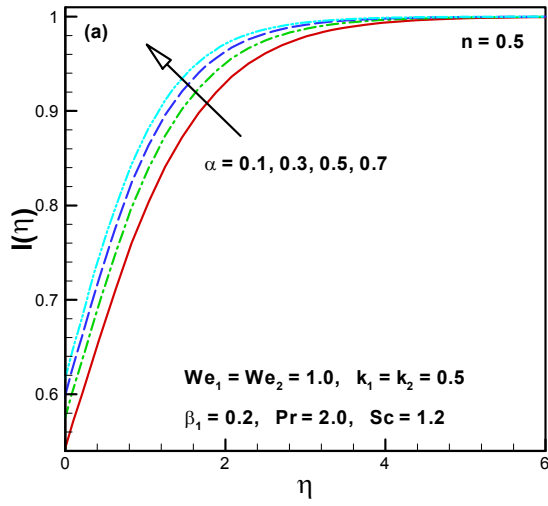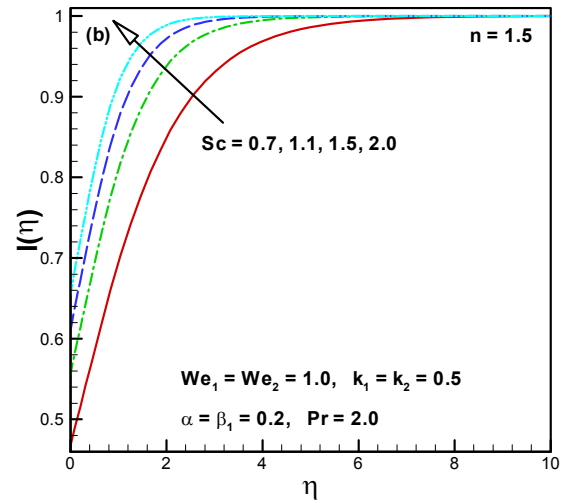
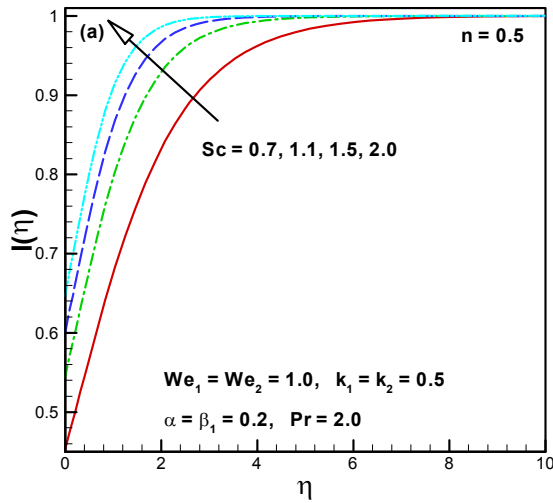**Figure 8.5(a, b):** Influence of α on $l(\eta)$.
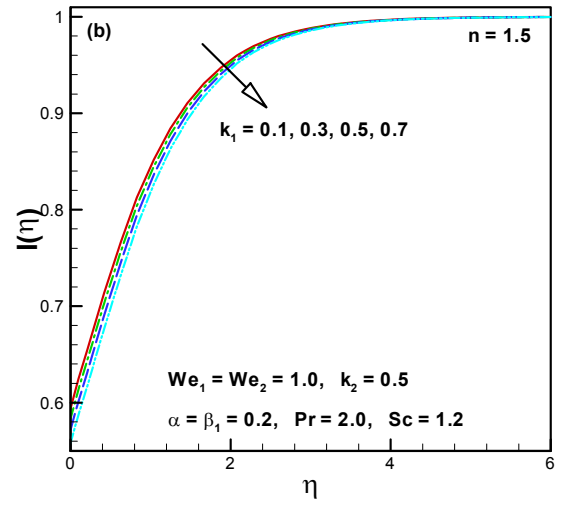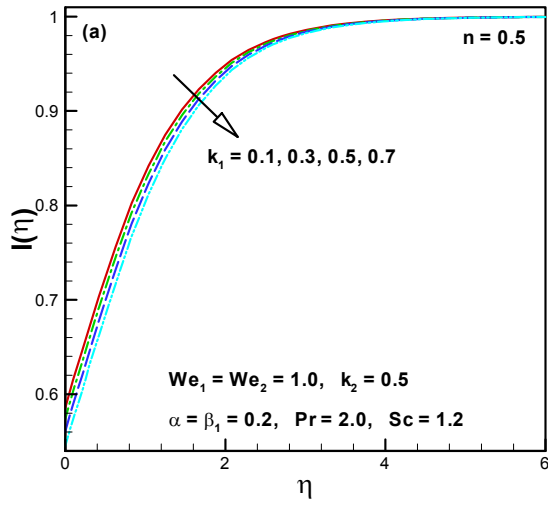

Figure 8.6(a, b): Influence of Sc on $l(\eta)$.

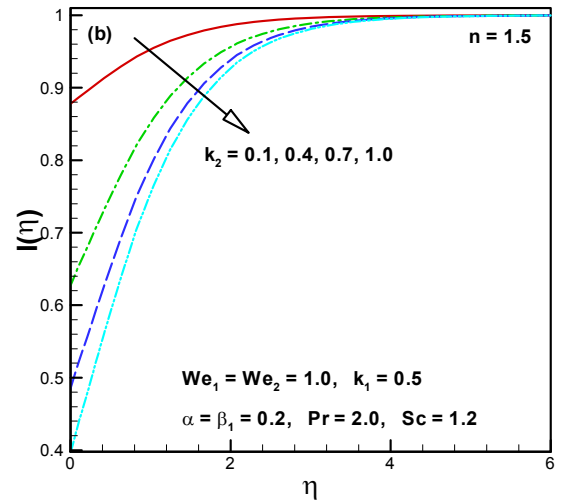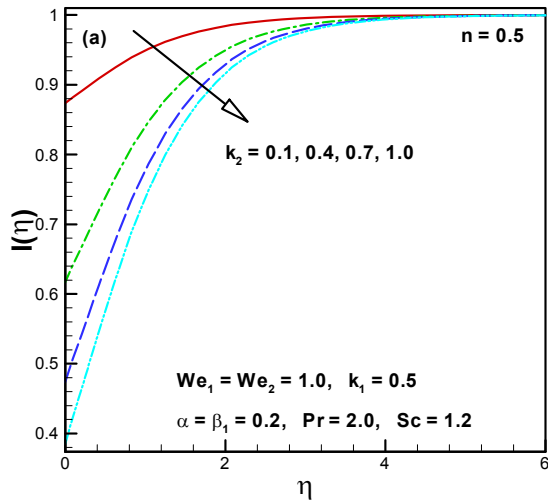**Figure 8.7(a, b):** Influence of k_1 on $l(\eta)$.

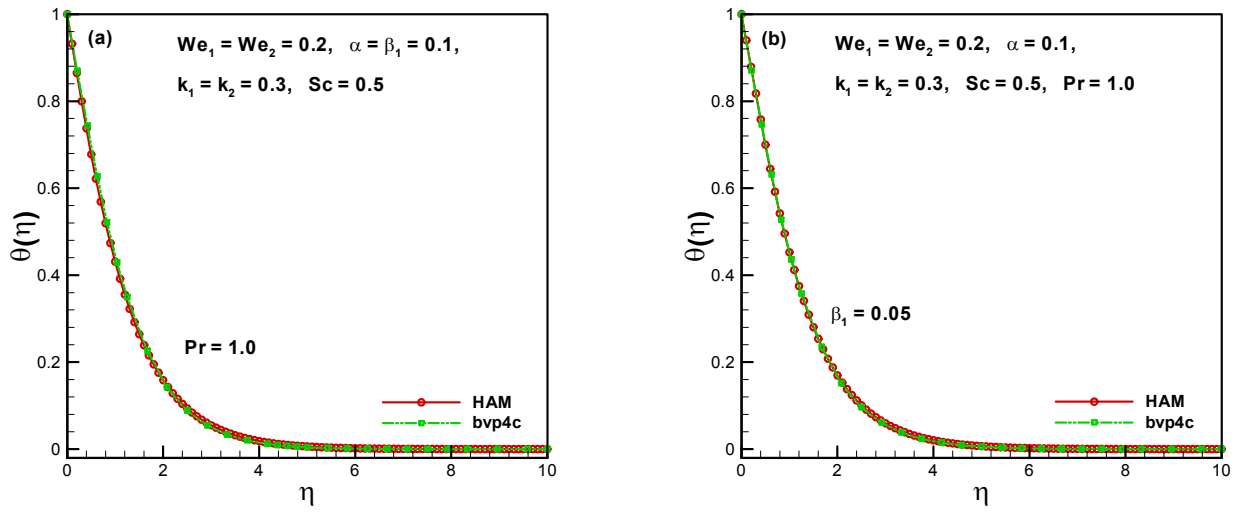**Figure 8.8(a, b):** Influence of k_2 on $l(\eta)$.

Figure 8.9(a, b): Graphical assessment between bvp4c and HAM for Pr and β_1 on $\theta(\eta)$.

Table 8.1: A comparison of $f''(0)$ between bvp4c and HAM in limiting cases when $We_1 = We_2 = 0$ and $n = 1$ are fixed.

α	$f''(0)$				
	Wang [117]	Liu and Anderson [118]	Munir *et al.* [119]	Present(bvp4c)	Present (HAM)
0.0	-1	-1	-1	-1	-1
0.25	-1.048813	-1.048813	-1.048818	-1.048813	-1.048810
0.50	-1.093097	-1.093096	-1.093098	-1.093095	-1.093095
0.75	-1.134485	-1.134486	-1.134487	-1.134485	-1.134486
1.0	-1.173720	-1.173721	-1.173721	-1.173720	-1.173720

Table 8.2: A comparison of $g''(0)$ between bvp4c and HAM in limiting cases when $We_1 = We_2 = 0$ and $n = 1$ are fixed.

α	$g''(0)$				
	Wang [117]	Liu and Anderson [118]	Munir *et al.* [119]	Present(bvp4c)	Present (HAM)
0.0	0	0	0	-1	-1
0.25	-0.194564	-0.194565	-0.194567	-0.1945649	-0.1945645
0.50	-0.465205	-0.465206	-0.465207	-0.4652052	-0.4652049
0.75	-0.794622	-0.794619	-0.794619	-0.7946182	-0.7946182
1.0	-1.173720	-1.173721	-1.173721	-1.1737205	-1.1737210

Table 8.3: A comparison of $\theta'(0)$ between bvp4c and HAM in limiting cases when $We_1 = We_2 = \beta = 0$ and $n = 1$ are fixed.

α	$\theta'(0)$			
	Liu and Anderson [118]	Munir *et al*. [119]	Present(bvp4c)	Present (HAM)
0.25	-0.665933	-0.665939	-0.665933	-0.665926
0.50	-0.735334	-0.735336	-0.735335	-0.735332
0.75	-0.796472	-0.796472	-0.796473	-0.796471

Table 8.4: A comparison of $-\theta'(0)$ between bvp4c and HAM for Pr when $We_1 = We_2 = \beta = 0$ and $n = 1$ are fixed.

Pr	$-\theta'(0)$				
	Khan and Pop [2]	Wang [122]	Gorla and Sidawi [123]	Present(bvp4c)	Present(HAM)
0.70	0.4539	0.4539	0.4539	0.453935	0.453933
1.0	-	-	-	0.581979	0.581977
1.3	-	-	-	0.693029	0.693023
1.5	-	-	-	0.760293	0.760298
1.7	-	-	-	0.823311	0.823327
2.0	0.9113	0.9114	0.9114	0.911362	0.911336
7.0	1.8954	1.8954	1.8954	1.895420	-
20.0	3.3539	3.3539	3.3539	3.353950	-
70.0	6.4621	6.4622	6.4622	6.462250	-

Chapter 9

Impact of Cattaneo–Christov Double Diffusion in 3D Carreau Fluid Flow

Here the steady 3D flow of a Carreau liquid influenced by bidirectional stretched surface. With Cattaneo–Christov double diffusion and temperature-dependent thermal conductivity, the heat and mass transfer mechanisms have been scrutinized. The alteration of nonlinear PDEs to nonlinear ODEs is equipped via apposite conversions and then resolved numerically by means of bvp4c scheme. The graphical depiction is exposed to portray the essential features of somatic parameters on Carreau liquid temperature and concentration distributions. This study indicates that the variable conductivity parameter enhances the liquid temperature, while the thermal relaxation time parameter and Prandtl number are diminishing functions of temperature field. Furthermore, these results illustrate that the concentration relaxation time parameter and Schmidt number diminish the concentration field. The assertion of present outcome is asserted by emergent assessment with former outcomes presented in prose, which sets a benchmark for execution of computational methodology. Moreover, graphical assessment is also reported for two altered techniques, the analytical one (HAM) and numerical one (bvp4c).

9.1   Description of the Problem

We analyze the steady 3D flow of Carreau liquid influenced by a bidirectional stretched surface. The flow is influenced owed to the stretching surface in two nearby $x-$ and $y-$directions with

linear velocities $u = ax$ and $v = by$, respectively, in which $a, b > 0$ are occupied to be constants relating to stretching rates and the flow presence constrained in the region $z > 0$. The heat and mass transfer mechanisms are explored via Cattaneo–Christov double diffusion relationships. The constant temperature and concentration at the wall are represented by (T_w, C_w) while the ambient values attain as $z \to \infty$, take on the constant values (T_∞, C_∞), respectively.

Under these concerns, the governing equations of 3D Carreau liquid are

$$\frac{\partial u}{\partial x} + \frac{\partial v}{\partial y} + \frac{\partial w}{\partial z} = 0, \tag{9.1}$$

$$u\frac{\partial u}{\partial x} + v\frac{\partial u}{\partial y} + w\frac{\partial u}{\partial z} = \nu\frac{\partial^2 u}{\partial z^2}\left[1 + \Gamma^2\left(\frac{\partial u}{\partial z}\right)^2\right]^{\frac{n-1}{2}}$$
$$+ \nu(n-1)\Gamma^2\left(\frac{\partial u}{\partial z}\right)^2\left(\frac{\partial^2 u}{\partial z^2}\right)\left[1 + \Gamma^2\left(\frac{\partial u}{\partial z}\right)^2\right]^{\frac{n-3}{2}}, \tag{9.2}$$

$$u\frac{\partial v}{\partial x} + v\frac{\partial v}{\partial y} + w\frac{\partial v}{\partial z} = \nu\frac{\partial^2 v}{\partial z^2}\left[1 + \Gamma^2\left(\frac{\partial v}{\partial z}\right)^2\right]^{\frac{n-1}{2}}$$
$$+ \nu(n-1)\Gamma^2\left(\frac{\partial v}{\partial z}\right)^2\left(\frac{\partial^2 v}{\partial z^2}\right)\left[1 + \Gamma^2\left(\frac{\partial v}{\partial z}\right)^2\right]^{\frac{n-3}{2}}, \tag{9.3}$$

$$u\frac{\partial T}{\partial x} + v\frac{\partial T}{\partial y} + w\frac{\partial T}{\partial z}$$

$$+ \lambda_1\left[\begin{array}{c} u^2\frac{\partial^2 T}{\partial x^2} + v^2\frac{\partial^2 T}{\partial y^2} + w^2\frac{\partial^2 T}{\partial z^2} + 2uv\frac{\partial^2 T}{\partial x \partial y} \\ + 2vw\frac{\partial^2 T}{\partial y \partial z} + 2uw\frac{\partial^2 T}{\partial x \partial z} + \left(u\frac{\partial u}{\partial x} + v\frac{\partial u}{\partial y} + w\frac{\partial u}{\partial z}\right)\frac{\partial T}{\partial x} \\ + \left(u\frac{\partial v}{\partial x} + v\frac{\partial v}{\partial y} + w\frac{\partial v}{\partial z}\right)\frac{\partial T}{\partial y} + \left(u\frac{\partial w}{\partial x} + v\frac{\partial w}{\partial y} + w\frac{\partial w}{\partial z}\right)\frac{\partial T}{\partial z} \end{array}\right] = \frac{1}{(\rho c)_f}\frac{\partial}{\partial z}\left(K(T)\frac{\partial T}{\partial z}\right), \tag{9.4}$$

$$u\frac{\partial C}{\partial x} + v\frac{\partial C}{\partial y} + w\frac{\partial C}{\partial z}$$

$$+ \lambda_2\left[\begin{array}{c} u^2\frac{\partial^2 C}{\partial x^2} + v^2\frac{\partial^2 C}{\partial y^2} + w^2\frac{\partial^2 C}{\partial z^2} + 2uv\frac{\partial^2 C}{\partial x \partial y} \\ + 2vw\frac{\partial^2 C}{\partial y \partial z} + 2uw\frac{\partial^2 C}{\partial x \partial z} + \left(u\frac{\partial u}{\partial x} + v\frac{\partial u}{\partial y} + w\frac{\partial u}{\partial z}\right)\frac{\partial C}{\partial x} \\ + \left(u\frac{\partial v}{\partial x} + v\frac{\partial v}{\partial y} + w\frac{\partial v}{\partial z}\right)\frac{\partial C}{\partial y} + \left(u\frac{\partial w}{\partial x} + v\frac{\partial w}{\partial y} + w\frac{\partial w}{\partial z}\right)\frac{\partial C}{\partial z} \end{array}\right] = D_m\frac{\partial^2 C}{\partial z^2}, \tag{9.5}$$

$$u = U_w(x) = ax, \quad v = V_w(y) = by, \quad w = 0, \quad T = T_w, \quad C = C_w \quad \text{at} \quad z = 0, \qquad (9.6)$$

$$u \to 0, \quad v \to 0, \quad T \to T_\infty, \quad C \to C_\infty, \quad \text{as} \quad z \to \infty, \qquad (9.7)$$

where (λ_2, D_m) are the relaxation time of mass flux and molecular diffusivity of the concentration respectively.

9.1.1 Appropriate Conversions

The following are the appropriate conversions

$$\theta(\eta) = \frac{T - T_\infty}{T_w - T_\infty}, \quad \phi(\eta) = \frac{C - C_\infty}{C_w - C_\infty}. \qquad (9.8)$$

In vision of above the alterations and Eq. (2.27) (cf. Chapter 2), the condition of incompressibility is satisfied automatically and Eqs. (9.2) $-$ (9.7) yield

$$f'''[1 + We_1^2 f''^2]^{\frac{n-3}{2}}[1 + nWe_1^2 f''^2] - f'^2 + f''(f + g) = 0, \qquad (9.9)$$

$$g'''[1 + We_2^2 g''^2]^{\frac{n-3}{2}}[1 + nWe_2^2 g''^2] - g'^2 + g''(f + g) = 0, \qquad (9.10)$$

$$(1 + \varepsilon\theta)\theta'' + \varepsilon\theta'^2 + \Pr(f + g)\theta' - \Pr\beta_1[(f + g)(f' + g')\theta' + (f + g)^2\theta''] = 0, \qquad (9.11)$$

$$\phi'' + Sc(f + g)\phi' - Sc\beta_2[(f + g)(f' + g')\phi' + (f + g)^2\phi''] = 0, \qquad (9.12)$$

$$f(0) = 0, \quad g(0) = 0, \quad f'(0) = 1, \quad g'(0) = \alpha, \quad \theta(0) = 1, \quad \phi(0) = 1, \qquad (9.13)$$

$$f' \to 0, \quad g' \to 0, \quad \theta \to 0, \quad \phi \to 0 \quad \text{as} \quad \eta \to \infty. \qquad (9.14)$$

Here $\beta_2(= a\lambda_2)$ is the concentration relaxation time parameter.

9.2 Engineering and Industrial Quantities of Interest

A critical structure of flow are the local skin friction coefficients C_{fx} and C_{fy} which are defined as

$$C_{fx} = \frac{\tau_{xz}}{\frac{1}{2}\rho U_w^2} \quad and \quad C_{fy} = \frac{\tau_{yz}}{\frac{1}{2}\rho U_w^2}, \qquad (9.15)$$

and the overhead expressions in the dimensionless form yield

$$\tfrac{1}{2} C_{fx} \operatorname{Re}_x^{\frac{1}{2}} = f''(0)[1 + We_1^2 f''^2(0)]^{\frac{n-1}{2}}, \tag{9.16}$$

$$\tfrac{1}{2} \left(\tfrac{U_w}{V_w} \right) C_{fy} \operatorname{Re}_x^{\frac{1}{2}} = g''(0)[1 + We_2^2 g''^2(0)]^{\frac{n-1}{2}}. \tag{9.17}$$

9.3   Graphical Illustration and Analysis

This portion is established to infer the influence of non-Fourier's heat and non-Fick's mass flux relations in *3D* flow of Carreau liquid. The numerical study is established for some descriptive values of numerous apposite parameters. The resultant non-linear ODEs are resolved numerically by bvp4c and the outcomes are designed graphically.

To envision the influence of ratio of stretching rates parameter (α) and thermal conductivity parameter (ε) on the Carreau liquid temperature field $\theta(\eta)$, **figures 9.1(a, b)** and **9.2(a, b)** are depicted for both instants $(n < 1)$ and $(n > 1)$. These conspiracies show that the temperature of Carreau fluid diminishes for larger α. Strengthening values of α cause that the velocity in $y-$direction is lower then velocity in $x-$direction and the particles collision increases. Hence, the liquid temperature of Carreau liquid declines when α increases. Additionally, the divergent tendency to be instigated for higher values of ε. Physically, the thermal conductivity of Carreau liquid rises for enhancing value of ε because of huge heat transfer quantity from the sheet to the material and therefore the temperature of Carreau liquid boosts up. **Figures 9.3(a, b)** and **9.4(a, b)** are drafted to deduce the features of Prandtl number (Pr) and thermal relaxation parameter (β_1) for both conditions. These outcomes display that the higher value of Pr and β_1, diminish both the liquid temperature and its thickness of the thermal boundary layer. As Prandtl number and thermal diffusivity have conflicting correlation. Because of this datum higher Pr declines the Carreau liquid temperature. Moreover, a similar performance is being remarked for β_1 which decays the temperature of Carreau liquid for both $(n < 1)$ and $(n > 1)$. Physically, from **figures 9.4(a, b)**, this ensue owing to the datum that for collective values of β_1, the liquid material desires additional time to transport of heat to its adjacent particle which enhances the temperature gradient and therefore, the liquid temperature declines.

Figures 9.5(a, b) and **9.6(a, b)** depict the aspects of Schmidt number (Sc) and solutal

relaxation time parameter (β_2) on $\phi(\eta)$. Both Sc and β_2 diminish the concentration of Carreau liquid and allied thickness of concentration boundary layer. As Sc is the relation of the viscous diffusion rate to the molecular diffusion rate. Though, advanced value of Sc resemble the larger viscous diffusion amount, which is adequate to exaggerate the liquid concentration. Furthermore, the results indicated that for shear thinning/thickening liquids, increasing values of Sc and β_2 are declining functions of concentration distribution.

9.3.1 Confirmation of Numerical Outcomes

For the legitimacy of the numerical outcomes an assessment of different values of ratio of stretching rates parameter (α) with the analytical results attained through the HAM is displayed in **Tables 9.1** to **9.3**. Moreover, an assessment table for diverse values of ε and Pr in limiting circumstance is presented as **Table 9.4**. From these tables, compared upshots with earlier presented valid prose as a brilliant instance of the problem and exceptional settlement is being remarked.
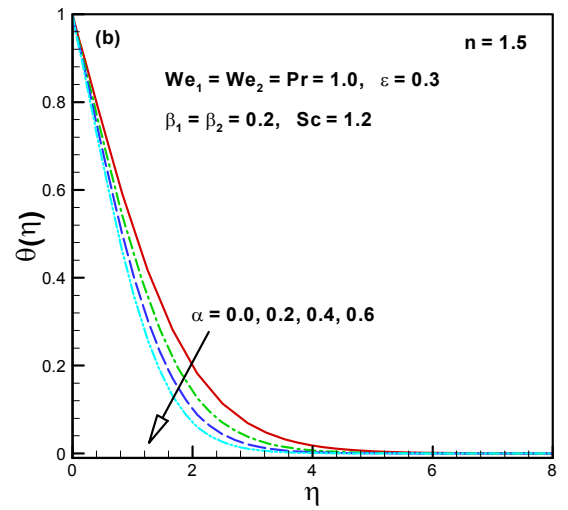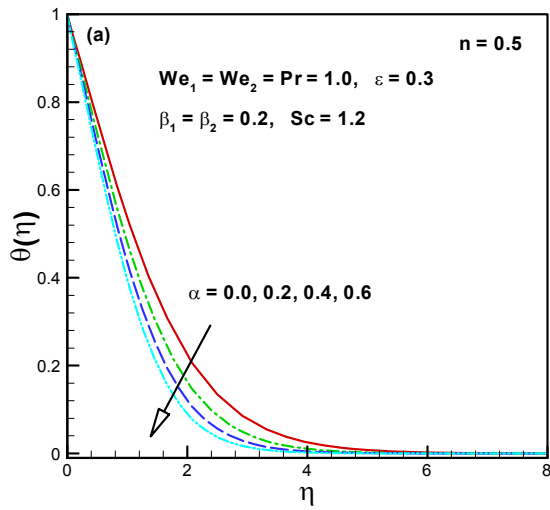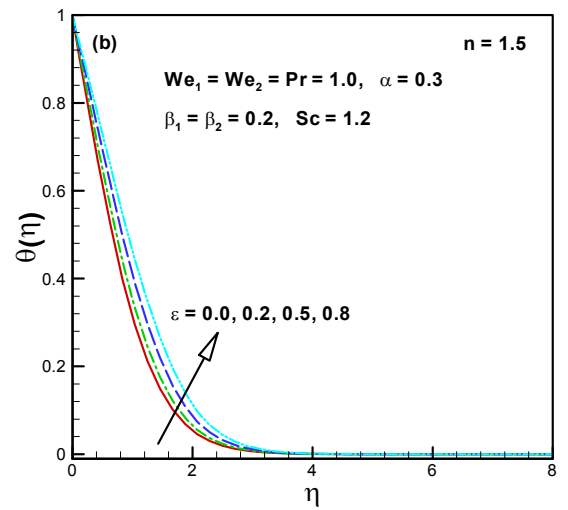
Figure 9.1(a, b): Influence of α on $\theta(\eta)$.
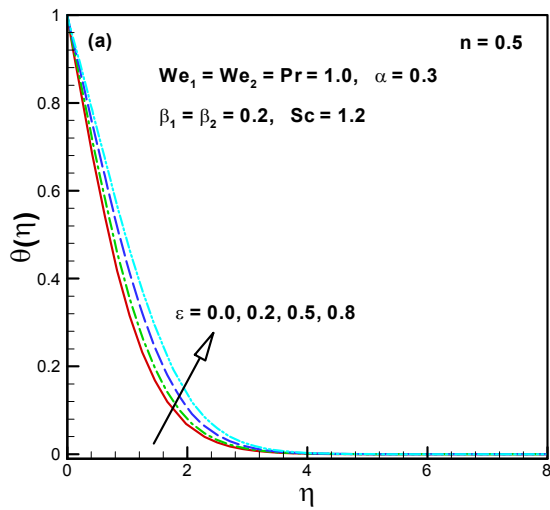
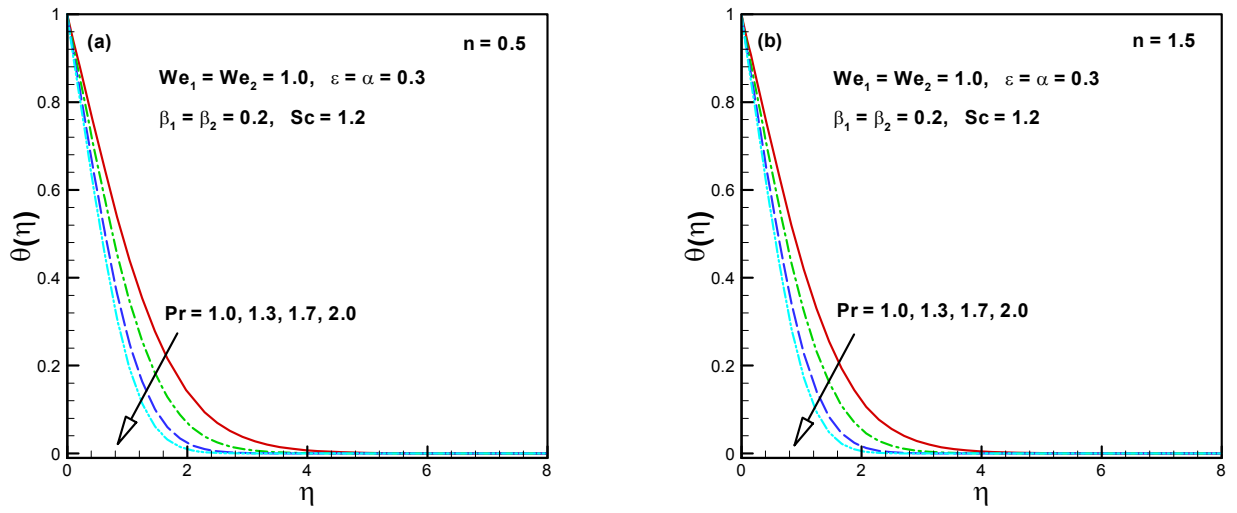**Figure 9.2(a, b):** Influence of ε on $\theta(\eta)$.

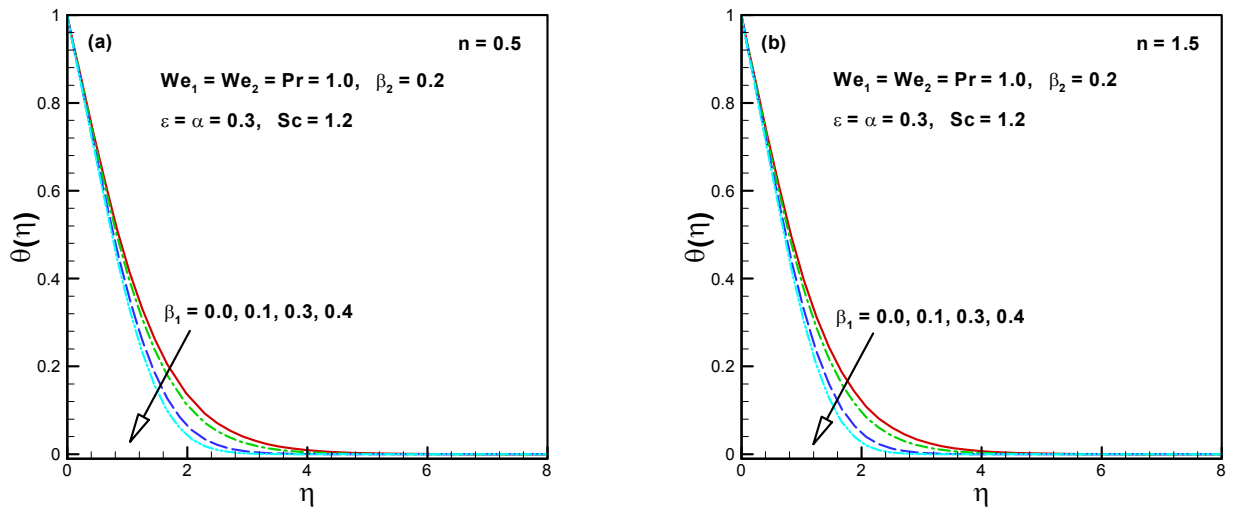**Figure 9.3(a, b):** Influence of Pr on $\theta(\eta)$.

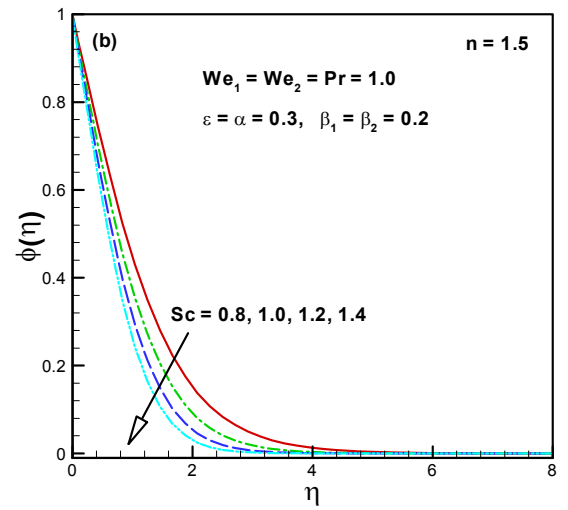
Figure 9.4(a, b): Influence of β_1 on $\theta(\eta)$.
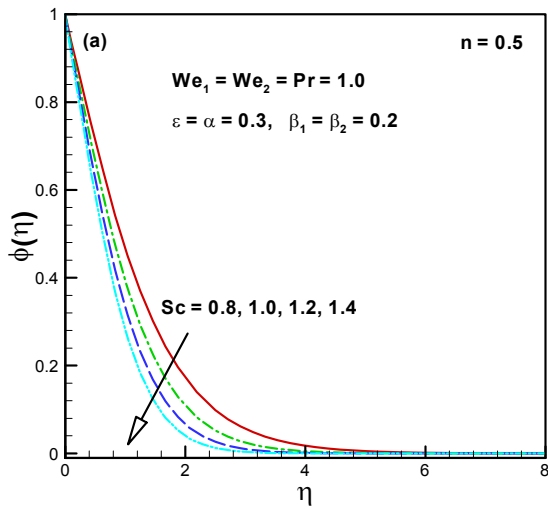
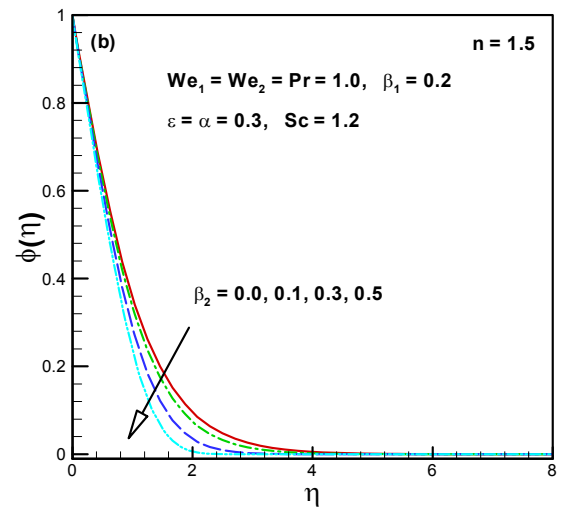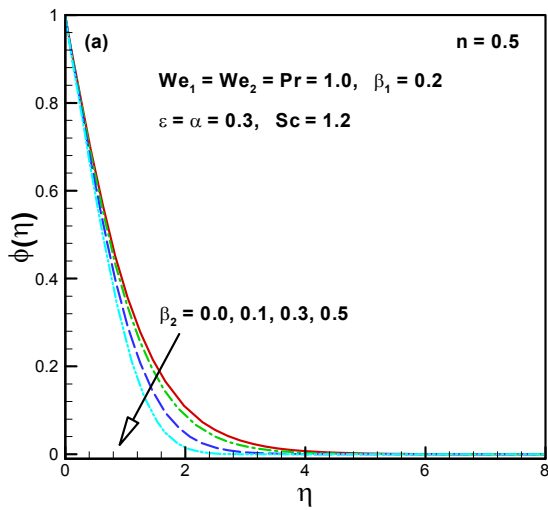**Figure 9.5(a, b)**: Influence of Sc on $\phi(\eta)$.

Figure 9.6(a, b): Influence of β_2 on $\phi(\eta)$.

Table 9.1: A comparison of $\left(\frac{1}{2}C_{fx}\,\mathrm{Re}_x^{\frac{1}{2}}\right)$ between HAM and bvp4c in limiting circumstances when $We_1 = We_2 = 0$ and $n = 1$ are fixed.

α			$f''(0)$		
	Wang [117]	Liu and Anderson [118]	Munir *et al.* [119]	Present (bvp4c)	Present (HAM)
0.0	-1	-1	-1	-1	-1
0.25	-1.048813	-1.048813	-1.048818	-1.0488125	-1.0488101
0.50	-1.093097	-1.093096	-1.093098	-1.0930951	-1.0930952
0.75	-1.134485	-1.134486	-1.134487	-1.1344845	-1.1344855
1.0	-1.173720	-1.173721	-1.173721	-1.1737201	-1.1737201

Table 9.2: A comparison of $\left(\frac{1}{2}\left(\frac{U_w}{V_w}\right)C_{fy}\,\mathrm{Re}_x^{\frac{1}{2}}\right)$ between HAM and bvp4c in limiting circumstances when $We_1 = We_2 = 0$ and $n = 1$ are fixed.

α			$g''(0)$		
	Wang [117]	Liu and Anderson [118]	Munir *et al.* [119]	Present (bvp4c)	Present (HAM)
0.0	0	0	0	-1	-1
0.25	-0.194564	-0.194565	-0.194567	-0.19456491	-0.19456446
0.50	-0.465205	-0.465206	-0.465207	-0.46520520	-0.46520485
0.75	-0.794622	-0.794619	-0.794619	-0.79461815	-0.79461822
1.0	-1.173720	-1.173721	-1.173721	-1.17372051	-1.17372100

Table 9.3: A comparison of $-\theta'(0)$ between HAM and bvp4c in limiting circumstances when $We_1 = We_2 = \epsilon = \beta_1 = \beta_2 = Sc = 0$ and $\Pr = n = 1$ are fixed.

α	$-\theta'(0)$			
	Liu and Anderson [118]	Munir *et al.* [119]	Present(bvp4c)	Present(HAM)
0.25	0.665933	0.665939	0.665933	0.665926
0.50	0.735334	0.735336	0.735335	0.735332
0.75	0.796472	0.796472	0.796473	0.796471

Table 9.4: A comparison of $-\theta'(0)$ between HAM and bvp4c in limiting circumstances $We_1 = We_2 = \beta_1 = \beta_2 = Sc = 0$ and $n = 1$ are fixed.

| ε	$\Pr$	$-\theta'(0)$		
		Khan *et.al* [60]	Present(bvp4c)	Present(HAM)
0.2	1.3	0.604568	0.6045730	0.6045650
0.3		0.569570	0.5695749	0.5695719
0.4		0.539040	0.5390454	0.5390411
0.2	1.5	0.664040	0.6640454	0.6640446
	1.7	0.719773	0.7197816	0.7197711
	2.0	0.797638	0.7976520	0.7976410

Chapter 10

Homogeneous-Heterogeneous Reactions in 3D Unsteady Nonlinear Radiative Flow of Carreau Fluid

This chapter scrutinize unsteady 3D bidirectional stretched flow of a magneto-Carreau liquid with non-linear thermal radiation. The convective properties for heat transfer mechanisms are investigated with heat sink/source aspects. Additionally, the proposed model of heterogeneous-homogeneous processes with equivalent diffusivities for autocatalysis and reactants are considered. The modeled boundary layer equations are reduced to a system of nonlinear ODEs using the appropriate transformations. The resulting equations are then solved by utilizing the two different techniques, namely the bvp4c function in Matlab and the homotopic algorithm. The numerical data for the velocities, temperature and concentration fields are graphically sketched and characteristics of the influential parameters are deliberated in detail. Moreover, the velocity gradients and the amount of heat transfer at the stretched surface for diverse value of the pertaining parameters are given in tabulated form. It is observed that the temperature profile enhances for the higher values of magnetic parameter (M) and heat generation parameter $(\delta > 0)$, whereas it declines for augmented values of heat absorption $(\delta < 0)$ parameter. In addition, the concentration profile declines for increasing values of homogeneous reaction parameter (k_1) and unsteadiness parameter (S). To see the validity of the numerical computa-

tions, the results of the numerical techniques, namely bvp4c with an efficient analytical method, the homotopy analysis method (HAM) are compared and perceived an outstanding correlation between these techniques.

10.1 Description of the Problem

Let us scrutinize unsteady 3D flow of a magneto-Carreau liquid with velocities $U_w(x,t)$ and $V_w = (x,t)$, in which x is the coordinate measured beside the sheet and t the time. Additionally, convective heat transfer mechanism is carried out in the presence of nonlinear thermal radiation and heat source/sink. Furthermore, the flow analysis is considered here by utilizing the heterogeneous-homogeneous processes (Merkin [41]). A magnetic field of strength $B(t) = \frac{B_0}{\sqrt{1-ct}}$ is applied along $z - axis$. Because of the small magnetic Reynolds number the impact of the induced magnetic field is neglected here. Moreover, we assume that hot liquid below the sheet with temperature T_f transform the heat to the sheet with coefficient of heat transfer h_f. The homogeneous processes for cubic autocatalysis be written as

$$G_1 + 2H_1 \rightarrow 3H_1, \quad \text{rate} = k_c g_1 h_1^2, \tag{10.1}$$
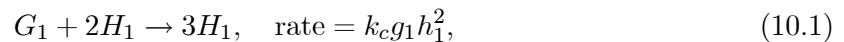
while on the catalyst surface, the first-order isothermal response is

$$G_1 \rightarrow H_1, \quad \text{rate} = k_s g_1, \tag{10.2}$$

where (g_1, h_1) are the concentration and (k_c, k_s) the rate constants of the chemical species (G_1, H_1), respectively. Furthermore, with the notion of both isothermal processes and distant from the sheet at the ambient fluid, for G_1 reactant, g_{1_0} is a constant concentration, whereas there is no autocatalyst H_1.

Governing equations of the existing unsteady flow under these aforementioned assumptions discussed above are given by

$$\frac{\partial u}{\partial x} + \frac{\partial v}{\partial y} + \frac{\partial w}{\partial z} = 0, \tag{10.3}$$

173

$$\frac{\partial u}{\partial t} + u\frac{\partial u}{\partial x} + v\frac{\partial u}{\partial y} + w\frac{\partial u}{\partial z} = \nu\frac{\partial^2 u}{\partial z^2}\left[1 + \Gamma^2\left(\frac{\partial u}{\partial z}\right)^2\right]^{\frac{n-1}{2}}$$

$$+\nu(n-1)\Gamma^2\left(\frac{\partial u}{\partial z}\right)^2\left(\frac{\partial^2 u}{\partial z^2}\right)\left[1 + \Gamma^2\left(\frac{\partial u}{\partial z}\right)^2\right]^{\frac{n-3}{2}} - \frac{\sigma B_0^2}{\rho_f}u, \quad (10.4)$$

$$\frac{\partial v}{\partial t} + u\frac{\partial v}{\partial x} + v\frac{\partial v}{\partial y} + w\frac{\partial v}{\partial z} = \nu\frac{\partial^2 v}{\partial z^2}\left[1 + \Gamma^2\left(\frac{\partial v}{\partial z}\right)^2\right]^{\frac{n-1}{2}}$$

$$+\nu(n-1)\Gamma^2\left(\frac{\partial v}{\partial z}\right)^2\left(\frac{\partial^2 v}{\partial z^2}\right)\left[1 + \Gamma^2\left(\frac{\partial v}{\partial z}\right)^2\right]^{\frac{n-3}{2}} - \frac{\sigma B_0^2}{\rho_f}v, \quad (10.5)$$

$$\frac{\partial T}{\partial t} + u\frac{\partial T}{\partial x} + v\frac{\partial T}{\partial y} + w\frac{\partial T}{\partial z} = \alpha_1\frac{\partial^2 T}{\partial z^2} - \frac{1}{(\rho c)_f}\frac{\partial q_r}{\partial z} + \frac{Q_0}{(\rho c)_f}(T - T_\infty), \quad (10.6)$$

$$\frac{\partial g_1}{\partial t} + u\frac{\partial g_1}{\partial x} + v\frac{\partial g_1}{\partial y} + w\frac{\partial g_1}{\partial z} = D_{G_1}\frac{\partial^2 g_1}{\partial z^2} - k_c g_1 h_1^2, \quad (10.7)$$

$$\frac{\partial h_1}{\partial t} + u\frac{\partial h_1}{\partial x} + v\frac{\partial h_1}{\partial y} + w\frac{\partial h_1}{\partial z} = D_{H_1}\frac{\partial^2 h_1}{\partial z^2} + k_c g_1 h_1^2. \quad (10.8)$$

The boundary condition of flow problems are

$$u = U_w(x,t) = \frac{ax}{1-\beta t}, \quad v = V_w(x,t) = \frac{by}{1-\beta t}, \quad w = 0,$$

$$-k\frac{\partial T}{\partial z} = h_f[T_f - T], \quad D_{G_1}\frac{\partial g_1}{\partial z} = k_s g_1, \quad D_{H_1}\frac{\partial h_1}{\partial z} = -k_s g_1 \quad \text{at} \quad z = 0, \quad (10.9)$$

$$u \to 0, \quad v \to 0, \quad T \to T_\infty, \quad g_1 \to g_{1_0}, \quad h_1 \to 0 \quad \text{as} \quad z \to \infty, \quad (10.10)$$

10.1.1   Appropriate Conversions

We introduce the following appropriate conversions:

$$\theta\left(\eta\right) = \frac{T - T_\infty}{T_f - T_\infty}, \quad g_1 = g_{1_0}l(\eta) \quad h_1 = h_{1_0}r(\eta). \quad (10.11)$$

In vision of the above conversions and Eq. (6.9) (cf. Chapter 6), the condition of incompressibility is satisfied automatically and Eqs. (11.4) − (11.10) yield

$$f'''[1 + We_1^2 f''^2]^{\frac{n-3}{2}}[1 + nWe_1^2 f''^2] - S\left(f' + \frac{1}{2}\eta f''\right) - f'^2 + f''(f+g) - M^2 f' = 0, \quad (10.12)$$

174

$$g'''[1 + We_2^2 g''^2]^{\frac{n-3}{2}}[1 + nWe_2^2 g''^2] - S\left(g' + \frac{1}{2}\eta g''\right) - g'^2 + g''(f+g) - M^2 g' = 0, \quad (10.13)$$

$$\frac{d}{d\eta}[\{1 + R_d(1 + (\theta_f - 1)\theta)^3\}\theta'] - \Pr S\left(\theta + \frac{1}{2}\eta\theta'\right) + \Pr(f+g)\theta' + \Pr\delta\theta = 0, \quad (10.14)$$

$$\frac{1}{Sc}l'' + (f+g)l' - k_1 l r^2 - \frac{S}{2}\eta l' = 0, \quad (10.15)$$

$$\frac{\lambda_c}{Sc}r'' + (f+g)r' + k_1 l r^2 - \frac{S}{2}\eta r' = 0, \quad (10.16)$$

$$f(0) = 0, \quad g(0) = 0, \quad f'(0) = 1, \quad g'(0) = \alpha, \quad \theta'(0) = -\gamma_1[1 - \theta(0)], \quad (10.17)$$

$$l'(0) = k_2 l(0), \quad \lambda_c r'(0) = -k_2 l(0), \quad (10.18)$$

$$f' \to 0, \quad g' \to 0, \quad \theta \to 0, \quad (10.19)$$

$$l \to 1, \quad r \to 0 \quad \text{as} \quad \eta \to \infty. \quad (10.20)$$

In physical situations, the diffusion coefficients D_{G_1} and D_{H_1} are occupied to be equal i.e. $\lambda_c = 1$, which will give us

$$l(\eta) + r(\eta) = 1. \quad (10.21)$$

Now consequently, Eqs. (10.15) and (10.16) yield

$$\frac{1}{Sc}l'' + (f+g)l' - \frac{S}{2}\eta l' - k_1(1-l)^2 l = 0, \quad (10.22)$$

with boundary conditions (10.18) and (10.20), we have

$$l'(0) = k_2 l(0), \quad l \to 1 \quad \text{as } \eta \to \infty. \quad (10.23)$$

10.2   Engineering and Industrial Quantities of Interest

The surface drag forces (C_{fx}, C_{fy}) and heat transport amount (Nu_x) are stated below

$$C_{fx} = \frac{\tau_{xz}}{\frac{1}{2}\rho_f U_w^2} \quad \text{and} \quad C_{fy} = \frac{\tau_{yz}}{\frac{1}{2}\rho_f U_w^2}, \quad (10.24)$$

175

$$Nu_x = \frac{xq_r}{k\,(T_f - T_\infty)} - \frac{x}{(T_f - T_\infty)} \left.\left(\frac{\partial T}{\partial z}\right)\right|_{z=0}, \tag{10.25}$$

while in dimensionless variables, these are

$$\tfrac{1}{2}C_{fx}\,\mathrm{Re}_x^{\frac{1}{2}} = f''(0)[1 + We_1^2 f''^2]^{\frac{n-1}{2}}, \tag{10.26}$$

$$\tfrac{1}{2}\left(\tfrac{U_w}{V_w}\right)C_{fy}\,\mathrm{Re}_x^{\frac{1}{2}} = g''(0)[1 + We_2^2 g''^2]^{\frac{n-1}{2}}, \tag{10.27}$$

$$\mathrm{Re}_x^{-\frac{1}{2}}\,Nu_x = -[1 + R_d\{1 + (\theta_f - 1)\theta(0)\}^3]\theta'(0). \tag{10.28}$$

10.3   Graphical Illustration and Analysis

The main attention of this section is to infer the physical structures of nonlinear thermal radiation and heterogeneous-homogeneous reactions in unsteady 3D magneto-Carreau liquid with convective heat transport. Additionally, characteristics of heat absorption/generation are deliberated. The set of Eqs.$(10.12) - (10.14)$ and (10.20) with boundary restrictions $(10.17), (10.19)$ and (10.23) are established and elucidated via bvp4c approach. Tables of skin friction coefficients and Nusselt number are structured for shear thinning/thickening liquids. Additionally, the tabular assessment between numerical (bvp4c) and analytical (HAM) schemes are presented.

Figures 10.1(a − d) are prepared to highlight the characteristics of local Weissenberg number (We_1) for both $(n = 0.5)$ and $(n = 1.5)$ on the velocity components $f'(\eta)$ and $g'(\eta)$. It is reported from these drafts that when values of We_1 rise the velocity component $f'(\eta)$ decays for $(n < 1)$, while conflicting depiction is being identified for the velocity component $g'(\eta)$ for $(n < 1)$. Similarly, it is also detected that for $(n > 1)$ local Weissenberg number We_1 boosts up the liquid velocity $f'(\eta)$ whereas, it reduces the liquid velocity component $g'(\eta)$ for amassed values of We_1 as exposed in **figures 10.1(b)** and **10.1(d)**. Physical, We_1 is the relation of relaxation time of material and a specific process time. So higher estimation of relaxation time leads to enhancement of thickness of material. Thus, higher We_1 corresponds to a decrease in velocity. Moreover, We_1 is the relation of relaxation time of liquid and a certain progression in which time growing the liquid viscosity. Hence, outcomes decline the liquid velocity $g'(\eta)$.

The behavior of local Weissenberg number (We_2) on the velocity components $f'(\eta)$ and $g'(\eta)$ is noticed through **figures 10.2(a − d)** for shear thinning/thickening liquids. It is noted from these strategies, the intensifying value of We_2 enhances the velocity components $f'(\eta)$ whereas the reverse trend is detected for the velocity component $g'(\eta)$ for $(n < 1)$. However, it is anticipated from the graphical data that opposite behavior of velocity components is acknowledged for shear thinning liquid i.e., $(n < 1)$.

Figures 10.3(a, b) and **10.4(a, b)** are plotted to interpret the impact of local Weissenberg numbers $(We_1$ and $We_2)$ on the temperature $\theta(\eta)$ of magneto-Carreau liquid. The progressive values of We_1 and We_2 enhance the liquid temperature for $(n < 1)$ and a reverse behavior is identified for $(n > 1)$. Physically, We_1 and We_2 are the proportion of viscous to the elastic forces, so strengthening values of We_1 and We_2 result in an amplification in the liquid viscosity. Consequently, flow becomes extra resistive and therefore, the temperature field enriches for $(n < 1)$ and reduced for $(n > 1)$. **Figures 10.5(a, b)** and **10.6(a, b)** are schemed to comprehend the impact of radiation parameter (R_d) and temperature ratio parameter (θ_f) for both shear thinning/thickening liquids on the temperature of Carreau liquid. From these plots it is notable that the temperature of Carreau liquid and associated thermal boundary layer rise for augmenting values of R_d and θ_f. Physically, when R_d enhances, the mean absorption coefficient declines due to which radiative heat transfer amount of the fluid rise. Therefore, the liquid temperature and its associated thermal boundary layer increase. The variation in the temperature of Carreau liquid for $(n < 1)$ and $(n > 1)$ is sketched in **figures 10.7(a, b)** and **10.8(a, b)** for different values of the heat absorption phenomenon $(\delta < 0)$ and heat generation phenomenon $(\delta > 0)$. The temperature of Carreau liquid increases as the value of heat generation $\delta > 0$ is increased due to the fact that $\delta > 0$ gives more heat to the fluid that corresponds to an increase in the temperature profile and the thermal boundary layer thickness while the opposite trend is detected for $\delta < 0$. Impact of magnetic parameter (M) and thermal Biot number (γ_1) on the temperature field are delineated through **figures 10.9(a, b)** and **10.10(a, b)**. It is apparent from these graphs that M and γ_1 are increasing functions of temperature field. Physically, this is due to the fact that the Lorentz force is a resistive force which opposes the liquid motion due to which collusion between the liquid particles enhances. Therefore, the temperature of Carreau liquid and its associated thermal boundary layer thickness rise. Additionally, it is observed

from the graphs, γ_1 has a significant effect on the temperature profile. When γ_1 is increased, the internal thermal resistance of the surface enhances. Therefore, a build in γ_1 increases fluid temperature effectively.

To visualize the impact of the local Weissenberg numbers (We_1 and We_2) on the concentration profile $l(\eta)$ for both values of $n = 0.5$ and 1.5, **figures 10.11(a, b)** and **10.12(a, b)** are plotted. From these plots we noted that when we enhance values of We_1 and We_2 the concentration profile reduces for ($n < 1$) while conflicting trend is observed for ($n > 1$). Furthermore, it is noted that the outcomes for the concentration of Carreau liquid are more prominent for lesser values of We_1 and We_2 when compared with the velocity and temperature fields. **Figures 10.13(a, b)** and **10.14(a, b)** are enlisted to envision the characteristics of homogeneous reaction parameter (k_1) and unsteadiness parameter (S) on concentration of Carreau liquid. The increasing values of homogeneous reaction parameter (amount of strength of homogeneous reaction) decline both the concentration and its associated thickness of concentration boundary layer for both instances. Although conflicting behavior is observed for accumulated values of S for concentration field. Chemically, during a chemical reaction reactant is consumed when enhance k_1. Owing to this circumstance concentration distribution shows diminishing trend for higher values of k_1. **Figures 10.15(a, b)** and **10.16(a, b)** are exposed to envision the influence of magnetic parameter (M) and Schmidt number (Sc) for ($n < 1$) and ($n > 1$) on concentration profiles. A conflicting behavior for both M and Sc on concentration profile is observed. Augmented values of M diminish the concentration distribution and its related thickness of concentration boundary layer; however, the concentration of Carreau fluid enriches for Sc. It is essential to note that Sc is the amount of momentum diffusivity to mass diffusivity. Augmented values of Sc resemble to greater momentum diffusivity due to which concentration profile rises.

10.3.1   Tabular Representations

Tables 10.1 and **10.2** are presented to inspect the characteristics of the different flow parameter on the skin friction coefficients $\left(\frac{1}{2} C_{fx} \, \mathrm{Re}_x^{\frac{1}{2}}, \frac{1}{2} \left(\frac{U_w}{V_w} \right) C_{fy} \, \mathrm{Re}_x^{\frac{1}{2}} \right)$ and amount of heat transfer $\left(Nu_x \, \mathrm{Re}_x^{-\frac{1}{2}} \right)$, respectively. It is noted that magnitude of $\left(\frac{1}{2} C_{fx} \, \mathrm{Re}_x^{\frac{1}{2}}, \frac{1}{2} \left(\frac{U_w}{V_w} \right) C_{fy} \, \mathrm{Re}_x^{\frac{1}{2}} \right)$ and $\left(Nu_x \, \mathrm{Re}_x^{-\frac{1}{2}} \right)$ augment for higher M and S. Moreover, the larger values of R_d, γ_1 and Pr

decrease the $\left(Nu_x \operatorname{Re}_x^{-\frac{1}{2}} \right)$ for both $(n < 1)$ and $(n > 1)$ cases.

10.3.2 Confirmation of Numerical Outcomes

Tables 10.3 and **10**.4 present the comparison between two different schemes, namely bvp4c and HAM. From these tables, we found an outstanding agreement between these two techniques. The accuracy of numerical significances is also recognized by comparison with the numerical outcomes (bvp4c) and analytical consequences attained by the HAM as displayed in **Tables 10.5** to **10.7**. Moreover, these outcomes are compared with previous published results and achieved an excellent agreement between these results.

(a) n = 0.5

$We_2 = Pr = 2.0,$ $\alpha = S = R_d = 0.3,$ $Sc = 1.5$

$\theta_f = 1.2,$ $M = \gamma_1 = 0.5,$ $\delta = k_1 = k_2 = 0.2$

$We_1 = 1.0, 2.0, 3.0, 4.0$

f''(η)

η

(b) n = 1.5

$We_2 = Pr = 2.0,$ $\alpha = S = R_d = 0.3,$ $Sc = 1.5$

$\theta_f = 1.2,$ $M = \gamma_1 = 0.5,$ $\delta = k_1 = k_2 = 0.2$

$We_1 = 1.0, 2.0, 3.0, 4.0$

f''(η)

η

(c) n = 0.5

$We_2 = Pr = 2.0,$ $\alpha = S = R_d = 0.3,$ $Sc = 1.5$

$\theta_f = 1.2,$ $M = \gamma_1 = 0.5,$ $\delta = k_1 = k_2 = 0.2$

$We_1 = 1.0, 2.0, 3.0, 4.0$

g'(η)

η

(d) n = 1.5

$We_2 = Pr = 2.0,$ $\alpha = S = R_d = 0.3,$ $Sc = 1.5$

$\theta_f = 1.2,$ $M = \gamma_1 = 0.5,$ $\delta = k_1 = k_2 = 0.2$

$We_1 = 1.0, 2.0, 3.0, 4.0$

g'(η)

η
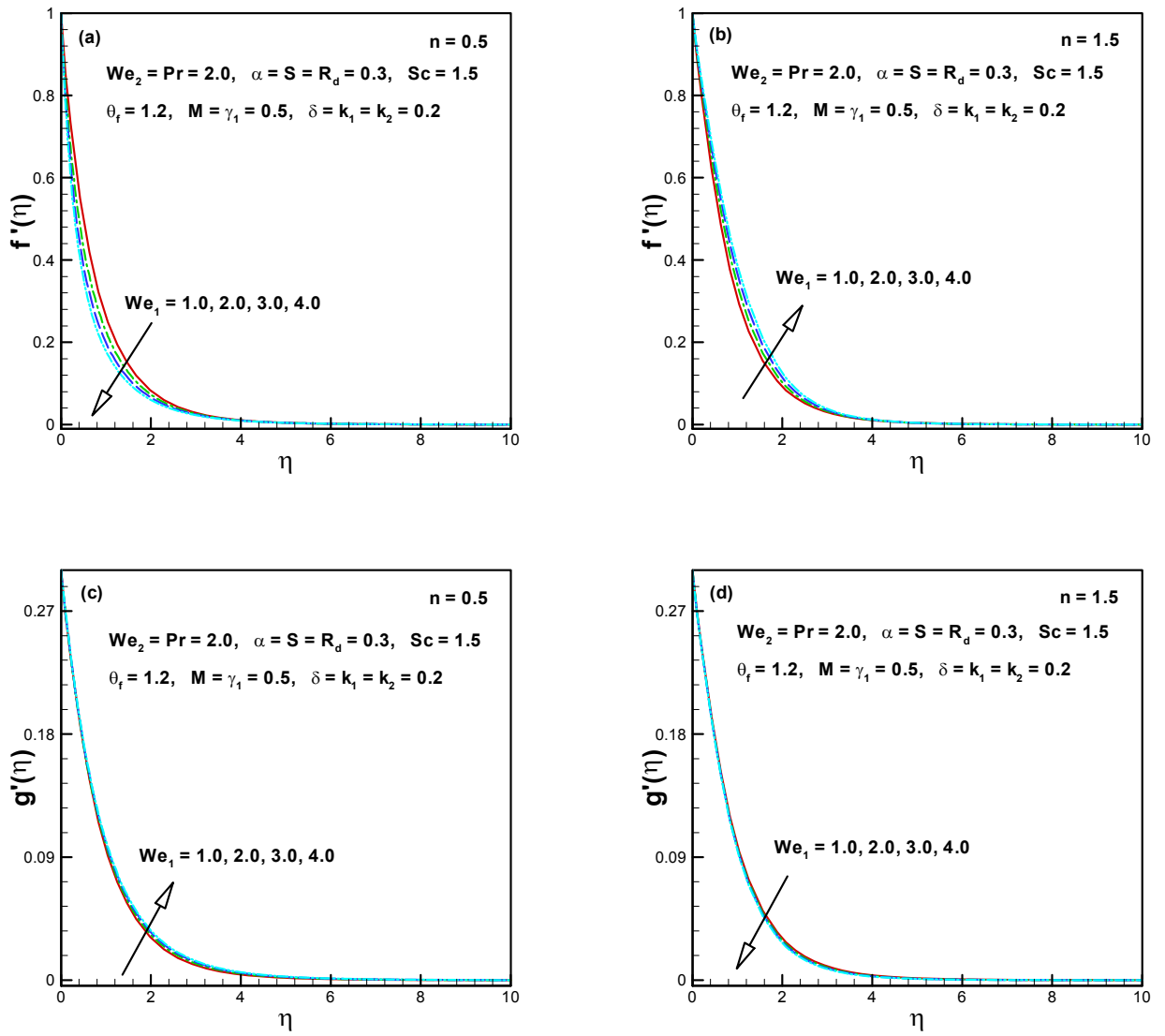
Figure 10.1(a − d): Influence of We_1 on $f'(\eta)$ and $g'(\eta)$.
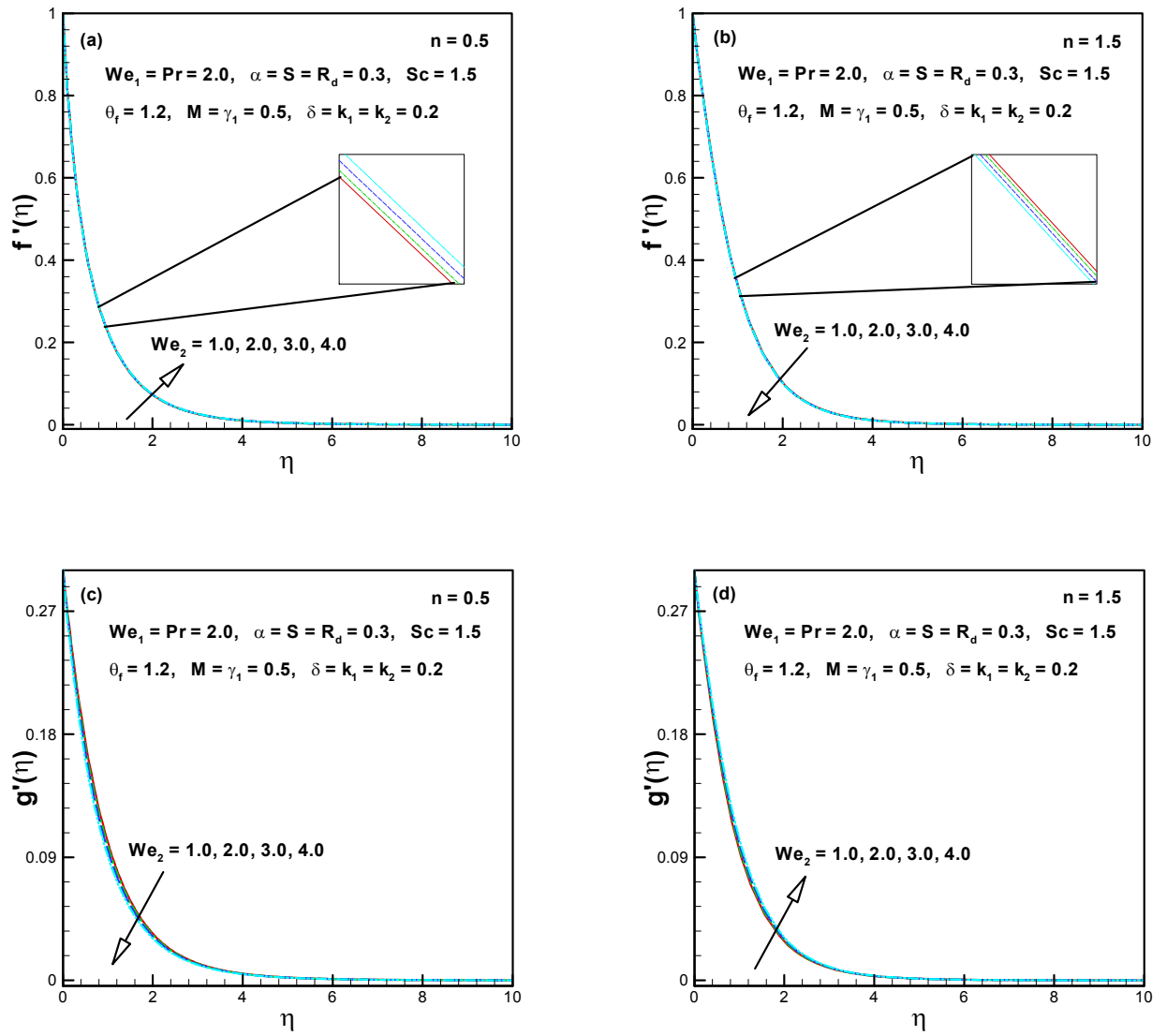
Figure 10.2(a − d): Influence of We_2 on $f'(\eta)$ and $g'(\eta)$.
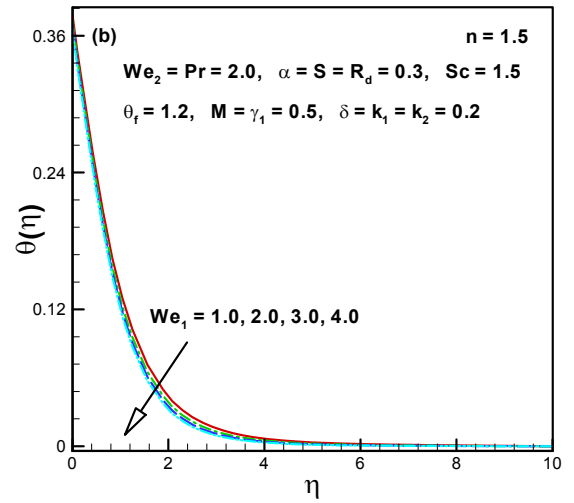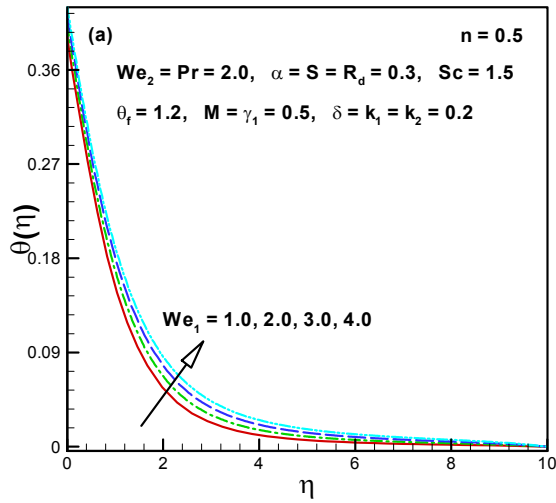
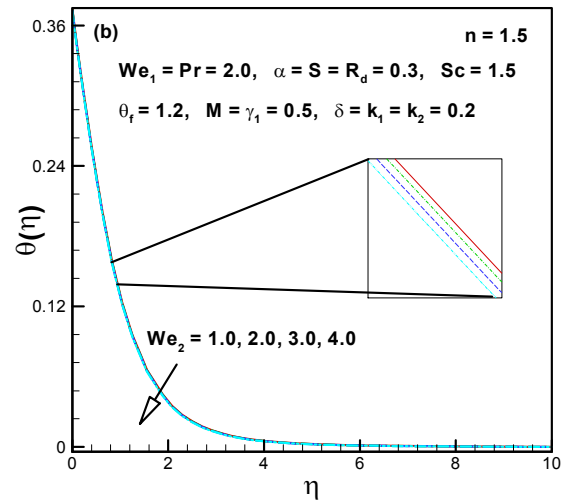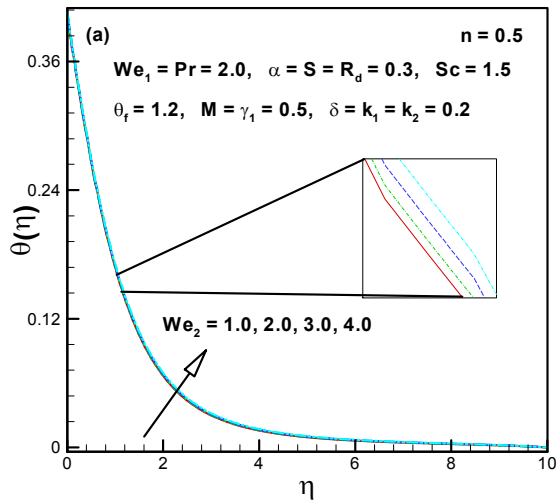**Figure 10.3(a, b):** Influence of We_1 on $\theta(\eta)$.

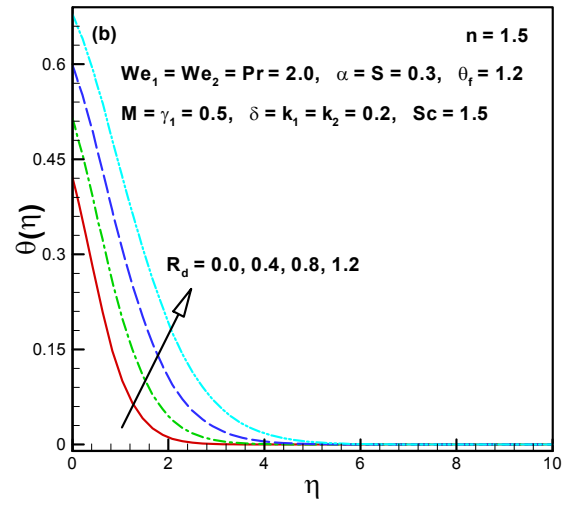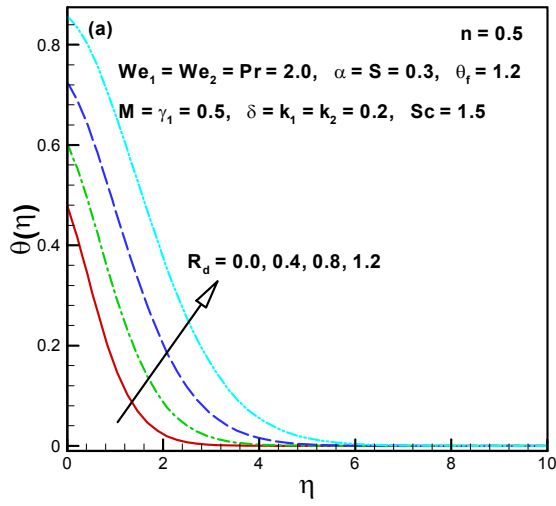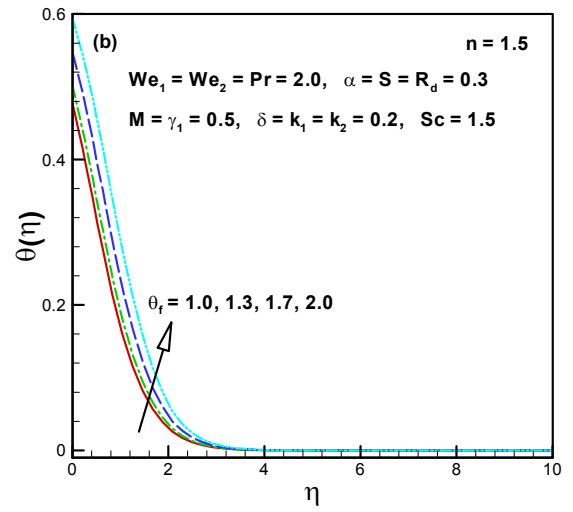**Figure 10.4(a, b):** Influence of We_2 on $\theta(\eta)$.
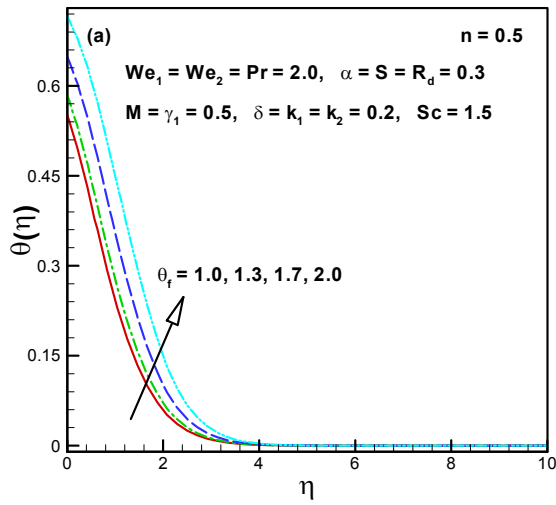
Figure 10.5(a, b): Influence of R_d on $\theta(\eta)$.
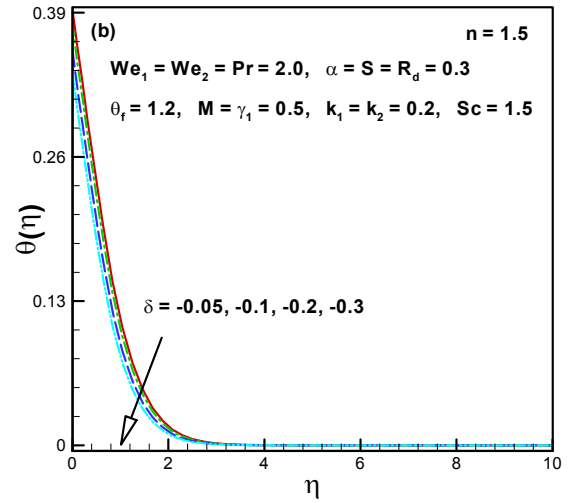

Figure 10.6(a, b): Influence of θ_f on $\theta(\eta)$.
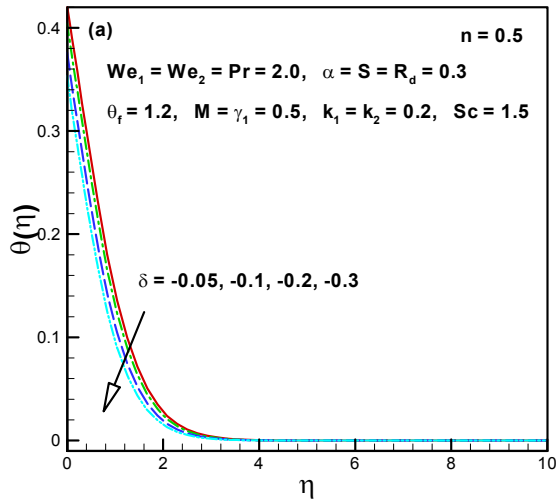
Figure 10.7(a, b): Influence of $\delta < 0$ on $\theta(\eta)$.
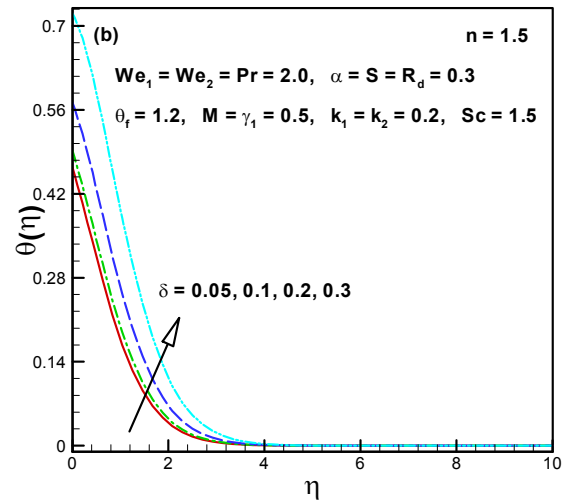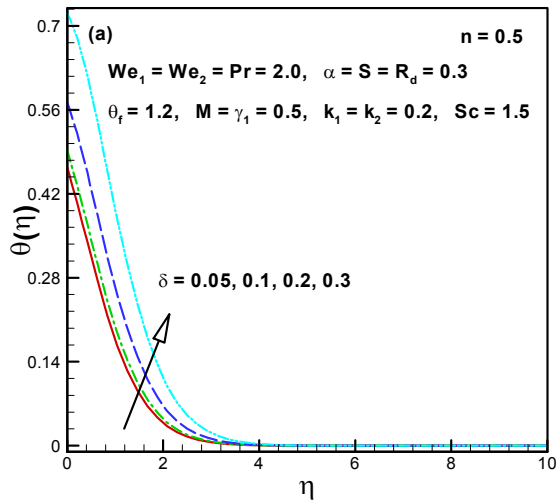
Figure 10.8(a, b): Influence of $\delta > 0$ on $\theta(\eta)$.

184
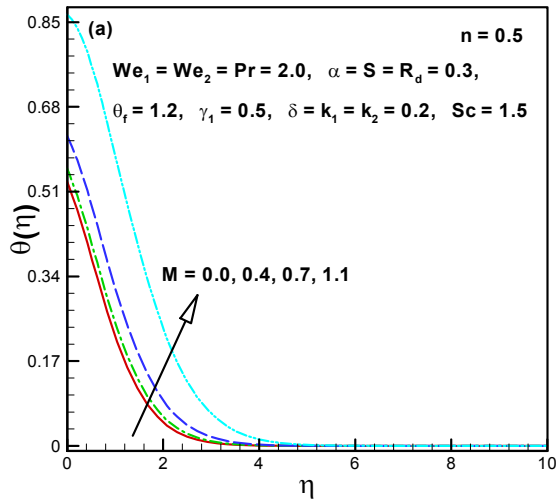
Figure 10.9(a, b): Influence of M on $\theta(\eta)$.

Figure 10.10(a, b): Influence of γ_1 on $\theta(\eta)$.

Figure 10.11(a, b): Influence of We_1 on $l(\eta)$.
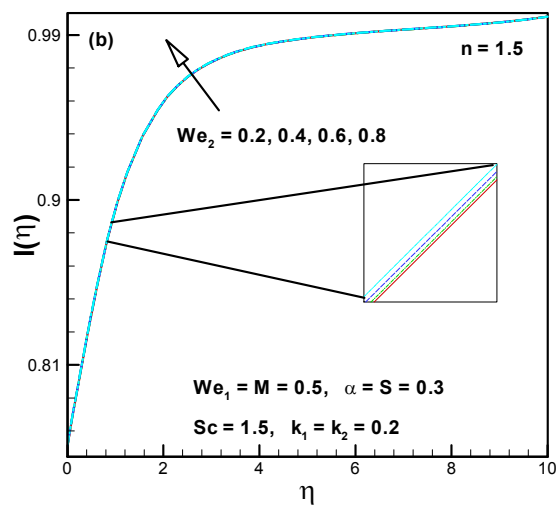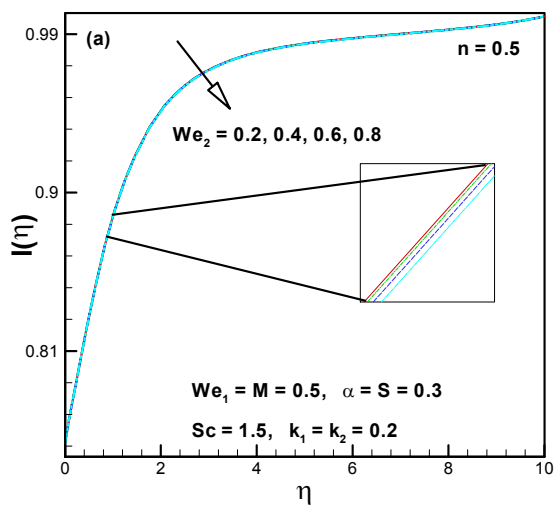
Figure 10.12(a, b): Influence of We_2 on $l(\eta)$.
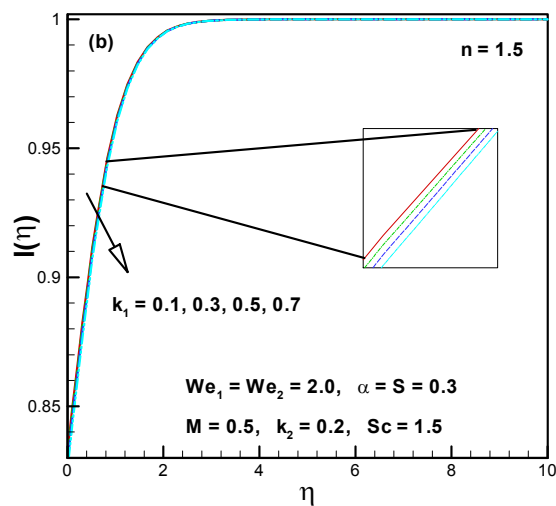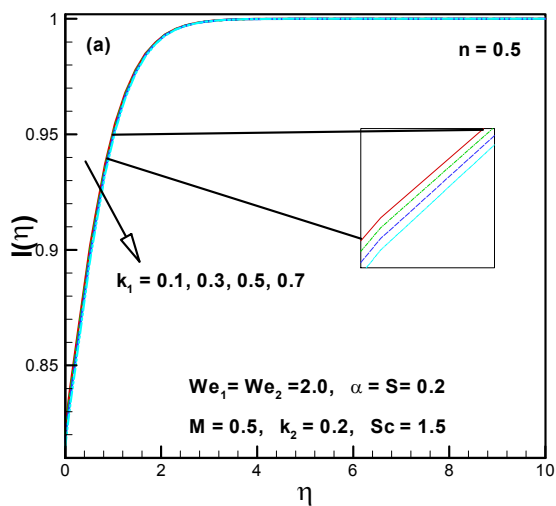
Figure 10.13(a, b): Influence of k_1 on $l(\eta)$.
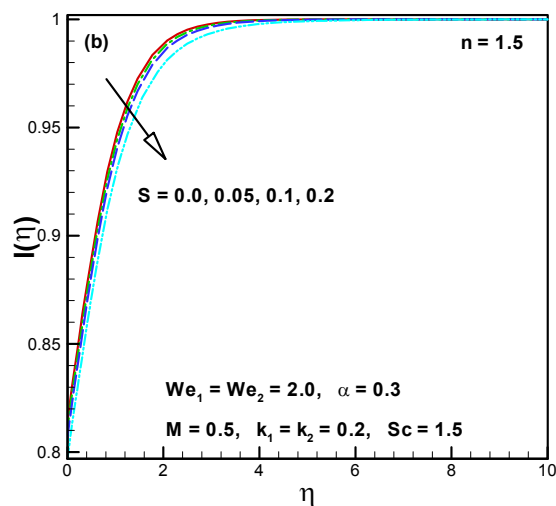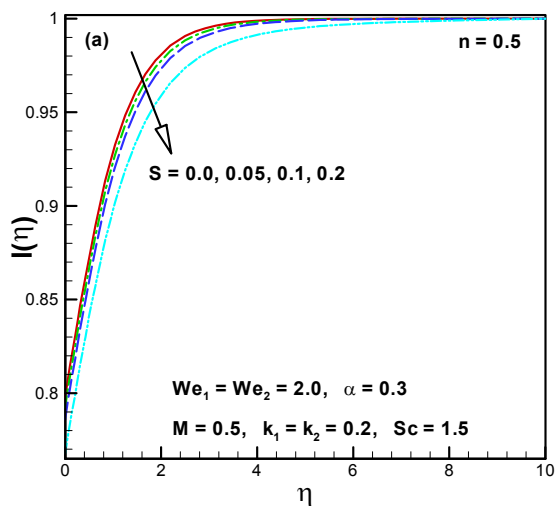
Figure 10.14(a, b): Influence of S on $l(\eta)$.
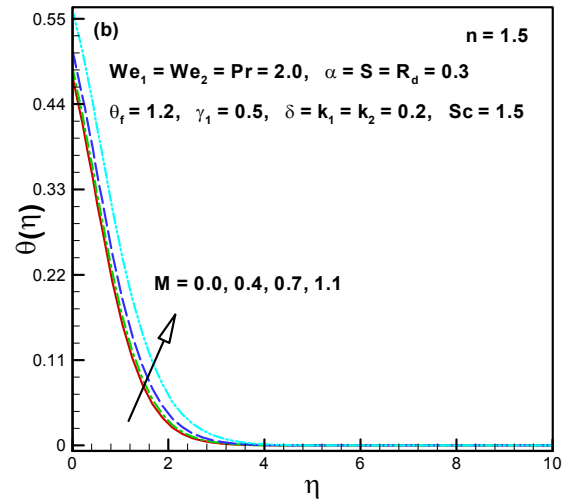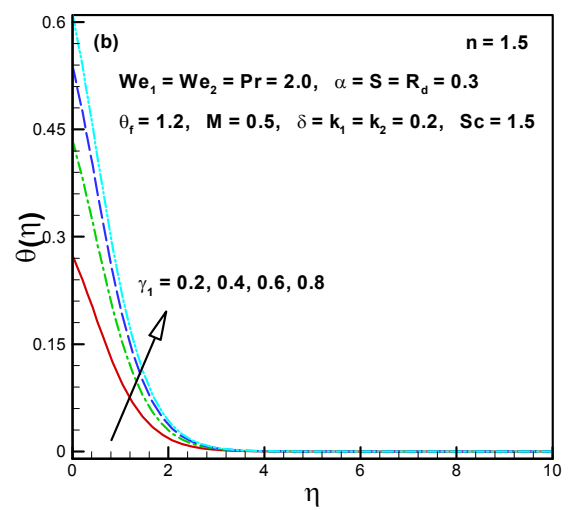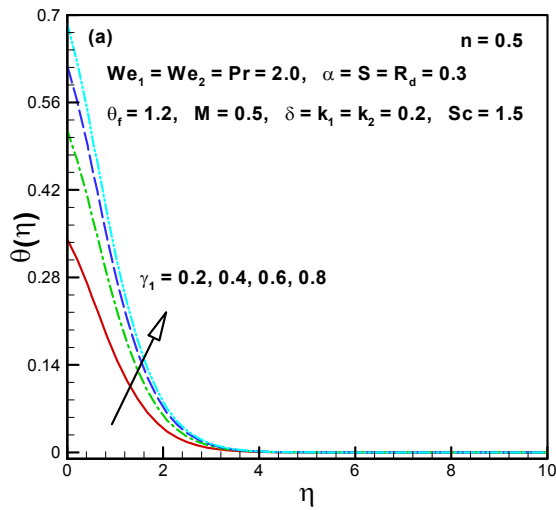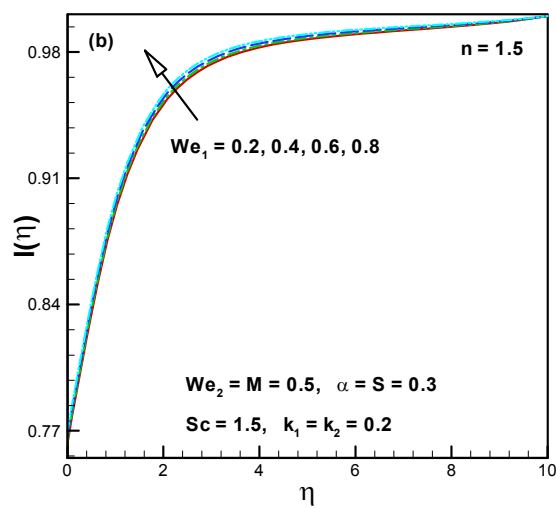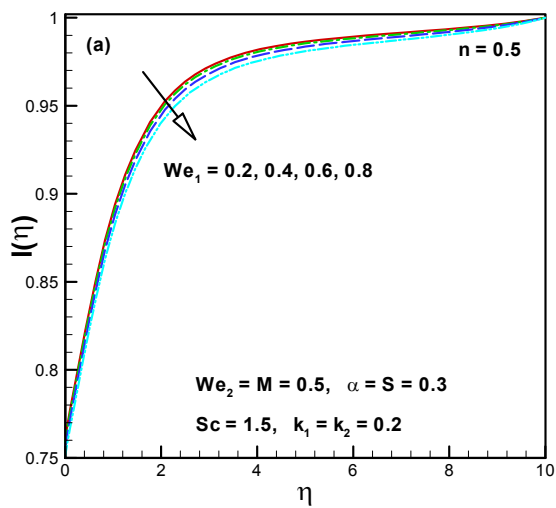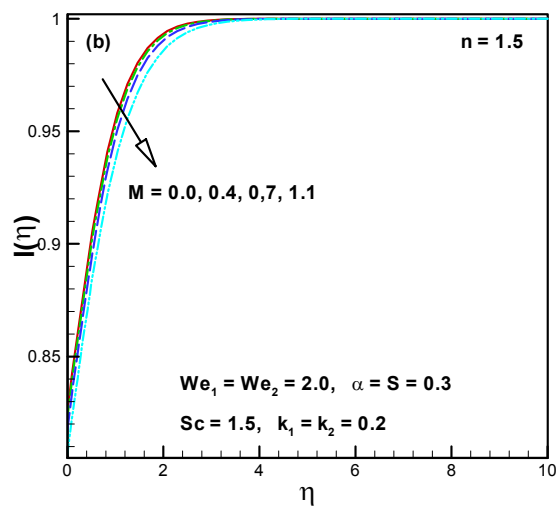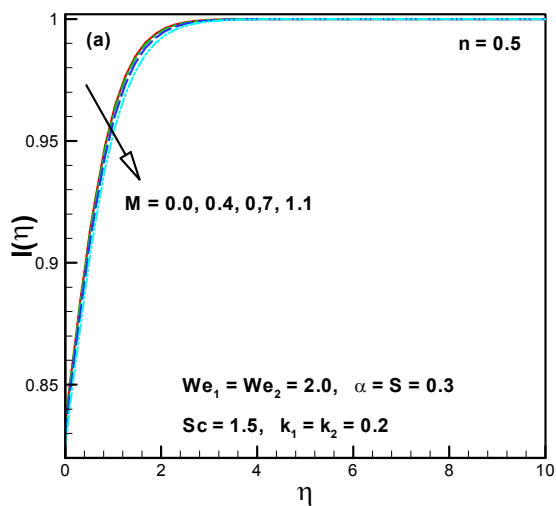
Figure 10.15(a, b): Influence of M on $l(\eta)$.
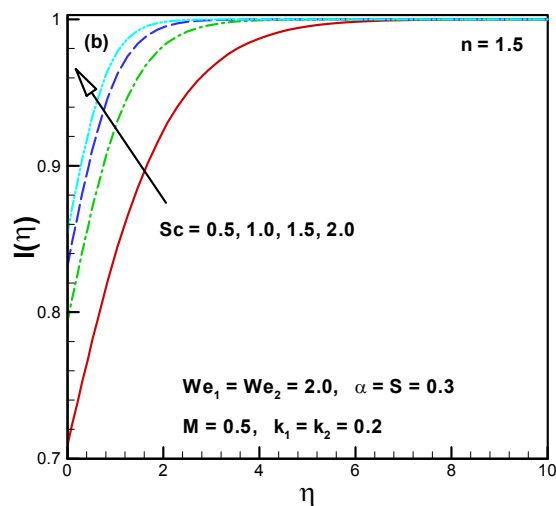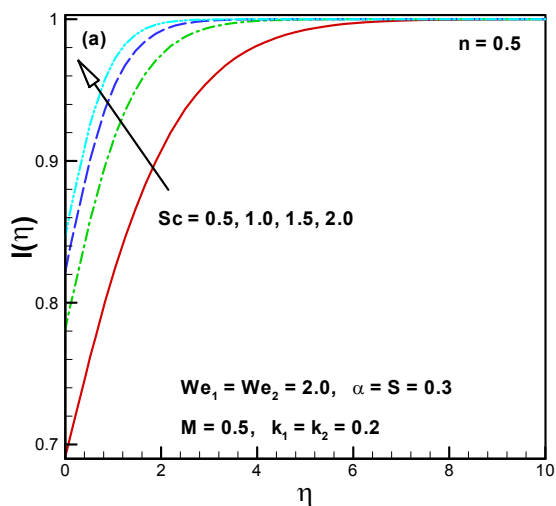
Figure 10.16(a, b): Influence of Sc on $l(\eta)$.

188

Table 10.1: Outcomes of $\left(\frac{1}{2}C_{fx}\,\mathrm{Re}_x^{\frac{1}{2}}, \frac{1}{2}\left(\frac{U_w}{V_w}\right)C_{fy}\,\mathrm{Re}_x^{\frac{1}{2}} \right)$ when $\alpha = 0.3$, $\gamma_1 = 0.5$, $\delta = 0.2$, $R_d = 0.3$, $\theta_f = 1.2$ and $\mathrm{Pr} = 2.0$ are fixed.

We_1	We_2	S	M	$\frac{1}{2}C_{fx}\,\mathrm{Re}_x^{\frac{1}{2}}$		$\frac{1}{2}\left(\frac{U_w}{V_w}\right)C_{fy}\,\mathrm{Re}_x^{\frac{1}{2}}$	
				$n = 0.5$	$n = 1.5$	$n = 0.5$	$n = 1.5$
2.0	2.0	0.3	0.5	-2.046435	-4.702709	-0.3300503	-0.4125359
2.5				-2.240301	-6.062783	-0.3281542	-0.4141052
3.0				-2.407694	-7.539750	-0.3265503	-0.4154563
3.5				-2.555124	-9.120284	-0.3251771	-0.4166335
2.0	2.5			-2.045798	-4.704881	-0.3414938	-0.4574357
	3.0			-2.045067	-4.707137	-0.3548244	-0.5079346
	3.5			-2.044266	-4.709401	-0.3695934	-0.5631292
	2.0	0.4		-2.117672	-4.919199	-0.3424575	-0.4302965
		0.5		-2.188601	-5.139543	-0.3547994	-0.4482203
		0.6		-2.259131	-5.363385	-0.3670574	-0.4662761
		0.3	0.0	-1.804023	-3.938287	-0.2843380	-0.3471551
			0.2	-1.843686	-4.059568	-0.2919741	-0.3578008
			0.4	-1.960615	-4.425757	-0.3141013	-0.3892843

Table 10.2: Outcomes of $\left(Nu_x \operatorname{Re}_x^{-\frac{1}{2}}\right)$ when $We_1 = We_2 = 2.0$, $\alpha = 0.3$, $\delta = 0.2$, $\theta_f = 1.2$ and $\Pr = 2.0$ are fixed.

S	M	R_d	γ	$\Pr$	$Nu_x \operatorname{Re}_x^{-\frac{1}{2}}$	
					$n = 0.5$	$n = 1.5$
0.3	0.5	0.3	0.5	2.0	0.411062	0.429949
0.4					0.424277	0.439151
0.5					0.435556	0.447557
0.6					0.445239	0.455161
0.3	0.0				0.418642	0.433624
	0.2				0.417404	0.433017
	0.4				0.413749	0.431242
	0.5	0.0			0.324812	0.337217
		0.4			0.438037	0.459293
		0.8			0.537834	0.569123
		0.3	0.1		0.116831	0.118229
			0.2		0.211790	0.216517
			0.4		0.355621	0.369532
			0.5	1.0	0.328768	0.352512
				1.3	0.360871	0.383626
				1.7	0.392740	0.413299

Table 10.3: A comparison of $\left(\frac{1}{2} C_{fx} \operatorname{Re}_x^{\frac{1}{2}}, \frac{1}{2} \left(\frac{U_w}{V_w} \right) C_{fy} \operatorname{Re}_x^{\frac{1}{2}} \right)$ between HAM and bvp4c when $We_1 = We_2 = \delta = 0.2$, $\alpha = \gamma_1 = R_d = 0.3$, $\theta_f = 1.2$, $n = 3$ and $\Pr = 1.3$ are fixed.

S	M	$\frac{1}{2} C_{fx} \operatorname{Re}_x^{\frac{1}{2}}$		$\frac{1}{2} \left(\frac{U_w}{V_w} \right) C_{fy} \operatorname{Re}_x^{\frac{1}{2}}$	
		bvp4c	HAM	bvp4c	HAM
0.2	0.5	-1.245683	-1.24569	-0.3061175	-0.306114
0.3		-1.275457	-1.27546	-0.3161997	-0.316197
0.4		-1.304997	-1.30499	-0.3261552	-0.326155
0.2	0.1	-1.139945	-1.13995	-0.2683624	-0.268361
	0.2	-1.153643	-1.15366	-0.2733681	-0.273365
	0.3	-1.176149	-1.17615	-0.2815117	-0.281515

Table 10.4: A comparison of $\left(Nu_x\,\mathrm{Re}_x^{-\frac{1}{2}}\right)$ between HAM and bvp4c when $We_1 = We_2 = \delta = 0.2,\ \alpha = 0.3,\ \theta_f = 1.2$ and $n = 3$ are fixed.

S	M	R_d	γ	Pr	$Nu_x\,\mathrm{Re}_x^{-\frac{1}{2}}$ bvp4c	HAM
0.2	0.5	0.3	0.3	1.3	0.263464	0.263461
0.3					0.272514	0.272512
0.4					0.280134	0.280130
0.2	0.1				0.268427	0.268429
	0.2				0.267809	0.267806
	0.3				0.266779	0.266774
	0.5	0.0			0.209058	0.209055
		0.5			0.296467	0.296469
		1.0			0.368989	0.368985
		0.3	0.1		0.112420	0.112424
			0.4		0.315951	0.315953
			0.7		0.423164	0.423167
			0.3	1.0	0.224571	0.224570
				1.3	0.250787	0.250789
				1.7	0.268741	0.268747

Table 10.5: A comparison of $f''(0)$ between HAM and bvp4c in limiting cases when $We_1 = We_2 = \alpha = 0$ and $n = 1$ are fixed.

			$f''(0)$		
S	Sharidan *et al.* [120]	Chamkha *et al.* [121]	[cf. Chapter 6] Table 6.4	Present (bvp4c)	Present (HAM)
0.8	-1.261042	-1.261512	-1.261044	-1.261043	-1.261043
1.2	-1.377722	-1.378052	-1.377728	-1.377725	-1.377752
2.0	-1.587362	-	-1.587371	-1.587381	-1.587362

Table 10.6: A comparison of $\theta'(0)$ between HAM and bvp4c in limiting cases when $We_1 = We_2 = S = M = \delta = \theta_f = R_d = 0$ and $n = 1$ are fixed.

		$\theta'(0)$		
α	Liu and Anderson [118]	Munir *et al.* [119]	Present(bvp4c)	Present(HAM)
0.25	-0.665933	-0.665939	-0.665933	-0.665926
0.50	-0.735334	-0.735336	-0.735335	-0.735332
0.75	-0.796472	-0.796472	-0.796473	-0.796471

Table 10.7: A comparison of $-\theta'(0)$ between HAM and bvp4c in limiting cases when $We_1 = We_2 = S = \delta = \theta_f = R_d = 0$, $\gamma \to \infty$ and $n = 1$ are fixed.

Pr			$-\theta'(0)$		
	Khan and Pop [2]	Wang [122]	Gorla and Sidawi [123]	Present (bvp4c)	Present (HAM)
0.70	0.4539	0.4539	0.4539	0.453935	0.453933
1.0				0.581979	0.581977
1.3				0.693029	0.693023
1.5				0.760293	0.760298
1.7				0.823311	0.823327
2.0	0.9113	0.9114	0.9114	0.911362	0.911336
7.0	1.8954	1.8954	1.8954	1.895420	
20.0	3.3539	3.3539	3.3539	3.353950	
70.0	6.4621	6.4622	6.4622	6.462250	

Chapter 11

Closing Remarks and Future Research Work

11.1   Closing Remarks

The research in this thesis has been initiated to elaborate the mathematical modeling and analysis for three-dimensional flows of Carreau fluid. The diverse characteristics of flow, heat and mass transport inside the boundary influenced by a bidirectional stretching surface have been explored. Particularly, both time-independent and time-dependent flows were reported. The formulated partial differential equations were converted in view of compatible conversions and then solved numerically via bvp4c. The confirmation of the results of this work is also done by making comparison through a numerical as well as analytical technique. This chapter provides in brief the highlights of the work presented in this thesis. Hence, the notable conclusions that are inferred from this exertion are enumerated as follows:

- The velocity component $f'(\eta)$ declined for $n = 0.5$ and enhanced for $n = 1.5$ for increasing local Weissenberg number (We_1). However, a conflicted behavior was reported for velocity component $g'(\eta)$.

- The behavior of the local Weissenberg number (We_2) was noted totally opposite for both $n < 1$ and $n > 1$ on velocity components $f'(\eta)$ and $g'(\eta)$, while temperature field enhanced for $n = 0.5$ and diminished for $n = 1.5$.

- A similar trend was remarked for higher value of power law exponent (n) on $f'(\eta)$ and $g'(\eta)$ for both shear thinning/thickening cases.

- The higher values of magnetic parameter (M) and unsteadiness parameter (S) caused a reduction in $f'(\eta)$ and $g'(\eta)$ and allied thickness of the boundary layer, whereas a conflicted performance was reported for temperature and concentration fields.

- The augmented values of thermal radiation (R_d), temperature ratio parameter (θ_f) and thermal Biot number (γ_1) intensified the temperature $\theta(\eta)$ of Carreau fluid.

- The Brownian motion (N_b) and thermophrosis (N_t) parameters, respectively, boosted the temperature of Carreau fluid for $n < 1$ and $n > 1$. However, conflicted performance of N_b and N_t were observed on concentration of Carreau nanofluid.

- The thermal stratification (S_1) and mass stratification (S_2) parameters diminished the temperature $\theta(\eta)$ and concentration $\phi(\eta)$ fields, respectively, while a conflicted trend was noted for larger mass Biot number (γ_2) for concentration field.

- The thermal relaxation time parameter (β_1) and concentration relaxation time parameter (β_2) reduced the temperature $\theta(\eta)$ and concentration $\phi(\eta)$, respectively.

- It was scrutinized that the homogeneous (k_1) and heterogeneous (k_2) reaction parameters have the aptitude to reduce the concentration $l(\eta)$ of Carreau fluid.

- The higher reaction rate (Λ), temperature difference parameters (Λ^*) and fitted rate constant (m) acknowledged a decay in the concentration field $\phi(\eta)$; however, the activation energy parameter (E) was augmented $\phi(\eta)$.

11.2   Future Research Work

In this thesis the main focus was to scrutinize the three-dimensional flows of Carreau fluid influenced by a bidirectional stretched surface. Although this thesis covers a wide-range of aspects regarding mathematical modeling and numerical computation of Carreau fluid, there are still a few suggestions for future work:

- In this thesis, the three-dimensional flows of Carreau fluid over planner stretching surface were investigated. This work can be extended for flows over curved stretching surface as well as flows due to rotating disk.

- This work could be extended forward to account for non-zero infinite shear rate viscosity for 3D flows of Carreau fluid.

- This study can be extended to explore the multiple solutions.

- Regarding the numerical simulation method, it would be interesting to perform a comparative study with different numerical methods.

Bibliography

[1] L.J. Crane, Flow past a stretching plate, *ZAMP*, **21** (1970) 645–647.

[2] W.A. Khan and I. Pop, Boundary-layer flow of a nanofluid past a stretching sheet, *Int. J. Heat Mass Transf.,* **53** (2010) 2477-2483.

[3] I.C. Liu, H.H. Wang and Y.F. Peng, Flow and heat transfer for three-dimensional flow over an exponentially stretching surface, *Chem. Eng. Commun.,* **200** (2013) 253–268.

[4] A. Ara, N.A. Khan, H. Khan and F. Sultan, Radiation effect on boundary layer flow of an Eyring–Powell fluid over an exponentially shrinking sheet, *Ain Shams Eng. J.,* **5** (2014) 1337-1342.

[5] N. Ishfaq, Z.H. Khan, W.A. Khan and R.J. Culham, Estimation of boundary-layer flow of a nanofluid past a stretching sheet, A revised model, *J. Hydro. Ser. B,* **28** (2016) 596-602.

[6] R.V. Williamson, The flow of pseudoplastic materials, *Ind. Eng. Chem.,* **21** (1929) 1108-1111.

[7] R.B. Bird, C.F. Curtiss, R.C. Armstrong and O. Hassager, Dynamics of Polymeric Liquids, John Wiley and Sons Inc., New York, USA, 1987.

[8] J.P. Pascal and H. Pascal, On some non-linear shear flows of non-Newtonian fluids, *Int. J. Non-Linear Mech.,* **130** (1995) 487-500.

[9] R. Ponalagusamy, Mathematical analysis of flow of non-Newtonian fluid due to metachronal beating of cilia in a tube and its physiological applications, *Appl. Math. Comput.,* **337** (2018) 545-561.

[10] P.J. Carreau, Rheological equations from molecular network theories, *Trans. Soc. Rheol.,* **116** (1972) 99–127.

[11] R.P. Chhabra and P.H.T. Uhlherr, Creeping motion of spheres through shear-thinning elastic fluids described by the Carreau viscosity equation, *Rheologica Acta,* **19** (1980) 187-195.

[12] N.S. Akbar and S. Nadeem, Carreau fluid model for blood flow through a tapered artery with a stenosis, *Ain Shams Eng. J.,* **5** (2014) 1307-1316.

[13] M. Khan and Hashim, Boundary layer flow and heat transfer to Carreau fluid over a nonlinear stretching sheet, *AIP Adv.,* **5** (2015) 107203.

[14] M. Khan, M.Y. Malik, T. Salahuddin and I. Khan, Heat transfer squeezed flow of Carreau fluid over a sensor surface with variable thermal conductivity: A numerical study, *Results Phy.,* **6** (2016) 940–945.

[15] T. Hayat, M. Waqas, S.A. Shehzad and A. Alsaedi, Stretched flow of Carreau nanofluid with convective boundary condition, *Pramana J. Phy.,* **86** (2016) 3-17.

[16] Hashim and M. Khan, On Cattaneo–Christov heat flux model for Carreau fluid flow over a slendering sheet, *Results Phy.,* **7** (2017) 310–319.

[17] K.G. Kumar, B.J. Gireesha, N.G. Rudraswamy and S. Manjunatha, Radiative heat transfers of Carreau fluid flow over a stretching sheet with fluid particle suspension and temperature jump, *Results Phy.,* **7** (2017) 3976-3983.

[18] S.U. Mamatha, C.S.K. Raju, G. Madhavi and Mahesha, Unsteady 3D MHD Carreau and Casson fluids over a stretching sheet with non-uniform heat source/sink, *Chem. Process Eng. Res.,* **52** (2017) 10-23.

[19] M. Khan, M. Irfan, L. Ahmad and W.A. Khan, Simultaneous investigation of MHD and convective phenomena on time-dependent flow of Carreau nanofluid with variable properties: Dual solutions, *Phy. Letters A,* **382** (2018) 2334-2342.

[20] S.T. Chaffin and J.M. Rees, Carreau fluid in a wall driven corner flow, *J. Non-Newtonian Fluid Mech.,* **253** (2018) 16-26.

[21] G.H.R. Kefayati and H. Tang, MHD thermosolutal natural convection and entropy generation of Carreau fluid in a heated enclosure with two inner circular cold cylinders, using LBM, *Int. J. Heat Mass Transf.,* **126-B** (2018) 508-530.

[22] S.U.S. Choi, Enhancing thermal conductivity of fluids with nanoparticles, *ASME Int. Mech. Eng.,* **66** (1995) 99–105.

[23] J. Buongiorno's, Convective transport in nanofluids, *ASME J. Heat Transf.,* **128** (2006) 240–250.

[24] R. Ellahi, M. Hassan and A. Zeeshan, Shape effects of nanosize particles in $Cu - H_2O$ nanofluid on entropy generation, *Int. J. Heat Mass Transf.,* **81** (2015) 449–456.

[25] M. Khan and W.A. Khan, Forced convection analysis for generalized Burgers nanofluid flow over a stretching sheet, *AIP Adv.,* **5** (2015) 107138; doi: 10.1063/1.4935043.

[26] B. Mahanthesh, B.J. Gireesha, R.S.R. Gorla, F.M. Abbasi and S.A. Shehzad, Numerical solutions for magnetohydrodynamic flow of nanofluid over a bidirectional non-linear stretching surface with prescribed surface heat flux boundary, *J. Magn. Magn. Mater.,* **417** (2016) 189–196.

[27] M. Khan and W.A. Khan, MHD boundary layer flow of a power law nanofluid with new mass flux condition, *AIP Adv.,* **6** (2016) 025211; doi: 10.1063/1.4942201.

[28] M. Khan, W.A. Khan and A.S. Alshomrani, Non-linear radiative flow of three-dimensional Burgers nanofluid with new mass flux effect, *Int. J. Heat Mass Transf.,* **101** (2016) 570-576.

[29] T. Hayat, M.I. Khan, M. Waqas, A. Alsaedi and M. Farooq, Numerical simulation for melting heat transfer and radiation effects in stagnation point flow of carbon-water nanofluid, *Comput. Methods Appl. Mech. Eng.,* **315** (2017) 1011–1024.

[30] W.A. Khan, M. Irfan, M. Khan, A.S. Alshomrani, A.K. Alzahrani and M.S. Alghamdi, Impact of chemical processes on magneto nanoparticle for the generalized Burgers fluid, *J. Mol. Liq.,* **234** (2017) 201-208.

[31] M. Waqas, M.I. Khan, T. Hayat and A. Alsaedi, Numerical simulation for magneto Carreau nanofluid model with thermal radiation: A revised model, *Comp. Methods Appl. Mech. Eng.,* **324** (2017) 640-653.

[32] A.S. Dogonchi and D.D. Ganji, Analytical solution and heat transfer of two-phase nanofluid flow between non-parallel walls considering Joule heating effect, *Powder Tech.,* **318** (2017) 390-400.

[33] T. Hayat, M. Rashid, M. Imtiaz and A. Alsaedi, Nanofluid flow due to rotating disk with variable thickness and homogeneous-heterogeneous reactions, *Int. J. Heat Mass Transf.,* **113** (2017) 96–105.

[34] C.S.K Raju, M.M. Hoque, N.N. Anika, S.U. Mamatha, and P. Sharma, Natural convective heat transfer analysis of MHD unsteady Carreau nanofluid over a cone packed with alloy nanoparticles, *Powder Tech.,* **317** (2017) 408-416.

[35] T. Hayat, M. Rashid, A. Alsaedi and B. Ahmad, Flow of nanofluid by nonlinear stretching velocity, *Results Phy.,* **8** (2018) 1104-1109.

[36] M. Sheikholeslami, R. Ellahi and K. Vafai, Study of Fe_3O_4-water nanofluid with convective heat transfer in the presence of magnetic source, *Alex. Eng. J.,* **57** (2018) 565-575.

[37] M. Mustafa, A. Mushtaq, T. Hayat and A. Alsaedi, Modeling MHD swirling flow due to rough rotating disk with non-linear radiation and chemically reactive solute, *Int. J. Numer. Methods Heat Fluid Flow,* **28** (2018) 2342-2356.

[38] M. Irfan, M. Khan, W.A. Khan and M. Ayaz, Modern development on the features of magnetic field and heat sink/source in Maxwell nanofluid subject to convective heat transport, *Phy. Letters A,* **382** (2018) 1992-2002.

[39] A. Hamid, M. Khan and Hashim, Impacts of binary chemical reaction with activation energy on unsteady flow of magneto-Williamson nanofluid, *J. Mol. Liq.,* **262** (2018) 435–442.

[40] B. Mahanthesh, B.J. Gireesha and I.L. Animasaun, Exploration of non-linear thermal radiation and suspended nanoparticles effects on mixed convection boundary layer flow of nanoliquids on a melting vertical surface, *J. Nanofluids,* **7** (2018) 833-843.

[41] J.H. Merkin, A model for isothermal homogeneous-heterogeneous reactions in boundary-layer flow, *Math. Comput. Model.,* **24** (1996) 125-136.

[42] M.A. Chaudhary and J.H. Merkin, A simple isothermal model for homogeneous-heterogeneous reactions in boundary-layer flow, I. Equal diffusivities, *Fluid Dyn. Res.,* **16** (1995) 311–333.

[43] H. Xu, A homogeneous-heterogeneous reaction model for heat fluid flow in the stagnation region of a plane surface, *Int. Commun. Heat Mass Transf.,* **87** (2017) 112-117.

[44] T. Hayat, R. Sajjad, R. Ellahi, A, Alsaedi and T. Muhammad, Homogeneous-heterogeneous reactions in MHD flow of micropolar fluid by a curved stretching surface, *J. Mol. Liq.,* **240** (2017) 209–220.

[45] J. Chen, B. Liu, X. Gao, L. Yan and D. Xu, Effects of heterogeneous–homogeneous interaction on the homogeneous ignition in hydrogen-fueled catalytic microreactors, *Int. J. Hydro. Energy,* **41** (2016) 11441-11454.

[46] C.S.K. Raju, N. Sandeep and S. Saleem, Effects of induced magnetic field and homogeneous–heterogeneous reactions on stagnation flow of a Casson fluid, *Eng. Sci. Tech. Int. J.,* **19** (2016) 875-887.

[47] Q. Lu, J. Pan, W. Yang, A. Tang, S. Bani and X. Shao, Interaction between heterogeneous and homogeneous reaction of premixed hydrogen–air mixture in a planar catalytic micro-combustor, *Int. J. Hydro. Energy,* **42** (2017) 5390-5399.

[48] M. Sajid, S.A. Iqbal, M. Naveed and Z. Abbas, Effect of homogeneous-heterogeneous reactions and magnetohydrodynamics on Fe3O4 nanofluid for the Blasius flow with thermal radiations, *J. Mol. Liq.,* **233** (2017) 115-121.

[49] B.J. Gireesha, P.B.S. Kumar, B. Mahanthesh, S.A. Shehzad and A. Rauf, Nonlinear 3D flow of Casson-Carreau fluids with homogeneous–heterogeneous reactions: A comparative study, *Results Phy.,* **7** (2017) 2762-2770.

[50] M.I. Khan, M. Waqas, T. Hayat, M.I. Khan and A. Alsaedi, Numerical simulation of nonlinear thermal radiation and homogeneous-heterogeneous reactions in convective flow by a variable thicked surface, *J. Mol. Liq.,* **246** (2017) 259-267.

[51] J.B.J. Fourier, Theorie analytique ee la chaleur, Paris, 1822.

[52] C. Cattaneo, Sulla conduzione del calore, Atti. Semin. Mat. Fis Univ. Modena Reggio Emilia, **3** (1948) 83–101.

[53] C.I. Christov, On frame indifferent formulation of the Maxwell–Cattaneo model of finite-speed heat conduction, *Mech. Res. Commun.,* **36** (2009) 481–486.

[54] V. Tibullo and V. Zampoli, A uniqueness result for the Cattaneo-Christov heat conduction model applied to incompressible fluids, *Mech. Res. Commun.,* **38** (2011) 77–79.

[55] K. Rubab and M. Mustafa, Cattaneo-Christov heat flux model for MHD three-dimensional flow of Maxwell fluid over a stretching sheet, *PLOS ONE*, **11** (2016) e0153481; doi: 10.1371/journal.pone.0153481.

[56] M. Khan and W.A. Khan, Three-dimensional flow and heat transfer to Burgers fluid using Cattaneo-Christov heat flux model, *J. Mol. Liq.,* **221** (2016) 651–657.

[57] M. Waqas, T. Hayat, M. Farooq, S.A. Shehzad and A. Alsaedi, Cattaneo-Christov heat flux model for flow of variable thermal conductivity generalized Burgers fluid, *J. Mol. Liq.,* **220** (2016) 642–648.

[58] L. Liu, L. Zheng, F. Liu and X. Zhang, Anomalous convection diffusion and wave coupling transport of cells on comb frame with fractional Cattaneo-Christov flux, *Commun. Nonlinear Sci. Numer. Simulat.,* **38** (2016) 45–58.

[59] J. Sui, L. Zheng, and X. Zhang, Boundary layer heat and mass transfer with CattaneoeChristov double-diffusion in upper-convected Maxwell nanofluid past a stretching sheet with slip velocity, *Int. J. Therm. Sci.,* **104** (2016) 461–468.

[60] W.A. Khan, M. Irfan and M. Khan, An improved heat conduction and mass diffusion models for rotating flow of an Oldroyd-B fluid, *Results Phy.,* **7** (2017) 3583-3589.

[61] M. Mustafa, T. Hayat and A. Alsaedi, Rotating flow of Maxwell fluid with variable thermal conductivity: An application to non-Fourier heat flux theory, *Int. J. Heat Mass Transf.,* **106** (2017) 142-148.

[62] M.E. Ali and N. Sandeep, Cattaneo-Christov model for radiative heat transfer of magnetohydrodynamic Casson-ferrofluid: A numerical study, *Results Phy.,* **7** (2017) 21-30.

[63] A.S. Dogonchi and D.D. Ganji, Impact of Cattaneo–Christov heat flux on MHD nanofluid flow and heat transfer between parallel plates considering thermal radiation effect, *J. Taiwan Inst. Chem. Eng.,* **80** (2017) 52-63.

[64] M. Khan, L. Ahmad, W.A. Khan, A.S. Alshomrani. A.K. Alzahrani and M.S. Alghamdi, A 3D Sisko fluid flow with Cattaneo-Christov heat flux model and heterogeneous-homogeneous reactions: A numerical study, *J. Mol. Liq.,* **238** (2017) 19-16.

[65] L. Liu, L. Zheng, F. Liu and X. Zhang, Heat conduction with fractional Cattaneo–Christov upper-convective derivative flux model, *Int. J. Ther. Sci.,* **112** (2017) 421-426.

[66] S. Nadeem, S. Ahmad and N. Muhammad, Cattaneo-Christov flux in the flow of a viscoelastic fluid in the presence of Newtonian heating, *J. Mol. Liq.,* **237** (2017) 180-184.

[67] S.U. Mamatha, Mahesha and C.S.K. Raju, Cattaneo-Christov on heat and mass transfer of unsteady Eyring Powell dusty nanofluid over sheet with heat and mass flux conditions, *Inform. Medicine Unlocked,* **9** (2017) 76-85.

[68] A. Aziz, A similarity solution for laminar thermal boundary layer over a flat plate with a convective surface boundary condition, *Commun. Nonlin. Sci. Numer. Simulat.,* **14** (2009) 1064-1068.

[69] T. Hayat, Y. Saeed, A. Alsaedi and S. Asad, Effects of convective heat and mass transfer in flow of Powell-Eyring fluid past an exponentially stretching sheet, *PLOS ONE,* **10** (2015) e0133831; doi: 10.1371/journal.pone.0133831.

[70] T. Hayat, M. Rashid and A. Alsaedi, MHD convective flow of magnetite-Fe3O4 nanoparticles by curved stretching sheet, *Results Phy.,* **7** (2017) 3107-3115.

[71] Y.J. Zhuang and Q.Y. Zhu, Numerical study on combined buoyancy–Marangoni convection heat and mass transfer of power-law nanofluids in a cubic cavity filled with a heterogeneous porous medium, *Int. J. Heat Fluid Flow,* **71** (2018) 39-54.

[72] Consequence of convective conditions for flow of Oldroyd-B nanofluid by a stretching cylinder, *J. Braz. Soc. Mech. Sci. Eng.,* **41** (2019), doi: 10.1007/s40430-019-1604-3.

[73] M.A. Hossain, M.A. Alim and D.A.S. Rees, Effect of radiation on free convection from a porous vertical plate, *Int. J. Heat Mass Transf.,* **42** (1999) 181-191.

[74] N.S. Akbar, S. Nadeem, R.U. Haq and Z.H. Khan, Numerical solutions of magnetohydrodynamic boundary layer flow of tangent hyperbolic fluid towards a stretching sheet, *Indian J. Phy.,* **87** (2013) 1121-1124.

[75] N.S. Akbar, S, Nadeem, R.U. Haq and Z.H. Khan, Radiation effects on MHD stagnation point flow of nanofluid towards a stretching surface with convective boundary condition, *Chinese J. Aeronaut.,* **26** (2013) 1389-1397.

[76] T. Hayat, M. Rashid, M, Imtiaz and A. Alsaedi, Magnetohydrodynamic (MHD) flow of Cu-water nanofluid due to a rotating disk with partial slip, *AIP Adv.,* **6** (2015) 067169; doi: dx.doi.org/10.1063/1.4923380.

[77] W.A. Khan and M. Khan, Impact of thermophoresis particle deposition on three-dimensional radiative flow of Burgers fluid, *Results Phy.,* **6** (2016) 829-836.

[78] M. Farooq, M.I. Khan, M. Waqas, T. Hayat, A. Alsaedi and M.I. Khan, MHD stagnation point flow of viscoelastic nanofluid with non-linear radiation effects, *J. Mol. Liq.,* **221** (2016) 1097-1103.

[79] M. Khan, M. Irfan and W.A. Khan, Impact of nonlinear thermal radiation and gyrotactic microorganisms on the magneto-Burgers nanofluid, *Int. J. Mech. Sci.,* **130** (2017) 375-382.

[80] S.S. Ghadikolaei, K. Hosseinzadeh, M. Hatami, D.D. Ganji and M. Armin, Investigation for squeezing flow of ethylene glycol (C2H6O2) carbon nanotubes (CNTs) in rotating stretching channel with nonlinear thermal radiation, *J. Mol. Liq.,* **263** (2018) 10-21.

[81] F.A. Soomro, M. Usman, R.U. Haq and W. Wang, Melting heat transfer analysis of Sisko fluid over a moving surface with nonlinear thermal radiation via Collocation method, *Int. J. Heat Mass Transf.,* **126 A***,* (2018) 1034-1042.

[82] A.S. Alshomrani, M. Irfan, A. Saleem and M. Khan, Chemically reactive flow and heat transfer of magnetite Oldroyd-B nanofluid subject to stratifications, *Appl. Nanoscience,* **8** (2018) 1743–1754.

[83] C. Sulochana, S.P. Samrat and N. Sandeep, Numerical investigation of magnetohydrodynamic (MHD) radiative flow over a rotating cone in the presence of Soret and chemical reaction, *Propulsion Power Res.,* **7** (2018) 91-101.

[84] M. Rashid, M.I. Khan, T. Hayat, M.I. Khan and A. Alsaedi, Entropy generation in flow of ferromagnetic liquid with nonlinear radiation and slip condition, *J. Mol. Liq.,* **276** (2019) 441-452.

[85] W.A. Khan, M. Khan and R. Malik, Three-dimensional flow of an Oldroyd-B nanofluid towards stretching surface with heat generation/absorption, *PLOS ONE,* **9** (2017) e105107; doi: 10.1371/journal.pone.0105107.

[86] M. Khan and W.A. Khan, Steady flow of Burgers nanofluid over a stretching surface with heat generation/absorption, *J. Braz. Soc. Mech. Sci. Eng.,* **38** (2016) 2359–2367.

[87] M.I. Khan, T. Hayat, M. Waqas, M.I Khan and A. Alsaedi, Impact of heat generation/absorption and homogeneous-heterogeneous reactions on flow of Maxwell fluid, *J. Mol. Liq.,* **233** (2017) 465–470.

[88] B.J. Gireesha, P. Venkatesh, N.S. Shashikumar and B.C. Prasannakumara, Boundary layer flow of dusty fluid over a radiating stretching surface embedded in a thermally stratified porous medium in the presence of uniform heat source, *Nonlinear Eng.,* **6** (2017) 31-41.

[89] G.K Ramesh, B.C. Prasannakumara, B.J. Gireesha, S.A. Shehzad and F.M. Abbasi, Three dimensional flow of Maxwell fluid with suspended nanoparticles past a bidirectional porous stretching surface with thermal radiation, *Ther. Sci. Eng. Progr.,* **1** (2017) 6-14.

[90] T.C. Chiam, Heat transfer with variable conductivity in a stagnation-point flow towards a stretching sheet, *Int. Commun. Heat Mass Transf.,* **23** (1996) 239-248.

[91] H.S. Chu and C.J. Tseng, Conduction-radiation interaction in absorbing, emitting and scattering media with variable thermal conductivity, *J. Thermophysics Heat Transf.,* **6** (1992) 537-540.

[92] S.M. Upadhya, Mahesha and C.S.K. Raju, Comparative study of Eyring and Carreau fluids in a suspension of dust and nickel nanoparticles with variable conductivity, *Eur. Phy. J. Plus,* **133** (2018) 156; doi: 10.1140/epjp/i2018-11979-x.

[93] T. Hayat, S. Farooq, B. Ahmad and A. Alsaedi, Consequences of variable thermal conductivity and activation energy on peristalsis in curved configuration, *J. Mol. Liq.,* 263 (2018) 258-267.

[94] S. Mukhopadhyay and A. Ishak, Mixed convection flow along a stretching cylinder in a thermally stratified medium, *J. Appl. Math.,* **2012** (2012) 1-8.

[95] B. Mahanthesh, B.J. Gireesha and R.S.R. Gorla, Heat and mass transfer effects on the mixed convective flow of chemically reacting nanofluid past a moving/ stationary vertical plate, *Alex. Eng. J.,* **55** (2016) 569–581.

[96] M. Imtiaz, T. Hayat and A. Alsaedi, Mixed convection flow of Casson nanofluid over a stretching cylinder with convective boundary conditions, *Adv. Powder Tech.,* **27** (2016) 2245-2256.

[97] M. Waqas, M.I. Khan, T. Hayat and A. Alsaedi, Stratified flow of an Oldroyd-B nanoliquid with heat generation, *Results Phy.,* **7** (2017) 2489–2496.

[98] P. Besthapu, R.U. Haq, S. Bandari and Q.M. Al-Mdallal, Mixed convection flow of thermally stratified MHD nanofluid over an exponentially stretching surface with viscous dissipation effect, *J. Taiwan Inst. Chem. Eng.,* **71** (2017) 307-314.

[99] S.M. Ibrahim, G. Lorenzini, P.V. Kumar and C.S.K. Raju, Influence of chemical reaction and heat source on dissipative MHD mixed convection flow of a Casson nanofluid over a nonlinear permeable stretching sheet, *Int. J. Heat Mass Transf.,* **111** (2017) 346-355.

[100] M.I. Khan, M. Waqas, T. Hayat, M.I. Khan and A. Alsaedi, Behavior of stratification phenomenon in flow of Maxwell nanomaterial with motile gyrotactic microorganisms in the presence of magnetic field, *Int. J. Mech. Sci.,* **131-132** (2017) 426-434.

[101] A.R. Bestman, Radiative heat transfer to flow of a combustible mixture in a vertical pipe, *Int. J. Energy Res.,* **15** (1991) 179–184.

[102] K.L. Hsiao, To promote radiation electrical MHD activation energy thermal extrusion manufacturing system efficiency by using Carreau-nanofluid with parameters control method, *Energy,* **130** (2017) 486–499.

[103] M. Mustafa, J.A. Khan, T. Hayat and A. Alsaedi, Buoyancy effects on the MHD nanofluid flow past a vertical surface with chemical reaction and activation energy, *Int. J. Heat Mass Transf.,* **108** (2017) 1340–1346.

[104] M.I. Khan, S. Qayyum, T. Hayat, M. Waqas, M.I. Khan and A. Alsaedi, Entropy generation minimization and binary chemical reaction with Arrhenius activation energy in MHD radiative flow of nanomaterial, *J. Mol. Liq.,* **259** (2018) 274–283.

[105] A. Zeeshan, N. Shehzad and R. Ellahi, Analysis of activation energy in Couette-Poiseuille flow of nanofluid in the presence of chemical reaction and convective boundary conditions, *Results Phy.,* **8** (2018) 502–512.

[106] M.I. Khan, T. Hayat, M.I. Khan and A. Alsaedi, Activation energy impact in nonlinear radiative stagnation point flow of Cross nanofluid, *Int. Commun. Heat Mass Transf.,* **91** (2018) 216-224.

[107] M. Irfan, M. Khan, W.A. Khan and L. Ahmad, Influence of binary chemical reaction with Arrhenius activation energy in MHD nonlinear radiative flow of unsteady Carreau nanofluid: Dual solutions, *Appl. Phy. A,* **125** (2019), doi: 10.1007/s00339-019-2457-4.

[108] L.F. Shampine, I. Gladwell and S. Thompson, Solving ODEs with MATLAB, (1st Edn.), Cambridge University Press, Cambridge, (2003).

[109] S.J. Liao, Beyond Perturbation: Introduction to Homotopy Analysis Method, Chapman and Hall, CRC Press, Boca Raton, (2003).

[110] S.J. Liao, Homotopy Analysis Method in Non-linear Differential Equations, Springer and Higher Education Press, Heidelberg, (2012).

[111] S. Abbasbandy, E. Shivanian and K. Vajravelu, Mathematical properties of $\hbar$-curve in the frame work of the homotopy analysis method, *Commun. Nonlinear Sci. Numer. Simulat.,* **16** (2011) 4268-4275.

[112] A. Mastroberardino, Homotopy analysis method applied to electrohydrodynamic flow, *Commun. Nonlinear Sci. Numer. Simulat.,* **16** (2011) 2730–2736.

[113] O.A. Beg, M.M. Rashidi, T.A. Beg and M. Asadi, Homotopy analysis of transient magneto-bio-fluid dynamics of micropolar squeeze film in a porous medium: A model for magneto-bio-rheological lubrication, *J. Mech. Medicine Biology,* **12** (2012) 1250051; doi: 10.1142/S0219519411004642.

[114] M. Turkyilmazoglu, An effective approach for evaluation of the optimal convergence control parameter in the homotopy analysis method, *Filomat,* **30** (2016) 1633-1650.

[115] P.D. Ariel, The three-dimensional flow past a stretching sheet and the homotopy, *Comput. Math. Appl.,* **54** (2007) 920–925.

[116] T. Hayat, I. Ullah, T. Muhammad, A. Alsaedi and S.A. Shehzad, Three-dimensional flow of Powell-Eyring nanofluid with heat and mass flux boundary conditions, *Chin. J. Phy.,* **25** (2016) 074701.

[117] C.Y. Wang, The three dimensional flow due to a stretching flat surface, *Phys. Fluids,* **27** (1984) 1915-1917.

[118] I.C. Liu and H.I. Anderson, Heat transfer over a bidirectional stretching sheet with variable thermal conditions, *Int. J. Heat Mass Transf.,* **51** (2008) 4018-4024.

[119] A. Munir, A. Shahzad and M. Khan, Convective flow of Sisko fluid over a bidirectional stretching surface, *PLOS ONE*, **10** (2015) e0130342; doi: 10.1371/journal.pone.0130342.

[120] S. Sharidan, T. Mahmood and I. Pop, Similarity solutions for the unsteady boundary layer flow and heat transfer due to a stretching sheet, *Int. J. Appl. Mech. Eng.,* **11** (2006) 647–654.

[121] A.J. Chamkha, A.M. Aly and M.A. Mansour, Similarity solution for unsteady heat and mass transfer from a stretching surface embedded in a porous medium with suction/injection and chemical reaction effects, *Chem. Eng. Commun.,* **197** (2010) 846–858.

[122] C.Y. Wang, Free convection on a vertical stretching surface, *J. Appl. Math. Mech., (ZAMM),* **69** (1989) 418-420.

[123] R.S.R. Gorla and I. Sidawi, Free convection on a vertical stretching surface with suction and blowing, *Appl. Sci. Res.,* **52** (1994) 247-257.

turnitin Turnitin Originality Report

On Stretched Flows of Carreau Fluid with Heat Transfer: Modeling and Analysis by Muhammad Irfan .

From DRSM (DRSML)

- Processed on 02-Dec-2019 14:21 PKT
- ID: 1225004688
- Word Count: 44329

Similarity Index
17%
Similarity by Source

Internet Sources:
  3%
Publications:
  11%
Student Papers:
  13%

sources:
1

1% match (student papers from 06-Jun-2018)

Submitted to Higher Education Commission Pakistan on 2018-06-06
2

1% match (publications)

Latif Ahmad, Masood Khan, Waqar Azeem Khan. "Numerical investigation of magneto-nanoparticles for unsteady 3D generalized Newtonian liquid flow", The European Physical Journal Plus, 2017
3

1% match (student papers from 22-Feb-2019)

Submitted to Higher Education Commission Pakistan on 2019-02-22
4

1% match (Internet from 11-May-2019)

https://www.science.gov/topicpages/h/heat+transfer+nanofluids.html
5

< 1% match (Internet from 26-Mar-2019)

https://www.science.gov/topicpages/h/heat+conduction+code.html
6

< 1% match (student papers from 07-Nov-2017)

Submitted to Higher Education Commission Pakistan on 2017-11-07